

**MINERALOGY, GEOCHEMISTRY, AND GEOCHRONOLOGY OF THE KIN  
PROPERTY PEGMATITES IN EASTERN BRITISH COLUMBIA**

by

Dana Caudle

B.S., Iowa State University, 2013

A THESIS SUBMITTED IN PARTIAL FULFILLMENT OF THE REQUIREMENTS FOR

THE DEGREE OF

MASTER OF SCIENCE

in

THE FACULTY OF GRADUATE AND POSTDOCTORAL STUDIES

(Geological Sciences)

THE UNIVERSITY OF BRITISH COLUMBIA

(Vancouver)

April, 2016

© Dana Caudle, 2016

## Abstract

Rare earth element- and Nb-bearing NYF-type pegmatites are located on the KIN property, approximately 95 km northeast of Revelstoke, British Columbia. They intrude amphibolite grade rocks of the Neoproterozoic Horsethief Creek Group in the Omineca Belt of the Canadian Cordillera. The Cordillera has traditionally been associated with LCT-type pegmatites, making the presence of NYF-type pegmatites on the KIN property particularly unusual. These pegmatites are found *in-situ* in four localities and contain significant amounts of allanite-(Ce), monazite-(Ce), chevkinite-(Ce), aeschynite-(Ce), euxenite-(Y), Nb-rich rutile, ilmenite, amphibole, and fluorapatite within plagioclase and Ba-rich feldspar and quartz. Additionally, the pegmatites contain textures and minerals, such as epidote-rimmed allanite and the breakdown of monazite into apatite and allanite in a corona texture, which can be attributed to Ca, F, and Si-rich fluids having been introduced during metamorphism. These pegmatites were dated by U-Pb zircon methods at approximately 79 Ma, and likely formed from an A-type source. Along with the NYF-type pegmatites, A-type REE-bearing syenites, coarse grained I-/S-type granites, and tourmaline bearing granitic pegmatite float samples are located on the property. The granite and syenite were identified as potential parental rocks for the mineralized pegmatites and this hypothesis was tested using geochemistry and geochronology. The granite is undeformed and has been dated by U-Pb zircon methods at approximately 76 Ma; this evidence, along with its geochemical signature suggests that the granite cannot be the parent for the pegmatites. Geochemical and elemental characteristics within the syenites suggest possible linkage to the pegmatites; however, syenite in the immediate area has been dated to 378 Ma, nearly 300 million years older than the pegmatites. In view of this the geochemical match and age discrepancy, it is possible that the pegmatites formed from partial melting of these older syenites at approximately 79 Ma.

## **Preface**

Chapter 1. Figures 1.1, 1.2, 1.3, 1.4, 1.5, 1.8, and 1.13 along with Tables 1.1, 1.2, and 1.3 are used with permission from applicable sources.

I was responsible for the majority of the thesis project design and organization, data collection and analysis and wrote the manuscript for the final dissertation. Cempírek, J. and Škoda, R. were involved in electron microprobe data collection at Masaryk University in Brno Czech Republic. Geochronological data collection and analyses were performed by the Pacific Centre for Isotope and Geochemical Research at the University of British Columbia and whole rock geochemical data was provided by Acme Laboratories, in Vancouver, British Columbia. Millonig, L. and Mortensen, J. contributed to chapter edits. My supervisor Groat, L.A., along with Cempírek, J., was involved with the project throughout with contributions to project design and chapter edits.

## Table of Contents

Abstract.....	ii
Preface.....	iii
Table of Contents.....	iv
List of Tables.....	ix
List of Figures.....	xi
Acknowledgements.....	xix
1. Introduction.....	1
1.1 Pegmatites.....	1
1.1.1 Pegmatite Definition.....	1
1.1.2 Pegmatite Classification.....	2
1.1.3 Parental Magmas.....	3
1.1.4 Pegmatite Internal Zoning.....	4
1.1.5 Pegmatite Formation.....	5
1.1.6 Importance of Rare Earth Elements.....	6
1.2 KIN Property.....	7
1.2.1 Regional Geology.....	7
1.2.2 Previous work on the KIN property.....	9
1.2.3 KIN Property Locality and Pegmatites.....	10
1.3 Materials & Methods.....	14
2. Petrography.....	32
2.1 Pegmatites.....	32
2.1.1 Border Zone.....	32
2.1.2 Wall Zone.....	33
2.1.3 Intermediate Zone.....	34
2.1.4 Core Zone.....	35

2.2	Granitic Pegmatite .....	36
2.3	Granite.....	37
2.4	Syenite.....	37
3.	Mineralogy .....	50
3.1	Silicates.....	50
3.1.1	Feldspar.....	50
3.1.2	Mica .....	51
3.1.3	Amphibole.....	52
3.1.4	Garnet.....	53
3.1.5	Zircon.....	55
3.1.6	Thorite.....	55
3.1.7	Titanite .....	55
3.1.8	Beryl and Bertrandite.....	56
3.1.9	Tourmaline.....	56
3.2	REE silicate minerals.....	57
3.2.1	Epidote Group minerals .....	57
3.2.2	Chevkinite group minerals.....	59
3.3	Phosphate Minerals.....	61
3.3.1	Monazite .....	61
3.3.2	Apatite.....	63
3.3.3	Xenotime.....	64
3.4	Oxide Minerals.....	64
3.4.1	Columbite.....	64
3.4.2	Rutile and ilmenite-pyrophanite.....	65
3.4.3	Aeschnyrite, Niobaeschnyrite, Euxenite, and Fersmite.....	66
3.5	Carbonate Minerals.....	68
3.5.1	Lanthanite .....	68

4. Whole-Rock Geochemistry and Geochronology .....	110
4.1 Whole-Rock Geochemistry .....	110
4.2 Geochronology .....	112
5. Discussion .....	125
5.1 Mineralogy Characterization and Discussion .....	125
5.1.1 Hyalophane Feldspar .....	125
5.1.2 Allanite .....	126
5.1.3 Aeschynite and Euxenite .....	127
5.1.4 Chevkinite Group Minerals .....	128
5.1.5 Phosphates: Monazite and Apatite .....	129
5.1.6 Columbite .....	130
5.2 Parental Magma Determination and Pegmatite Classification .....	131
5.2.1 Parental Magma Determination .....	131
5.2.2 Pegmatite Classification .....	133
5.3 Metamorphic Conditions and Effects .....	134
5.3.1 Evidence for Metamorphism and Effects .....	134
5.3.2 Metamorphic Conditions .....	135
5.3.3 Potential Causes of Metamorphism .....	137
5.4 Locality Comparison .....	137
6. Conclusions .....	141
7. Suggestions for Future Work .....	143
References .....	145
Appendices .....	156
Appendix A: EMPA Methods .....	156
A.1 Feldspar .....	156
A.2 Mica, Beryl, and Bertrandite .....	156
A.3 Amphibole .....	157

A.4	Garnet.....	157
A.5	Zircon.....	158
A.6	Titanite.....	158
A.7	Tourmaline.....	159
A.8	Epidote Group Minerals.....	159
A.9	Chevkinite Group Minerals.....	160
A.10	Monazite and Thorite.....	160
A.11	Apatite.....	161
A.12	Columbite.....	161
A.13	Rutile and Ilmenite-Pyrophanite.....	162
A.14	Aeschnynite, Niobaeschnynite, Euxenite, and Fersmite.....	162
A.15	Lanthanite.....	163
Appendix B: EMPA Results.....		164
B.1:	Feldspar.....	164
B.2:	Micas.....	169
B.3:	Amphibole.....	174
B.4:	Garnet.....	177
B.5:	Zircon.....	182
B.6:	Titanite.....	184
B.7:	Beryl+Bertrandite.....	186
B.8:	Tourmaline.....	187
B.9:	Epidote Group Minerals.....	189
B.10:	Chevkinite Group Minerals.....	208
B.11:	Monazite and Thorite.....	216
B.11:	Apatite.....	221
B.13:	Columbite.....	223
B.14:	Oxides.....	229

B.15: Aeschnite, Nioboaeschnite, Euxenite, and Fersmite .....	230
B.16: Lanthanite.....	242
Appendix C: Full Petrographic Descriptions .....	243
C.1 Pegmatites .....	243
C.2 Granitic Pegmatite.....	252
C.3 Granite.....	252
C.4 Syenite.....	253
Appendix D: Geochronology Results .....	269
D.1: Pegmatite Radiometric Dating Report.....	269
D.2: Granite Radiometric Dating Report.....	276

## List of Tables

Table 1.1 Principal subdivision and characteristics of the five classes of granitic pegmatites [Table 2 from Černý & Ercit, (2005)].....	18
Table 1.2 Subdivision of granitic pegmatites of the rare-element class [Table 5 from Černý & Ercit (2005)].....	19
Table 1.3 Mineral composition of typical pegmatite zones (Simmons, et al., 2003). ....	20
Table 1.4 KIN Property Locality Coordinates.....	23
Table 2.1 Border zone petrography. ....	38
Table 2.2 Wall zone petrography.....	40
Table 2.3 Intermediate zone petrography. ....	42
Table 2.4 core zone petrography.....	46
Table 3.1 Thin sections analyzed by EMP and their locality. ....	68
Table 3.2 Feldspar: Thin sections and zones with analyzed samples. ....	68
Table 3. 3 Mica: Thin sections and zones with analyzed samples.....	71
Table 3. 4 Amphibole: Thin sections and zones with analyzed samples.....	74
Table 3. 5 Garnet: Thin sections and zones with analyzed samples.....	77
Table 3.6 Zircon: Thin sections and zones with analyzed samples.....	81
Table 3.7 Thorite: Thin sections and zones with analyzed samples.....	82
Table 3.8 Titanite: sections and zones with analyzed samples.....	82
Table 3.9 Epidote Group Minerals: Thin sections and zones with analyzed samples.....	86
Table 3.10 Chevkinite: Thin sections and zones with analyzed samples. ....	94
Table 3.11 Monazite: Thin sections and zones with analyzed samples.....	97
Table 3.12 Apatite: Thin sections and zones with analyzed samples. ....	100

Table 3.13 Columbite: Thin sections and zones with analyzed samples.....	102
Table 3.14 Oxides: Thin sections and zones with analyzed samples. ....	104
Table 3.15 REE-bearing oxides: Thin sections and zones with analyzed samples. ....	105
Table 4.1 Major element whole rock geochemical results. ....	113
Table 4.2 Minor element whole rock geochemistry results.....	114
Table 4.3 Trace element analyses for Trident Mountain syenites. ....	116

## List of Figures

Figure 1.1 Example of typical internal structure of rare element pegmatites (Černý, 1991). .....	20
Figure 1.2 Geologic map of British Columbia and KIN property location [figure from Massey, et al. (2005)]......	21
Figure 1.3 Alkaline igneous rock occurrences within British Columbia. The KIN pegmatite occurrence is found close to the Trident Mountain locality shown on the map [from Pell (1994)]. .....	22
Figure 1.4 Location of the KIN property within the Selkirk-Cariboo-Monashee complex near the Mica Creek area [map from Crowley et al. (2000)]......	22
Figure 1.5 Map of KIN property with pegmatite and float localities marked. [underlying map with syenite trace from Brown (2011); geology based on Massey et al., (2005)]......	24
Figure 1.6 Top: Pegmatite at locality KIN-130 seen intruding within strike of host rocks.....	25
Figure 1.7 Coarse grains of allanite and columbite within feldspar at locality KIN-130. ....	26
Figure 1.8 Locality KIN-133 (Millonig, 2011).....	26
Figure 1.9 Coarse black allanite within feldspar at locality KIN-134. ....	27
Figure 1.10 Top: Coarse allanite from the wall zone at locality KIN-135. ....	28
Figure 1.11 Coarse molybdenite grains (sample Rad 2).....	29
Figure 1.12 Float PGM sample with white matrix and tourmaline grain. ....	29
Figure 1.13 Location of all granite points overlying the original syenite trace described in the company report [from Brown (2011)]. ....	30
Figure 1.14 Top: Coarse grained granitic rock (G18) composed primarily of quartz, feldspar, and muscovite. ....	31
Figure 2.1 Border zone in hand sample from locality KIN-133. ....	38

Figure 2.2 Primary monazite breaks down to form secondary fluorapatite, thorite, and allanite-(Ce) in a corona in sample KIN-133c.....	39
Figure 2.3 Primary aeschynite-(Ce) and ferrocolumbite with secondary allanite-(Ce) with thorite in sample KIN-133c.....	39
Figure 2.4 Garnet clusters surrounded by clinozoisite with phlogopite in border zone sample KIN-134-4.....	40
Figure 2.5 Wall zone thin section blanks (left to right are samples KIN-133e, KIN-135a, Rad 1, KIN-133b, and KIN133d) to show texture and appearance, as well as similarities between this zone across localities.....	41
Figure 2.6 Poikiloblastic texture of amphibole and phlogopite within sample KIN-133b.....	41
Figure 2.7 Secondary zoned allanite grains in the intermediate zone in sample KIN-130a.....	43
Figure 2.8 Primary columbite with euxenite-(Y) in fractures and fersmite as a secondary product in section KIN-130b.....	43
Figure 2.9 Hand sample from the intermediate zone at locality KIN-134.....	44
Figure 2.10 Blank from thin section KIN-135b.....	44
Figure 2. 11 Images from thin section Rad 2a showing mica (phlogopite and muscovite) in vein (top) and tourmaline (bottom).....	45
Figure 2.12 Undulose extinction and migratory boundaries visible in the quartz within the core at locality KIN-130.....	47
Figure 2.13 Primary amphibole grains demonstrating cleavage planes within quartz in the quartz core from locality KIN-130.....	47
Figure 2.14 Quartz core with visible quartz and red garnet at locality KIN-134. The top of the photo shows the contact between the core and the intermediate zone.....	48

Figure 2.15 Allanite and apatite within quartz in sample Rad 2c.....	48
Figure 2.16 Ferrocolumbite and monazite-(Ce) within almandine in sample PGM 1.....	49
Figure 2.17 Ferriallanite grains in syenite sample JBTD018.....	49
Figure 3.1 Feldspar classification diagram.....	69
Figure 3.2 Variation in Ba and Ca within feldspars.....	69
Figure 3.3 Ca, K, and Na ratios within feldspars.....	70
Figure 3.4 Ratios of K, Ba, and Na within feldspars. The hyalophane trend towards Na instead of K is visible.....	70
Figure 3.5 Mica classification diagram for all KIN samples.....	71
Figure 3.6 Biotite classification diagram.....	72
Figure 3.7 Graph showing variations of Ti in biotite and muscovite (circled). Note higher Ti contents in lower Mg/Mg+Fe points.....	72
Figure 3.8 Primary biotite with secondary almandine and primary magnesiohornblende and columbite in the wall zone at locality KIN-133.....	73
Figure 3.9 Secondary sericite after plagioclase in the intermediate zone from locality KIN-130.....	73
Figure 3.10 Biotite and muscovite in association in sample Rad 2a.....	74
Figure 3.11 Amphibole classification diagram.....	75
Figure 3.12 Compositional diagram for amphibole, showing tschermakite and edenite substitution trends.....	76
Figure 3.13 Primary magnesiohornblende with secondary almandine, pyrite, and lanthanite-(Ce) in the core at locality KIN-130.....	76

Figure 3. 14 a (above) Type I and Type II garnets differentiated by high and low Ca contents. Type I on the right, Type II on the left. Fe <sup>2+</sup> is blue, Mn is red, and Mg is green. ....	78
Figure 3. 15 Garnet classification diagram. ....	79
Figure 3.16 Garnet compositional diagram showing generally low amounts of Mg present in all garnet types. ....	79
Figure 3.17 Garnet I in quartz with poikiloblastic texture in the border zone at locality KIN-133. ....	80
Figure 3.18 Garnet I with titanite in the wall zone at locality KIN-135. ....	80
Figure 3.19 Primary altered garnet II replaced by muscovite, chlorite, and xenotime within the granite. ....	81
Figure 3.20 Primary garnet II with almandine in PGM 1 with feldspar and tourmaline. ....	81
Figure 3.21 Thorite exsolutions in allanite-(Ce) in the intermediate zone at locality KIN-130. ...	82
Figure 3.22 Ilmenite II in symplectite with columbite III and phlogopite after titanite in the wall zone at locality KIN-133. ....	83
Figure 3. 23 REE levels in titanite normalized to chondrite. Each color/shape combination represents a different sample point. ....	83
Figure 3.24 Zoned tourmaline in sample Rad 2a. ....	84
Figure 3.25 Classification diagram for tourmaline using X-site cation ratios. ....	84
Figure 3.26 Classification diagram for tourmaline, using W-site cation ratios. ....	85
Figure 3.27 Diagram for Y-site cation distribution in tourmaline. ....	85
Figure 3.28 EGM classification diagram. The same data sets are present in both diagrams, however a (top) shows the classification based on zone and locality whereas b (bottom) shows	

the classification based on allanite type (classification based on Armbruster et al., 2006 and Ercit, 2002).	87
Figure 3.29 REE distribution within EGM.	88
Figure 3.30 REE levels in EGM normalized to chondritee. Each color/shape combination represents a different sample point.	88
Figure 3.31 Allanite III after primary monazite in the border zone at locality KIN-133.	89
Figure 3.32 Secondary allanite III with secondary aeschynite-(Ce) with ferrocolumbite in the border zone at locality KIN-133.	89
Figure 3.33 Large, zoned, allanite I/II crystal in the wall zone at locality KIN-135.	90
Figure 3.34 M3 –site vacancies in allanite. The line is to draw attention to the similar level found within the primary allanite I grains.	90
Figure 3.35 Zone allanite I (and II on edges) with an inclusion of chevkinite in the wall zone at locality KIN-133.	91
Figure 3.36 Zoned allanite III in the intermediate zone (130a).	91
Figure 3.37 Secondary allanite III after monazite-(Ce) with apatite and thorite from the intermediate zone at locality KIN-134.	92
Figure 3.38 Secondary allanite III after monazite with apatite in the intermediate zone at locality KIN-134.	92
Figure 3.39 M <sup>3+</sup> vs Ti for allanite grains. The line is to draw attention to the trend found within the primary allanite I grains.	93
Figure 3.40 REE vs Ti for allanite grains. The line is to draw attention to the trend found within the primary allanite I grains.	93

Figure 3.41 $M^{2+}$ vs. Ti for allanite grains. The line is to draw attention to the trend found within the primary allanite I grains. ....	94
Figure 3.42 Distribution of chevkinite and perrierite subgroup samples (Modeled after Macdonald and Belkin, 2002).....	95
Figure 3.43 REE amounts present in chevkinite normalized to chondrite. Each color/shape combination represents a different sample point. ....	95
Figure 3.44 Primary chevkinite and secondary perrierite present in the wall zone at locality KIN-135.....	96
Figure 3.45 Primary chevkinite with partial replacement by aeschynite in allanite.....	96
Figure 3.46 REE distribution within monazite. ....	97
Figure 3.47 REE values present in monazite normalized to chondrite. Each color/shape combination represents a different sample point. ....	98
Figure 3.48 Huttonite/thorite and cheralite substitution trends in monazite (based on Ondrejka, 2012). ....	98
Figure 3. 49 Primary monazite with secondary allanite and apatite with chevkinite in the wall zone at locality KIN-133.....	99
Figure 3. 50 Monazite in sample KIN 136 with rutile and exsolved columbite IV.....	99
Figure 3. 51 Monazite in sample PGM 1 with columbite.....	100
Figure 3.52 REE vs Si showing the low values of REE present in KIN property apatite. ....	101
Figure 3.53 The KIN property apatites contain elevated levels of Sr.....	101
Figure 3.54 Columbite classification diagram. ....	102
Figure 3.55 Columbite with allanite in the wall zone at locality KIN-135.....	103

Figure 3.56 Columbite I with fersmite and euxente-(Y) in the intermediate zone at locality KIN-130. The lighter columbite present is secondary columbite II grains. ....	103
Figure 3.57 Rutile following trend towards columbite. ....	104
Figure 3.58 Ilmenite, pyrophanite and geikielite classification diagram.....	105
Figure 3.59 REE distribution of AGM and EMG. The two visible trends (those that favor LREEs and those that favor HREEs) differentiate AGM and EGM. Each color/shape combination represents a different sample point. ....	106
Figure 3.60 Aeschynite-(Ce) and euxenite-(Y) (with fergusonite) are found in their respective sections based on REE preference. ....	106
Figure 3.61 Classification and differentiation of aeschynite-(Ce), euxenite-(Y), fersmite, and fergusonite-(Y).....	107
Figure 3.62 Classification and overlap of REE-bearing oxide minerals present .....	108
Figure 3.63 Ilmenite with nioboaeschynite-(Ce) exsolution with titanite in the wall zone at locality KIN-133. ....	108
Figure 3.64 Euxenite with columbite in the intermediate zone at locality KIN-130.....	109
Figure 4.1 Locations of all samples used in geochemical studies. ....	117
Figure 4.2 Zr/Hf and Nb/Ta ratios. The top graph shows the entire sample set, while the axis is cut in the bottom graph to better show variation among the other samples. Syenite sample names have been shortened to contain the first three letters and final two digits to decrease sample name length.....	118
Figure 4. 3 U/U+Th and Y/Y+REE ratios present in the samples.....	119
Figure 4.4 Top: Chondrite-normalized REE values of KIN property samples (using McDonough & Sun (1995)). ....	120

Figure 4.5 LREE and HREE+Y concentrations found in the samples. ....	121
Figure 4. 6 Sr, Nb, and Zr concentrations.....	121
Figure 4.7 Granite and bulk pegmatite classification based on the alumina index molar diagram with I-type and S-type boundary added from Chappel and White in blue (2004). Granite samples are marked in black whereas the pegmatite sample is red. A/CNK is $Al_2O_3/(CaO + Na_2O + K_2O)$ and A/NK is $Al_2O_3/(Na_2O + K_2O)$ .....	122
Figure 4.8 Granite and bulk pegmatite classification (based on Whalen et al., 1989). ....	123
Figure 4. 9 Top: U-Pb zircon age analyses from granite sample. Bottom: U-Pb zircon age analyses from pegmatite sample. ....	124

## **Acknowledgements**

I would first like to thank my supervisors Lee Groat and Jan Cempírek for their tremendous support and guidance during this process. I would also like to thank Leo Millonig for his initial work on the project and help getting started, along with all his edits.

Mati Raudsepp, Edith Czech, Elisabetta Pani, Jenny Lai, and Lan Kato were instrumental to this thesis for their assistance at UBC with data collection and sample preparation along with Radek Škoda and Petr Gadas at Masaryk University in Brno, Czech Republic for their assistance collecting EMP data.

Additionally, thanks to Jim Mortensen and Craig Hart for their help, advice and edits, and additional thanks to Jim and Rich Friedman for collecting radiometric data used in this thesis.

I would also like to acknowledge Mackenzie Parker for all her help editing and the writing advice she provided.

Thank you to everyone else who took a look, helped me remember that one word, told me that a sentence didn't work that way, and generally provided help with writing. And finally, thanks to my family, friends, lab mates, and everyone special to me for all their support.

## **1. Introduction**

The information presented here represents the results of mineralogical, geochemical, and geochronological research done on igneous rocks found on the KIN property, located approximately 95 km northwest of Revelstoke, British Columbia. These rocks were studied in order to, 1) characterize the mineralogy and classify the main pegmatites; 2) attempt to identify the parental source magma for these pegmatites, and 3) describe effects and conditions of metamorphism that the host rocks in the study have experienced.

Although this project is primarily focused on the KIN property pegmatites and the study of pegmatites as a whole, rare earth element (REE) mineralization is commonly found in these types of pegmatites and associated rocks and a deeper understanding of their formation could lead to more REE-enriched pegmatite discoveries. This would add to the base knowledge of REEs and the minerals in which they occur in Canada.

### **1.1 Pegmatites**

#### **1.1.1 Pegmatite Definition**

Pegmatites are igneous intrusions that commonly form elongate, dyke like bodies that can attain tens of meters in size, and are defined as “very coarse- to gigantic-sized textures in intrusive igneous rocks” (Simmons et al., 2003). Although pegmatites are known for their large crystals, they also can contain interesting textures with large and small crystals intermixed and may contain rare element-bearing minerals not found in any other rock type.

Pegmatites are textural variants of many intrusive rocks (granites, syenites, carbonatites, gabbros, etc.), but most commonly granite, to the extent that the term “pegmatite”, without further clarification, is commonly used for granitic pegmatites specifically (London & Kontak,

2012). In addition, there is a significant degree of variation in granitic pegmatites and the minerals and elements found in them; to the extent that explicit classification schemes have been implemented to organize the variation.

The large crystal size and rare minerals found in pegmatites have attracted a wide variety of researchers to pegmatites over the years. Igneous petrologists are interested in their formation, economic geologists in their resources including gems and rare elements, and more common minerals like quartz and feldspar; and mineralogists for their usual mineral compositions (London & Kontak, 2012). Pegmatite research is a continuously expanding field with many facets.

### **1.1.2 Pegmatite Classification**

Although, there is some debate in the scientific community as to the best method to classify these rocks (e.g., Dill, 2015), granitic pegmatites are generally classified using Petr Černý's classification scheme (Černý, 1991). Černý groups pegmatites into five classes based broadly on emplacement depth; these are the abyssal, muscovite, muscovite-rare element, rare-element, and miarolitic classes. These classes are can be further subdivided into subclasses and families, such as the MI-REE and MI-Li subclasses of the miarolitic (MI) class (Černý & Ercit, 2005) (Table 1.1).

The rare element class is the most researched of the pegmatite groups and includes pegmatites formed by differentiation from granitic plutons that are emplaced at intermediate to shallow depths (Černý & Ercit, 2005). This class contains two subclasses: the REL-REE, [Nb>Ta geochemical signature] subtype, which commonly forms in extensional crustal settings, and the REL-Li (Li, Rb, Cs geochemical signature) subtype found in compressional orogenic

settings (Černý & Ercit, 2005). Finally, each of these subclasses is further broken down into types based on the specific mineralogy found in each (Table 1.2).

In addition to the classification into classes and subclasses, two main families within pegmatites, specifically rare element pegmatites, can be defined based on geochemical signatures. These are the NYF-type and LCT-type families, although they can also be found as NYF-LCT mixed type, which contain elements and minerals common to both families. NYF-type pegmatites are named for their elevated levels of niobium, yttrium, and fluorine, and are further characterized by elevated amounts of Y, REE, Ti, U, Th, Zr, Nb>Ta, and F, with a bulk composition that is typically sub- to metaluminous (Černý, 1991). LCT-type pegmatites are named for their elevated levels of lithium, cesium, and tantalum, and are further characterized by elevated levels of Li, Rb, Cs, Be, Sn, Ga, Ta>Nb, with a bulk composition that is typically peraluminous (Černý, 1991).

It is worth noting that although these classifications seem fairly straight forward, there can be significant overlap among classes as some minerals can be seen in multiple classes.

### **1.1.3 Parental Magmas**

Pegmatites form through the process of fractional crystallization from magmas, most commonly from granites (this process is described in more detail in section 1.1.5) (London, 2008). Although granites are the most frequent parental rock, other alkaline rocks including carbonatites and syenites can also form pegmatites, as can mafic rocks such as gabbro (London, 2008). Pegmatites typically form as marginal or exterior bodies to the parental pluton (Simmons et al., 2003) and the composition of this parent can play a significant role in determining the characteristics of the pegmatite and its mineralogy.

Parental rocks are usually determined based on mineralogy, geochemical signatures, and geochronology (as they will have similar crystallization ages). If no apparent parent can be found, there is the possibility of a hidden parental body at depth. An additional theory of anatectic pegmatites exists, whereby there is no direct parental magma. Instead, the pegmatites form from partial melting of preexisting rocks. These pegmatites can be considered members of the abyssal class of pegmatites (Černý & Ercit, 2005; Novák et al., 2013).

#### **1.1.4 Pegmatite Internal Zoning**

Rare-element pegmatites form in one of three structural patterns: homogeneous, zoned, and layered (Černý, 1991). Homogeneous pegmatites are just that; they contain a uniform distribution of minerals and contain little variety whereas zoned pegmatites show much more variety. Layered pegmatites are similar to zoned, however they are the “extreme” cases of these rocks (Černý, 1991).

Zoned pegmatites are the most common and generally form as concentric shells (Fig. 1.1) and are named, from the margin inward: the border zone, wall zone, intermediate zone, and core zone (Černý, 1991). Although the compositions of these zones can vary, the most common minerals found in these zones and their textures can be seen in Table 1.3. The border zone is commonly thin and the most fine grained of the zones, the wall zone is coarser and can contain a wide variety of minerals. The intermediate zone is coarser yet and is dominated by a single mineral phase, such as plagioclase feldspar, and the core is commonly mostly composed of quartz (London, 2008). Trends found when moving towards the core include a coarsening of grains and a decrease in the number of rock forming units (Černý, 1991).

### 1.1.5 Pegmatite Formation

Due to the abnormally large crystals found within pegmatites, their unique mineralogy, and the rare textures found within them [such as the graphic intergrowth of quartz and feldspar (graphic granite)] and apparent complicated variation of grain size, scientists have long sought the process by which they form. Current theory states that pegmatites form due to fractional crystallization within magmas and concentration of fluids and rare elements in residual melt (Simmons et al., 2003; London, 2008). It is due to this fractionation that elements and minerals uncommon in these parental rocks are found within pegmatites. Major rock-forming elements are used up in the formation of these more common parental rocks leaving the incompatible elements (F, Cl, Li, Na, K, Rb, Cs, Be, H<sub>2</sub>O, PO<sub>4</sub><sup>3-</sup>, etc.) in the melt in higher abundances. This leads to the crystallization of rare minerals that contain these elements within the pegmatite (Thomas et al., 2012). Although this is the widely accepted theory, it is not the only one (see Simmons & Webber, 2008; and Thomas et al., 2012).

There is again a prevailing theory among pegmatite researchers regarding the large, yet variable, grain size found within pegmatites, as well as their pegmatitic textures. Original schools of thought held that crystals of such large size could only be found within rocks that had cooled over extended periods of time under stable conditions (London, 2008). However, this theory could not explain the variety of textures observed within pegmatites, such as graphic granite. It is now believed that these grain sizes are due to the crystallizing magma being undercooled (London, 2008). Undercooling is the process by which a liquid is cooled below its freezing point, but does not freeze. The cooler and shallower environments that pegmatite magmas enter as they move further from the parental magma prevents the viscous, highly evolved magma from flowing, and, in this solid-like state, the temperature can drop below the magma's freezing point

(London, 2008). At this point, the undercooled, incompatible element-rich magma starts crystallizing, cooling inward from the margin to the core. During this process, a boundary layer of fluxed melt enriched in elements incompatible in the first crystallizing minerals (feldspars and quartz) forms at the crystallization front. During the course of the crystallization, the boundary layer dissolves the viscous undercooled magma and allows fast diffusion of compatible elements to the crystallization front while it further concentrates fluid and incompatible elements (“constitutional zone refining,” London, 2008, 2014). The nucleation rate of new crystals gradually decreases during increase of fluids in the boundary layer, which promotes growth of large crystals. Once the bulk of the undercooled melt is consumed by the boundary layer and it becomes eventually undersaturated in elements compatible with so-far crystallizing minerals (feldspars, quartz, but also accessory minerals specific for each pegmatite, e.g. biotite, Fe-tourmaline, garnet, etc.), crystallization of the boundary layer produces core zones, which typically are the albite-lepidolite zone and the quartz core (London, 2008, 2014).

#### **1.1.6 Importance of Rare Earth Elements**

Rare earth elements are divided into two main groups: the light rare earths (LREEs) and the heavy rare earths (HREEs). Elements La to Gd plus Sc are considered LREEs whereas Tb to Lu plus Y are HREEs. Both groups contain elements that are crucial components in modern technologies such as plasma screens, smart phones, and hybrid cars. However, as of 2012, over 97% of the mining and refinement of REEs occurs in China (Mancheri, 2012). As a result, China has a near monopoly on the REE market, making much of the world dependent upon it for their REE supplies.

China is currently far ahead of the rest of the world in terms of understanding REEs and development due to large amounts of REEs available there and the research and technologies developed using these elements (Kremmidas, 2012). Information to be gained within Canada regarding REE mineralization is therefore invaluable. Rare earth elements are not rare within Canada, with a number of mining companies hoping to enter the market, and a goal to be producing 20% of the global share of REEs by 2018 (Els, 2014).

## **1.2 KIN Property**

### **1.2.1 Regional Geology**

Alkaline intrusive rocks (primarily carbonatites, nepheline and sodalite syenites) are present in several parts of the Canadian Cordillera and were described and documented by Pell (1994). The Cordillera formed by the accretion of terranes along the western edge of ancestral North America (Hinchey et al., 2006), forming thin, north to south trending bands of terranes in what is now eastern British Columbia (Fig. 1.2). The alkaline rocks were emplaced prior to the Jura-Cretaceous Columbian orogeny (Pell, 1994). The parental magmas of alkaline igneous rocks commonly form deep in the mantle and intrude tectonically stable regions that have shown little tectonic history in recent times (Heinrich, 1966; Dawson, 1980). However, British Columbia is not a stable region and is different from those generally studied, and as such, provides a new opportunity to study alkaline rocks in a compressional and active geologic setting (Pell, 1994).

This suite of alkaline rocks is found in broad zones on either side of the Rocky Mountain Trench within three discrete areas: 1) the Foreland Belt, 2) the eastern edge of the Omineca Belt, and 3) the region of the Omenica Belt near the Frenchman Cap Dome and Trident Moutain, a

known syenite locality (Fig. 1.3, from Pell, 1994). The KIN property is located within the Omineca Belt and is hosted by metamorphosed Precambrian rocks, specifically by the Neoproterozoic Horsethief Creek Group (Perkins, 1983) within the Mica Creek area (Ghent & Villeneuve, 2006) in the Selkirk-Monashee-Cariboo complex (Crowley et al., 2000) (Figure 1.4).

The Canadian Cordillera has experienced three episodes of alkaline and carbonatite magmatism: ~800-700 Ma, ~500 Ma, and most recently ~360-340 Ma. Prior to this most recent period of magmatism, an intra-plate continental margin within the Cordillera became a convergent inter-plate boundary at ~390 Ma (Monger & Price, 2002) and led to an extensional tectonic environment, likely caused by slab rollback which led to this latest period of magmatism (Millonig et al., 2012). In more recent times, various episodes of metamorphism have occurred in the Cordilleran rocks from ~155 to 50 Ma (Millonig et al., 2012). Zircons from the local Trident Mountain were dated to 359.2 Ma and 57.2 Ma, which were interpreted to provide an intrusion age of ~360 Ma and a metamorphic age of ~57 Ma (Millonig et al., 2012).

The Mica Creek area has undergone five known periods of tectonism ranging from 175-160, 142-120, 110, 100-90, and 75-50 Ma (Crowley et al., 2000). The most recent of these includes the intrusion of leucogranites and late-stage pegmatites [72-58 Ma (Sevigny et al., 1989)] with kyanite- and sillimanite-grade metamorphism and the introduction of fluids and coincides with the thrusting of the Selkirk-Monashee-Cariboo complex over the Monashee complex (Crowley et al., 2000). This area was divided into three domains with the KIN property located in the second, which experienced kyanite growth during peak metamorphism sometime after 73 Ma (Crowley et al., 2000).

The alkaline intrusive group found on the eastern edge of the Omineca Belt typically occurs as foliated, sill-like bodies that intrude Late Precambrian to Early Cambrian

metasedimentary rocks which were deformed and metamorphosed during the Columbian orogeny (Pell, 1994). This area of British Columbia is composed primarily of Late Proterozoic and Paleozoic rocks from Paleozoic-Mesozoic terranes that were thrust onto the North American rocks (Carr, 1991); (Fig. 1.2).

The alkaline, igneous rocks found on the KIN property intrude into schist belonging to the Neoproterozoic Horsethief Creek Group (Brown, 2012), which underlies much of the northernmost Purcell Mountains and adjacent Selkirk Mountains. This Group is regionally divided informally into grit, slate, carbonate, and upper clastic divisions (Poulton & Simony, 1980), and is present amphibolite grade meta-sedimentary rocks at the KIN property (Millonig, 2011).

### **1.2.2 Previous work on the KIN property**

Little work has been done on the KIN property; however, information regarding the nepheline syenites present on the neighboring Trident Mountain dates back to 1965, when they were first discovered by J. O. Wheeler during his geological mapping of the region (Wheeler, 1965).

The Trident Mountain area was first studied with an economic focus in 1987 during a survey conducted by the BC Ministry of Energy, Mines and Petroleum Resources, to record and collect information on syenite occurrences (White, 1989). Additional data was collected and samples assayed in 2006 and 2007. Structural studies were done in 2006, together with soil sampling in 2007 focusing on HREEs (Brown, 2012).

Reconnaissance exploration took place in 2010 when TerraLogic Exploration Services undertook silt and rock sampling on the Trident property in order to determine the source of the

high REE values discovered in soil samples. In addition, silt sampling on was carried out on the KIN property (Brown, 2012). This was the first instance of work occurring directly on the KIN property. In 2011, additional field work was done on the KIN property when rock samples were collected and analyzed; the initial findings of these analyses were the basis of a short company report (Millonig, 2011).

### **1.2.3 KIN Property Locality and Pegmatites**

The KIN property is located on Kinbasket Lake within the Canadian Cordillera, approximately 95 km northwest of Revelstoke, British Columbia and 13 km southeast of the separate property found on Trident Mountain (Fig. 1.2). The KIN property contains metamorphosed REE- and Nb-bearing minerals are found within apparent NYF-type pegmatites in the vicinity of granitic and syenitic bodies which intrude the same host rock (these pegmatites will be referred to as allanite pegmatites throughout this work, due to their high allanite content). The Trident Mountain property contains known rare earth element-(REE-) bearing syenites (Brown, 2012) and the KIN property contains potentially related syenites. These were not seen during field exploration, but were described in Millonig (2011) along with granites, and granitic pegmatites. GPS coordinates for the pegmatites, float samples, and granites are given in Table 1.4. Although the pegmatites and float coordinates are for these small sites, the granite coordinates are wider ranging and are more meant to show the trace of the granite, as the outcrop commonly extends between localities. The pegmatites and float samples can be seen in Figure 1.5 where the red lines designate original syenite traces added by the company (Brown, 2012).

Although pegmatites throughout much of Canada have been studied in more detail, those within British Columbia have not been, and building the knowledge base of these bodies is

critical to understanding their formation. The pegmatite bodies on the KIN property were discovered relatively recently, and therefore, very little research has been done on them. In addition, many of the Cordilleran pegmatite occurrences are LCT-type pegmatites (e.g., Mt. Begbie pegmatites, Dixon, 2013; Hellroaring Creek and Lighting Creek pegmatites, Brown, 2003; and Little Nahanni pegmatites, Barnes, 2010). This makes the KIN property pegmatites, which display apparent NYF-type signatures, somewhat anomalous. Research regarding these seemingly unusual REE- and Nb-bearing pegmatites, their minerals, and their formation is therefore invaluable for understanding pegmatite formation and parental magmas, especially as NYF-type pegmatites as a whole are poorly studied compared to LCT pegmatites (Ercit, 2004).

Four deformed allanite pegmatite bodies containing REE and Nb mineralization have been located at the KIN property and studied in detail: KIN-130, KIN-133, KIN-134, and KIN-135 (Fig. 1.5); the locality numbers follow that of Millonig (2011) who visited the locality during the 2011 exploration campaign and collected the first samples. The pegmatites form lenses parallel to foliation of their host rock at the KIN property, which, in this area, is a dark amphibolite grade meta-sedimentary schist and gneiss. Syenite and carbonatite samples collected by Brown (2012) indicate the presence of alkaline rocks southeast from the study area in addition to the non-metamorphosed granites exposed on the property. The host rock is mostly fine-grained gneiss with a well-developed schistose texture, containing garnets up to 1 cm in diameter and kyanite crystals up to 6 cm in length in a few localities.

The pegmatite outcrop at KIN-130 is distinctive as an easily visible elongate dyke (Fig. 1.6 a and b) with exposed, coarse mineralization (Fig. 1.7). The pegmatite forms a lensoidal body and is the least weathered of the localities, appearing mostly intact. The outcrop is approximately 2m wide and 12m long, and off-white to rusty brown-red in color. Coarse grained minerals such

as allanite, columbite and molybdenite up to 3 cm in size are present within feldspar. The pegmatite is zoned with wall and intermediate zones and a quartz core.

Locality KIN-133 was inaccessible during the 2014 field season; however, it has been previously described as being highly weathered and covered by large amounts of rock debris. Mineral aggregates of allanite, monazite, aeschynite, and columbite with feldspar, quartz, biotite, amphibole and garnet are found at this locality (Fig. 1.8; Millonig, 2011). Additionally, although the crystals found at localities KIN-130 and KIN-135 can be relatively large, grains of any mineral in this occurrence are rarely >1.0 cm in size (Millonig, 2011).

The main pegmatite body found at locality KIN-134 is the most distinctive, especially the border zone, which is recognized by its coarse-grained texture and dark, heterogeneous mineralization with allanite and monazite grains up to 2 cm in size (Fig. 1.9). Columbite, aeschynite, and biotite are all present within a quartz and feldspar matrix. The pegmatite at this locality is approximately 1m wide and moderately mechanically weathered with Fe-staining and contains core zone, intermediate zone, and border zone.

Locality KIN-135 is located up the slope from locality KIN-134 and is possibly an extension of the same dyke as found at KIN-134. The most recognizable zone present is the border zone which contains allanite forming large euhedral crystals up to 6 cm in length within quartz and feldspar. This zone is highly heterogeneous and dark in appearance (Fig. 1.10). In addition to the complex and dark mineralogy, light intermediate textural zones composed primarily of feldspar with some quartz and small amounts of accessory minerals are also present. The pegmatite dyke at this locality ranges between 50 cm and 1m in width and is approximately 8m in length (Fig. 1.10). This locality is moderately weathered and contains core, intermediate, and border zones.

Pegmatitic float samples were discovered and sampled during 2014 field work on the KIN property. Sample Rad 1 was a smaller apparent allanite pegmatite float sample that only contained wall zone textures similar to those found at locality KIN-135. The sample is dark, coarse grained and contains high amounts of REE-bearing minerals such as columbite, allanite, monazite, and aeschynite. Sample Rad 2 is a second allanite pegmatite float sample which is dark colored and has a similar appearance to samples found at locality KIN-130 and KIN-135. It contains molybdenite, allanite, and monazite within quartz and feldspar (Fig. 1.11) with wall, intermediate, and core zone textures present. Float sample PGM is a medium grained granitic pegmatite sample that is extremely light in color and contains tourmaline grains up to 2 cm in size (Fig. 1.12). Although Rad 1 and 2 appear similar to the *in situ* pegmatites, PGM is lighter in color with tourmaline and lacks the REE- and Nb-bearing minerals seen in the other pegmatite samples.

The “syenites” at KIN occur as light-colored sills within the host rock that have been folded back on themselves and intrude the host rock along strike (Brown, 2012), however, it is worth noting that within the report, it is denoted that the term “syenite” is used primarily as a field term to describe granitoids found within the rock; however, some are indeed true syenites (Brown, 2012), unfortunately, it is difficult to determine which are true syenites and which are granites based on the brief descriptions provided in the report.

The granites found on the KIN property were likely discovered during previous exploration; however, they were recorded as syenites and mapped as such and not described in detail (Brown, 2012). The granites and their more specific outcrop boundaries and descriptions were recorded during 2014 field work; they form sills approximately 5-30m thick and several hundred meters long and possibly were outlined in previous reports (Brown, 2012), but referred

to as syenite and poorly described. They can be seen in Figure 1.13; the red in the map represents the original placement of the syenite trace by the company. The granite is extremely coarse grained and blocky with muscovite books up to 5 cm in diameter and feldspar up to 10 cm in maximum dimension. In contrast to the pegmatites, the granites form continuous sills without apparent deformation, parallel to the host rock formation. These bodies are commonly broken into large blocks with large grains of quartz, feldspar, and mica (Fig. 1.14a), which locally appear to have fallen from higher elevations; however, the mapped granite localities are clearly *in situ* and are conformable with the host rock (Fig. 1.14b). The granite outcrops are quite widespread on the property and appear very similar in composition, although samples were only taken for detailed study from three of these localities (G17, G18, and G19).

Across the property, there is evidence for some structural control of the mineralization and syenite phases which can be seen from field observations (Millonig, 2011). Additional structural studies have found that fractures, faults, and fracture zones located near the property may be the source of these controlling features (Brown, 2012). The area studied for this project is only a portion of what is known as the Amy Carmen zone within the KIN property and was identified as an area of interest in the company reports (Brown, 2012).

### **1.3 Materials & Methods**

The materials for this project included samples from pegmatite outcrops at four localities (KIN-130, KIN-133, KIN-134, and KIN-135), four pegmatite float samples (Rad 1, Rad 2, PGM, and KIN-136), samples from three granite localities (G17, G18, and G19) and one syenite

sample (JBTDR018), all from the KIN-property. Additional geochemical data was obtained from a previous company report (Brown, 2012).

Initial samples for this project were collected by Leo Millonig and other members of the initial exploration team during the 2011 field season. *In situ* samples from four localities (JBTDR018, KIN-130, KIN-133, and KIN-134) were collected at that time, together with samples from two float localities (KIN-136 and JBTDR018). Eight thin sections were made from these samples. An initial report was written which reported hand sample identification and descriptions with additional scanning electron microscope (SEM) data (Millonig, 2011).

Additional field work was conducted by the author, together with Dr. Lee Groat, and Jan Cempírek, in August, 2014. Pegmatite localities KIN-130, KIN-134, and KIN-135 were revisited and additional samples were collected from these previously known localities. New granitic bodies were discovered and samples were collected from three localities (G17, G18, and G19), and four additional pegmatite float samples were discovered and sampled (Rad 1, Rad 2, and PGM). Field relationships and GPS coordinates were recorded and photographs were taken for all samples and localities.

Twenty additional thin sections were prepared from these new samples. These sections were made in order to have a complete suite of representative sections from all localities and zones. Additionally, those with particularly interesting mineralogy were sampled in more detail to create a larger sample size of these minerals and textures.

All 28 thin sections were first studied with a polarizing optical microscope, and basic mineralogy and textural relationships were identified. These samples were then studied with the SEM to identify unfamiliar minerals and to study crystals and relationships too small to see under the polarizing microscope.

Scanning electron microprobe data were collected at the Department of Earth, Ocean and Atmospheric Sciences at the University of British Columbia with a Philips XL30 electron microscope (Bruker Quantax 200 energy-dispersion X-ray microanalysis system, XFlash 6010 SDD detector, Robinson cathodoluminescence detector) using a 15 kV beam. Back-scattered electron imaging was used for visual identification.

Thirteen samples were selected for electron microprobe (EMP) analysis. Samples were selected to obtain data from a variety of zones and localities, in addition to samples with particularly interesting (i.e., REE-rich) mineralogy. A limited amount of data was collected on the EMP due to limits in time and resources available. Electron microprobe data were collected at Masaryk University in Brno, Czech Republic using a CAMECA SX100 instrument. Standards used are reported in the relevant appendices.

Four samples (three granite samples and one pegmatite sample) were submitted for whole rock geochemical analyses. An additional sample was included as a standard. These samples were chosen based on the amount of material available. Because these are very coarse grained rocks, large samples were needed to provide accurate composite data; hence only samples with an adequate amount of material were sent. Additionally, funding limited the number of samples that could be analyzed.

Whole rock geochemical analyses were performed at Acme Laboratories, in Vancouver, British Columbia. Samples were crushed and major elements were determined using XRF – fusion and reported in wt %. Most minor element amounts (all but Li and F) were determined using lithium fusion and reported in ppm. Lithium was determined using peroxide fusion – ICP-OES techniques and F was determined using a NaOH fusion digestion/potentiometric method. Both Li and F contents are also reported in ppm.

Zircons were separated from one sample each of the granite and pegmatite on the KIN property and were dated using U-Pb methods at the Pacific Centre for Isotope and Geochemical Research at the University of British Columbia. A total of 20 analyses of zircons were done from each sample, using standard laser ablation ICP-MS methods described by Tafti et al (2009). A New Wave UP-213 laser ablation system and a ThermoFinnigan Element 2 single collector, double-focusing, magnetic sector ICP-MS setup were used to collect the data. The Plešovice zircon standard (Sláma et al., 2007) was used as the primary reference for the analyses, and the Temora 2 zircon standard was used as an internal monitor. The separated zircons along with the standard and reference zircons were washed and polished and the portions determined to be free of alteration, inclusions, or inherited cores were chosen for analysis. Full descriptions of the methods and results can be found in appendices C and D.

**Table 1.1** Principal subdivision and characteristics of the five classes of granitic pegmatites [Table 2 from Černý & Ercit, (2005)].

Class Subclass	Typical minor elements	Metamorphic environment	Relation to granites
<b>Abyssal (AB)</b>			
<i>AB-HREE</i>	HREE, Y, Nb, Zr,U,Ti	(upper amphibolite to)	none (?)
<i>AB-LREE</i>	LREE, U, Th, Ti	low- to high-P granulite facies; ~4 to 9 kbar, ~700 to 800°C	(segregations of anatectic leucosome ?)
<i>AB-U</i>	U, Th, Zr, LREE		
<i>AB-BBe</i>	B, Be		
<b>Muscovite (MS)</b>			
	no rare-element mineralization (micas and ceramic minerals)	high-P, Barrovian amphibolite facies (kyanite–sillimanite) 5 to 8 kbar, ~650 to 580°C	none (anatectic bodies) to marginal and exterior
<b>Muscovite – Rare-element (MSREL)</b>			
<i>MSREL-REE</i>	Be, Y, REE, Ti, U, Th, Nb-Ta	moderate to high P, (T) amphibolite facies; 3 to 7 kbar, ~650 to 520°C	interior to exterior; locally poorly defined
<i>MSREL-Li</i>	Li, Be, Nb		
<b>Rare-element (REL)</b>			
<i>REL-REE</i>	Be, Y, REE, U, Th, Nb>Ta, F	variable, largely shallow and postdating regional events affecting the host rocks	interior to marginal (rarely exterior)
<i>REL-Li</i>	Li, Rb, Cs, Be, Ga, Sn, Hf, Nb-Ta, B, P, F	low-P, Abukuma amphibolite (andalusite–sillimanite) to upper greenschist facies; ~2 to 4 kbar, ~650 to 450°C	(interior to marginal to) exterior
<b>Miarolitic (MI)</b>			
<i>MI-REE</i>	Y, REE, Ti, U, Th, Zr, Nb, F	very low P, postdating regional events that affect the host rocks	interior to marginal
<i>MI-Li</i>	Li, Be, B, F, Ta>Nb	low-P amphibolite to greenschist facies, 3 to 1.5 kbar, 500 to 400°C	(interior to) marginal to exterior

**Table 1.2** Subdivision of granitic pegmatites of the rare-element class [Table 5 from Černý & Ercit (2005)].

<i>Subclass</i> Type	Subtype	Geochemical signature	Typical minerals
<i>REL-REE</i>	allanite- monazite	LREE, U, Th, (Be, Nb>Ta, F, [P])	allanite, monazite, zircon, rutile, fluorite, ilmenite
	euxenite	L-H-REE, Y, Ti, Zr, Nb>Ta, (F, P)	euxenite, monazite, xenotime, zircon, rutile, ilmenite, (fergusonite, aeschnite, zinnwaldite)
	gadolinite	Be, Y, HREE, Zr, Ti, Nb>Ta, F, (P)	gadolinite, fergusonite, samarskite, zircon, rutile, ilmenite, fluorite, (zinnwaldite)
<i>REL-Li</i>	beryl- columbite	Be, Nb-Ta, (±Sn, B)	beryl, columbite, tantalite, (rutile)
	beryl- columbite phosphate	Be, Nb-Ta, P, (Li, F; ±Sn, B)	beryl, columbite, tantalite, triphylite, triphylite
complex	spodu- mene	Li, Rb, Cs, Be, Ta-Nb, (Sn, P, F; ±B)	spodumene, beryl, colum- bite, tantalite, (amblygonite, lepidolite, pollucite)
	petalite	as above	petalite, beryl, columbite- tantalite, (amblygonite, lepidolite, pollucite)
	lepidolite	Li, F, Rb, Cs, Be, Ta-Nb, (Sn, P, B)	lepidolite, beryl, topaz, microcline, columbite- tantalite, (pollucite)

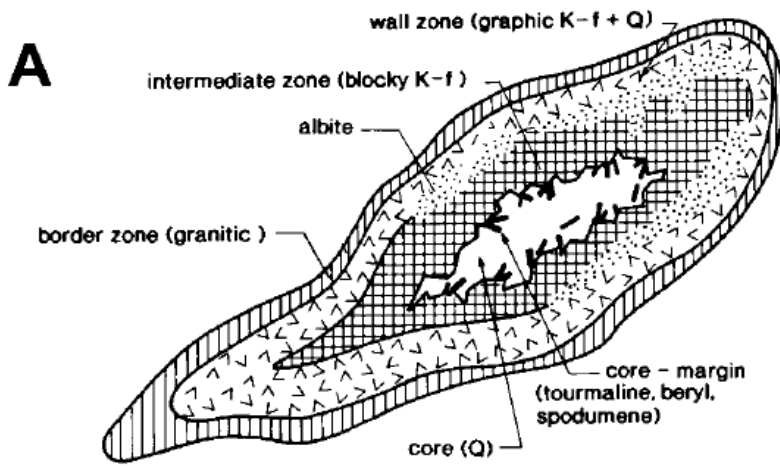
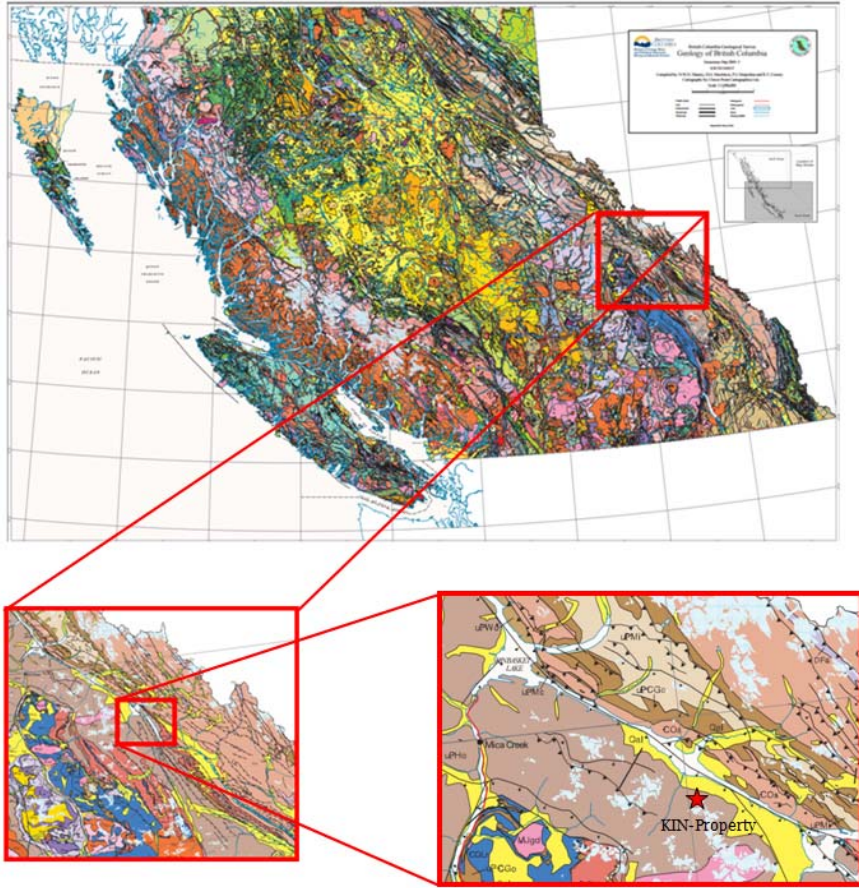


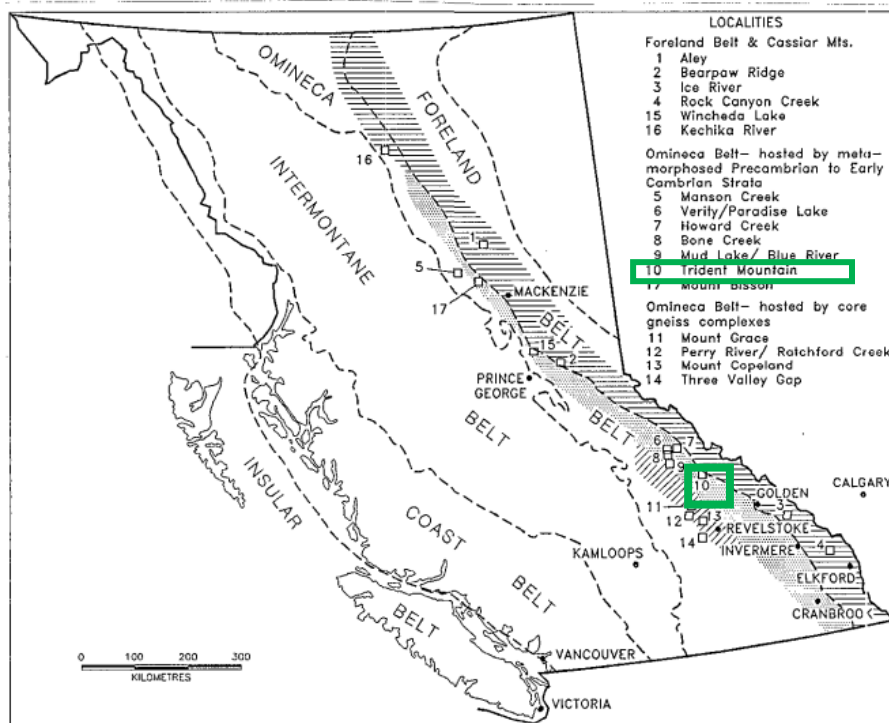
Figure 1.1 Example of typical internal structure of rare element pegmatites (Černý, 1991).

Table 1.3 Mineral composition of typical pegmatite zones (Simmons, et al., 2003).

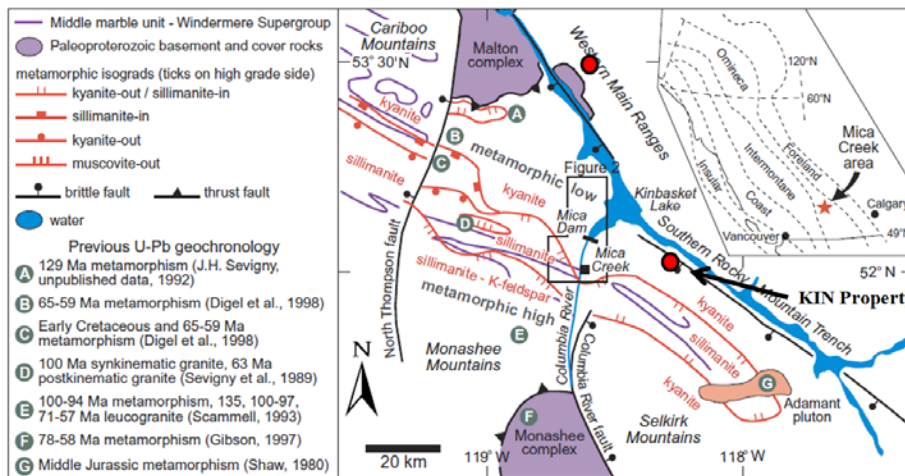
Zone	Texture	Principal Minerals	Accessory Minerals
Border zone	Fine grained	Plagioclase or microcline, quartz, ± muscovite	Schorl, garnet, magnetite, microcline or plagioclase
Wall zone	Coarser	Quartz, plagioclase, microcline, ± muscovite, ± biotite	Schorl, garnet, beryl, apatite
Outer Intermediate zone	Progressively coarser to giant size xls.; pocket development	Microcline, quartz	Schorl-elbaite, sodic plagioclase, muscovite, phosphates
Inner Intermediate zone (Core-margin)	Both coarse and fine, some giant xls; pocket development	Quartz, microcline, sodic plagioclase, ± muscovite, ± biotite	Schorl-elbaite, beryl, phosphate minerals, Nb-Ta minerals
Core		Quartz	Beryl, spodumene



**Figure 1.2** Geologic map of British Columbia and KIN property location [figure from Massey, et al. (2005)].



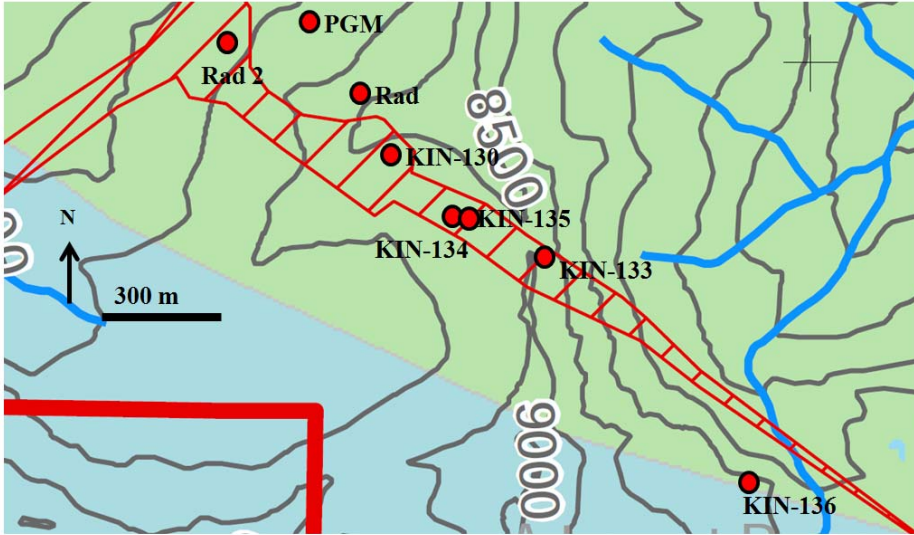
**Figure 1.3** Alkaline igneous rock occurrences within British Columbia. The KIN pegmatite occurrence is found close to the Trident Mountain locality shown on the map [from Pell (1994)].



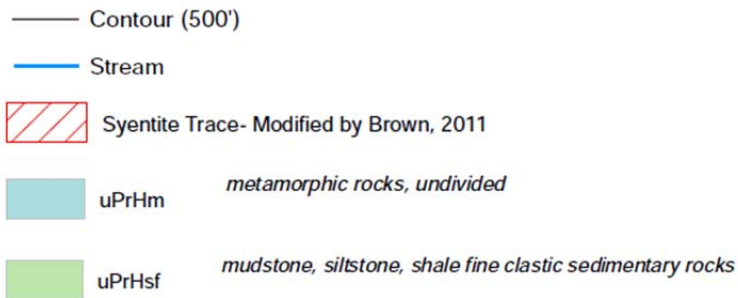
**Figure 1.4** Location of the KIN property within the Selkirk-Cariboo-Monashee complex near the Mica Creek area [map from Crowley et al. (2000)].

**Table 1.4** KIN Property Locality Coordinates

Sample Number	Latitude	Longitude
<b>Pegmatites</b>		
130	51°50'51.30"N	117°58'15.07"W
133	51°50'39.89"N	117°57'46.99"W
134	51°50'41.89"N	117°57'59.84"W
135	51°50'42.33"N	117°57'58.50"W
<b>Granites</b>		
G1	51°51'12.69"N	117°58'52.07"W
G2	51°51'13.15"N	117°58'54.59"W
G3	51°51'8.18"N	117°58'57.10"W
G4	51°51'3.64"N	117°59'1.54"W
G5	51°50'52.35"N	117°58'45.72"W
G6	51°50'51.47"N	117°58'46.28"W
G7	51°50'52.18"N	117°58'38.98"W
G8	51°50'52.31"N	117°58'37.88"W
G9	51°50'51.04"N	117°58'38.80"W
G10	51°50'50.82"N	117°58'38.53"W
G11	51°50'49.07"N	117°58'31.02"W
G12	51°50'49.13"N	117°58'27.67"W
G13	51°50'49.13"N	117°58'27.67"W
G14	51°50'48.03"N	117°58'26.92"W
G15	51°50'47.24"N	117°58'25.02"W
G16	51°50'47.35"N	117°58'24.03"W
G17	51°50'59.45"N	117°58'46.38"W
G18	51°51'2.70"N	117°59'1.73"W
G17	51°51'7.85"N	117°58'55.97"W
<b>Float</b>		
Rad	51°51'3.14"N	117°58'40.20"W
Rad2	51°51'8.28"N	117°58'56.47"W
PGM	51°51'11.74"N	117°58'39.87"W



**Figure 1.5** Map of KIN property with pegmatite and float localities marked. [underlying map with syentite trace from Brown (2011); geology based on Massey et al., (2005)].



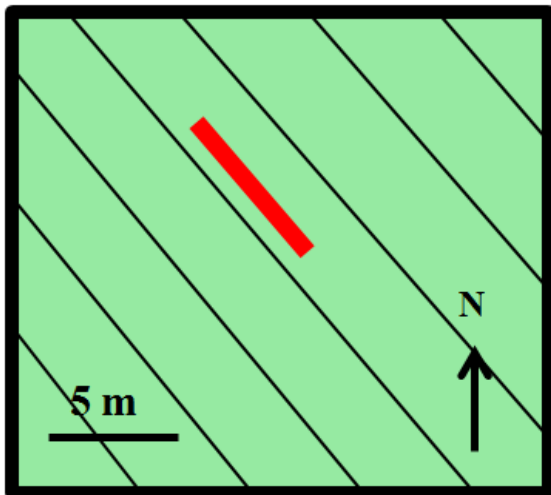


**Figure 1.6** Top: Pegmatite at locality KIN-130 seen intruding within strike of host rocks  
Bottom: Rough map sketch of size and orientation of pegmatite outcrop and its concordance with the host rock at locality KIN-130. Black lines represent the schistosity of the host rock.



**Figure 1.7** Coarse grains of allanite and columbite within feldspar at locality KIN-130.



**Figure 1.8** Locality KIN-133 (Millonig, 2011).



**Figure 1.9** Coarse black allanite within feldspar at locality KIN-134.



**Figure 1.10** Top: Coarse allanite from the wall zone at locality KIN-135.  
Bottom: Locality KIN-135 with coarse grains of allanite (top of the pegmatite) found along strike within the host rock (strike of the pegmatite shown with the arrow).



**Figure 1.11** Coarse molybdenite grains (sample Rad 2).



**Figure 1.12** Float PGM sample with white matrix and tourmaline grain.

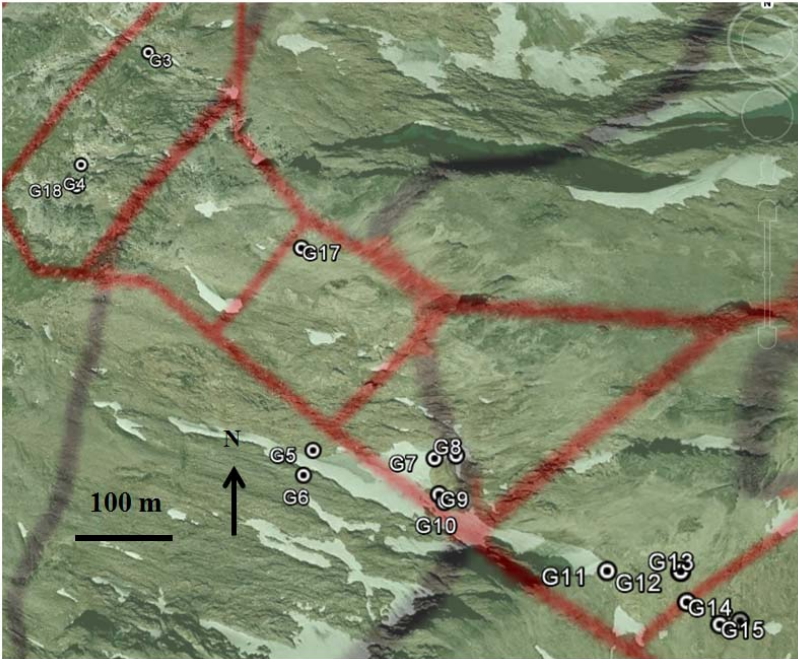


**Figure 1.13** Location of all granite points overlying the original syenite trace described in the company report [from Brown (2011)].



**Figure 1.14** Top: Coarse grained granitic rock (G18) composed primarily of quartz, feldspar, and muscovite. Bottom: Granite intrusions along strike within the host rock (right) at locality G3. The granite can be seen to extend several meters.

## **2. Petrography**

Four main rock types are present on the KIN property: pegmatites, granitic pegmatite, granite, and syenite. The non-classified pegmatites described first are the main focus of this research, although the granitic pegmatites, along with the granite and syenite samples, are included for completeness. This chapter contains tables of textures and minerals present with figures and additional text of textural description as needed. A full description and additional figures can be found in Appendix C.

The pegmatite localities found on the KIN property never contain material from each of the zones at surface, making some determinations, especially those based on spatial arrangements, difficult. Zones were determined primarily based on an increase of grain size and decreasing number of rock forming units from the margin inward (Černý, 1991) and an increase of quartz and Fe contents (specifically in biotite) towards the core (London, 2008). Also, zones locally vary significantly from one pegmatite body to another, so although these general characteristics may be similar, mineralogy and textures are commonly quite diverse.

### **2.1 Pegmatites**

#### **2.1.1 Border Zone**

Border zone textures were found in samples from localities KIN-133 and KIN-135. Table 2.1 lists elements present in each sample.

In hand sample, these samples are identified by their fine, “dark” mineralization and red garnet within cream-colored feldspar (Fig. 2.1). Minerals within this zone are not as large as those in other zones, with an approximate maximum of 2 mm in length for the phlogopite and

allanite grains. Thin sections KIN-133a, KIN-133c and KIN-134-4 represent this zone (the latter two sections were analyzed with EMP).

KIN-133: Allanite is generally found in two associations and never in isolation. These associations are: 1) allanite-(Ce), fluorapatite, and thorite with monazite in a corona texture (Fig. 2.2); and 2) allanite-(Ce) with aeschynite-(Ce), columbite, and thorite (Fig. 2.3). The first association is likely secondary allanite and apatite after monazite although the second association is less clear. This second association is commonly much larger than the corona shaped association type; however, both types feature anhedral minerals.

KIN-134: Garnet is generally found in “clusters” surrounded by clinozoisite within feldspar. Subhedral phlogopite grains are scattered throughout (Fig. 2.4).

### **2.1.2 Wall Zone**

Wall zone samples were collected from KIN-130, KIN-133 and KIN-135 localities and float sample RAD1. Table 2.2 contains the abundances of each mineral within the zone. Unlike other zones where there is variation in minerals and appearances across localities, the wall zone samples all look very similar (Fig. 2.5). They are recognizable in hand sample by their dark green and brown color with large subhedral to euhedral allanite grains. Thin sections KIN-133b, KIN-133d, KIN-133e, KIN-135a, KIN-135c, and Rad 1 are from this zone. Sections KIN-133d, KIN-135a, and KIN-135c were analyzed with the EMP.

Both primary and secondary allanite are present in this zone. The secondary grains are up to 3 mm size, anhedral, and are commonly associated with other REE-bearing phases such as secondary chevkinite and aeschynite with some remaining monazite-(Ce) and secondary apatite

with thorite. Primary allanite occurs as large (up to 1.5 cm) eu- to subhedral grains with darker REE-rich zones near the center of the grains and lighter REE-depleted rims.

The oxide minerals are commonly associated with each other and with the REE-bearing phases. Columbite and ilmenite occur as anhedral to subhedral primary grains whereas the other phases occur as secondary minerals.

In some parts of this zone, a poikiloblastic texture is visible within the phlogopite, almandine, and magnesiohornblende grains (Fig 2.6).

### **2.1.3 Intermediate Zone**

Unlike the wall zone, the intermediate zone samples vary significantly from locality to locality in terms of minerals present. Table 2.3 lists minerals and their abundances found within this zone at each locality. All (except KIN-136 and Rad 2a) contain large grains of REE- and/or Nb-bearing minerals within blocky cream colored feldspar. Intermediate zone samples were collected from the KIN-130, KIN-134, KIN-135, KIN-136, and Rad 2 localities with thin sections 130, 130a, 130b, and 130b-, 134-1, 134-2, 134-3, 135b, 136, and Rad 2a and Rad 2b representing this zone. Samples 130a, 130b, 134-2, 135b, 136, and Rad 2a were analyzed using EMP.

KIN-130: In hand sample, this zone can be identified by its near homogeneous light cream color except for large, dark, and commonly euhedral crystals of allanite (up to 5.0 cm) and columbite (up to 2 cm). These large crystals can be seen in thin section in Figures 2.7 and 2.8.

Sample 130b-1, however, appears different with higher garnet and biotite content and may represent a contact between zones. It contains significantly higher amounts of garnet (35%) and phlogopite (25%) with approximately 40% feldspar. It is classified as an intermediate-zone

sample due to its high feldspar content and the presence of Ba-rich feldspar, hyalophane, which is only seen in the intermediate zone.

KIN-134: In hand sample, this zone is characterized by the presence of large rusty red monazite/allanite grains (up to 1.0 cm) and biotite grains within cream colored feldspar (Fig. 2.9). REE- and Nb-bearing minerals are commonly associated and form mineral groups up to 2 cm in size. Primary and secondary relationships between these minerals are commonly unclear.

KIN-135: In hand sample, this zone is very similar to the intermediate zone seen at locality KIN-130, and it is predominately cream in color, with feldspar and quartz grains up to 1 cm in size, and smaller minor minerals. It is shown in hand sample in Figure 2.10.

KIN-136: The intermediate zone at locality KIN-136 is recognizable by its light color and high muscovite content. However, unlike the majority of the samples where the feldspar is cream in color, it appears grayer at this locality. It can

Rad 2: In hand sample, the intermediate zone at this locality appears similar to that found at locality KIN-130: large, dark grains within cream colored feldspar. However, these dark grains are more commonly dark gray, anhedral quartz and the accessory minerals, such as tourmaline are found as small, dark grains scattered throughout the rock. Figure 2.11 shows mica and tourmaline as seen in thin section.

#### **2.1.4 Core Zone**

Pegmatite core zones are consistently characterized by their high level of quartz content. Table 2.4 lists the approximate abundances of each mineral within each locality containing this zone. Although the accompanying accessory mineralogy may vary, all core zone sections are composed primarily of quartz. Quartz core samples were collected from the KIN-130, KIN-134,

KIN-135, and Rad 2 localities (thin sections 130b-2 and Rad 2c were the only thin sections created from these samples and section 130b-2 was the only one analyzed using EMP).

KIN-130: The core at this locality is distinguished by its translucent (blue) quartz color (boundary migration texture and undulose extinction found within the quartz seen in Fig. 2.12) with small green, anhedral amphibole grains which form a diamond shape that clearly demonstrates their  $124^{\circ}/56^{\circ}$  cleavage planes (Fig. 2.13) and can attain 1.0 cm in size.

KIN-134: No samples were taken from the quartz core of pegmatite 2; however, visual examination shows a high percentage of coarse-grained quartz occurring with red garnet, likely almandine (Fig. 2.14). In the figure below, the contact between the core and the intermediate zone is visible.

KIN-135: The core from sample KIN-135 is composed primarily of quartz (80%) with euhedral grains of allanite up to 1.5 cm long with muscovite up to 5 mm in length. No thin sections were prepared from this material.

Rad 2: In hand sample, this sample appears dark brown and gray with visible apatite and allanite grains up to 4 mm in size (Fig. 2.15) and contains brown, pyrite-filled veins.

## **2.2 Granitic Pegmatite**

Granitic pegmatite was only found in one float sample on the KIN-property: PGM (thin section PGM 1). This sample is finer-grained than the other pegmatite samples, with quartz and feldspar grains (which make up the majority of the sample) attaining approximately 1 mm in size.

This sample is composed primarily of albite and K-feldspar (80%) and quartz (10%). The remaining mineralogy is composed of monazite-(Ce), ferrocolumbite, euxenite-(Y), almandine, muscovite, schorl, pyrite, and zircon.

The garnet and tourmaline (up to 1 mm in size) are both primary. Accessory minerals usually occur as individual grains; however, they can also appear in small associations of accessory minerals (Fig. 2.16) within the feldspar and quartz.

### **2.3 Granite**

The granite on the KIN-property is extremely coarse-grained with muscovite grains up to 10 cm in size. Multiple thin sections were made (G17a, G17b, G18, and G19); however, the composition across the granites appears similar. G17a was analyzed by EMP.

The granite is primarily composed of quartz (25%), albite (35%), and muscovite (20%) with accessory almandine. Other accessory minerals include: fluorapatite, bismuthinite, chalcopyrite, monazite, xenotime, sericite, chlorite, bismuthinite, chalcopyrite, pyrite, iron oxide, and zircon. All rock forming mineral grains are anhedral.

### **2.4 Syenite**

Syenitic rocks were found on the KIN property during earlier company exploration, and one thin section of this material (JBTDR018) was provided to UBC for further study. The sample is primarily composed of allanite (50%; euhedral to subhedral grains up to 2 cm), feldspar (30%), biotite (20%; euhedral to subhedral grains up to 1 cm). Accessory minerals present are monazite, apatite, and muscovite. Iron staining is common throughout. The allanite forms large, elongate, and commonly twinned specimens (Fig. 2.17).

**Table 2.1** Border zone petrography.

Minerals													
	qz	fsp	phl	alm	czo	aln	clb	aesc	rt	ap	mnz	thr	zrn
KIN-133	5	40	15	10		x	x	x		x	x	x	x
KIN-134	5	15	7	35	25		x		x			x	x
Textures													
KIN-133	fine grained (grains rarely larger than 2mm) anhedral grains (subhedral phlogopite); poikiloblastic texture (almandine and phlogopite in feldspar); secondary almandine												
KIN-134	fine grained (almandine up to 2 mm and clinozoisite up to 5 mm); garnet "clusters" up to 10 mm												

(Numbers in boxes represent approximate percentage of rock composed of this minerals. Abbreviations are as follows: qz=quartz; fsp=feldspar; phl=phlogopite; czo=clinozoisite; aln=allanite; clb=columbite; aesc=aeschnite; rt=rutile; ap=apatite; mnz=monazite; thr=thorite; zrn=zircon.)



**Figure 2.1** Border zone in hand sample from locality KIN-133.

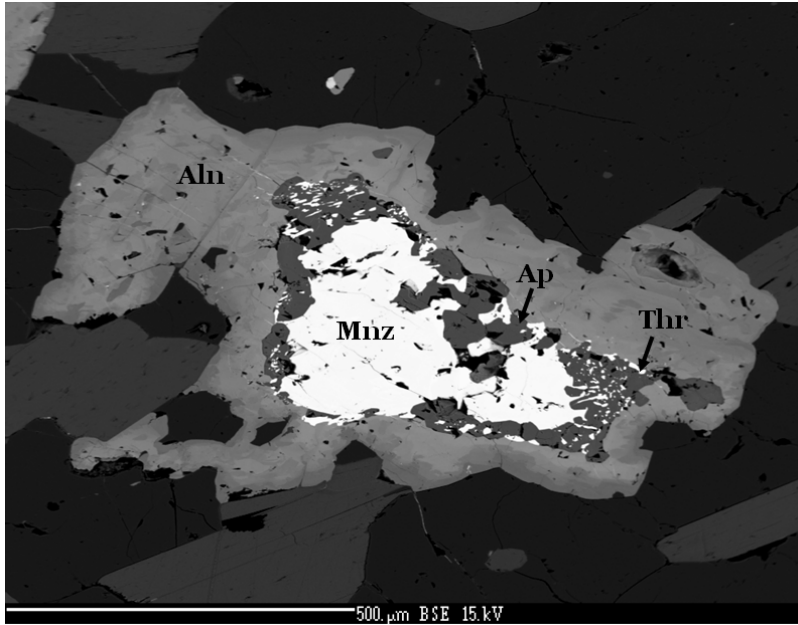


**Figure 2.2** Primary monazite breaks down to form secondary fluorapatite, thorite, and allanite-(Ce) in a corona in sample KIN-133c.

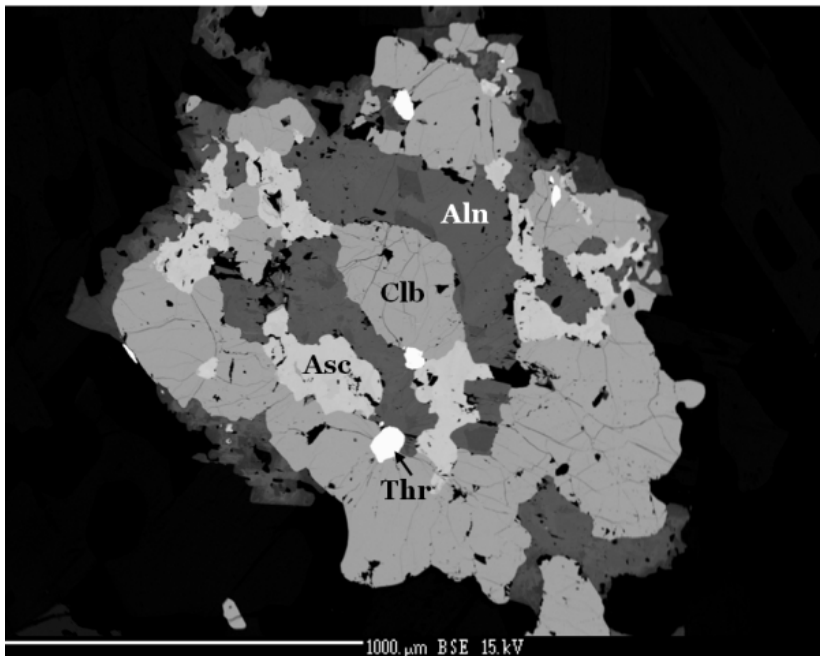


**Figure 2.3** Primary aeschynite-(Ce) and ferrocolumbite with secondary allanite-(Ce) with thorite in sample KIN-133c.



**Figure 2.4** Garnet clusters surrounded by clinozoisite with phlogopite in border zone sample KIN-134-4.

**Table 2.2** Wall zone petrography.

qz	fsp	hbl	alm	bt	aln	ap	mnz	chv	aesc	clb	ilm	rt	thr	ttn	zrn	py	sp	ox
15	x	25	6	9	15	5	5	x	x	x	x	x	x	x	x	x	x	x
Textures																		
Coarse and blocky; some poikiloblastic texture; REE-bearing phases commonly associated																		

(Numbers in boxes represent approximate percentage of rock composed of this minerals. Abbreviations are as follows: qz=quartz; fsp=feldspar; hbl=hornblende; alm=almandine; bt=biotite; ap=apatite; mnz=monazite; chv=chevkinite; aesc=aeschnite; clb=columbite; ilm=ilmenite; rt=rutile; thr=thorite; ttn=titanite; zrn=zircon; py=pyrite; sp=sphalerite; ox=Fe-oxides.)



**Figure 2.5** Wall zone thin section blanks (left to right are samples KIN-133e, KIN-135a, Rad 1, KIN-133b, and KIN133d) to show texture and appearance, as well as similarities between this zone across localities.

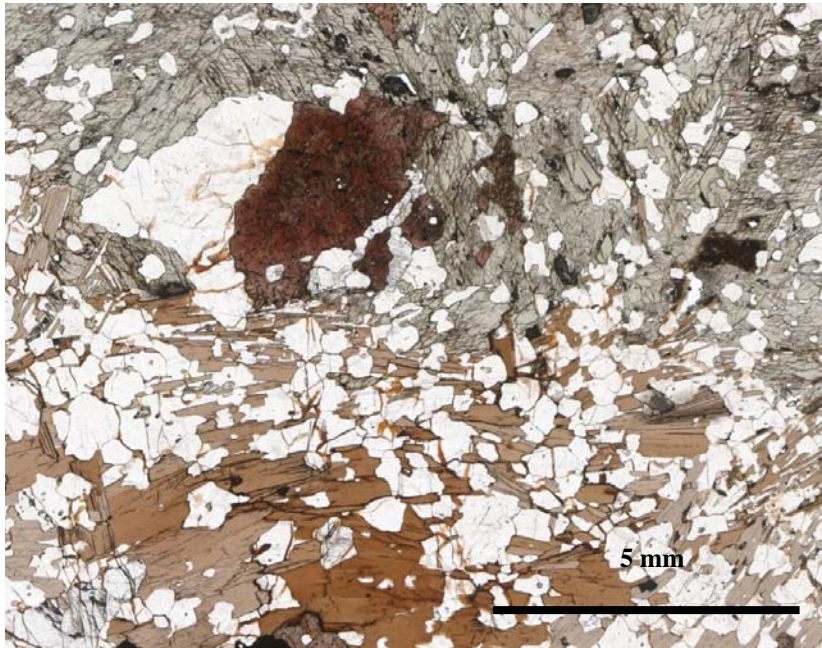


**Figure 2.6** Poikiloblastic texture of amphibole and phlogopite within sample KIN-133b.

**Table 2.3** Intermediate zone petrography.

	qz	plg	hya	grt	phl	msc	aln	clb	rt	tur	ap	mnz	chev	amph	thr	fers	aesc	eux	zrn	py
130	30	25	25	x	x	x	7	8			x			x	x	x		x		
134	15	20		x	10		20	x			10	15	x		x		x		x	
135	15	40	35	x	x							x								
136		55		x		35		x	x			7						x	x	
Rad 2	10	75			x	x	x			x	x	x								x
	Textures																			
130	Large anhedral quartz and feldspar (up to 1 cm); large euhedral to subhedral zoned (Fig. 2.1.7) allanite grains (up to 5 cm); large (up to 2.0 cm) euhedral columbite associate with euxenite; fersmite grains as exsolutions (Fig. 2.1.8).																			
134	Common allanite+apatite after monazite (sometimes in coronas), commonly associated with columbite, chevkinite, and aeschynite; subhedral phlogopite up to 2 mm																			
135	Very prevalent feldspar with quartz; scattered phlogopite, other accessory minerals are found within the phlogopite																			
136	Feldspar (anhedral, up to 0.50 cm) and muscovite (subhedral, up to 8 mm) dominated; columbite as exsolutions within rutile (can be associated with monazite) (Fig. 2.1.11); euxenite found within garnet (Fig. 2.1.12).																			
Rad 2	Bulk feldspar and quartz, micas found along fractures (Fig. 2.1.13), small tourmaline grains (up to 2 mm in size) (Fig. 2.1.13), high levels of sericitization; intergrowths of muscovite and quartz (Fig. 2.1.14)																			

(Numbers in boxes represent approximate percentage of rock composed of this minerals. Abbreviations are as follows: qz=quartz; plg=plagioclase feldspar; ksp=K-feldspar; hya=hyalophane feldspar; grt=garnet; phl=phlogopite; msc=muscovite; aln=allanite; clb=columbite; rt=rutile; tur=tourmaline; ap=apatite; mnz=monazite; chev=chevkinite; amph=amphibole; thr=thorite; fers=fersmite; aesc=aeschynite; eux=euxenite; zrn=zircon; py=pyrite.)

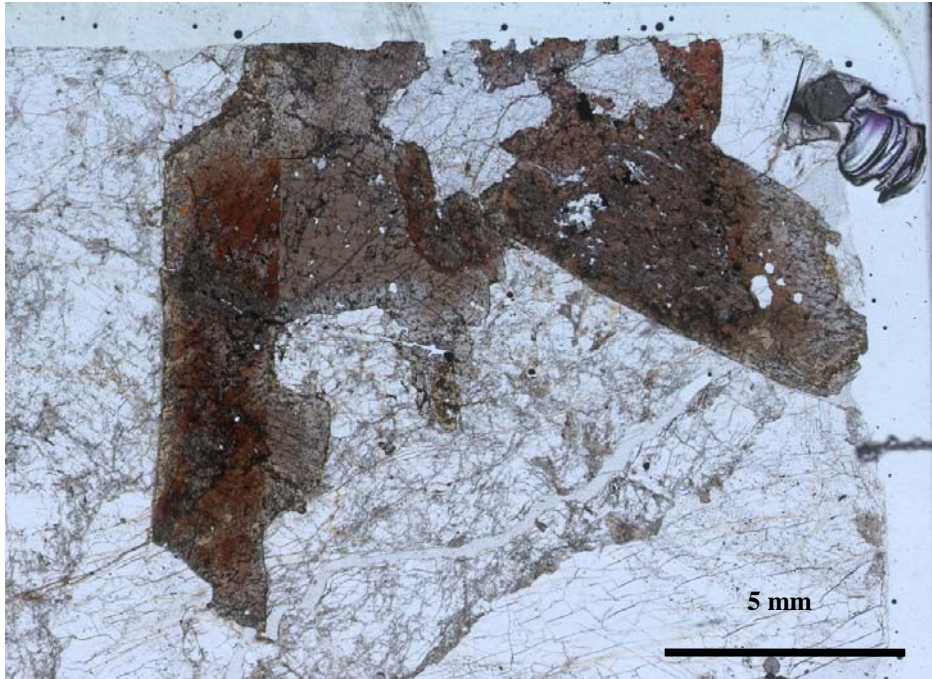


**Figure 2.7** Secondary zoned allanite grains in the intermediate zone in sample KIN-130a.

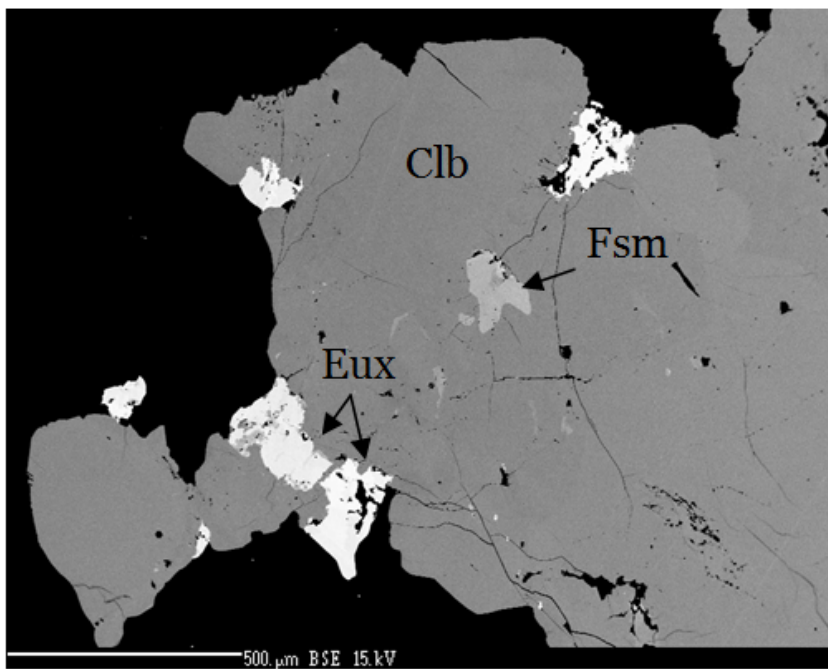


**Figure 2.8** Primary columbite with euxenite-(Y) in fractures and fersmite as a secondary product in section KIN-130b.



**Figure 2.9** Hand sample from the intermediate zone at locality KIN-134.



**Figure 2.10** Blank from thin section KIN-135b.

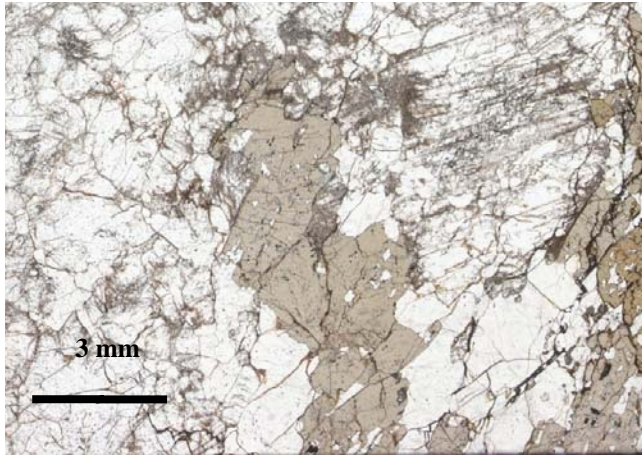
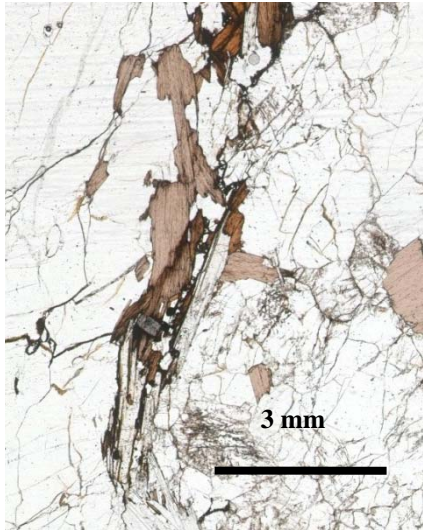


**Figure 2. 11** Images from thin section Rad 2a showing mica (phlogopite and muscovite) in vein (top) and tourmaline (bottom).

**Table 2.4** core zone petrography.

	qz	plg	hbl	msc	grt	ap	aln	aesc	zrn	py	wur	lan	ber
KIN-130	90		5		x					x	x	x	x
KIN-134	90				5		5						
KIN-135	80			s									
Rad 2	85	5				x	x	x	x	x			
	Textures												
KIN-130	All accessory mineralization occurs as replacement and fracture filling within the diamond shaped amphibole grains; undulose extinction in quartz (Fig. 2.1.15)												
KIN-134	High quartz content with garnet												
KIN-135	Quartz with euhedral allanite up to 1.50 cm and msc up to 5 mm in length												
Rad 2	Apatite and allanite are associate (Fig. 2.1.18) with small aeschynite grains found within (likely secondary after monazite); feldspar grains "fill" space between quartz grains												

(Numbers in boxes represent approximate percentage of rock composed of this minerals. Abbreviations are as follows: qz=quartz; plg=plagioclase feldspar; hbl=hornblende; msc=muscovite; grt=garnet; ap=apatite; aln=allanite; aesc=aeschynite; zrn=zircon; py=pyrite; wur=wurtzite; lan=lanthanite; ber=bertrandite..)

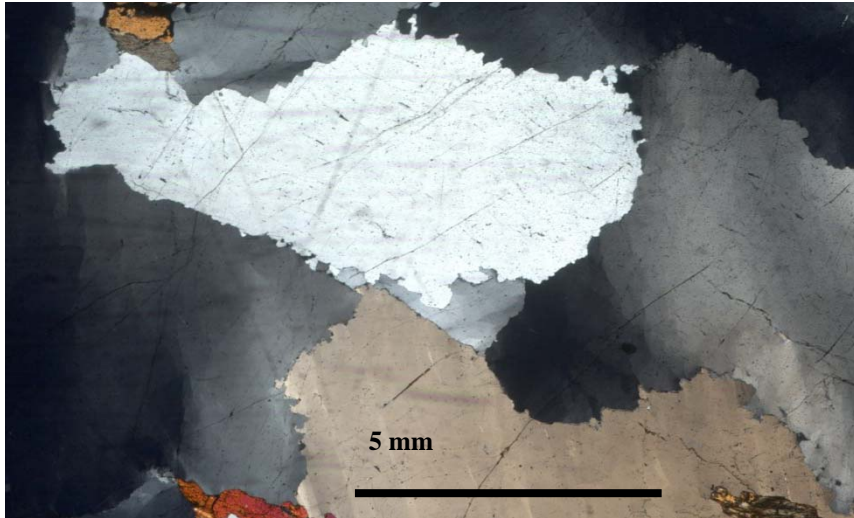


**Figure 2.12** Undulose extinction and migratory boundaries visible in the quartz within the core at locality KIN-130.



**Figure 2.13** Primary amphibole grains demonstrating cleavage planes within quartz in the quartz core from locality KIN-130.

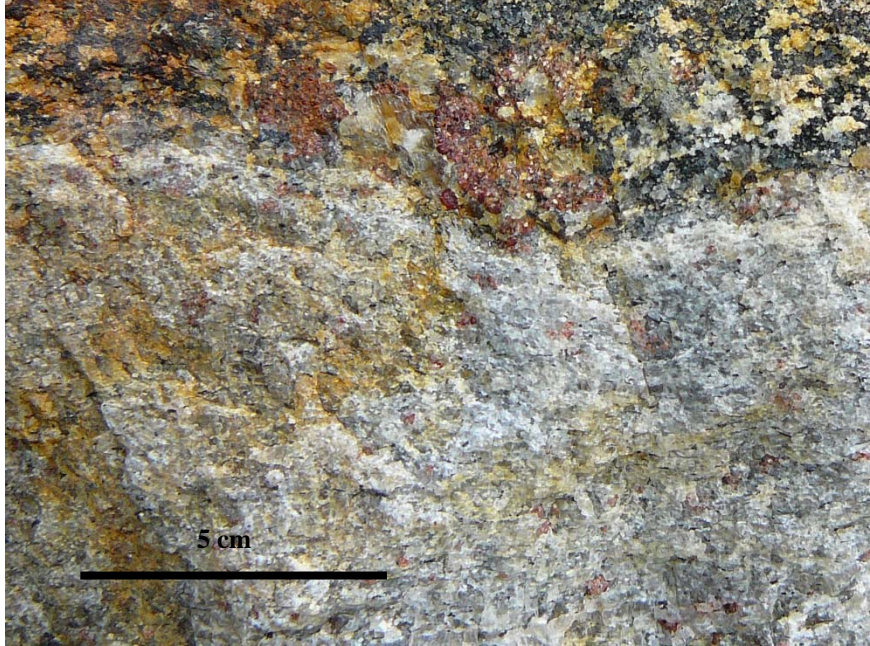


**Figure 2.14** Quartz core with visible quartz and red garnet at locality KIN-134. The top of the photo shows the contact between the core and the intermediate zone.

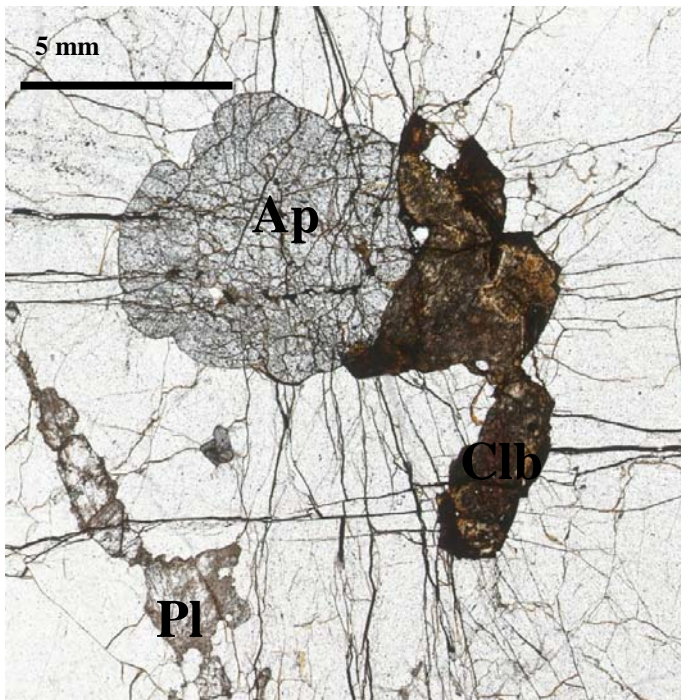


**Figure 2.15** Allanite and apatite within quartz in sample Rad 2c.

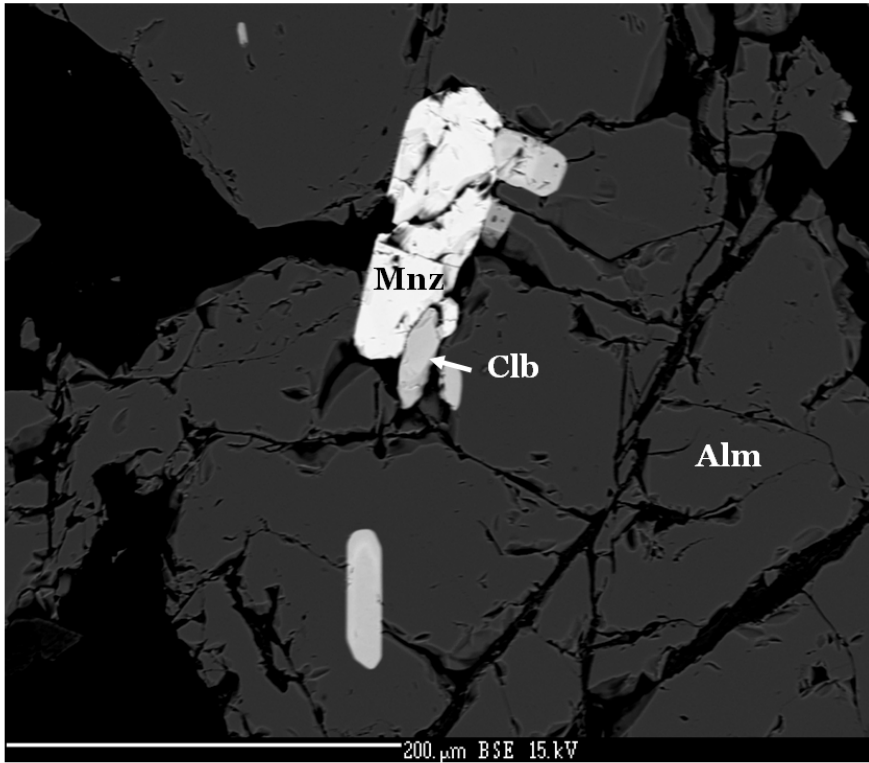


**Figure 2.16** Ferrocolumbite and monazite-(Ce) within almandine in sample PGM 1.

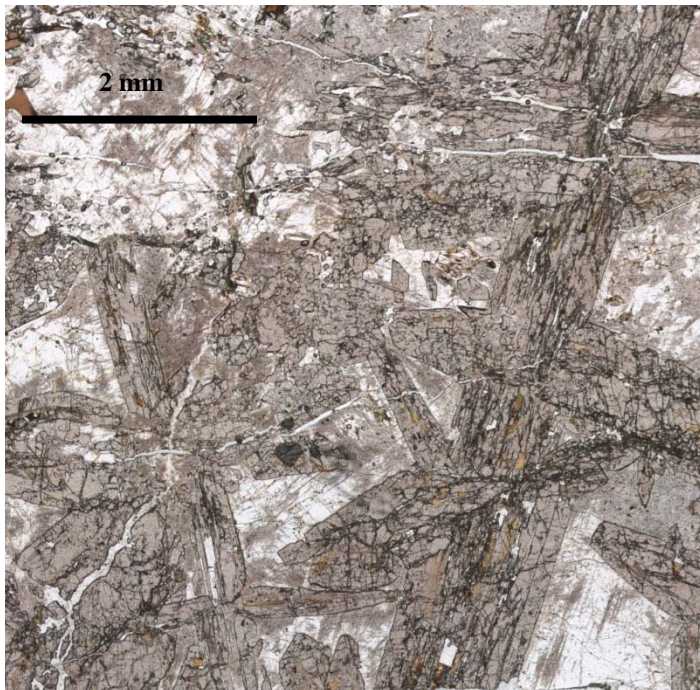


**Figure 2.17** Ferriallanite grains in syenite sample JBTDR018.

### 3. Mineralogy

The mineralogical information presented in this chapter is based on electron microprobe (EMP) data collected from a set of samples representative of each pegmatite zone and type of mineralization. Resources did not permit the collection of data from all samples, so although this is a comprehensive look at the minerals for which data was collected, not all minerals were analyzed. Table 3.1 lists all thin sections analyzed by EMP and their locality.

#### 3.1 Silicates

##### 3.1.1 Feldspar

Feldspars are common in most studied samples with plagioclase (albite and oligoclase) being the most abundant. Hyalophane,  $(K,Ba)[Al(Si,Al)Si_2O_8]$ , is present in the intermediate zone at locality KIN-130, and K-feldspar is only found in sample PGM 1. There is little overlap between these high and low Ca groups (Fig. 3.1 and 3.2). Regardless of composition, the feldspar in all of the samples is white to cream in color and blocky in texture. Table 3.2 lists samples containing feldspar and their type and Fig. 3.3 shows the distribution of Na, Ca, and K within the samples.

The feldspar present in the border zone is all oligoclase. Samples from locality KIN-133 reach a maximum level of 0.34 Ca apfu whereas those from locality KIN-134 have a maximum of 0.30 Ca apfu.

Both plagioclase and hyalophane are present in the intermediate zone at locality KIN-130. Calcium in the plagioclase ranges from 0.02 to 0.28 Ca apfu. The Ca-rich samples are oligoclase and the Ca-poor samples are albite. The hyalophane contains maximum K and Ba values of 0.44 apfu for both elements. The  $X_K$  (K/K+Ba) range varies from 0.49 to 0.55 within the hyalophane

grains. Compositions between K and Ba feldspars usually follow a solid solution from Ba-rich (celsian) to K-rich (orthoclase) as seen in Deer et al (2001), however, in the samples found at KIN, the opposite trend can be seen in Fig. 3.4 where the feldspar compositions trend towards Na. This will be discussed further in chapter 5.

At locality KIN-134, the intermediate zone feldspars are all oligoclase with a maximum Ca value of 0.30 Ca apfu, and samples from Rad 2 contain only albite with Na up to 0.93 Na apfu and 0.33 Ca apfu. The granite contains albite with Na levels of 1.14 Na apfu and Ca levels of 0.10 Ca apfu. Sample PGM 1 contains two types of feldspar: albite and orthoclase. The albite contains low levels of Ca (maximum 0.07 apfu) and the orthoclase features low amounts of Na (ca. 0.1 apfu) with no Ba.

### **3.1.2 Mica**

Mica group minerals are common accessory minerals in many of the zones present in the KIN samples. Both biotite and muscovite are present, with annite and phlogopite compositions for biotite. Mg/(Mg+Fe) trends are shown in Fig. 3.7. This is particularly significant in that lower Mg values are found in micas closer to the core and were used in zonal differentiation. Table 3.3 lists samples containing mica and their type.

Dark mica in the border zone at locality KIN-133 is phlogopite (Fig. 3.5), and contains an Mg# up to 0.69, the highest found; approximately 1.11 Al apfu, and little compositional variation. It is primary and commonly replaced by almandine with a poikiloblastic texture (Fig. 3.6).

The wall zone contains biotite (Fig. 3.5) of both phlogopite and annite compositions (Fig. 3.6). Both have been mostly replaced by almandine and are associated with magnesiohornblende (Fig. 3.8). The phlogopite (133d) has an Mg # of 0.59 and Al values of 1.13 Al apfu. The annite

(135c) is slightly altered (Fig. 3.5) with a single Al value attaining value of 1.46 Al apfu. It has a particularly high Ti content up to 0.31 Ti apfu (Fig. 3.7). This elevated Ti and variation in composition (Fig. 3.6) are likely due to the effects of the alteration.

The biotite at KIN-134 in the border zone is has an  $X_{Mg}$  value of 0.49 and is on the border between annite and phlogopite (Fig. 3.6). It is primary and is replaced locally by almandine.

The intermediate zone at locality KIN-134 contains phlogopite that is also close to the annite/phlogopite border with an  $X_{Mg}$  value of about 0.53 (Fig. 3.6). It is primary and has been replaced locally to form almandine.

Muscovite from the intermediate zone at locality KIN-130 (Fig. 3.5) occurs as secondary sericite after highly altered plagioclase (Fig. 3.9). It contains the highest Al+R<sup>3+</sup> and lowest Mg of all of the samples for which EMP data were collected with values of 1.97 Al+R<sup>3+</sup> apfu at the M-site (Fig. 3.5) and an Mg# of 0.29.

Both phlogopite and muscovite occur in sample Rad 2a (Fig. 3.5 and Fig. 3.6) as primary minerals in veins within quartz and feldspar. Only the biotite is associated with fluorapatite and they can be in association with each other (Fig. 3.10). The biotite has an Mg# of about 0.59 and the muscovite contains slightly more Mg with Mg# up to 0.67.

### 3.1.3 Amphibole

All of the amphiboles within the KIN samples belong to the calcium subgroup (<sup>B</sup>Ca = 1.66-1.86) and can be classified as magnesiohornblende (Hawthorne et al., 2012). Table 3.4 lists samples containing amphibole.

Wall zone amphibole is relatively Fe<sup>2+</sup>-rich for magnesiohornblende (Fig. 3.11). It's primary, commonly replaced by almandine in association with phlogopite, and contains pyrite-

filled veins. Small amounts of edenite substitution ( $\text{Na}_{\text{tot}}+\text{K}$ ) are found within these grains, with up to 0.15 Na apfu and 1.28  $\text{Al}_{\text{tot}}+\text{Fe}^{3+}$  apfu (Fig. 3.12). These trends are paralleled by slight decreases in the amount of Si present, with a minimum of 7.00 Si apfu.

The core zone amphibole contains primary magnesiohornblende that has been replaced by almadine/spessartine and fractures filled with pyrite, wurtzite, and lanthanite-(Ce) (Fig. 3.13). It has high Si levels for magnesiohornblende with almost 7.50 Si apfu present (Fig. 3.11). There is some edenite substitution present (Fig. 3.12) with up to 1.81 Na apfu, again associated with a slight decrease in the Si content. Similar amounts of tschermakite substitution are present (3.12) with  $\text{Al}_{\text{tot}}+\text{Fe}^{3+}$  totaling a maximum of 0.84  $\text{Al}_{\text{tot}}+\text{Fe}^{3+}$  apfu.

#### 3.1.4 Garnet

Garnet compositions comprise two groups, those with higher Ca and lower  $\text{Fe}^{2+}$  (type I), and those with lower Ca and higher  $\text{Fe}^{2+}$  (type II) (Fig. 3.14a and b). Type I garnets appear secondary, possibly after phlogopite, and type II garnets are likely primary. Although the type I samples have higher Ca, the garnets are still generally Fe-rich and are almost entirely almandine, and very rarely spessartine (Fig. 3.15). Table 3.5 lists samples containing mica and their type.

Garnets in the main pegmatite bodies plot close to middle composition among almandine, spessartine, and Ca-garnet in Fig. 3.15 with a slight prevalence of almandine component (except for two points in the core zone); samples from outside the main pegmatite bodies plot closer to the almandine corner (Fig. 3.15). Figure 3.16 gives a slightly different view of the sample compositions and is intended to showcase the general lack of Mg present in these samples, as all plots point along the solid solution of  $\text{Fe}^{2+}$  to Ca+Mn.

Border, wall, and intermediate zone garnets are all almandine in composition (Fig. 3.15).

Border zone garnets form with a poikiloblastic texture (Fig. 3.17).  $X_{Mn}$  [Mn/(Mn+Fe)] values range from 0.36 to 0.42 at locality KIN-133 and KIN-134 is  $X_{Mn}$  is 0.28. KIN-134 is found with significant amounts of what appears to be unreached phlogopite.

Garnets in the wall zone are prevalent as the majority of the phlogopite has undergone replacement and little primary material remains. It forms in association with magnesiohornblende and occasionally in primary titanite (Fig. 3.18).  $X_{Mn}$  values range from 0.31 to 0.37.

Garnet is abundant in the intermediate zone and  $X_{Mn}$  values have a larger range than those generally found at the KIN locality with a range of 0.27 to 0.36.

Garnets in the core zone occur as secondary grains within primary magnesiohornblende with fracture filling pyrite and lanthanite-(Ce) (Fig. 3.13). The garnet found here is very close to the almandine/spessartine boundary (Fig. 3.15) and is the most Mn-rich of all the garnet present, with up to 1.27 Mn apfu.  $X_{Mn}$  values range from 0.46 to 0.59.

Primary type II garnets in the granitic rocks (G17 and PGM 1) are more Fe-rich and contain more almandine component than Type I garnets from the allanite pegmatites (Fig. 3.15). Garnets in the granite have slightly lower  $X_{Mn}$  values than those found in type I garnets with a range of 0.18 to 0.22. These garnets are primary but have undergone severe deformation and replacement by chlorite, muscovite, and xenotime (Fig. 3.19). PGM 1 garnets are also primary and found within albite with tourmaline (Fig. 3.20). These garnets have  $X_{Mn}$  values with the same range as those found in sample KIN-135; 0.22 to 0.23, and they carry a similar almandine signature (Fig. 3.15).

### **3.1.5 Zircon**

Zircon is common in the pegmatites and is present in many samples. Table 3.6 lists samples containing zircon. The crystals are commonly primary and contain few impurities. In every case, individual crystals appear isolated and not involved in any reactions or growth relationships. The zircons also appear to show very little elemental substitution; the highest levels of Hf present are in sample PGM 1 with 0.03 Hf apfu. All other samples contain a minimum of 0.96 Zr apfu with the remaining 0.04 apfu from Hf, Y, or Al (neither Y nor Al are found in concentrations above 0.01 apfu).

### **3.1.6 Thorite**

Thorite occurs as small, secondary grains with compositions close to the ideal end member and with little substitution. Table 3.7 lists samples containing thorite.

In the border zone, thorite occurs two ways: 1) after monazite-(Ce) with allanite-(Ce) and fluorapatite, and 2) with secondary nioboaeschnite-(Ce), ferrocolumbite and ferriallanite-(Ce). In sample KIN-130a, it occurs as exsolutions within primary Th-rich allanite (Fig. 3.21), whereas KIN-134-2 contains thorite that is associated with chevkinite-(Ce) and nioboaeschnite-(Ce) in addition to allanite. The thorite in the intermediate zone contains the highest levels of impurities, with 0.03 Ce apfu and 0.07 P apfu.

### **3.1.7 Titanite**

Table 3.8 lists samples containing titanite. Titanite occurs as large primary grains in association with primary magnesiohornblende and phlogopite, and almandine, and is partially replaced by Nb-rich ilmenite, ferrocolumbite, and phlogopite in symplectite (Fig. 3.22). It

contains moderate amounts of Nb-substitution (up to 0.07 Nb apfu) and slightly elevated REEs (Fig. 3.23). The F content is low compared to published data (Cempírek et al., 2008) with a maximum of 0.08 F apfu. Contents of Al and Fe are also slightly elevated, with up to 0.14 Al+Fe apfu present in the samples.

### **3.1.8 Beryl and Bertrandite**

Beryllium-rich minerals are uncommon in the KIN property samples and were found in only two samples, both at locality KIN-130. Beryl was found within the intermediate zone (thin section 130a), as a small, most likely primary grain that was altered to quartz and albite. Potential bertrandite is present in the core zone (thin section 130b-2) on fractures in a primary amphibole, however it is unclear as the Be content cannot be analyzed.

### **3.1.9 Tourmaline**

Tourmaline was only found within two samples: Rad 2a and PGM 1. Crystals in Rad 2a are found within quartz and feldspar with quartz inclusions, and is compositionally zoned (Fig. 3.24). The X-site primarily contains Na, Ca, and minor K and vacancy, with slight compositional evolution towards Ca-enrichment in parts of the crystals (Fig. 3.24). The W-site is filled with prevailing F and minor Cl and shows solid solution from <sup>W</sup>OH-depleted to <sup>W</sup>OH-enriched composition with constant levels of F+Cl (Fig. 3.26), and the Y-site occupancy is dominated by Mg (Fig. 3.27). The tourmaline composition indicates that fluor-dravite is the major end-member present.

Tourmaline in sample PGM 1 is compositionally similar to that from Rad 2a; its X-site is dominated by Na (Fig. 3.25), but Ca contents are significantly lower. Also, W-site occupancy of

PGM 1 tourmaline is similar in its high and stable contents of F; however, OH prevails over F for most analytical points. The tourmaline composition evolves from OH-dominated to F,O-dominated with a fairly constant F+Cl component (Fig. 3.26). Finally, the Y-site of the PGM 1 tourmaline contains more Fe than Mg and little Al, classifying the PGM 1 tourmaline as Mg,F-rich schorl and fluor-schorl (Fig. 3.27). The PGM 1 tourmaline grains are found within albite and K-feldspar with garnet nearby (Fig. 3.20).

## 3.2 REE silicate minerals

### 3.2.1 Epidote Group minerals

Epidote group minerals (EGM) are commonly found in samples as both primary and secondary allanite with three textural types. Allanite I consists of fresh primary grains of ferriallanite-(Ce) [ideally  $(\text{CaCe})(\text{Fe}^{3+} \text{AlFe}^{2+})(\text{Si}_2\text{O}_7)(\text{SiO}_4)\text{O}(\text{OH})$ ] (Fig. 3.28). Allanite II formed from allanite I that has undergone some degree of recrystallization to create REE-depleted epidote (Fig. 3.28a and b), occasionally with higher levels of  $\text{M}^{3+}$  site vacancies and allanite III is secondary allanite-(Ce) [ideally  $(\text{CaCe})(\text{Al}_2\text{Fe}^{2+})(\text{Si}_2\text{O}_7)(\text{SiO}_4)\text{O}(\text{OH})$ ] (Fig. 3.28a and b). Table 3.9 lists samples containing epidote group minerals and their type.

Regardless of locality and textural type, EGM grains are zoned, both optically and compositionally, primarily due to variations in REE abundance. The grains have high Ti values present in these samples, which will be discussed more in Chapter 5. The EGMs present are consistently Ce-rich over La or Nd (Fig. 3.29) and the REE content, especially LREEs, is visually significantly elevated when normalized to chondrite (Fig. 3.30) (chondrite normalization here and for all minerals from McDonough & Sun (1995)).

EGM in the border zone are entirely secondary allanite III, which occur in one of two ways: 1) with fluorapatite and allanite-(Ce) after monazite-(Ce) in a corona (Fig. 3.31), and 2) with thorite and secondary niobaeschnite-(Ce) with ferrocolumbite (Fig. 3.32). The EGM grains are zoned with variable REE values (between 0.54 and 0.86 total REE apfu) and typically are allanite-(Ce) (Fig. 3.28a and b) with elevated Ti levels (up to 0.32 Ti apfu). At KIN-134, these grains are more commonly clinozoisite (0.38 total REE apfu) (Fig. 3.28a and b), but still found in similar secondary after monazite environments.

Wall zone grains are almost entirely primary allanite I and altered allanite II, with few allanite III grains (Fig. 3.33). Allanite I/II grains are large sub-euhedral grains with allanite I in the cores and allanite II on the grain boundaries. The allanite I grains are primarily ferriallanite-(Ce) (Fig. 3.28a and b) and allanite II is leached allanite I with high levels of vacancies at the M3 site (Fig. 3.34) and lower levels of REEs, and are primarily epidote in composition (Fig. 3.28 a and b). These primary and Fe-rich grains can also be associated with “exsolutions” of chevkinite (Fig. 3.35). Where present, allanite III grains are primarily allanite-(Ce) (Fig. 3.28a and b) and found after primary monazite-(Ce) with secondary aeschnite-(Ce), chevkinite-(Ce), and perrierite-(Ce).

Intermediate zone epidote group mineral grains are primary allanite I with altered allanite II rims and allanite or epidote in composition (Fig. 3.28a and b). At locality KIN-130 the allanite-(Ce) (with altered REE-depleted epidote at the border) grains commonly appear euhedral and zoned, suggesting a primary origin (Fig. 3.36). Both monazite and apatite are present, however, which suggests some degree of alteration and that portions of the grains, at least, are secondary allanite III grains instead of primary. The border material contains almost no Ti, whereas the cores of the allanite crystals are enriched (up to 0.20 Ti apfu).

In contrast, the intermediate zone at KIN-134 contains a significant amount of allanite III in a textural corona (Fig. 3.37 and 3.38), occasionally found in association with primary ferrocolumbite. These grains are strongly zoned (REE variation from 0.46 total REE apfu to 0.92 total REE apfu) allanite-(Ce) grains (except for a few clinozoisite grains) (Fig. 3.28 a and b). Rad 2 are secondary allanite III after monazite with the lowest Ce content of all the samples (maximum of 0.26 Ce apfu) (Fig. 3.28 a and b).

Visible trends among primary allanite I grains include a consistent level of vacancy at about 0.18 apfu (Fig. 3.34) along with a linear negative relationship between the total  $M^{3+}$  site versus Ti (Fig 3.39). Additionally, a positive correlation between the levels of REE and Ti exists (Fig. 3.40) as well as a less correlated, but still positive relationship between  $M^{2+}$  site totals and Ti (Fig. 3.41). In general, primary allanite plot as Fe-rich ferriallanite, however, it is interesting to note that some allanite II grains, the REE-depleted rims from allanite I, contain higher levels of  $Fe^{3+}$  than the primary grains. A hypothesis is that this is due to the chevkinite exsolutions that form in the allanite I grains: the  $Fe^{3+}$  is removed the allanite I and is incorporated into the chevkinite in these zones; the primary  $Fe^{3+}$  remains in the allanite II part of the grain.

### **3.2.2 Chevkinite group minerals**

Chevkinite group minerals seen here are chevkinite and perrierite, which are polymorphs (Table 3.10 lists samples containing chevkinite group minerals and mineral type). Both are monoclinic with different  $\beta$  angle ( $\sim 100^\circ$  for chevkinite and  $\sim 113^\circ$  for perrierite) and can be generally distinguished using their composition discrimination diagram (Fig. 3.42) proposed by Macdonald and Belkin (2002).

ChGM grains found at the KIN property are mostly chevkinite-(Ce) [ideally  $(\text{Ca,REE})_4\text{Fe}^{2+}(\text{Ti,Fe}^{3+},\text{Fe}^{2+},\text{Al})_2\text{Ti}_2\text{Si}_4\text{O}_{22}$ ] in composition with a few grains of perrierite-(Ce) [ideally  $(\text{Ce,Ca,Sr})_4\text{Fe}^{2+}(\text{Ti,Fe}^{3+},\text{Fe}^{2+},\text{Al})_2\text{Ti}_2\text{Si}_4\text{O}_{22}$ ]. Perrierite grains are entirely secondary and contain highly elevated levels of REEs, especially LREEs, when normalized to chondrite (Fig. 3.43).

Wall zone ChGM occur as both chevkinite-(Ce) and perrierite-(Ce) (Fig. 3.42) and commonly form as inclusions within allanite (3.35), where some of the Fe and Ti from allanite form pockets of chevkinite within allanite. Additionally, they can form with allanite as a secondary product after monazite. In grains with both minerals, the chevkinite crystals contain darker zones in BSE that are Ca- and Sr-enriched and represent perrierite-(Ce) (Fig. 3.44). The difference between mineral types is primarily seen in the decrease in REEs and Mn present in the samples (total REEs decrease from 3.25 REE apfu to 2.78 REE apfu); Ca and Sr increase from 0.64 Ca+Sr apfu to 1.02 Ca+Sr apfu.

ChGM found within the border zone are exclusively secondary chevkinite-(Ce) commonly in association with secondary allanite-(Ce) with fluorapatite after monazite-(Ce). All of the ChGM crystals are zoned, with varying levels of REEs (2.53 total REE apfu to 3.61 total REE apfu), Mn (0.14 to 0.39 Mn apfu), Ca (0.30 to 0.62 Ca apfu), Nb (0.19 to 0.50 Nb apfu), and Sr (0.05 to 0.50 Sr apfu). Only one grain of primary chevkinite-(Ce) was analyzed in KIN-134 samples was analyzed and is in association with secondary allanite-(Ce) and aeschynite after primary monazite (Fig. 3.45). It contains low levels of Mn (0.07 Mn apfu), Ca (0.39 Ca apfu), Nb (0.12 Nb apfu) and Sr (0.06 Sr apfu).

Typical chevkinite present in the KIN samples is secondary after monazite, commonly with secondary allanite. This implies that Si had to be introduced into the system in order to create the chevkinite and allanite present. This is further discussed in Chapter 5.

### **3.3 Phosphate Minerals**

#### **3.3.1 Monazite**

Monazite is a moderately common accessory mineral in samples. It is always primary monazite-(Ce) (with solid solution from monazite-(Ce) to monazite-(La) (Fig.3.46) and has commonly undergone replacement to form secondary allanite-(Ce) and fluorapatite. Table 3.11 lists samples with analyzed monazite. Figure 3.47 shows the elevated levels of REE minerals in relation to chondrite present in the monazite samples, particularly of the LREEs.

Two substitution trends are present in the monazite (Fig. 3.48). The first is the huttonite/thorite trend, where (Th,U)+Si substitute for (REE+P) (Ondrejka et al., 2012); the second substitution trend is the cheralite substitution where [Ca+U(Th)] substitutes for two REE atoms.

The monazite present in the border and wall zones is primary and has been replaced by fluorapatite, ferriallanite-(Ce), and thorite in a corona texture with the original monazite still present in the core (Fig. 3.31). Although monazite-(Ce) is present in border zone, it has commonly undergone complete replacement; additionally, little Si and Th substitution is present with 0.07 Si apfu and 0.07 Th apfu. Ca levels are low. It is only present in one sample from the wall zone where little primary material remains (most has undergone complete replacement) (Fig. 3.49). Samples from this zone demonstrate the huttonite/thorite substitution particularly well and

range from low levels of substitution (0.04 Si and Th apfu) to moderate levels (0.39 Si and Th apfu) (Fig. 3.48).

Although monazite is common in other sections, it is extremely prevalent in the intermediate zone at locality KIN-134. These are primary monazite-(Ce) grains that have undergone moderate replacement to form allanite-(Ce) and fluorapatite in association with primary ferrocolumbite. These reactions are similar to those found within the border and wall zones; however, there is significantly more unreacted monazite present (Fig. 3.37 and 3.38). Substitution is present with a maximum of 0.09 Si apfu and 0.09 Th apfu.

The intermediate zone at locality KIN 136 contains primary monazite-(Ce) in association with primary Nb-rich rutile. These grains have undergone little substitution with a maximum of 0.01 Si apfu, 0.07 Th apfu, and 0.07 Ca, and appear more euhedral than grains found in other samples (Fig. 3.50). Unlike the other samples, these grains are not associated with secondary allanite.

Rad 2a monazite is primary monazite-(Ce) with the highest levels of huttonite/thorite substitution (Th+U+Si and REE+Y+P values attain 1.12 and 0.77 apfu, respectively) Fig. 3.48). These grains are very small and have undergone replacement by allanite-(Ce) and fluorapatite with little primary material remaining. These samples contain the highest amounts of Nd (0.12 Nd apfu) found on the KIN property.

The samples from PGM 1 show the highest amount of cheralite substitution in the KIN property samples (Fig. 3.48) with up to 0.14 Ca apfu. These grains of monazite-(Ce) are primary and associated with primary ferrocolumbite. These grains appear the most homogeneous with little replacement (Fig. 3.51).

### 3.3.2 Apatite

The apatite present on the KIN property occurs almost entirely as secondary fluorapatite (Fig. 3.53) after monazite-(Ce) with consistently REE values (Fig. 3.53). Table 3.12 lists samples with analyzed apatite and their zones.

Border zone apatite grains are secondary after monazite-(Ce) and either associated with thorite and allanite-(Ce) (Fig. 3.31) in a textural corona or found with primary ferrocolumbite, secondary niobaeschynite-(Ce) and allanite-(Ce) with small monazite-(Ce) remnants within the apatite. This fluorapatite is particularly Sr-rich with 0.20 Sr apfu (3.3.9) and it also contains 1.01 F apfu; additionally it contains the highest levels of REE present in any apatite with a maximum value of 0.03 total REE apfu (Fig. 3.53).

Fluorapatite found within the wall zone contains a low level of REEs, with less than 0.01 total REE apfu (Fig. 3.53). It occurs as a secondary mineral after primary monazite-(Ce) with allanite-(Ce), and chevkinite-(Ce) (Fig. 3.49) with moderate Sr enrichment (up to 0.20 Sr apfu) (Fig. 3.3.10).

Intermediate zone fluorapatite is secondary after monazite-(Ce) with allanite-(Ce), and thorite (Fig. 3.37 and 3.38) and have the lowest Sr values of the main pegmatites (maximum of 0.05 Sr apfu) (Fig. 3.53), and 1.05 F apfu. Sample Rad 2a apatite crystals contain the least Sr of all the samples with a maximum of 0.03 Sr apfu present (3.53).

Throughout the samples, there appears to be a strong correlation between zone and the Sr concentrations (Fig. 3.53). Apatite found closer to the core contains the least amount of Sr and that in the border zone contains the most. Additionally, secondary apatite should contain appreciable levels of OH or Cl in place of F (London & Burt, 1982); however, that is not the case in these samples where there appears to be very little substitution (Fig. 3.52).

### 3.3.3 Xenotime

Xenotime ( $\text{YPO}_4$ ) is a rare mineral and is only found in the nearby granite (G17a), where it occurs as a secondary mineral within primary almandine that has been replaced by xenotime as well as chlorite and muscovite (Fig.3.19).

## 3.4 Oxide Minerals

### 3.4.1 Columbite

Minerals of the columbite-tantalite series were found in all but the core zones (Table 3.13 lists sections with analyzed columbite and their zone) and consistently contain little Ta and are Fe-rich, classifying grains as ferrocolumbite (Fig. 3.54) (with the exception of one data point that is manganocolumbite). Columbite is present in four textural types: columbite I is primary columbite, columbite II is secondary with inclusions of fersmite and euxenite, columbite III is a replacement product from titanite, and columbite IV is found as exsolutions within rutile.

Columbite-group minerals in the border zone are columbite I and mostly belong to the Mn-rich ferrocolumbite group with one sample of manganocolumbite. It is commonly replaced along fractures by allanite-(Ce), nioboaeschynite-(Ce) and thorite (Fig. 3.32) with  $X_{\text{Mn}}$   $[\text{Mn}/(\text{Mn}+\text{Fe}^{2+})]$  values of 0.27-0.52. These are the highest values of Mn present and include the only manganocolumbite compositions present in the KIN property data collected.

Columbite in the wall zone is present as primary grains that are overgrown by secondary allanite-(Ce) (Fig. 3.55), and secondary (columbite III) grains formed in association with ilmenite by the replacement of Nb-rich titanite with phlogopite (Fig. 3.22). It is strictly of ferrocolumbite composition (Fig. 3.54).

In the intermediate zone at locality KIN-130, the columbite occurs solely as ferrocolumbite and as both primary (columbite I) and secondary (columbite II) grains. Columbite I grains are relatively homogeneous and have been locally replaced by fersmite and euxenite-(Y) with secondary grains that appear more porous, heterogeneous, and commonly occur in association with thorite and euxenite-(Y) (Fig. 3.56). The ferrocolumbite contains an  $X_{Mn}$  range of 0.26-0.31.

KIN-134 columbite grains forms both as primary and secondary grains (columbite I and III), commonly in association with secondary aeschynite-(Ce), allanite-(Ce), and thorite.  $X_{Mn}$  is more variable than in other zones and ranges from 0.17 to 0.36.

In the muscovite-rich intermediate zone sample found at locality KIN-136 ferrocolumbite occurs as inclusions exsolved from Nb-rich rutile (Fig. 3.50). It is the most Fe-rich sample observed. It contains a maximum  $X_{Mn}$  value of 0.07.

PGM 1 columbite occurs as small, primary columbite I grains and is the most Ta rich of the samples with up to 13.40 wt.% Ta and has an  $X_{Mn}$  value of 0.26.

### **3.4.2 Rutile and ilmenite-pyrophanite**

Table 3.14 lists samples containing oxide minerals and their zone. Rutile in Rad 2a is likely primary Nb-rutile in phlogopite. Grains in KIN 136 are primary Nb-rich rutile with monazite-(Ce) and contain exsolved ferrocolumbite crystals (Fig. 3.50). The rutile in both samples is Nb-rich with up to 24.48 wt. %  $Nb_2O_5$  (0.163 Nb apfu) and generally follows the  $(Fe^{2+} + Nb^{5+}_2)_4 \rightarrow 3Ti^{4+}$  substitution (Fig. 3.57) towards columbite.

Ilmenite was in two textural types in the wall zone: 1) ilmenite I forms euhedral primary crystals with Nb-rich titanite, and 2) ilmenite II forms as a secondary product in symplectite with

ferrocolumbite and phlogopite after primary Nb-rich titanite (Fig. 3.22). Ilmenite I has elevated MnO and Nb<sub>2</sub>O<sub>5</sub> contents (8.55 wt. % MnO and 0.65 wt. % Nb<sub>2</sub>O<sub>5</sub>) with X<sub>Mn</sub> levels up to 0.18. The ilmenite II grains were too small for analysis.

Pyrophanite (Mn-analogue of ilmenite) is very rarely found and only in the wall zone) as a secondary product with aeschynite-(Ce), allanite-(Ce), and thorite replacing columbite (Fig. 3.58) Its X<sub>Mn</sub> value (0.61) is the highest recorded for ilmenite-group minerals at KIN.

### 3.4.3 Aeschynite, Nioboeschynite, Euxenite, and Fersmite

Euxenite- and aeschynite-group minerals have the same stoichiometry of AB<sub>2</sub>O<sub>6</sub> (A=REE+Y+Ca; B=Nb, Ti, Ta); they differ in crystal structure (euxenite-group minerals have space group *Pcan* and aeschynite-group minerals have space group *Pmnb*). Euxenite, (REE,Ca,U,Th)(Nb,Ti,Ta)<sub>2</sub>O<sub>6</sub>, and aeschynite, (REE,Ca,Fe)(Ti,Nb)<sub>2</sub>(O,OH)<sub>6</sub>, can be differentiated by euxenite's preference for Y and the heavy REEs. Aeschynite generally contains the light REEs (Fig. 3.59 and 3.60). Additionally, nioboeuxenite is distinguished from euxenite by Nb>Ti (Fig. 3.61). Fersmite, (Ca,Y)(Nb,Ta,Ti)<sub>2</sub>(O,OH)<sub>6</sub> is characterized by Ca>>REE (Fig. 3.62). Table 3.15 lists samples with these minerals and their zone.

Samples found in the border zone are classified as nioboeschynite-(Ce) with the exception of two aeschynite-(Ce) grains. The grains of both minerals are secondary and crystalline and found associated with primary ferrocolumbite and secondary allanite-(Ce), and thorite (figs. 3.32). The Nb content ranges from 0.99 Nb apfu to 1.51 Nb apfu with all but the two samples with the lowest Nb contents being nioboeschynite-(Ce). The fact that these grains are crystalline is of particular note due to the fact that aeschynite is commonly metamict (Ercit, 2005 ).

Samples from the wall zone are aeschynite-(Ce). These grains are secondary and found as small exsolutions in ilmenite (Fig. 3.63) and chevkinite and are associated with thorite and allanite-(Ce).

Euxenite is found within the intermediate zone at locality KIN-130, one sample point in the border zone, and in sample PGM 1. It can be classified as euxenite-(Y) for all samples. Zoned euxenite is found within the intermediate zone as secondary crystalline (optically anisotropic) grains along ferrocolumbite fractures (Fig. 3.64). As with aeschynite, euxenite is commonly metamict and the crystalline grains found here, along with the aeschynite grains found in other zones, provide an opportunity to learn more about the crystal structures of these minerals.

Additionally, intermediate zone samples from locality KIN-134 contain crystals with both aeschynite-(Ce) and nioboaeschynite-(Ce) signatures. Both types are found within larger allanite-(Ce) grains. The nioboaeschynite-(Ce) grains are secondary and associated with ferrocolumbite, thorite, and allanite-(Ce) (Fig. 3.14). The aeschynite-(Ce) samples are associated with chevkinite (Fig. 3.45).

Fersmite [ideally  $(\text{Ca}, \text{Y})(\text{Nb}, \text{Ta}, \text{Ti})_2(\text{O}, \text{OH})_6$ ] is found solely in the intermediate zone at locality KIN-130 as a secondary product replacing ferrocolumbite (Fig. 3.56). It contains 0.69 Ca apfu and is Nb rich with 1.85 Nb apfu (Pal et al., 2007) and is differentiated by its high Ca content (Fig. 3.63).

Fergusonite-(Y) [ideally  $\text{YNbO}_4$ ] is only found in the intermediate zone at locality KIN-136, as small, secondary, and altered samples within primary monazite-(Ce) and allanite-(Ce).

### 3.5 Carbonate Minerals

#### 3.5.1 Lanthanite

The quartz core at locality KIN-130 (thin section 130b-2) contains the only lanthanite crystal aggregate found within the KIN property samples and is classified as lanthanite-(Ce). It is a secondary replacement mineral on fractures in hornblende with pyrite and almandine (Fig. 3.13).

**Table 3.1** Thin sections analyzed by EMP and their locality.

Thin Section	KIN-130a	KIN-130b	KIN-130b-2	KIN-133c	KIN-133d	KIN-134-2	KIN-134-4	KIN-135a
Locality	KIN-130	KIN-130	KIN-130	KIN-133	KIN-133	KIN-134	KIN-134	KIN-135
Thin Section	KIN-134-2	KIN-134-4	KIN-135a	KIN-135c	KIN-136	Rad 2a	G17a	PGM 1
Locality	KIN-134	KIN-134	KIN-135	KIN-135	KIN-136	Rad 2	G17	PGM

**Table 3.2** Feldspar: Thin sections and zones with analyzed samples.

Zone/Sample type	Thin Section	Albite	Oligoclase	K-feldspar	Hyalophane
Border Zone	KIN-133c		x		
	KIN-134-4		x		
Intermediate Zone	KIN-130a	x	x		x
	KIN-130b	x	x		x
	KIN-134-2		x		
	Rad 2a				
Granite	G17a	x			
Granitic Pegmatite	PGM 1	x		x	

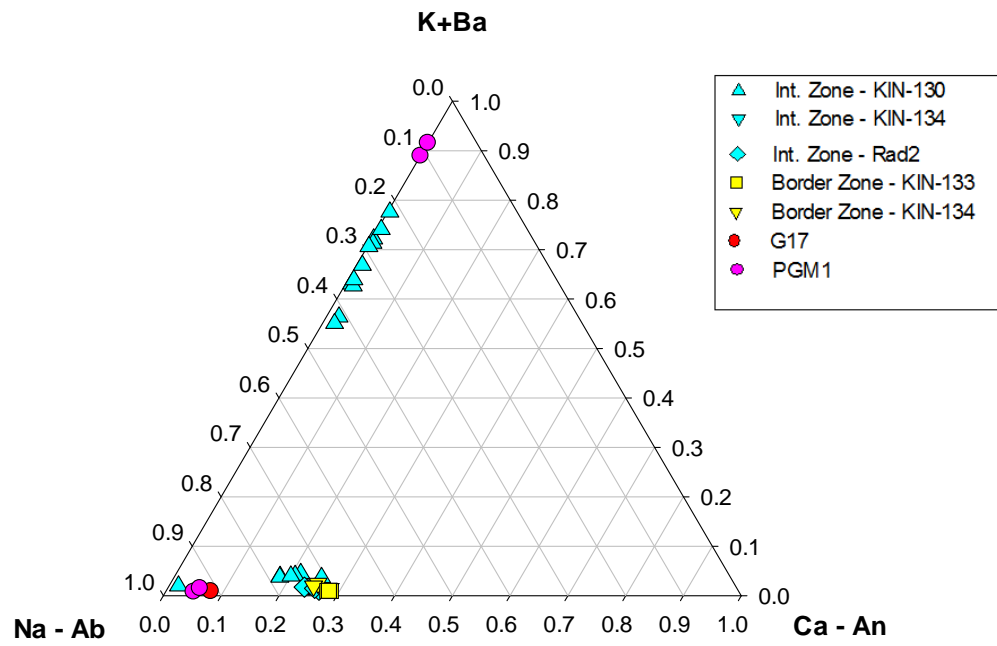


**Figure 3.1** Feldspar classification diagram.

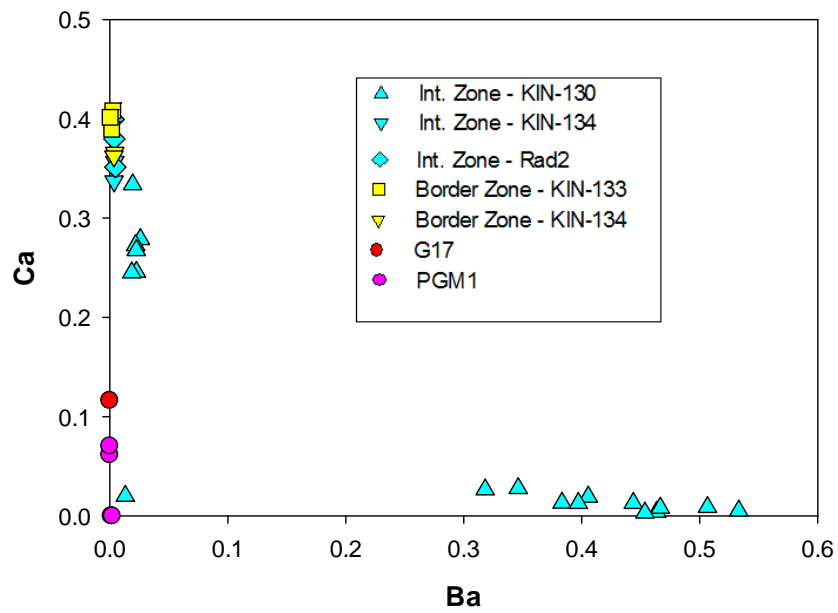


**Figure 3.2** Variation in Ba and Ca within feldspars.

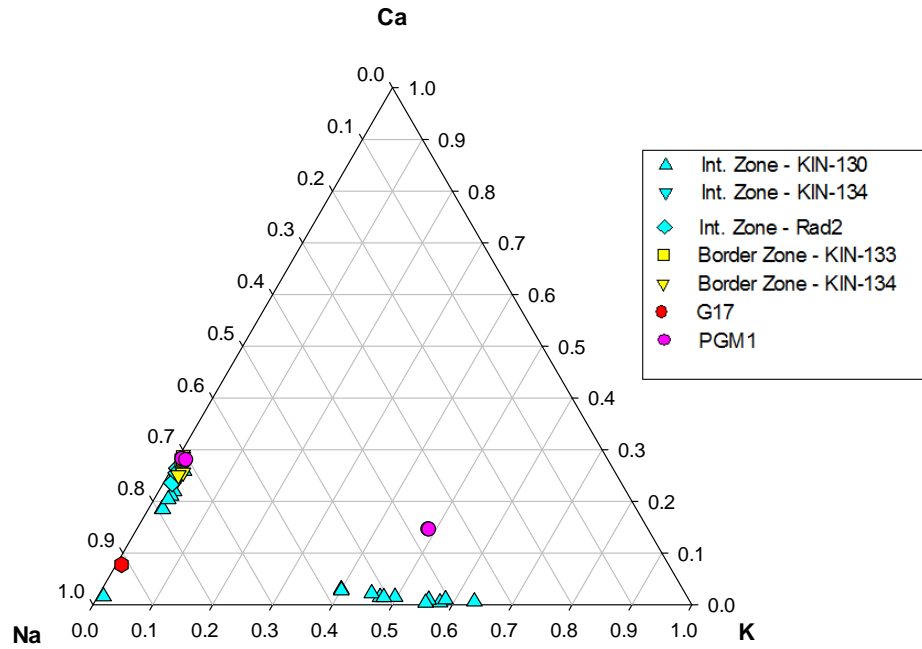


Figure 3.3 Ca, K, and Na ratios within feldspars.

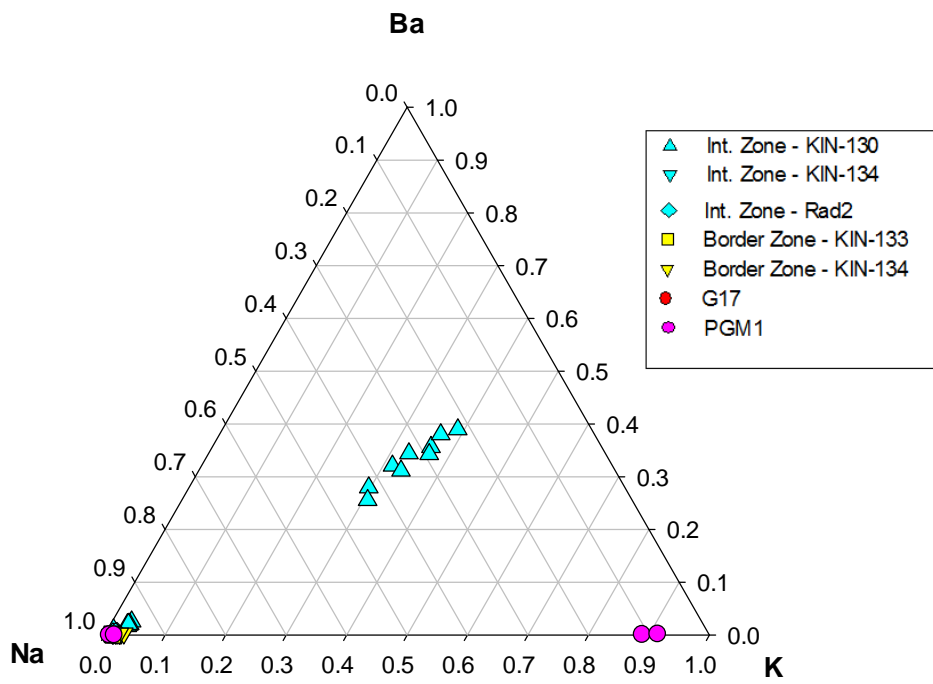
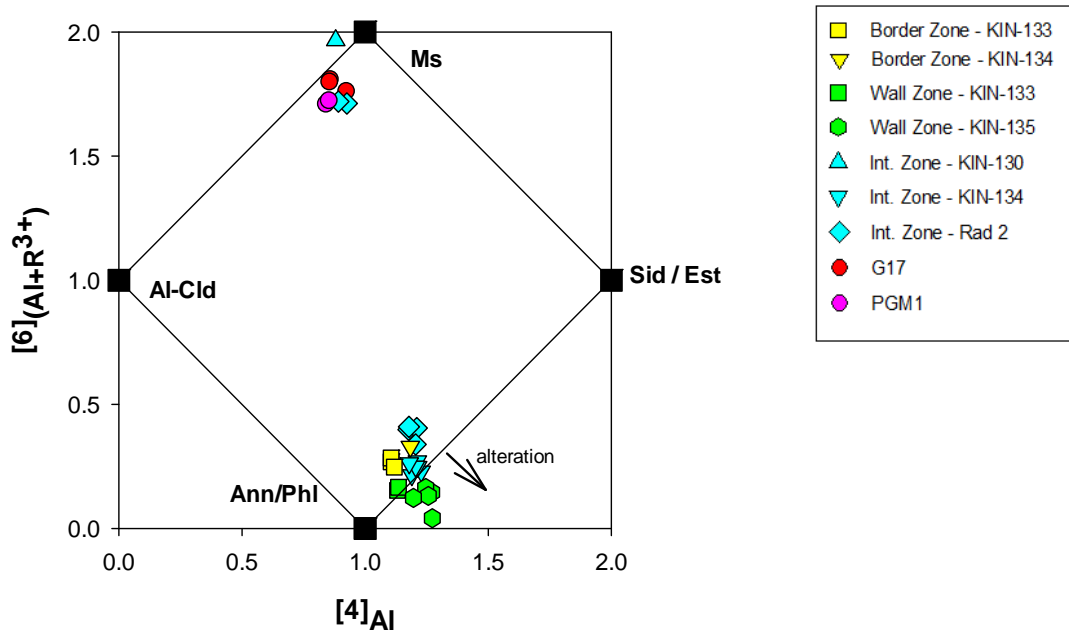


Figure 3.4 Ratios of K, Ba, and Na within feldspars. The hyalophane trend towards Na instead of K is visible.

**Table 3. 3** Mica: Thin sections and zones with analyzed samples.

Zone/Sample type	Thin Section	Biotite	Muscovite
Border Zone	KIN-133c	x	
	KIN-134-4	x	
Wall Zone	KIN-133d	x	
	KIN-135c	x	
Intermediate Zone	KIN-134-2	x	
	Rad 2a	x	x
	KIN-130b		x
Granite	G17a		x
Granitic Pegmatite	PGM 1		x



**Figure 3.5** Mica classification diagram for all KIN samples.

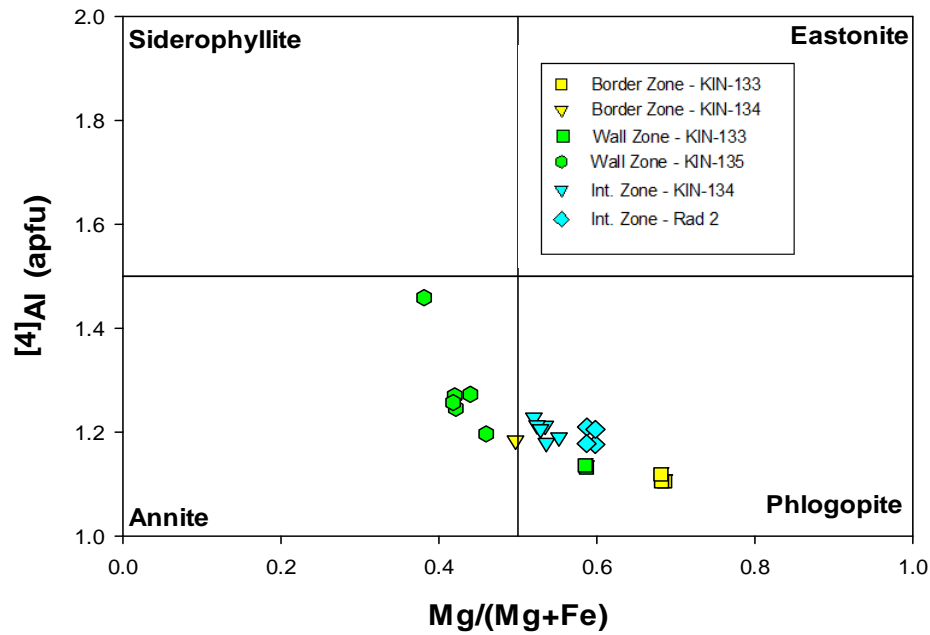


**Figure 3.6** Biotite classification diagram.

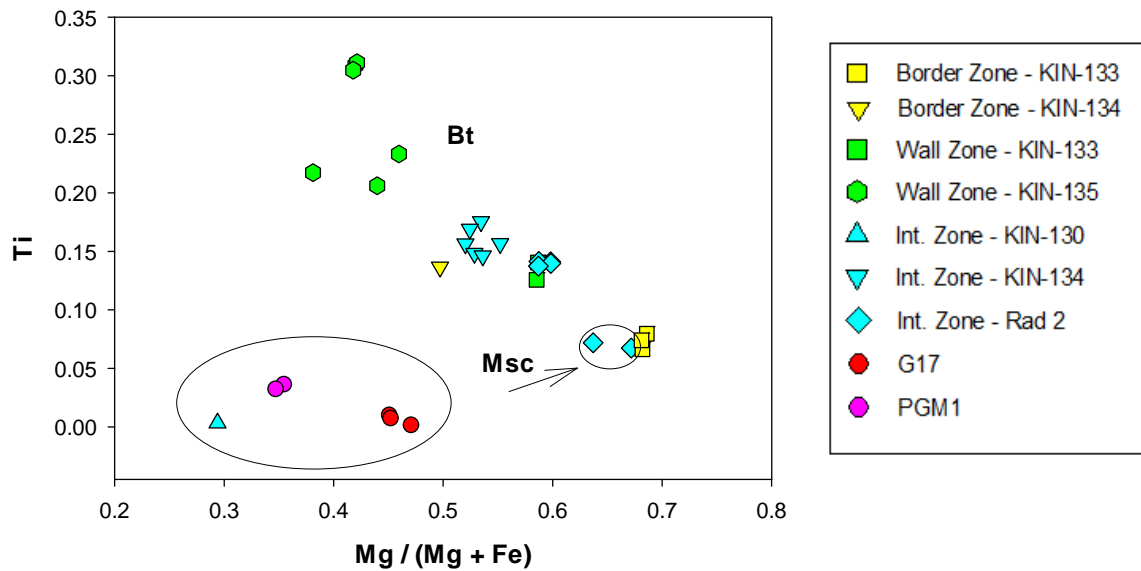


**Figure 3.7** Graph showing variations of Ti in biotite and muscovite (circled). Note higher Ti contents in lower Mg/Mg+Fe points.

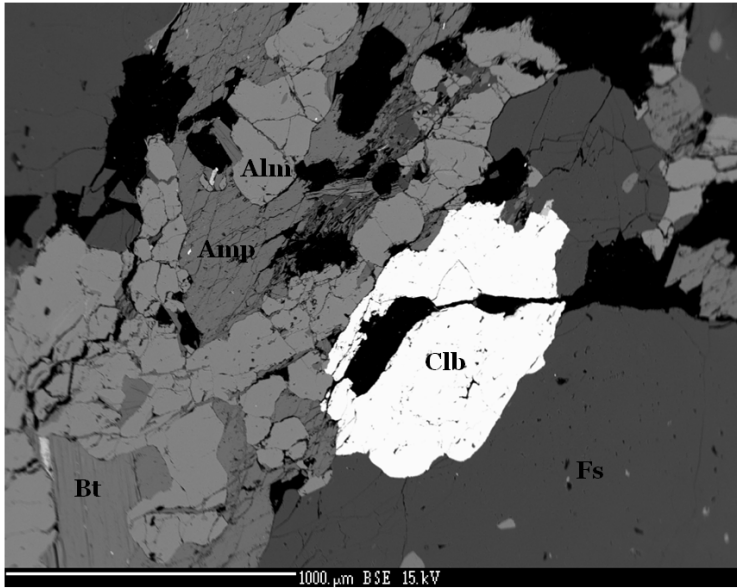


**Figure 3.8** Primary biotite with secondary almandine and primary magnesiohornblende and columbite in the wall zone at locality KIN-133.

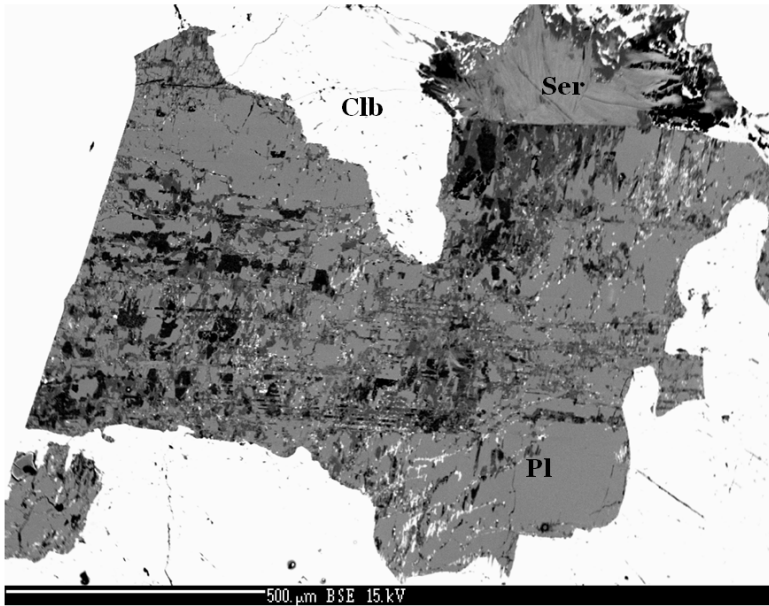


**Figure 3.9** Secondary sericite after plagioclase in the intermediate zone from locality KIN-130.

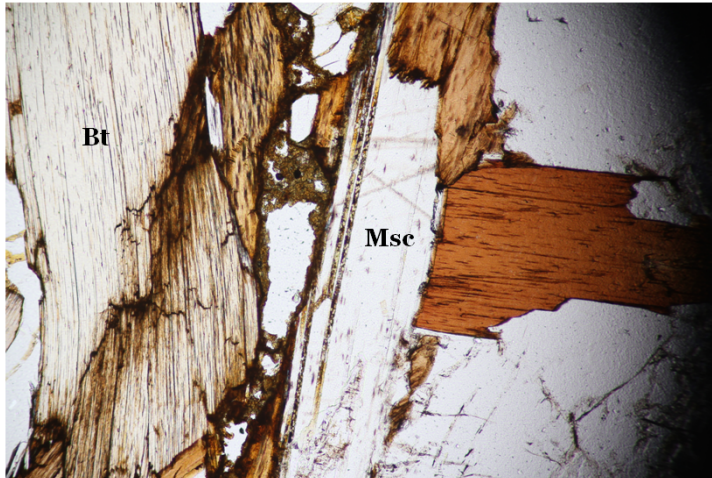


**Figure 3.10** Biotite and muscovite in association in sample Rad 2a

**Table 3. 4** Amphibole: Thin sections and zones with analyzed samples.

Zone/Sample type	Thin Section	Magnesiohornblende
Wall Zone	KIN-133d	x
	KIN-135a	x
	KIN-135c	x
Core Zone	KIN-130b-2	x

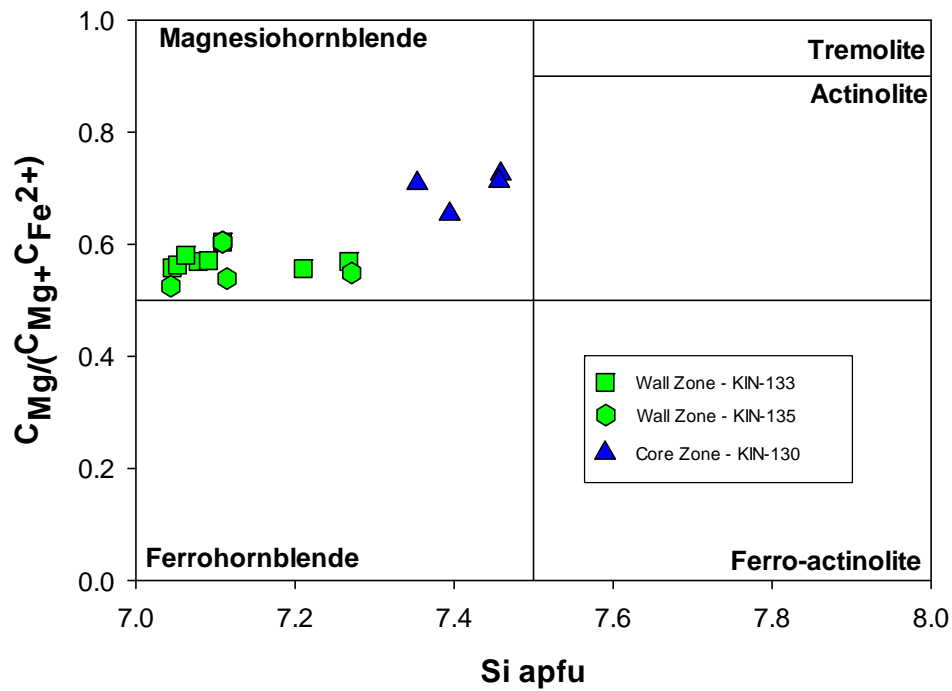
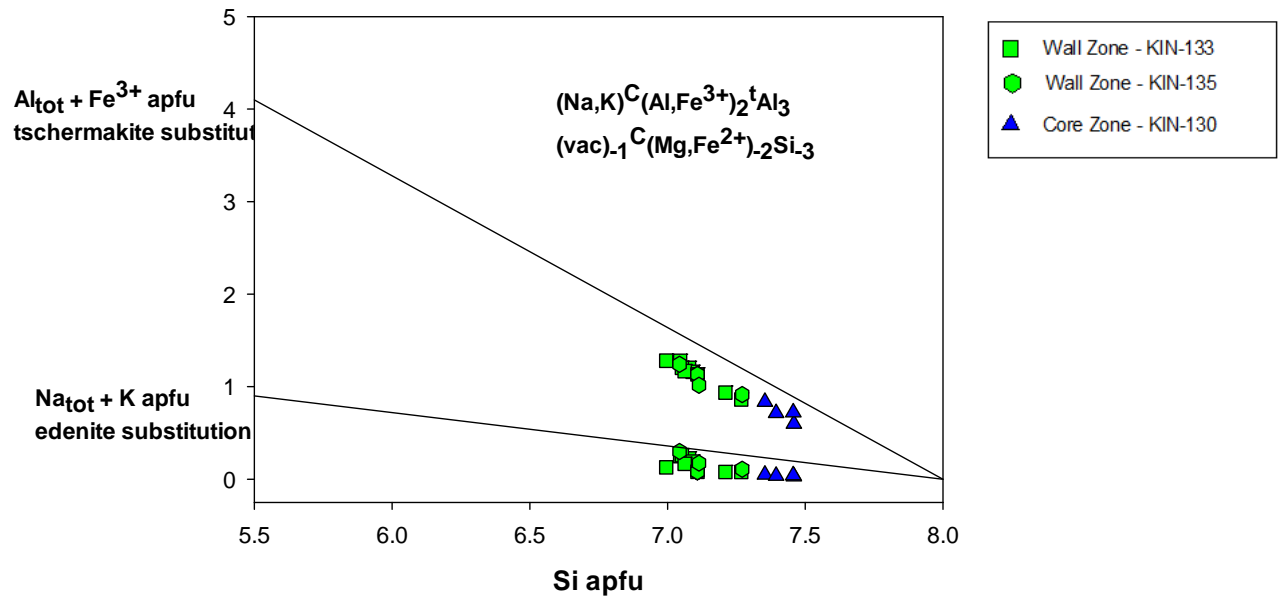
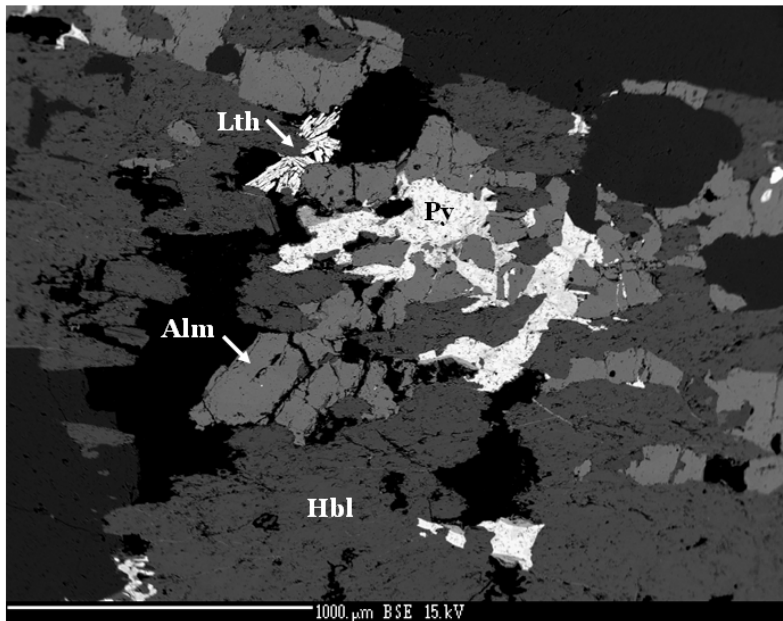


Figure 3.11 Amphibole classification diagram.



**Figure 3.12** Compositional diagram for amphibole showing tschermakite and edenite substitution trends.



**Figure 3.13** Primary magnesian hornblende with secondary almandine, pyrite, and lanthanite-(Ce) in the core at locality KIN-130.

**Table 3. 5** Garnet: Thin sections and zones with analyzed samples.

Zone/Sample type	Thin Section	Almandine	Spessartine	Type I	Type II
Border Zone	KIN-133c	x		x	
	KIN-134-4	x		x	
Wall Zone	KIN-133d	x		x	
	KIN-135a	x		x	
Intermediate Zone	KIN-1342	x		x	
Core Zone	KIN-130b-2	x	x	x	
Granite	G17a	x			x
Granitic Pegmatite	PGM 1	x			x

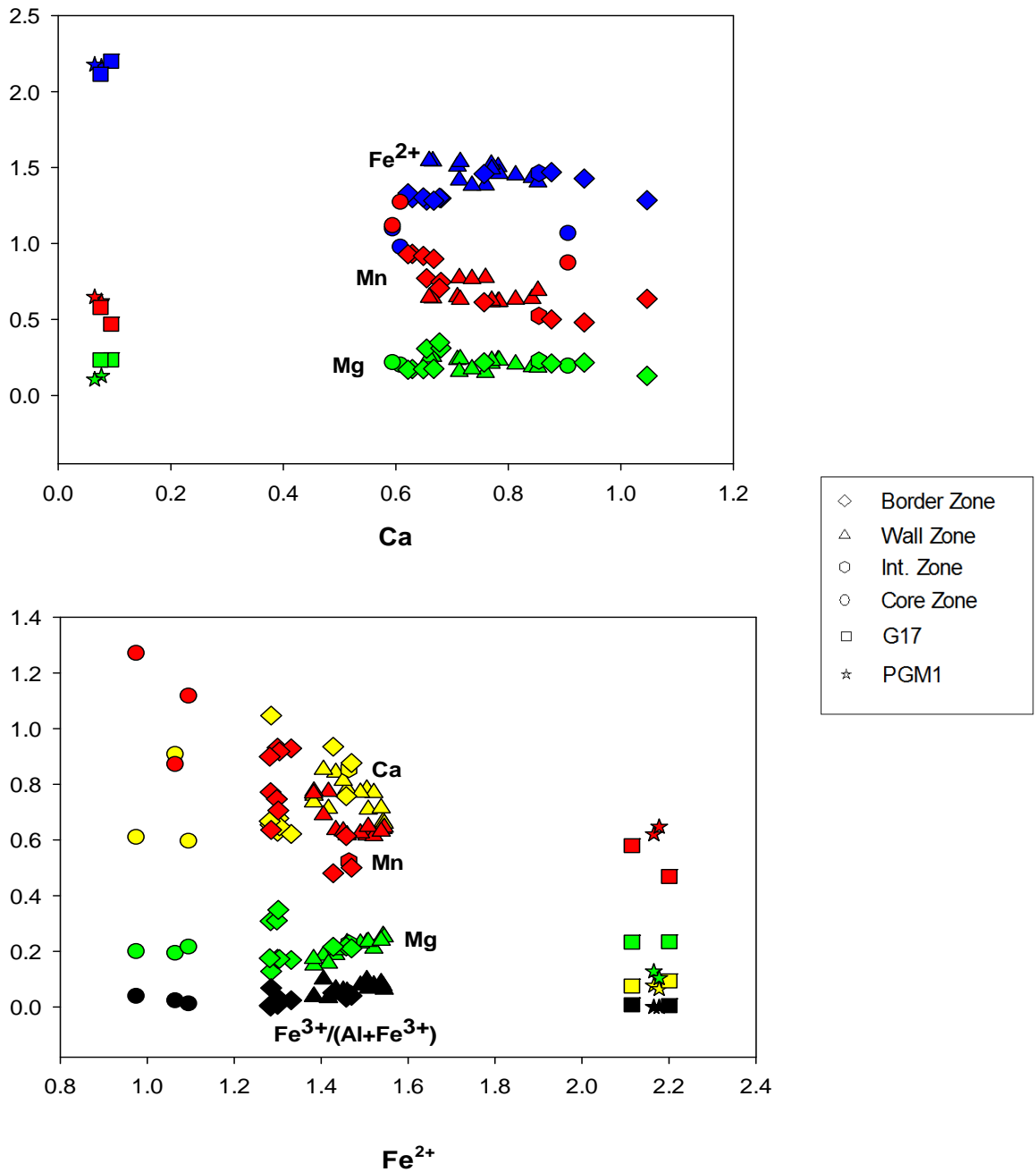


**Figure 3.14** a (top) Type I and Type II garnets differentiated by high and low Ca contents. Type I on the right, Type II on the left. Fe<sup>2+</sup> is blue, Mn is red, and Mg is green. b (below) Type I and Type II garnets differentiated by Fe<sup>2+</sup> content. Type I on the left and Type II on the right. Ca is yellow, Mn is red, Mg is green, and Fe<sup>3+</sup>/(Al+Fe<sup>3+</sup>) is black.

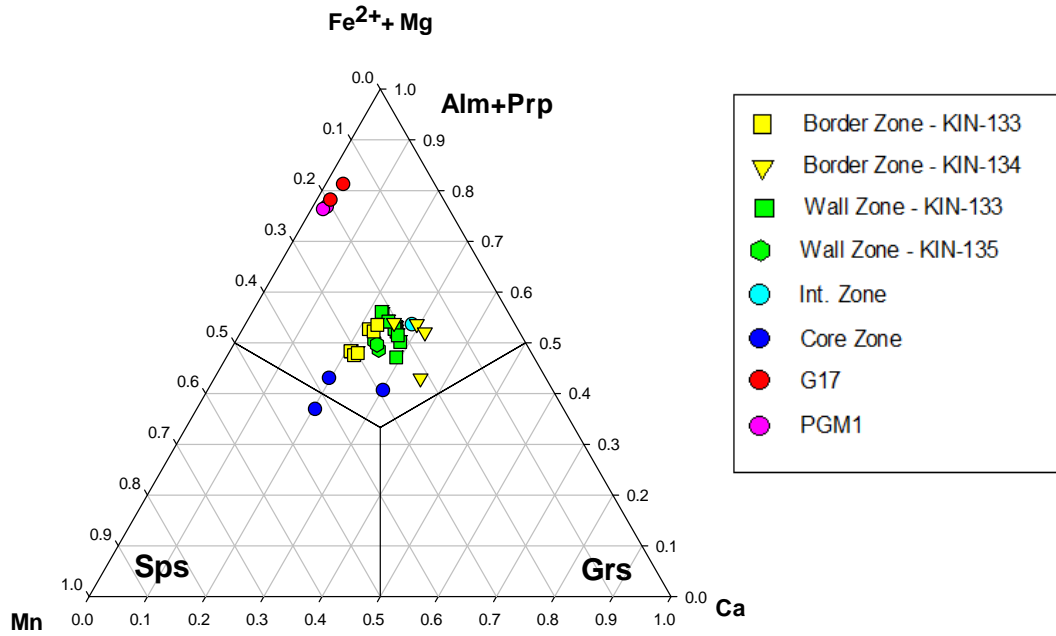


**Figure 3.15** Compositional diagram for amphibole showing tschermakite and edenite substitution trends.

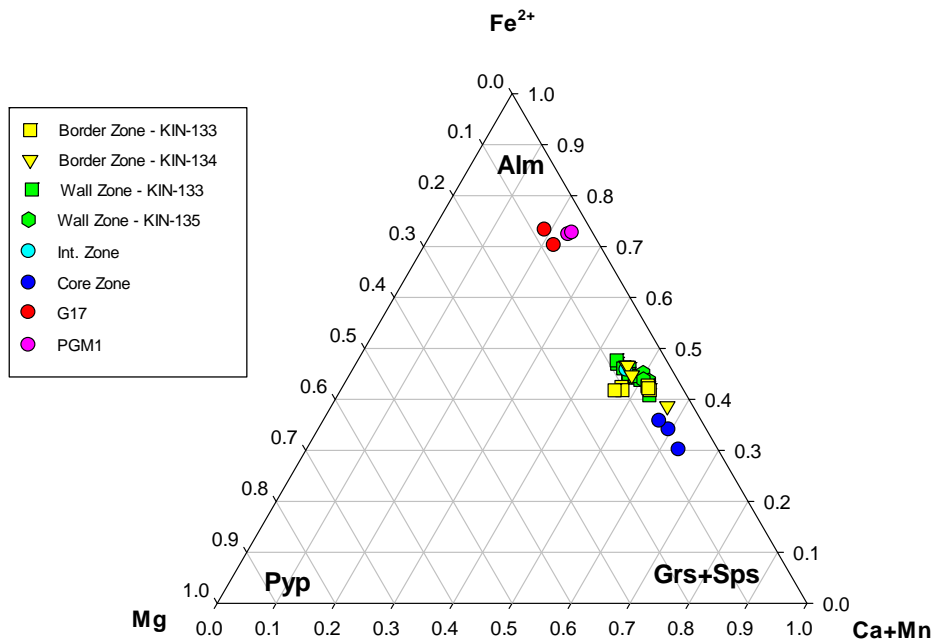


**Figure 3.16** Garnet compositional diagram showing generally low amounts of Mg present in all garnet types.

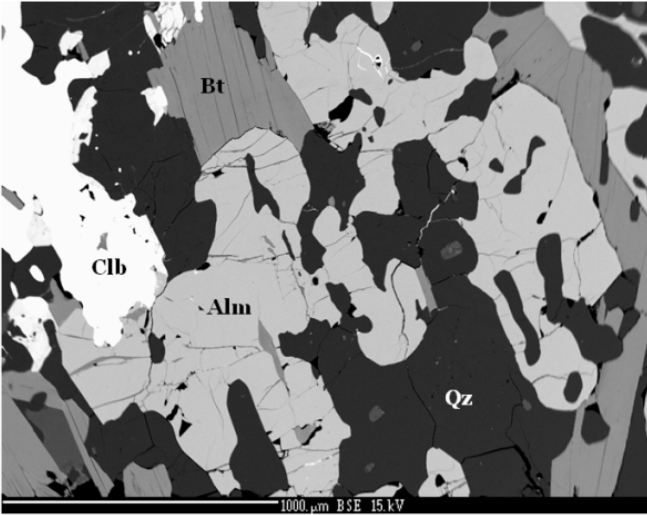


**Figure 3.17** Garnet I in quartz with poikiloblastic texture in the border zone at locality KIN-133.

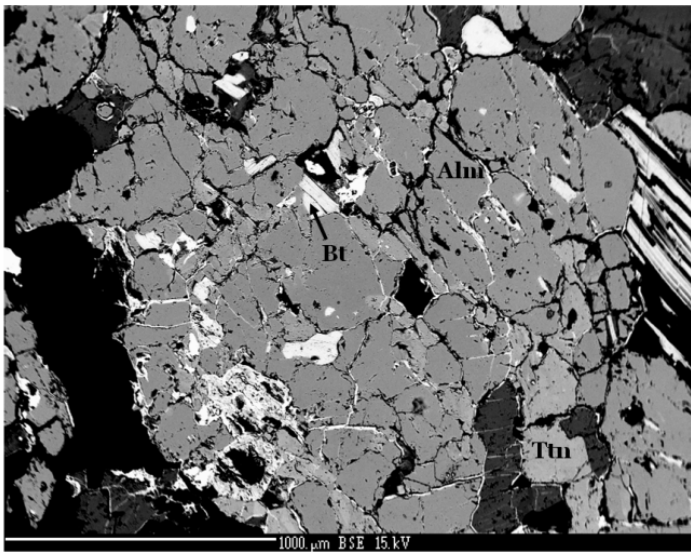


**Figure 3.18** Garnet I with titanite in the wall zone at locality KIN-135.

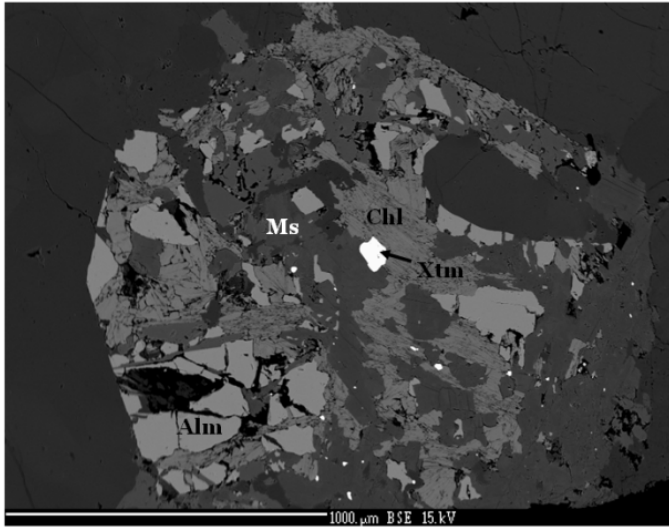


**Figure 3.19** Primary altered garnet II replaced by muscovite, chlorite, and xenotime within the granite.

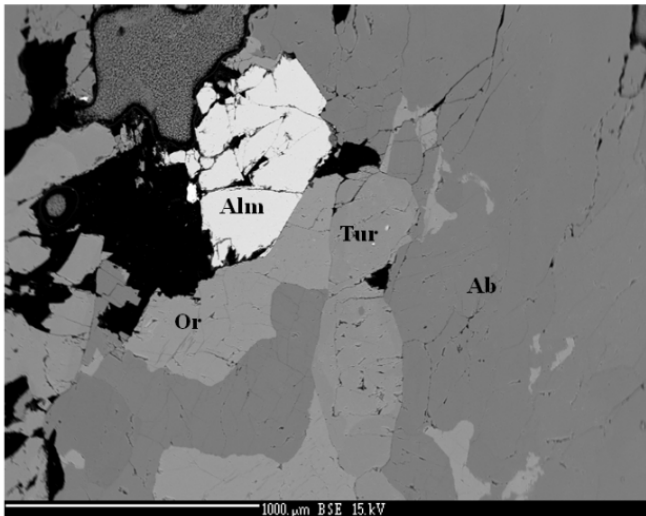


**Figure 3.20** Primary garnet II with almandine in PGM 1 with feldspar and tourmaline.

**Table 3.6** Zircon: Thin sections and zones with analyzed samples.

Zone/Sample type	Thin Section
Border Zone	KIN-133c
Wall Zone	KIN-134-4
	KIN-135a
Intermediate Zone	KIN-136
	Rad 2a
Granitic Pegmatite	PGM1

**Table 3.7** Thorite: Thin sections and zones with analyzed samples

Zone/Sample type	Thin Section
Border Zone	KIN-133c
Intermediate Zone	KIN-130a
	KIN-134-2

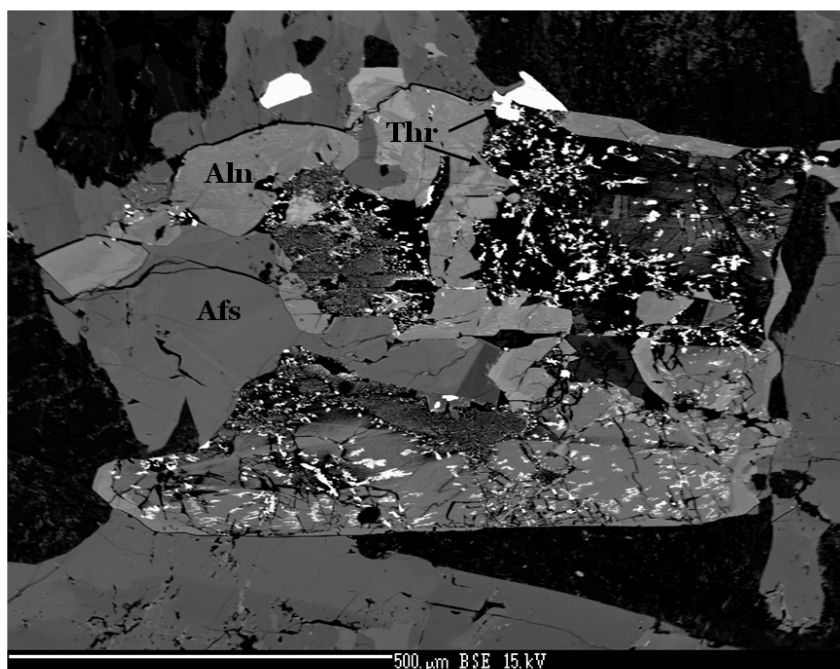


**Figure 3.21** Thorite exsolutions in allanite-(Ce) in the intermediate zone at locality KIN-130.

**Table 3.8** Titanite: sections and zones with analyzed samples.

Zone/Sample type	Thin Section
Wall Zone	KIN-133d
	KIN-135c

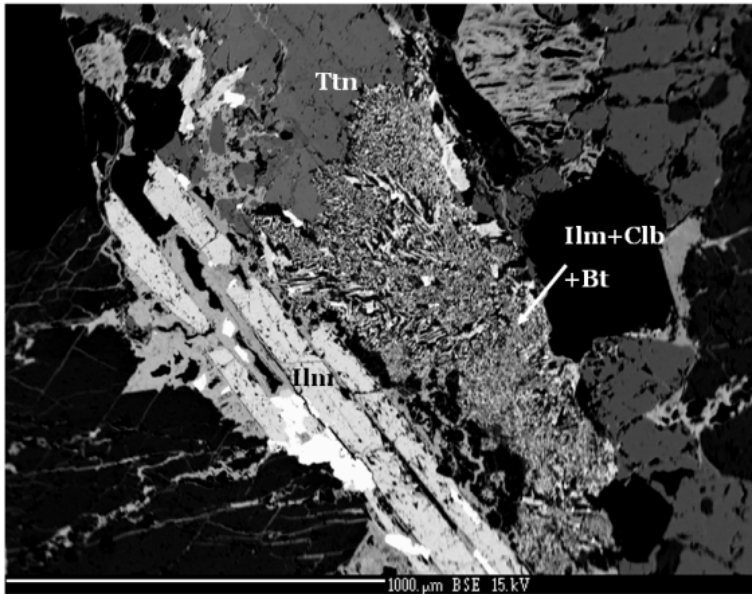


**Figure 3.22** Ilmenite II in symplectite with columbite III and phlogopite after titanite in the wall zone at locality KIN-133.

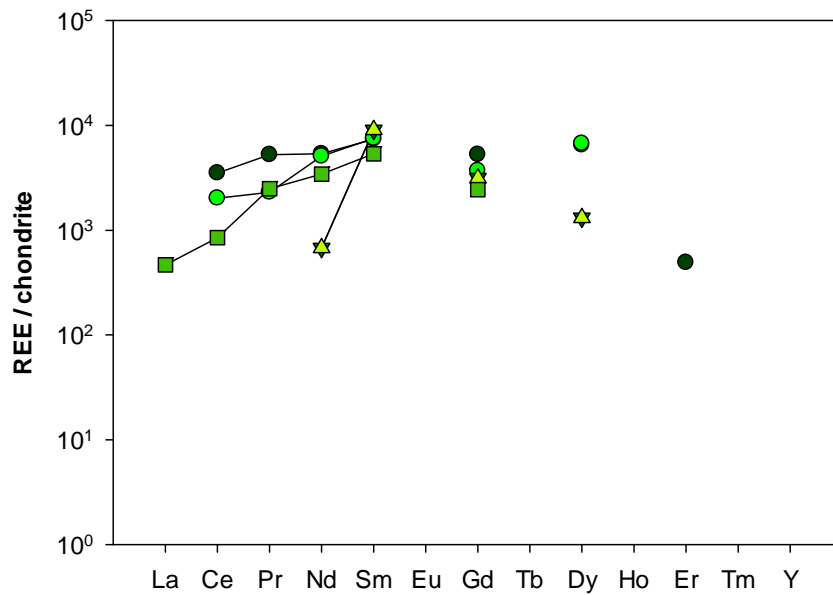


**Figure 3.23** REE levels in titanite normalized to chondrite. Each color/shape combination represents a different sample point.

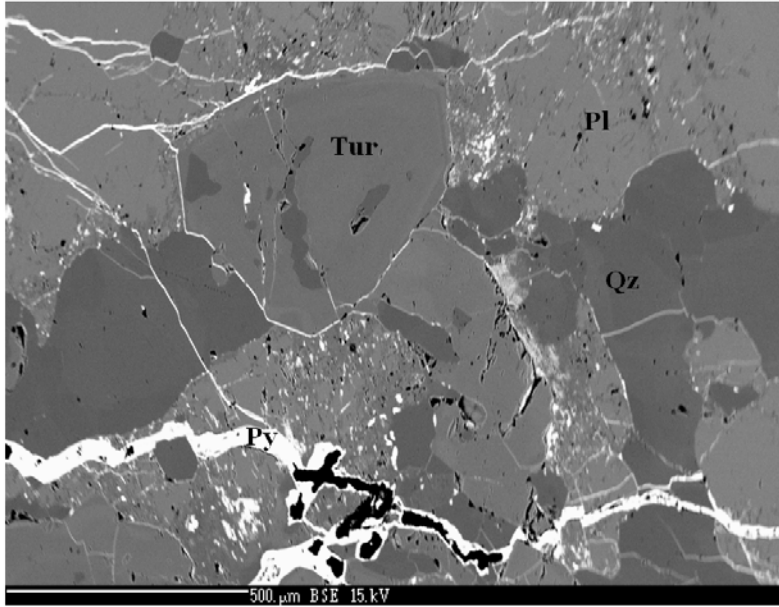


Figure 3.24 Zoned tourmaline in sample Rad 2a.

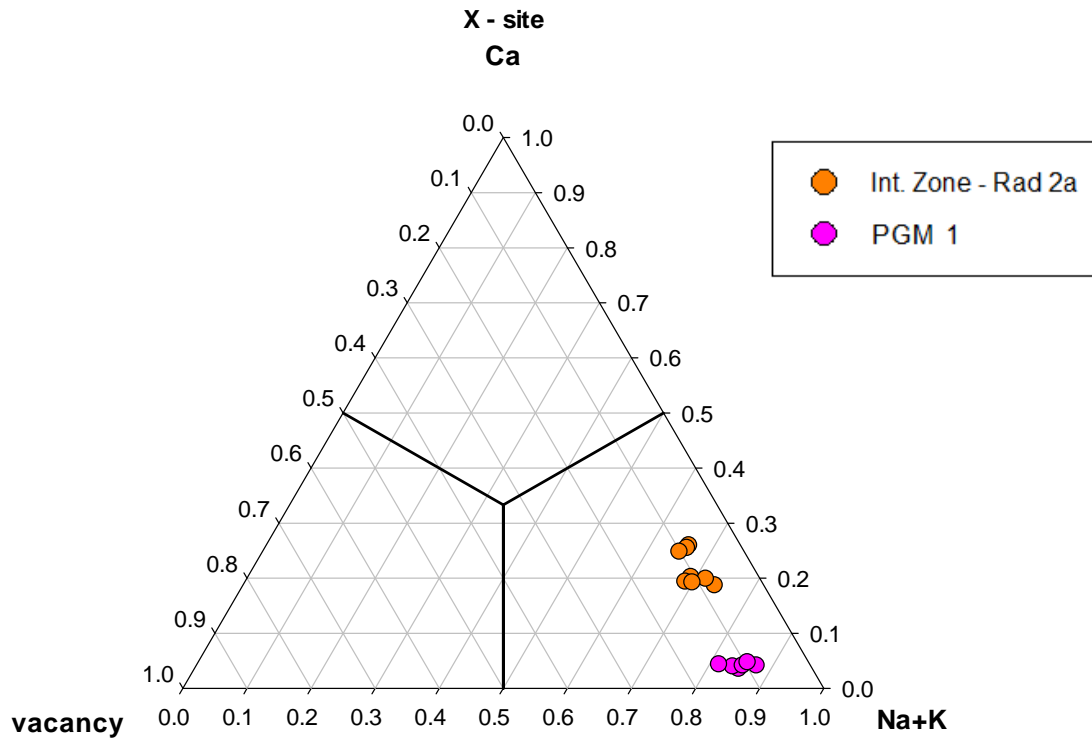


Figure 3.25 Classification diagram for tourmaline using X-site cation ratios.

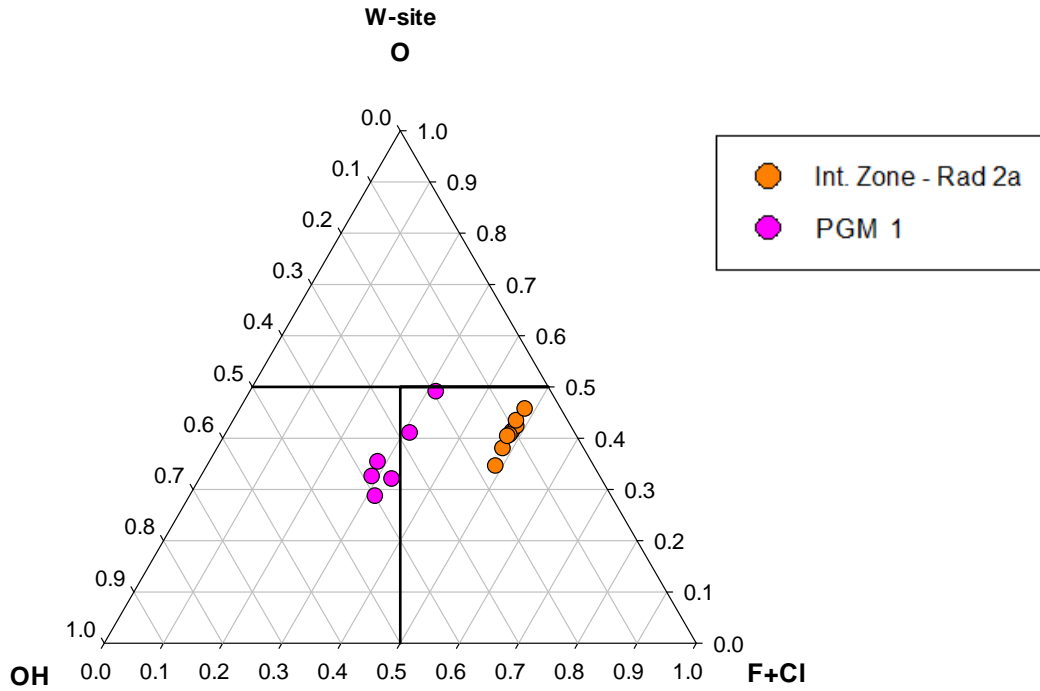


Figure 3.26 Classification diagram for tourmaline using W-site cation ratios.

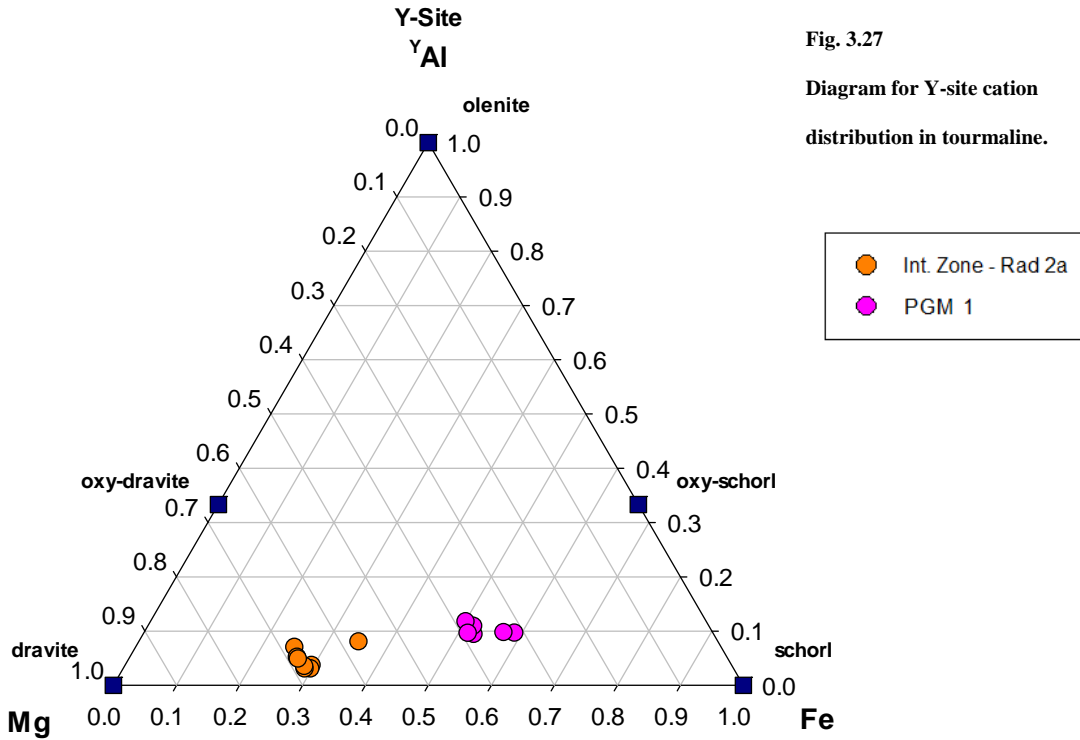
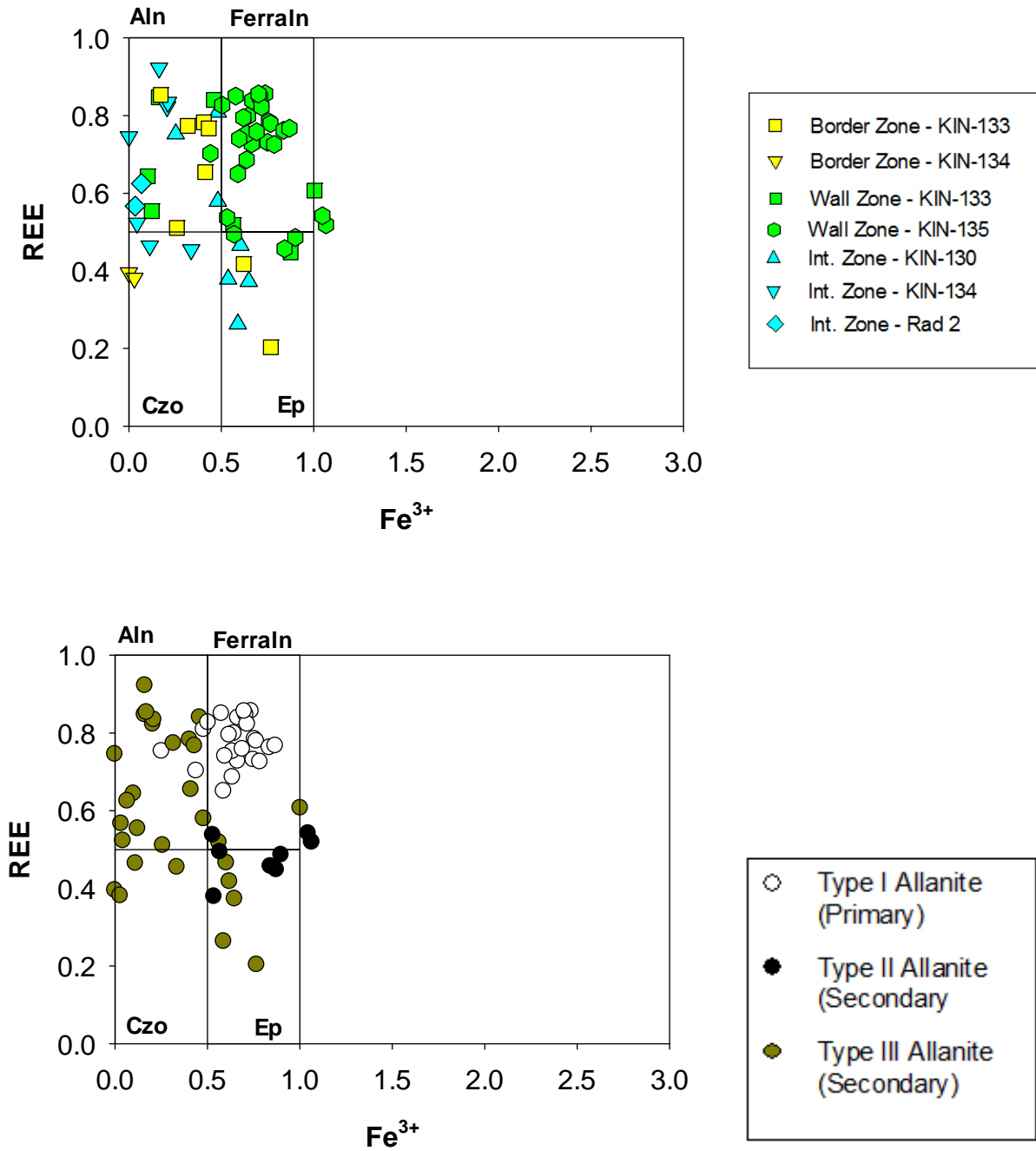


Fig. 3.27  
Diagram for Y-site cation distribution in tourmaline.

Figure 3.27 Classification diagram for tourmaline using Y-site cation ratios.

**Table 3.9** Epidote Group Minerals: Thin sections and zones with analyzed samples.

Zone/Sample type	Thin Section	Allanite I	Allanite II	Allanite III
Border Zone	KIN-133c			x
	KIN-134-4			x
Wall Zone	KIN-133d	x	x	±x
	KIN-135a	x	x	±x
	KIN-135c	x	x	±x
Intermediate Zone	KIN-130a			x
	KIN-130b			x
	KIN-134-2			x
	Rad 2a			x



**Figure 3.28** EGM classification diagram. The same data sets are present in both diagrams, however a (top) shows the classification based on zone and locality whereas b (bottom) shows the classification based on allanite type (classification based on Armbruster et al., 2006 and Ercit, 2002).

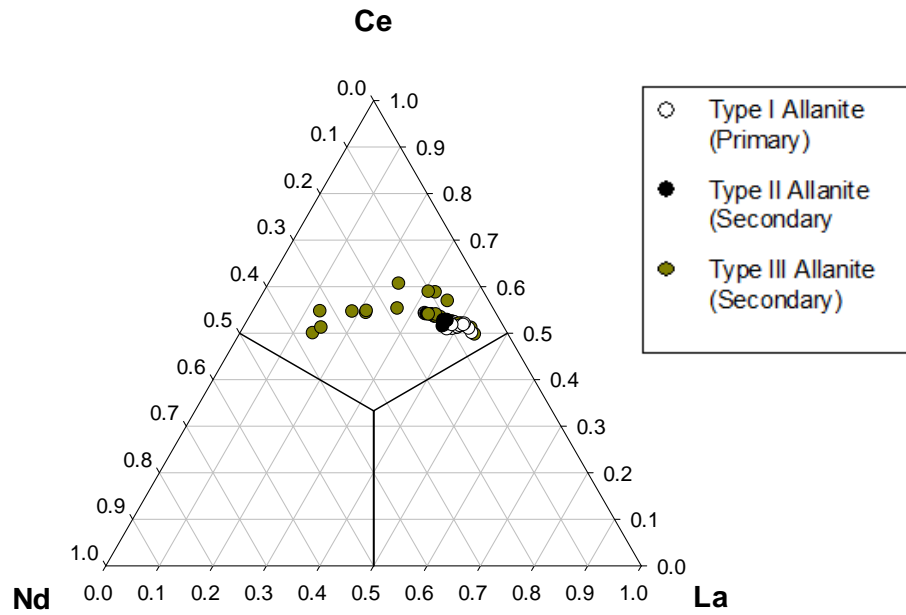


**Figure 3.29** REE distribution within EGM.

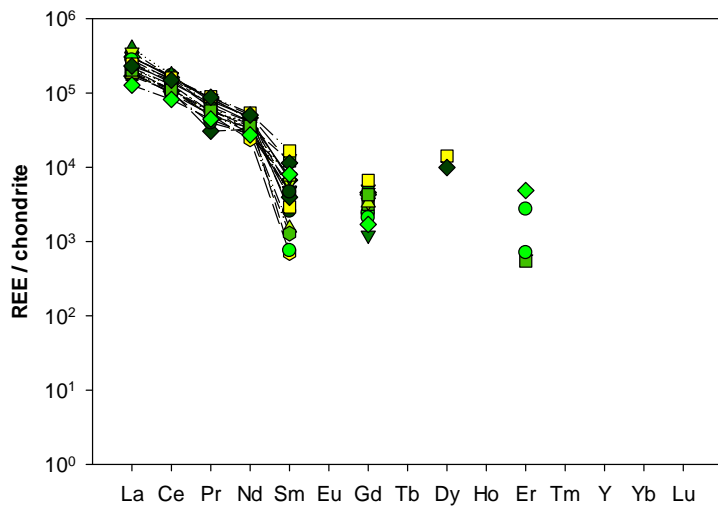


**Figure 3.30** REE levels in EGM normalized to chondrite. Each color/shape combination represents a different sample point.

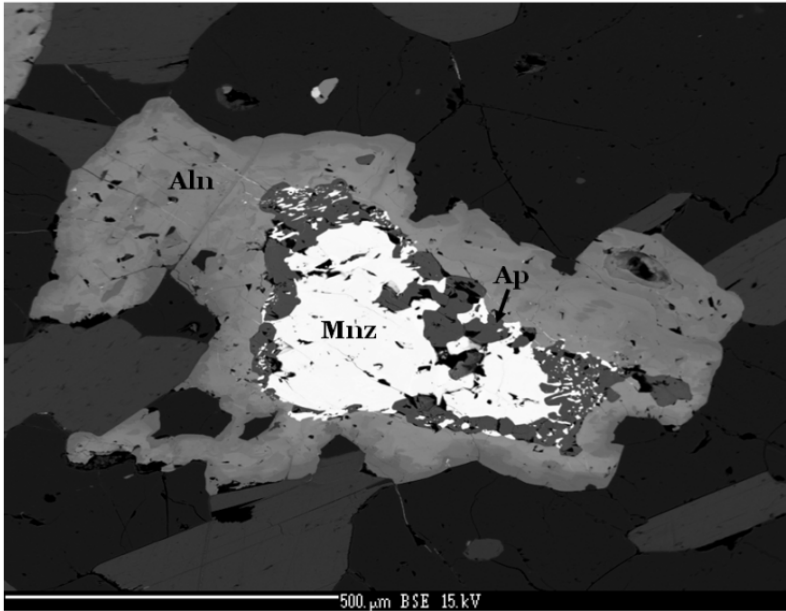


**Figure 3.31** Allanite III after primary monazite in the border zone at locality KIN-133.

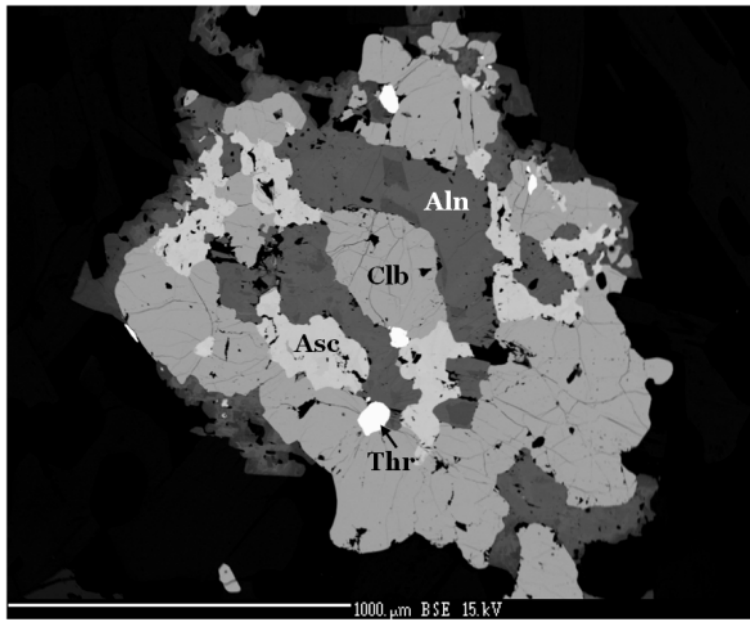


**Figure 3.32** Secondary allanite III with secondary aeschnite-(Ce) with ferrocolumbite in the border zone at locality KIN-133.

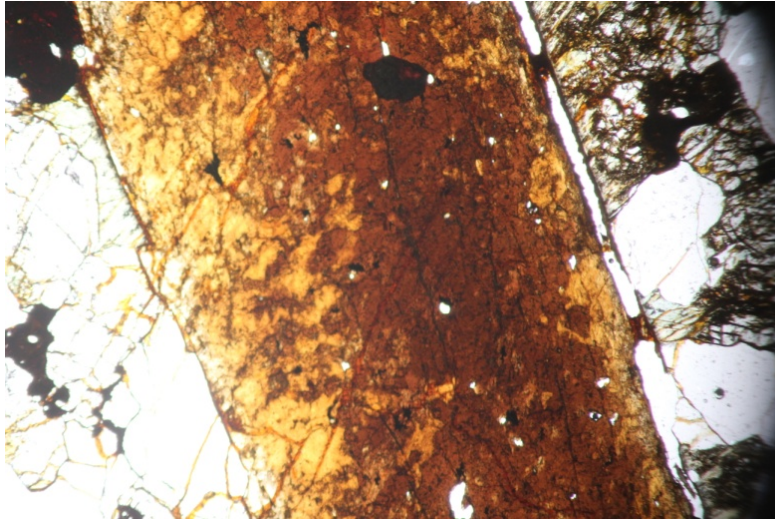


**Figure 3.33** Large, zoned, allanite I/II crystal in the wall zone at locality KIN-135.

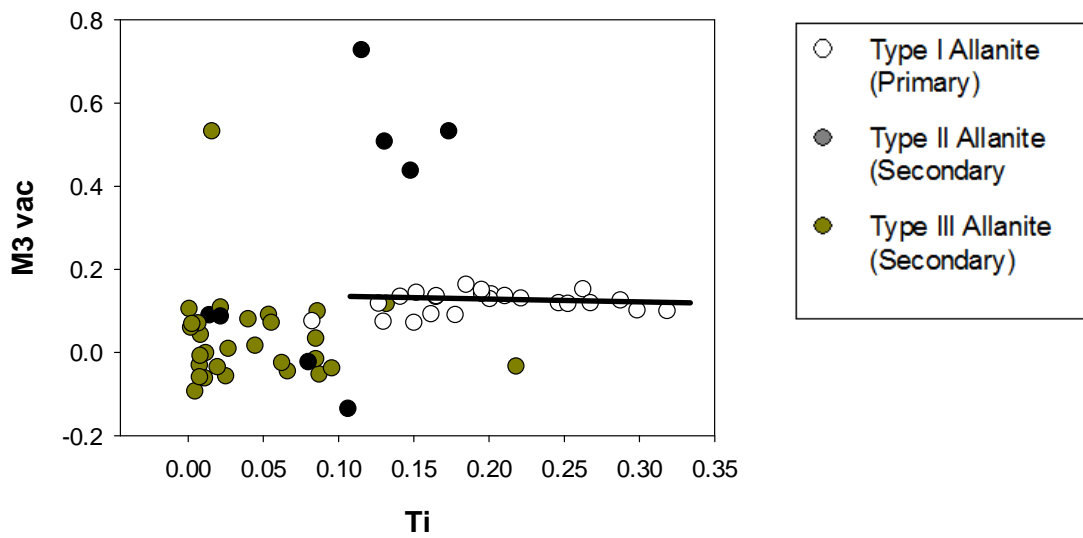


**Figure 3.34** M3 –site vacancies in allanite. The line is to draw attention to the similar level found within the primary allanite I grains.

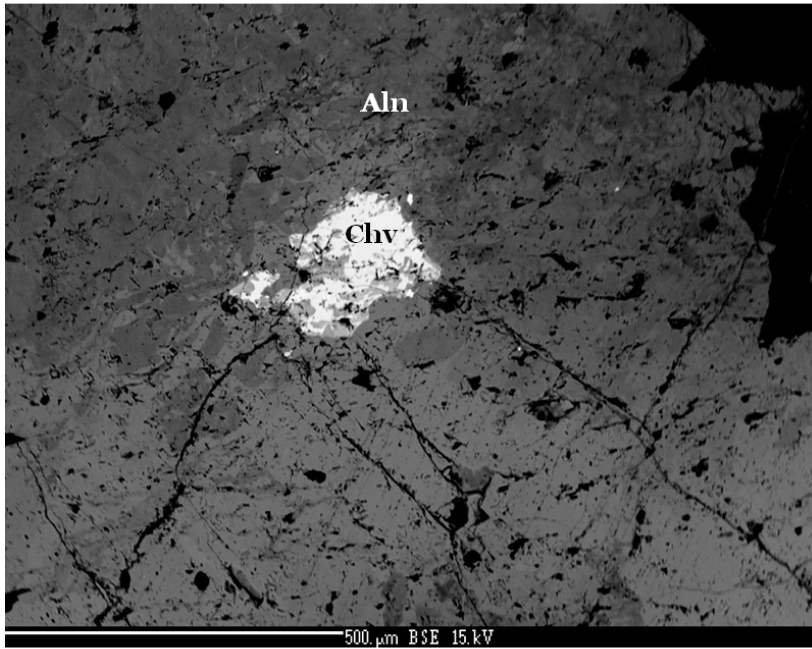


**Figure 3.35** Zone allanite I (and II on edges) with an inclusion of chevkinite in the wall zone at locality KIN-133.

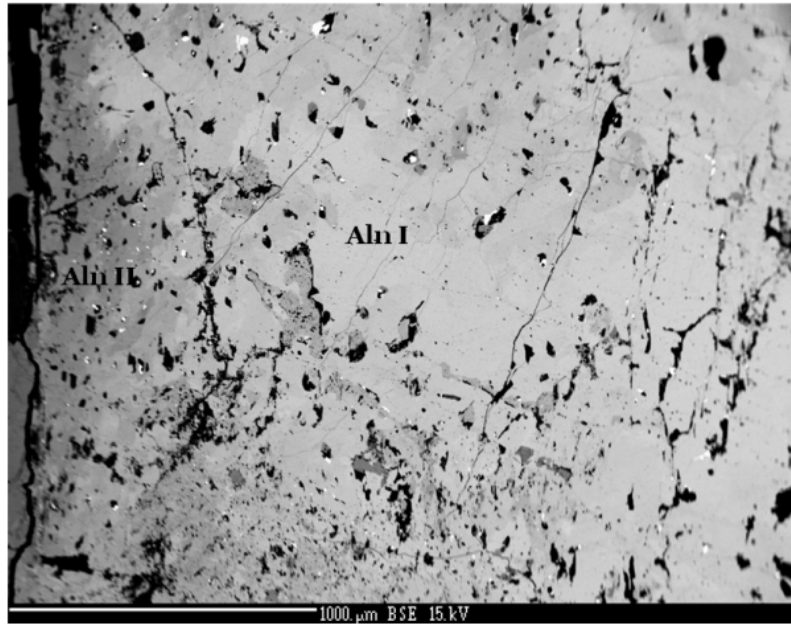


**Figure 3.36** Zoned allanite III in the intermediate zone (130a).

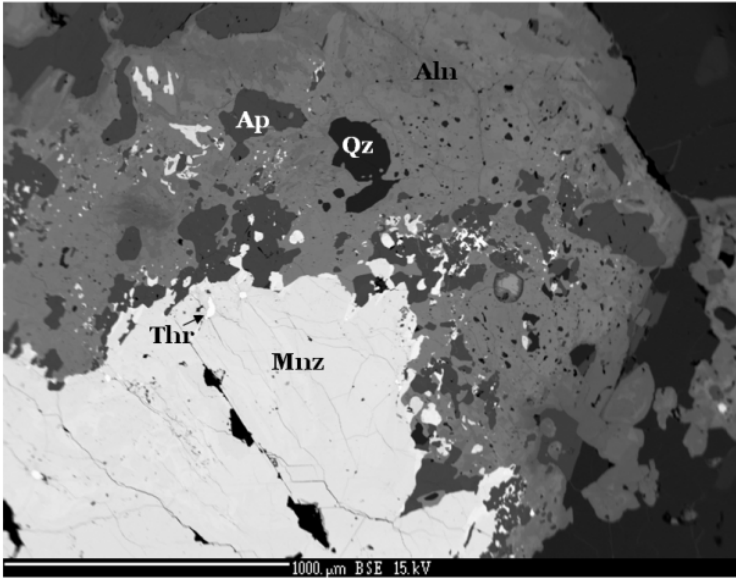


**Figure 3.37** Secondary allanite III after monazite-(Ce) with apatite and thorite from the intermediate zone at locality KIN-134.

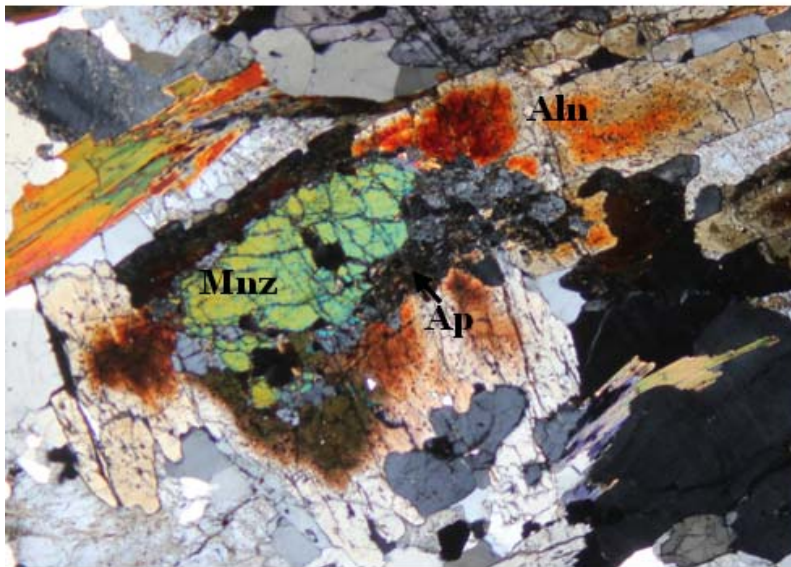


**Figure 3.38** Secondary allanite III after monazite with apatite in the intermediate zone at locality KIN-134.

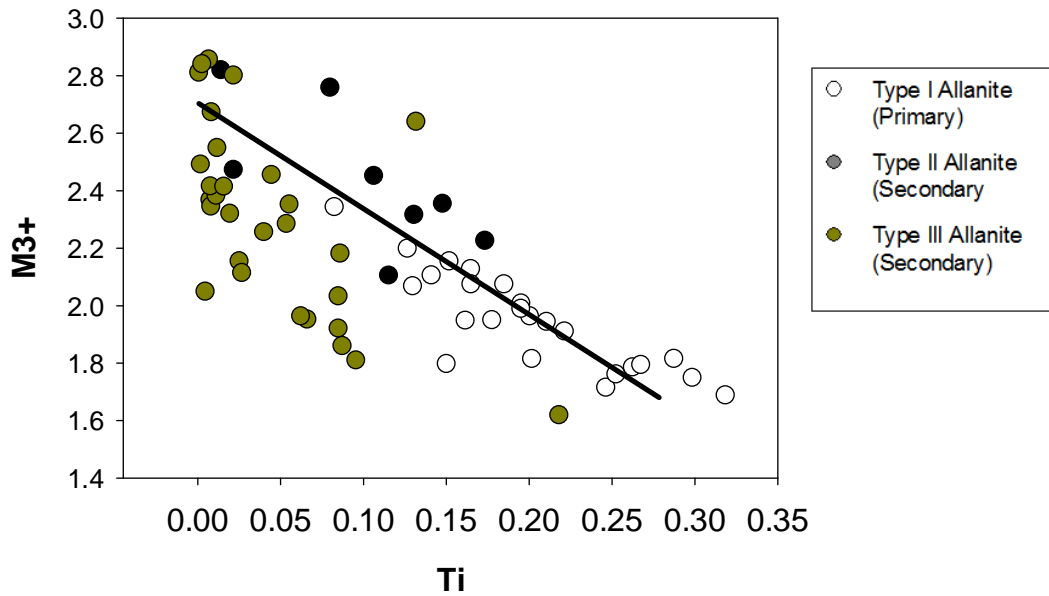


**Figure 3.39**  $M^{3+}$  vs Ti for allanite grains. The line is to draw attention to the trend found within the primary allanite I grains.

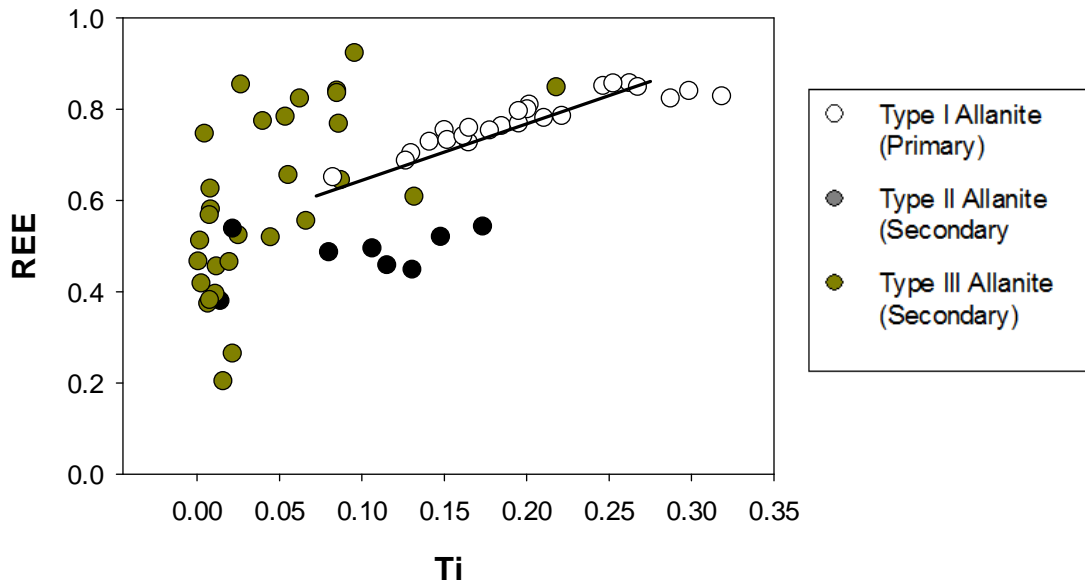


**Figure 3.40** REE vs Ti for allanite grains. The line is to draw attention to the trend found within the primary allanite I grains.

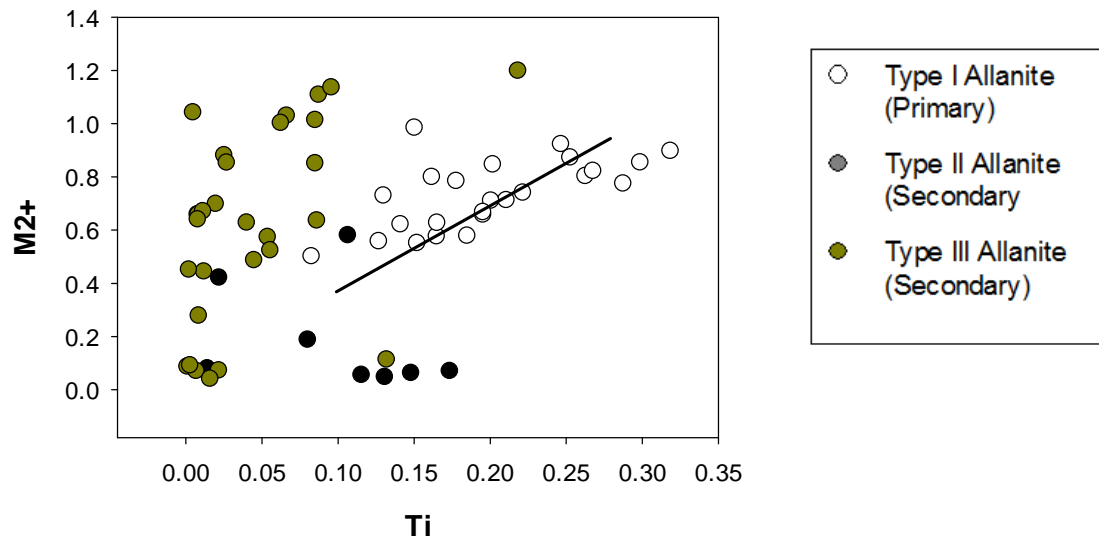


**Figure 3.41**  $M^{2+}$  vs. Ti for allanite grains. The line is to draw attention to the trend found within the primary allanite I grains.

**Table 3.10** Chevkinite: Thin sections and zones with analyzed samples.

Table 3.10 Chevkinite Group Minerals: Thin sections and zones with analyzed samples			
Zone/Sample type	Thin Section	Chevkinite	Perrierite
Wall Zone	KIN-133d	x	
	KIN-135a	x	
	KIN-135c	x	x
Intermediate Zone	KIN-134-2	x	

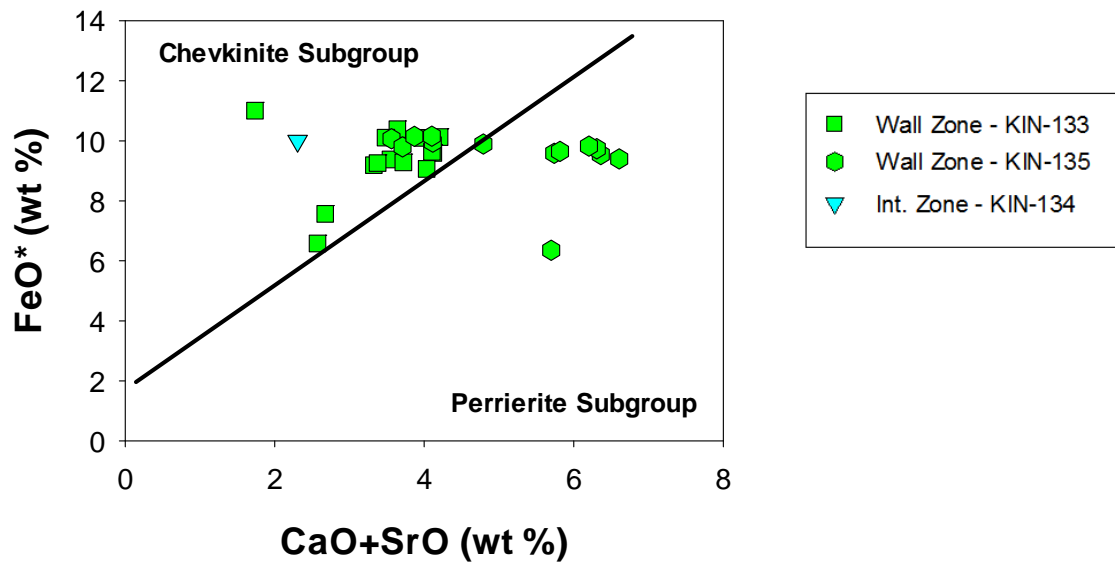


**Figure 3.42** Distribution of chevkinite and perrierite subgroup samples (Modeled after Macdonald and Belkin, 2002).

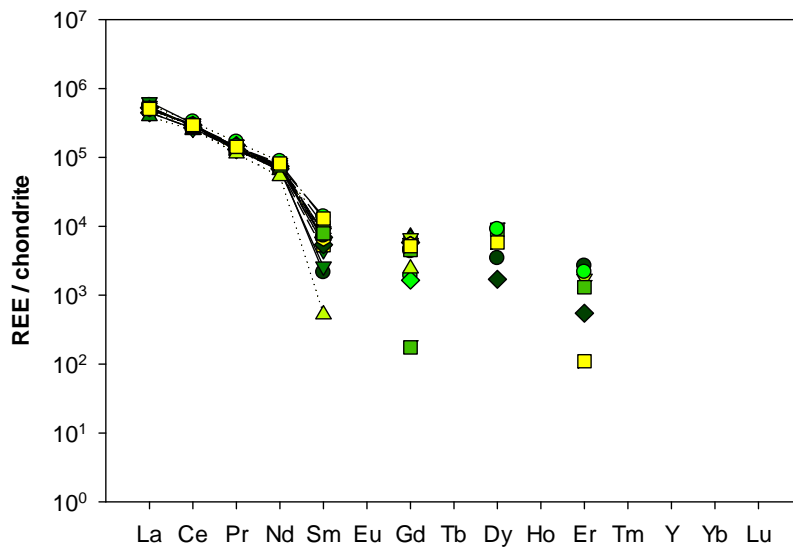


**Figure 3.43** REE amounts present in chevkinite normalized to chondrite. Each color/shape combination represents a different sample point.

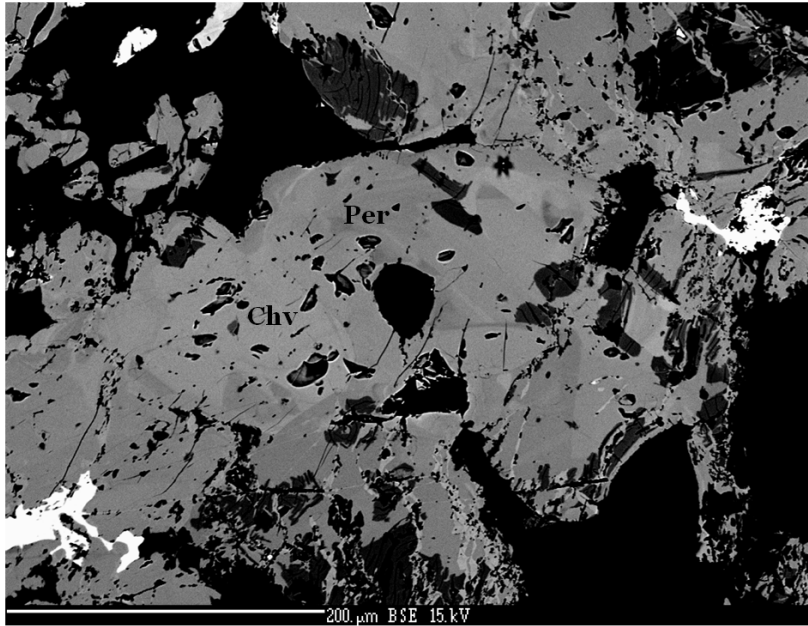


**Figure 3.44** Primary chevkinite and secondary perrierite present in the wall zone at locality KIN-135.

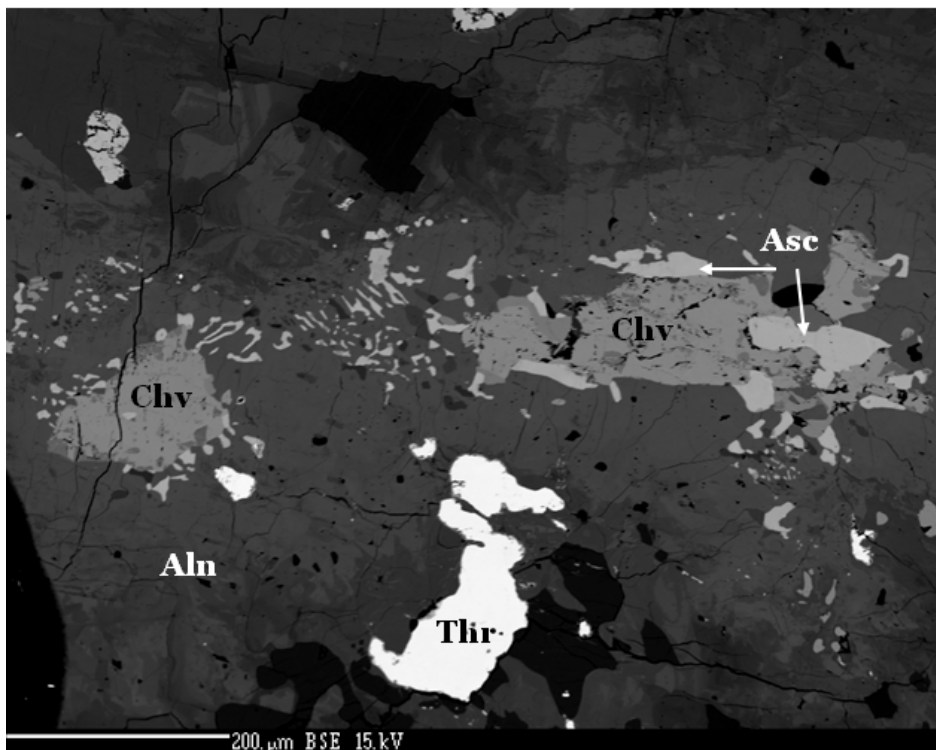


**Figure 3.45** Primary chevkinite with partial replacement by aeschynite in allanite.

**Table 3.11** Monazite: Thin sections and zones with analyzed samples.

Zone/Sample type	Thin Section
Border Zone	KIN-133c
Wall Zone	KIN-133d
Intermediate Zone	KIN-134-2
	KIN-136
	Rad 2a
Granitic Pegmatite	PGM 1

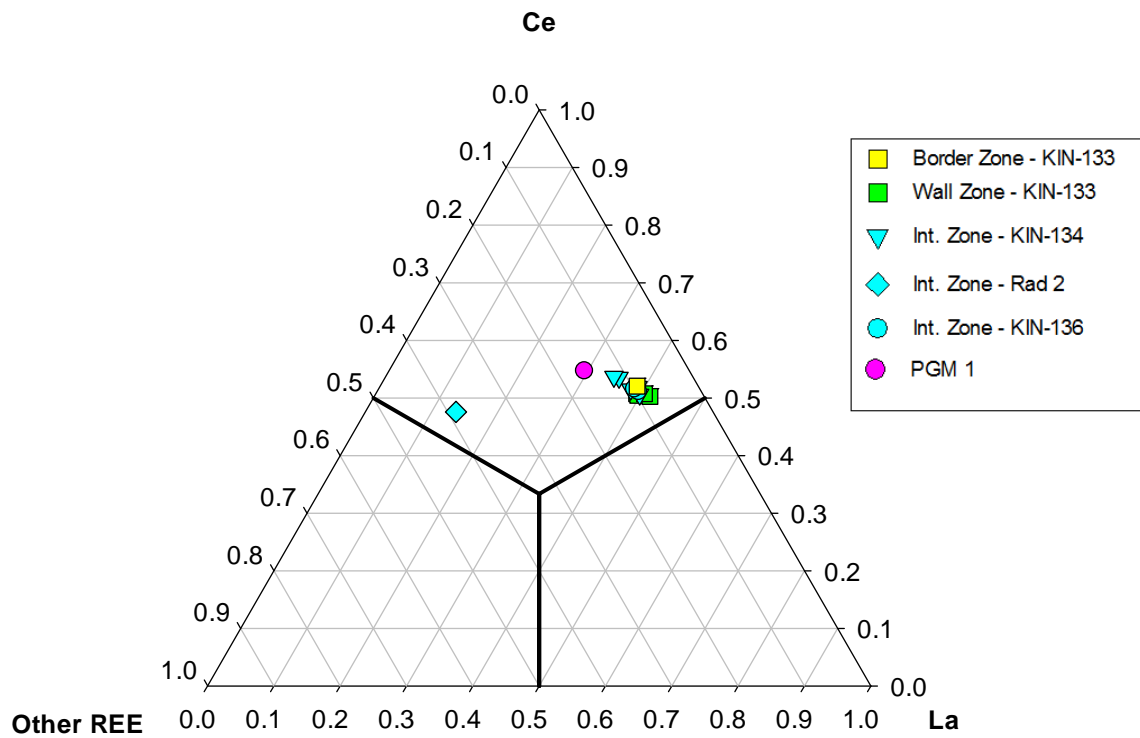


**Figure 3.46** REE distribution within monazite.

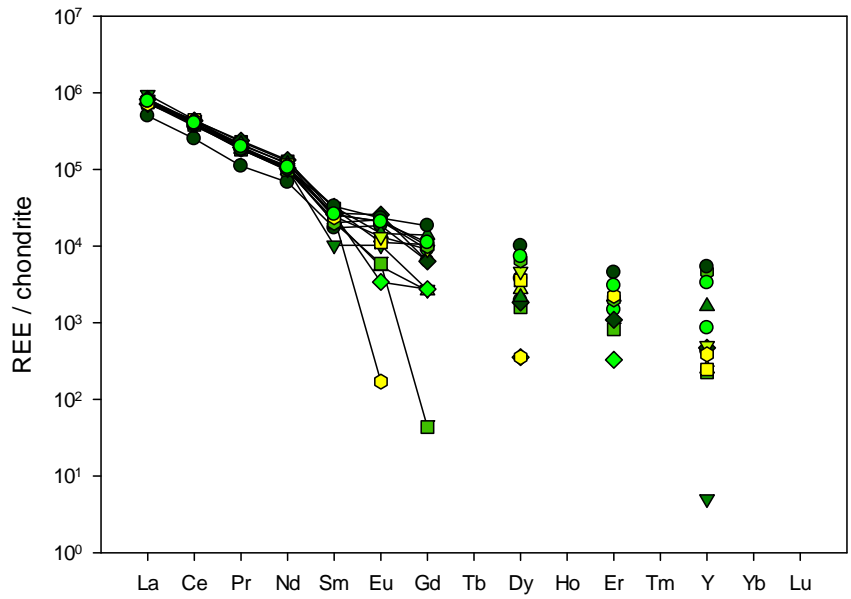


**Figure 3.47** REE values present in monazite normalized to chondrite. Each color/shape combination represents a different sample point.

Huttonite/Cheralite Substitutions - Ondrejka 2012

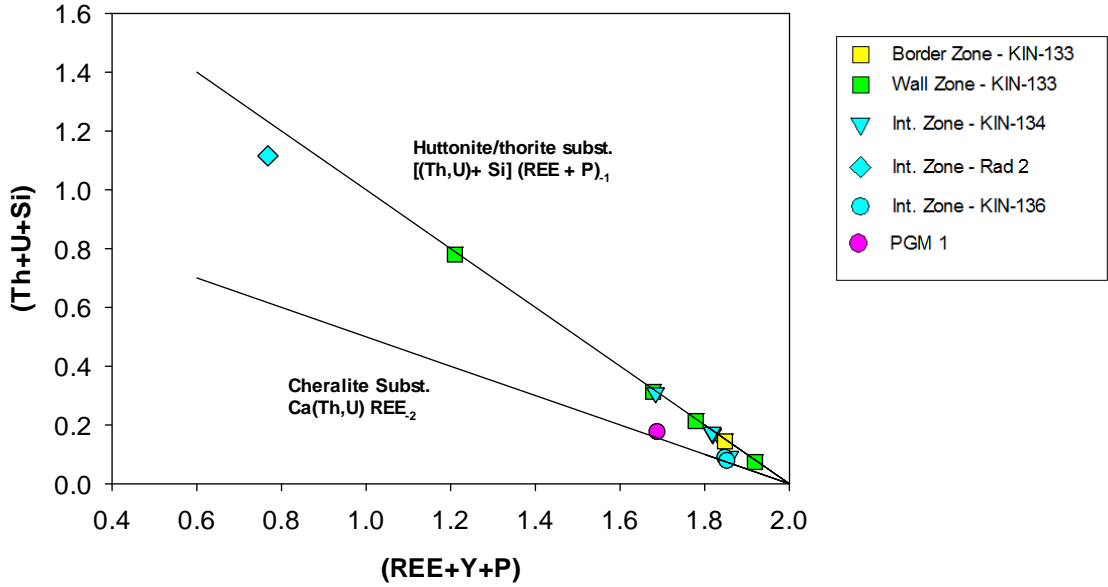


**Figure 3.48** Huttonite/thorite and cheralite substitution trends in monazite (based on Ondrejka, 2012).

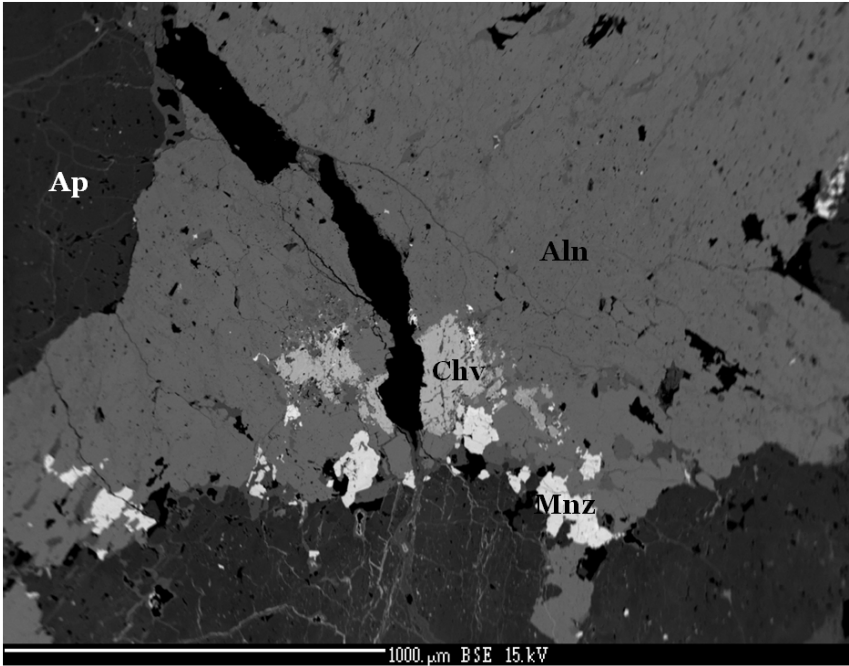


**Figure 3. 49** Primary monazite with secondary allanite and apatite with chevkinite in the wall zone at locality KIN-133.

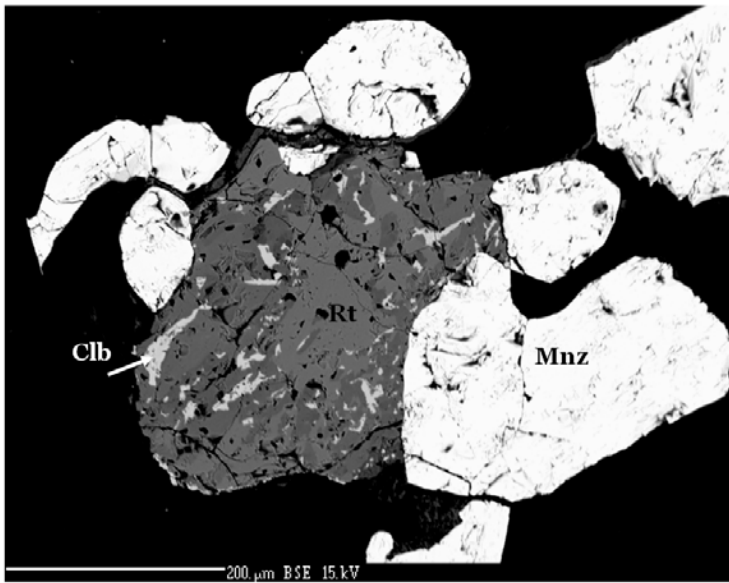


**Figure 3. 50** Monazite in sample KIN 136 with rutile and exsolved columbite IV.

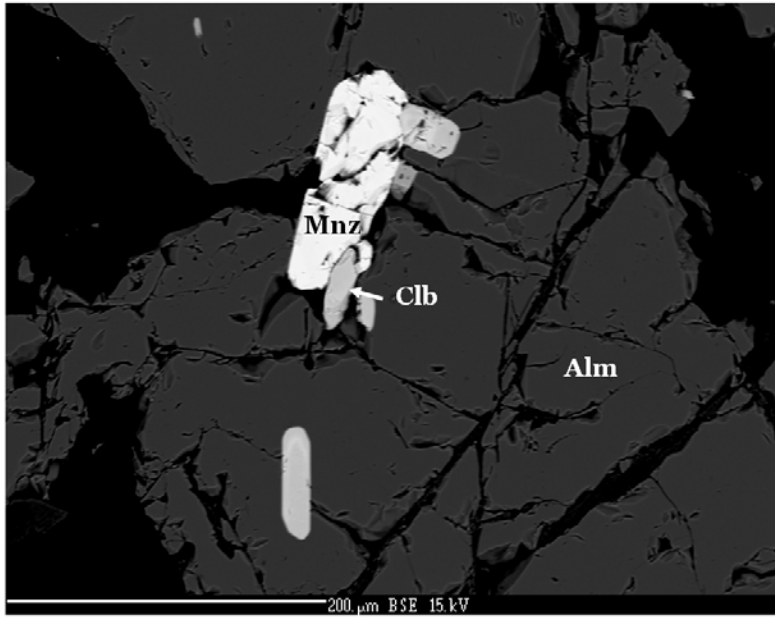


**Figure 3. 51** Monazite in sample PGM 1 with columbite.

**Table 3. 12** Apatite: Thin sections and zones with analyzed samples.

Zone/Sample type	Thin Section
Border Zone	KIN-133c
Wall Zone	KIN-133d
	KIN-135c
Intermediate Zone	KIN-130a
	KIN-134-2
	Rad 2a

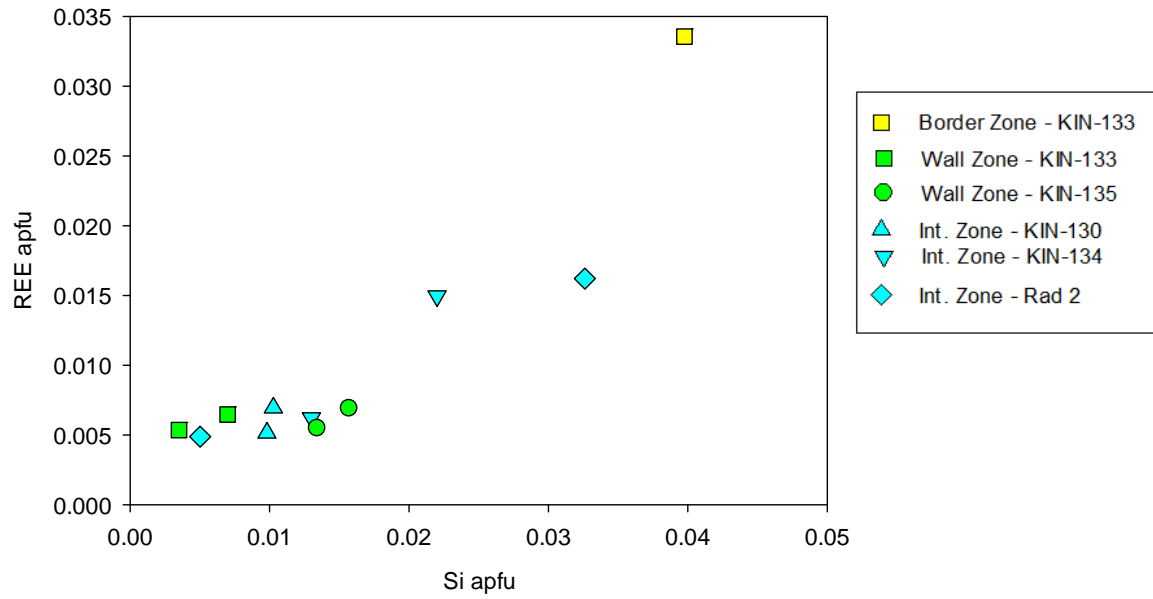


**Figure 3.52** REE vs Si showing the low values of REE present in KIN property apatite.

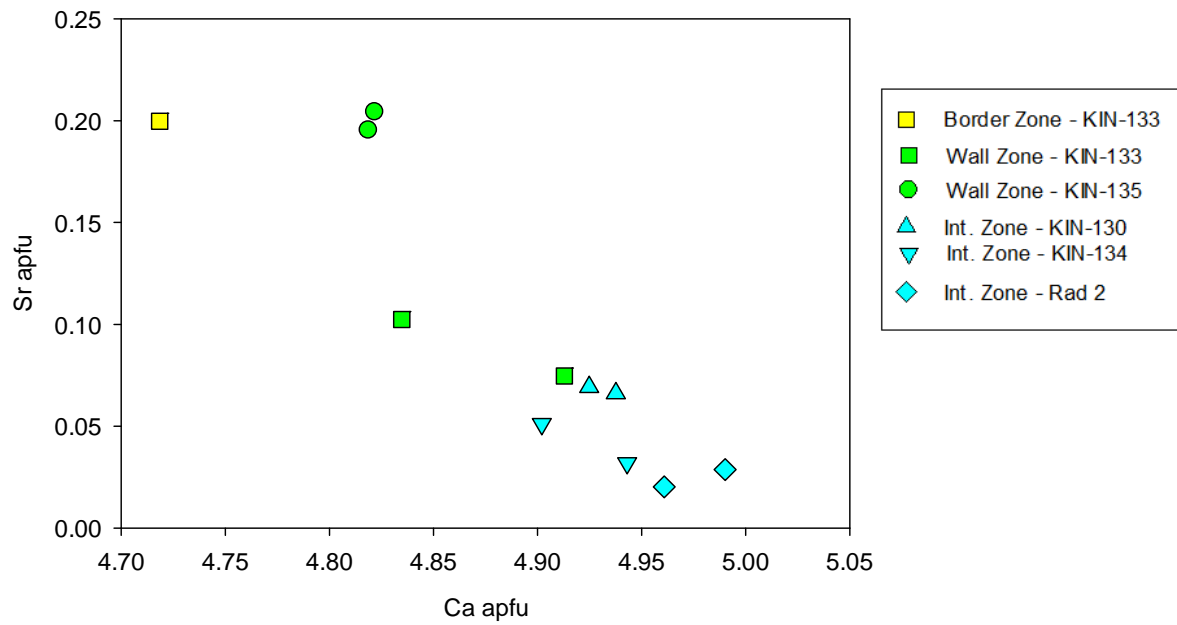


**Figure 3.53** The KIN property apatites contain elevated levels of Sr.

**Table 3. 13** Columbite: Thin sections and zones with analyzed samples.

Zone/Sample type	Thin Section	Columbite I	Columbite II	Columbite III	Columbite IV
Border Zone	KIN-133c	x			
Wall Zone	KIN-133d	x		x	
	KIN-135a	x		x	
Intermediate Zone	KIN-130a	x	x		
	KIN-130b	x	x		
	KIN-134-2	x			
	KIN-136				x
Granitic Pegmatite	PGM 1	x			

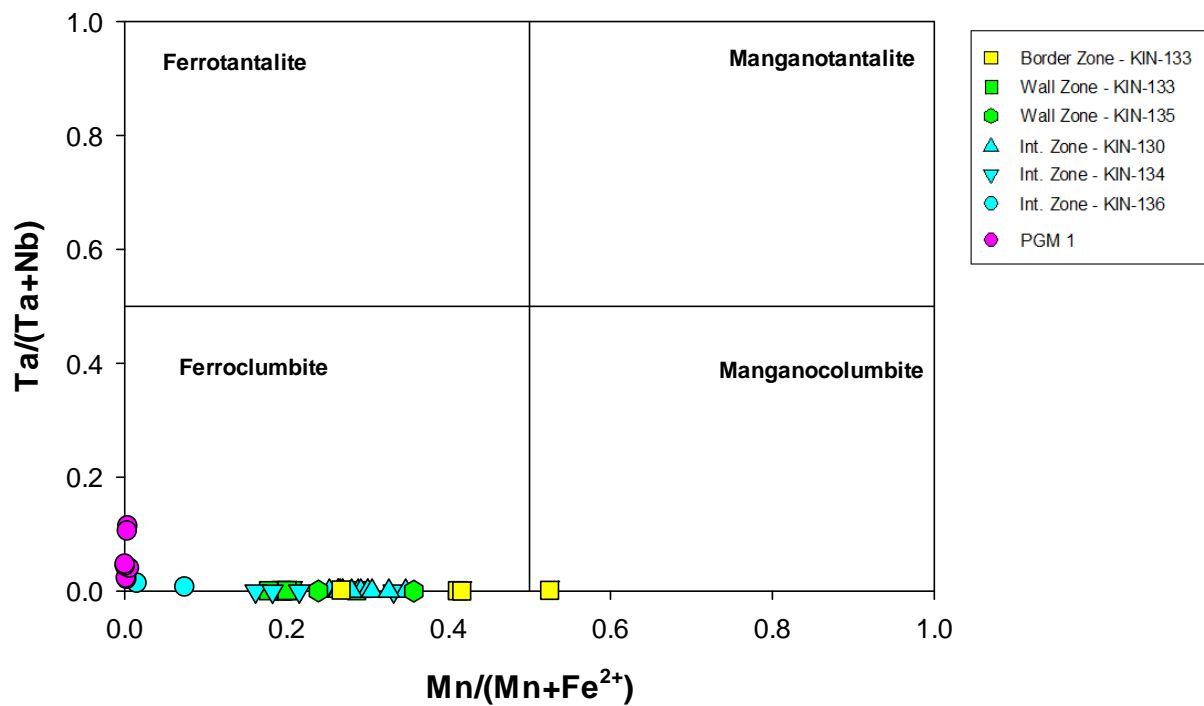


**Figure 3.54** Columbite classification diagram.

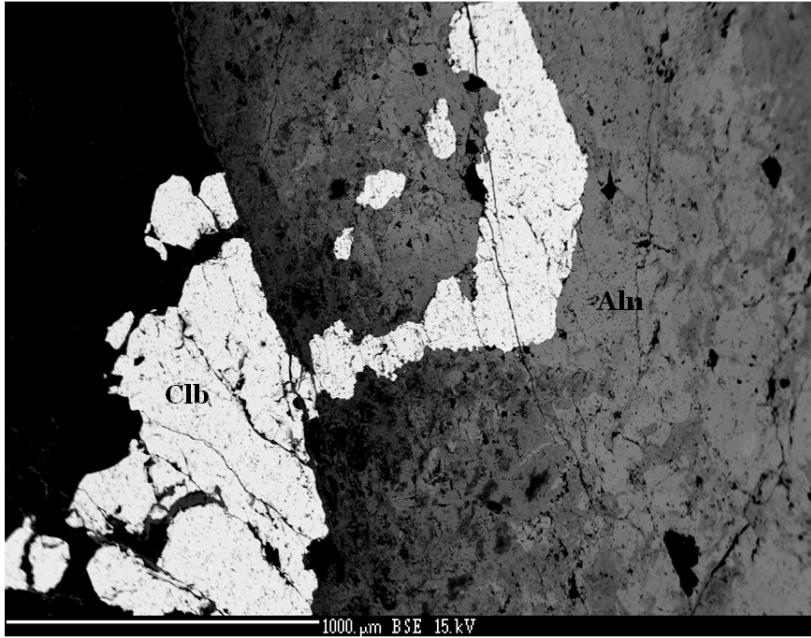


**Figure 3.55** Columbite with allanite in the wall zone at locality KIN-135.

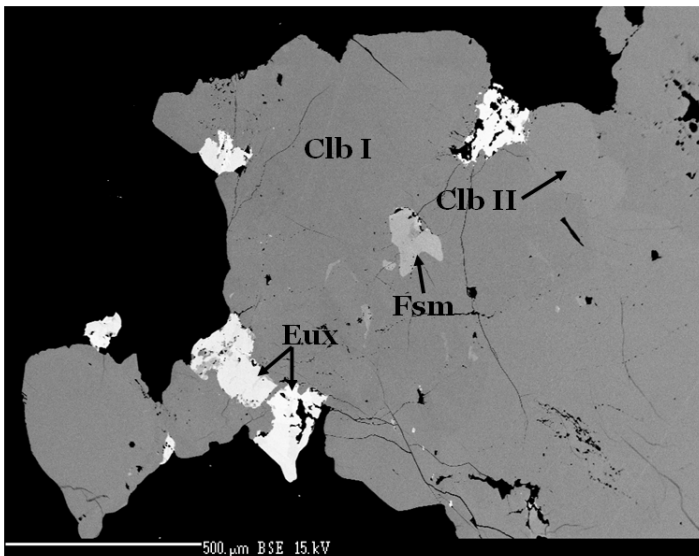


**Figure 3.56** Columbite I with fersmite and euxente-(Y) in the intermediate zone at locality KIN-130. The lighter columbite present is secondary columbite II grains.

**Table 3.14** Oxides: Thin sections and zones with analyzed samples.

Zone/Sample type	Thin Section	Rutile	Ilmenite	Pyrophanite
Border Zone	KIN-133d		x	
Wall Zone	KIN-133c			x
Intermediate Zone	KIN-136	x		
	Rad 2a	x		

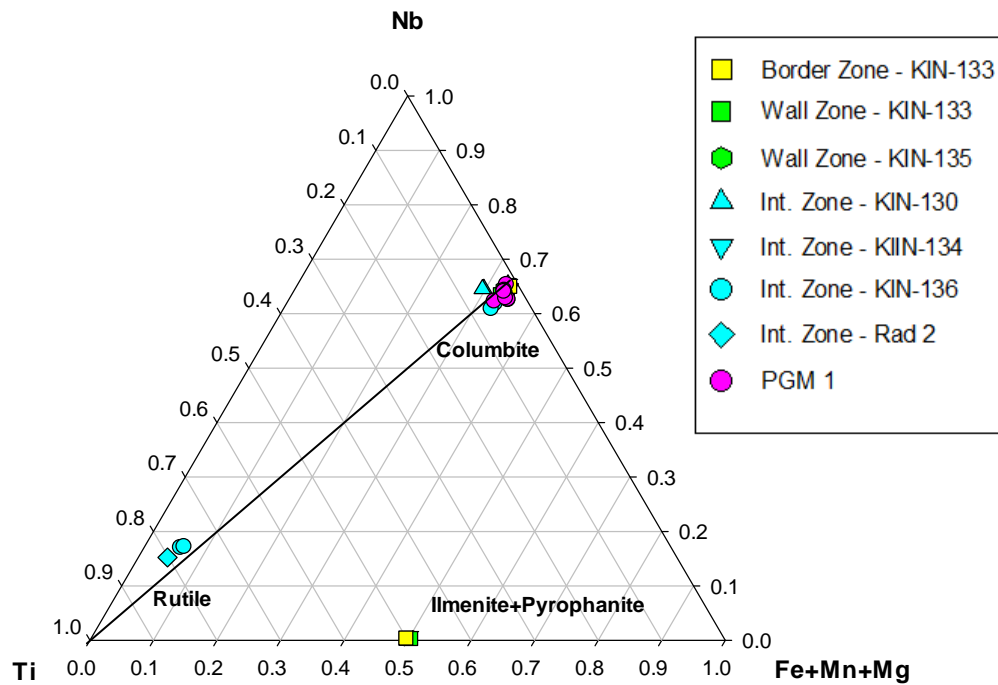


**Figure 3.57** Rutile following trend towards columbite.

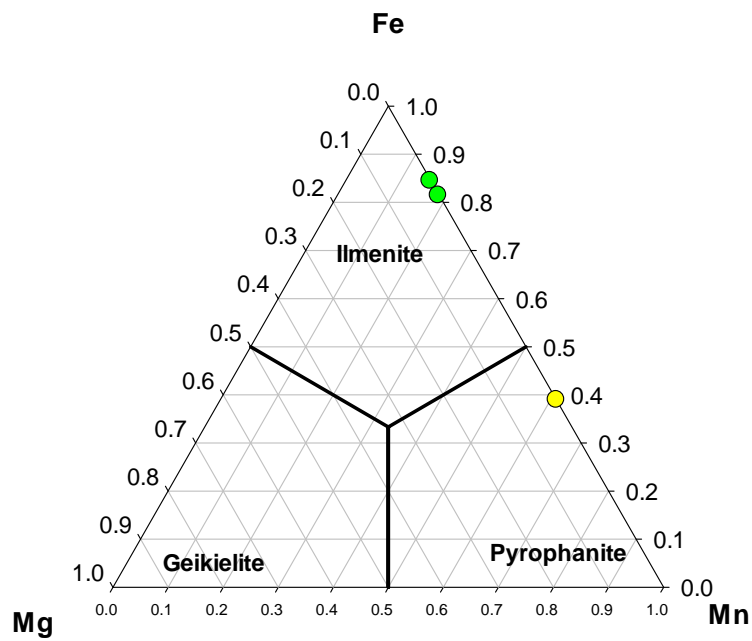


**Figure 3.58** Ilmenite, pyrophanite, and geikielite classification diagram.

**Table 3. 15** REE-bearing oxides: Thin sections and zones with analyzed samples.

Zone/Sample type	Thin Section	Aeschnyrite	Nb-aeschnyrite	Euxenite	Fersmite	Fergusonite
Border Zone	KIN-133d	x	x	x		
Wall Zone	KIN-133c	x				
Intermediate Zone	KIN-130a			x		
	KIN-130b			x	x	
	KIN-134-2	x	x			
	KIN-136					x
Granitic Pegmatite	PGM 1			x		

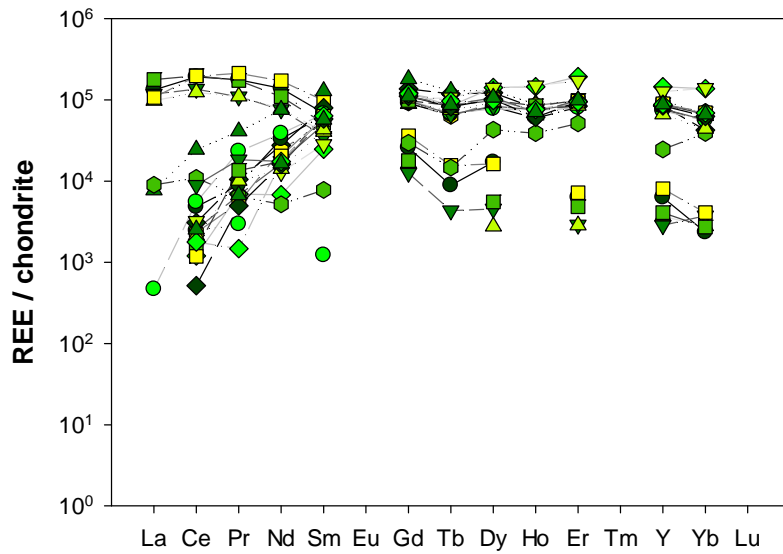


**Figure 3.59** REE distribution of AGM and EMG. The two visible trends (those that favor LREEs and those that favor HREEs) differentiate AGM and EGM. Each color/shape combination represents a different sample point.

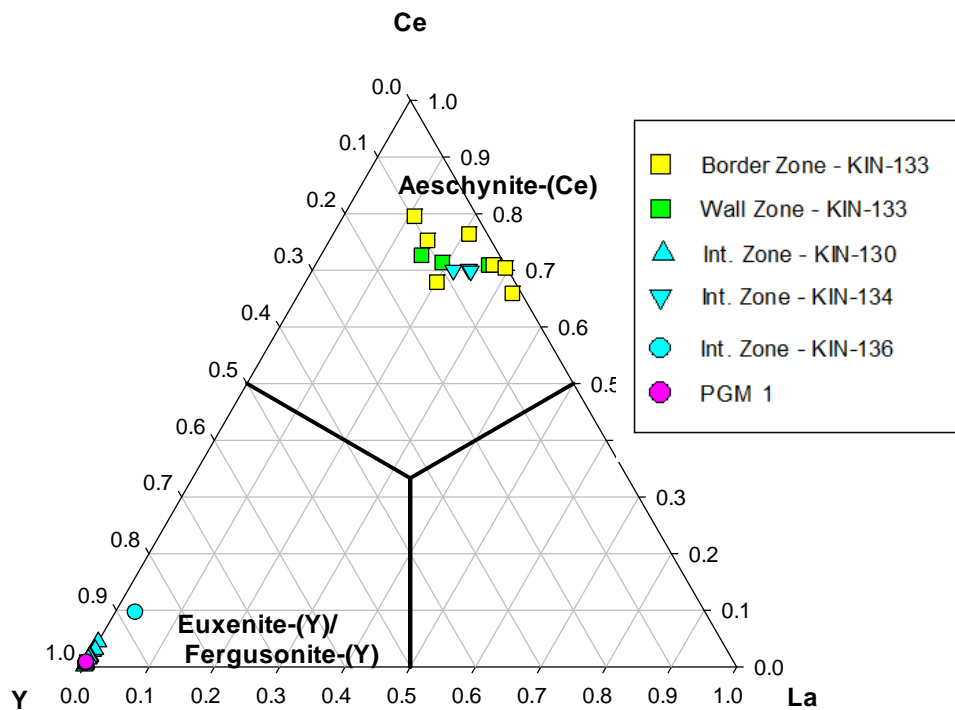


**Figure 3.60** Aeschnite-(Ce) and euxenite-(Y) (with fergusonite) are found in their respective sections based on REE preference.

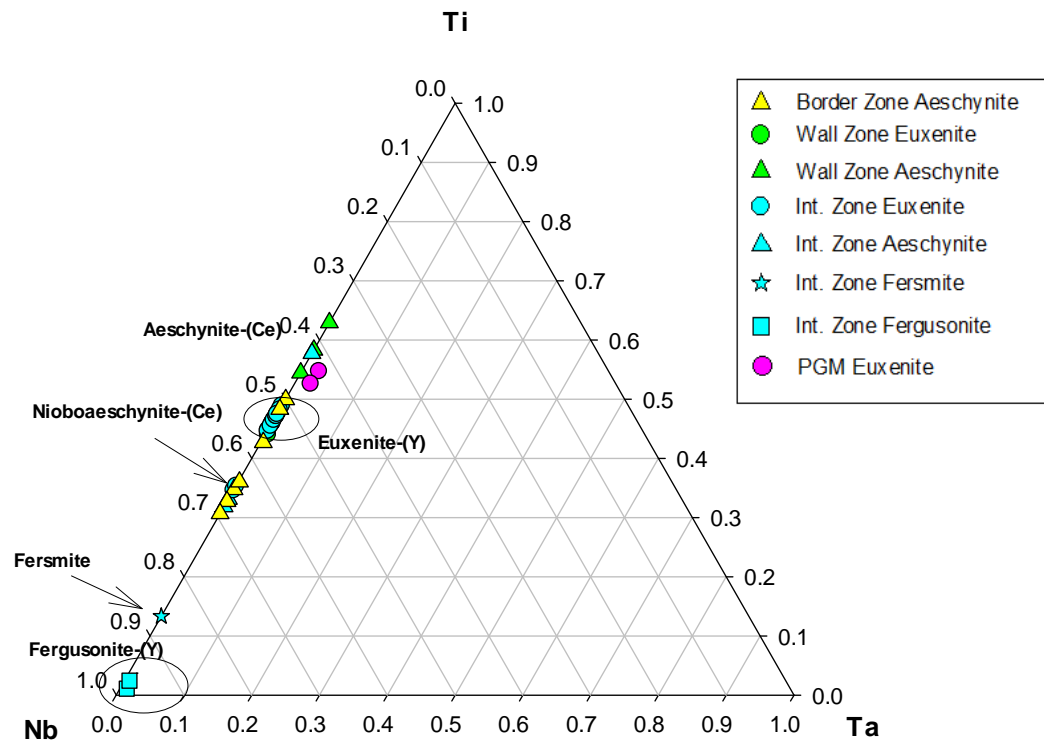


**Figure 3.61** Classification and differentiation of aeschnite-(Ce), euxenite-(Y), fersmite, and fergusonite-(Y).

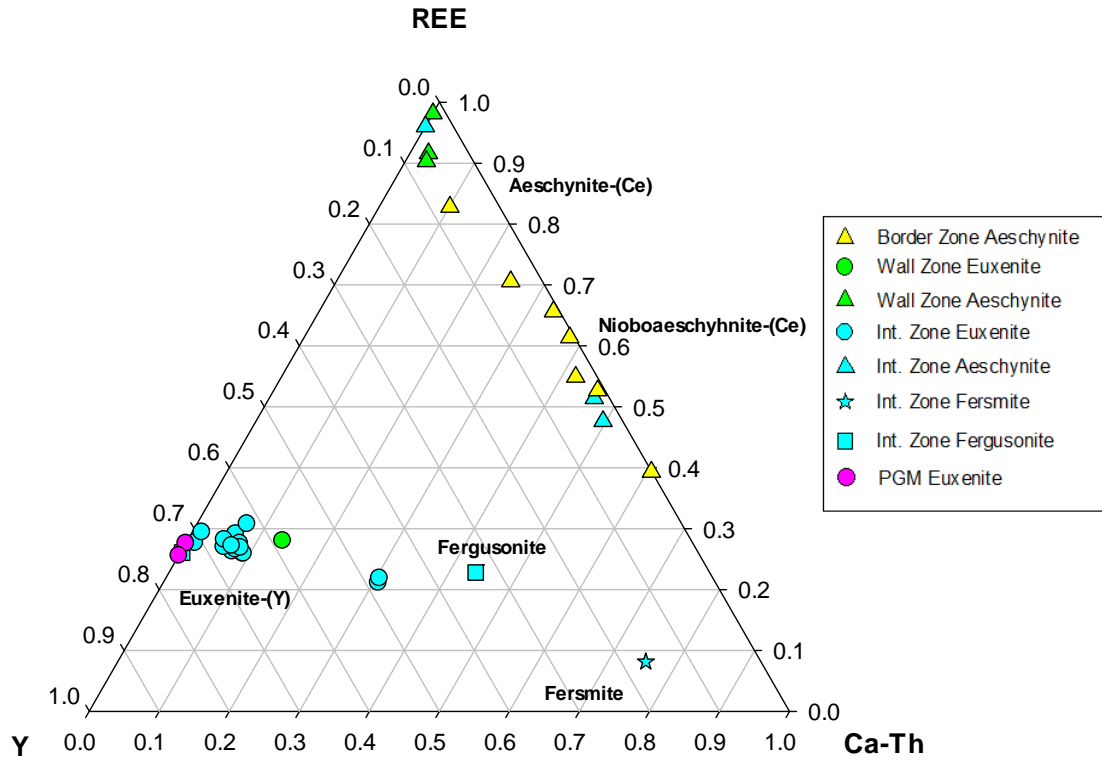


**Figure 3.62** Classification and overlap of REE-bearing oxide minerals present .

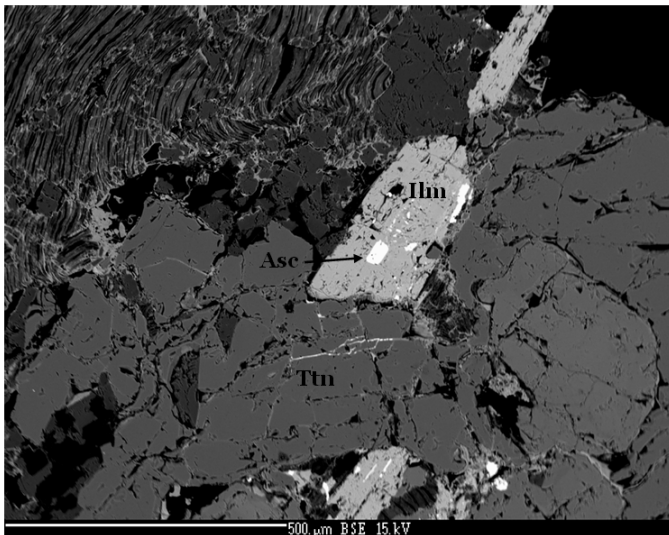


**Figure 3.63** Ilmenite with niobaeschnite-(Ce) exsolution with titanite in the wall zone at locality KIN-133.

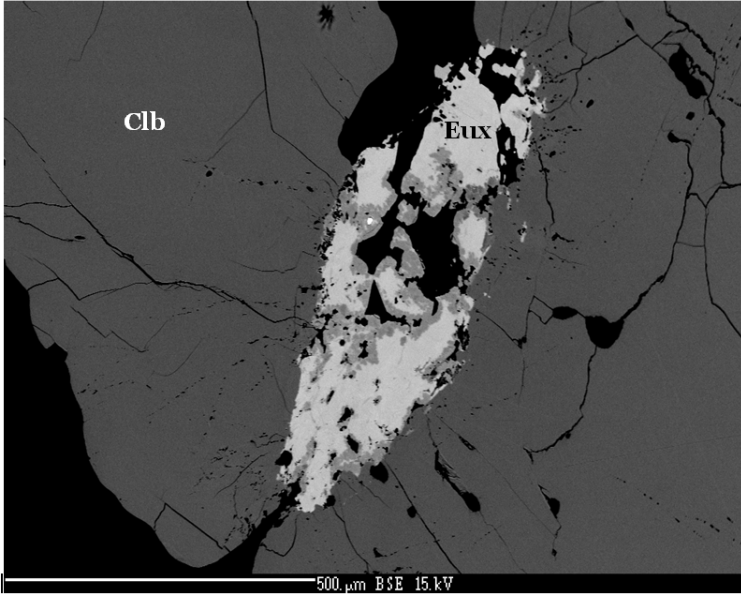


**Figure 3.64** Euxenite with columbite in the intermediate zone at locality KIN-130.

## 4. Whole-Rock Geochemistry and Geochronology

### 4.1 Whole-Rock Geochemistry

Four samples collected from the KIN property during the 2014 field season were submitted for whole rock geochemical analysis. The samples included three from the granite (G17, G18, and G19, from their respective localities) and one from the pegmatite locality KIN-135 (K135), the most REE-enriched pegmatite locality. The samples submitted were chosen to provide the most representative and heterogeneous mineral content as possible. The whole rock geochemical results for major elements are shown in Table 4.1 and trace element data, including that for syenite samples from Brown (2012), are shown in Table 4.2. The samples of Brown (2012) were not available for this study and were not analyzed for major element contents. Only syenite samples in close proximity to the pegmatites were chosen (Fig. 4.1). Additional trace element data from Trident Mountain syenites was provided in a separate report (Brown & Millonig, 2010) and are presented in Table 4.3

Figure 4.2 shows the Zr/Hf and Nb/Ta and Figure 4.3 the U/(U+Th) and Y/(Y+REE) ratios of the investigated samples. These ratios can be used to indicate the degree of fractionation within the pegmatites as higher ratios indicate increased degrees of fractionation (London, 2008). The Zr/Hf has maximums of 26.00 in the granite and 38.93 in the pegmatite, whereas the syenites show a range from 32.70 to 85.27. In the case of Nb/Ta, the granite samples contain a maximum ratio of 31.67, the syenites show a range from 17.50 to 118.45. The pegmatite contains extremely high levels of Nb/Ta with a ratio of 1201.30. Additionally, Figure 4.3 shows U/(U+Th) and Y/(Y+REE) ratios; higher ratios indicate increased levels of fractionation, and again, the pegmatite point is shown to be very low (Škoda & Novák, 2007). The data suggests that the pegmatite has experienced relatively low degrees of fractionation.

In Figure 4.4, syenite and pegmatite samples from KIN and Trident Mountain syenites have been normalized to chondrite using values from McDonough and Sun (1995). Here, it is apparent that the pegmatite sample (K135) is the most LREE-enriched of all of the samples analyzed. The Eu anomaly is most visible as a positive anomaly in samples G19 and JBTDR013. A very slight negative anomaly is visible in sample K135. In comparing pegmatite and the two main potential parental rocks, it is apparent that the REE enrichment can be quite different. The pegmatite is extremely enriched in LREEs (16793 ppm LREE; this value may not be representative of the pegmatite as a whole, due to sampling with a bias for REE-rich material). The granite shows little enrichments, and syenite shows a moderate amount, with values up to 3806 ppm LREEs (Fig.4.5). Little research has been done on syenite pegmatites due to their relative rarity, however, it has been reported that these bodies are commonly enriched in Zr, Th, and LREE, with anomalously high concentrations of Sr and Nb (London, 2008). Strontium, Nb, and Zr concentrations are shown in Figure. 4.6, and the Nb and Sr levels especially appear high.

NYF-type pegmatites are typically derived from A-type granites (London, 2008) whereas LCT-type pegmatites are typically derived from I and S type granites (Simmons et al., 2003). Additionally, NYF-type pegmatites have a subaluminous to metaluminous bulk composition whereas LCT-type have peraluminous to subaluminous bulk composition (Černý & Ercit, 2005). Major element analyses would be required to determine the bulk compositions of the syenites. Figure 4.7 and 4.8 show the granite present on the KIN property appears to be an I-type, peraluminous/metaluminous borderline granite whereas the pegmatite sample and the Trident Mountain syenites have a metaluminous bulk chemistry and A-type composition.

## 4.2 Geochronology

Dates from the syenite, granite, and main pegmatite localities (samples from KIN-134 and KIN-135 were submitted) were obtained to better understand the geologic history of the area.

The Trident Mountain syenite body was previously dated by Pell (1994) who obtained U/Pb zircon ages of  $378 \pm 7$  Ma and  $138 \pm 9$  Ma. The older date is regarded as the intrusion age.. In contrast, the younger date is interpreted to result from resetting during Jurassic metamorphism (Pell, 1994).

Samples from both the granite and pegmatites were submitted to the Pacific Centre for Isotope and Geochemical Research at the University of British Columbia for zircon dating. Samples were prepared using standard techniques and analyzed using laser ablation ICP-MS methods. A total of 19 zircon crystals from the granite were analyzed and provided a weighted average  $^{206}\text{Pb}/^{238}\text{U}$  age of  $76.6 \pm 0.5$  Ma. Similarly, 20 zircon crystals from the pegmatite were dated and provided a weighted average  $^{206}\text{Pb}/^{238}\text{U}$  age of  $79.4 \pm 0.5$  Ma (Fig. 4.9 a and b).

It is worth noting that although the zircons from the pegmatites appeared to contain a significant amount of irregular zonation (including scalloping, potentially from resorption). However, the analytical data indicates that the age and composition of the altered zircons is indistinguishable from the original material. The alteration must therefore have occurred very soon after the initial crystallization of the zircon. Photos and full dating reports can be found in appendix D.

**Table 4.1** Major element whole rock geochemical results.

Sample		G17	G18	G19	K135
Description		Granite	Granite	Granite	Pegmatite
SO3	wt. %	<0.002	<0.002	<0.002	<0.002
P2O5	wt. %	0.06	0.3	0.12	0.79
V2O5	wt. %	<0.002	<0.002	<0.002	<0.002
SiO2	wt. %	74.5	73.9	69.2	59.7
TiO2	wt. %	<0.01	0.03	0.04	0.73
Al2O3	wt. %	15.58	16.4	18.64	14.43
Fe2O3	wt. %	0.28	0.42	0.54	5
MgO	wt. %	0.07	0.13	0.17	1.61
CaO	wt. %	0.81	1.32	1	2.24
MnO	wt. %	0.02	0.01	<0.01	0.67
Na2O	wt. %	5.68	6.04	6.27	2.44
K2O	wt. %	2.93	1.75	2.97	2.68
Cr2O3	wt. %	0.002	<0.001	<0.001	<0.001
Ni	wt. %	<0.01	<0.01	<0.01	<0.01
Cu	wt. %	<0.01	<0.01	<0.01	<0.01
Zn	wt. %	<0.001	<0.001	0.001	0.037
Sr	wt. %	0.027	0.023	0.031	1.156
Zr	wt. %	0.003	<0.002	<0.002	0.009
Ba	wt. %	0.04	0.02	0.04	3.85
Pb	wt. %	0.01	0.01	0.01	0.04
LOI	wt. %	0.49	0.75	0.91	0.56
SUM	wt. %	100.55	101.08	99.9	96.57

**Table 4.2** Minor element whole rock geochemistry results.

Sample		G17	G18	G19	K135	JBKNR014	JBKNR015	JBKNR016	JBKNR017	MKKNR012	JBTDR012	JBTDR013	JBTDR014
Description		Granite	Granite	Granite	Pegmatite	Syenite							
Li	ppm	<0.01	<0.01	<0.01	<0.01	--	--	--	--	--	--	--	--
Be	ppm	9	21	11	54	4	3	2	3	28	10	6	10
F	ppm	110	305	348	1688	--	--	--	--	--	--	--	--
V	ppm	14	<8	<8	41	35	58	201	22	20	164	8	110
Co	ppm	<0.2	0.3	0.3	8.1	5.1	10.2	33.6	2.7	2.9	8	0.4	3.8
Cu	ppm	0.3	0.3	1.5	5.2	4.8	3.6	1.5	1.5	9.3	13.3	1.5	3.6
Ni	ppm	0.2	0.1	0.3	16.1	6.5	7.1	64.4	2.8	1.6	20.8	2	1.7
Zn	ppm	1	2	3	323	25	122	162	19	129	159	3	42
Ga	ppm	15.6	19.5	19.3	21.1	9.5	19.8	21.6	15.6	19.2	27.8	14	17.1
As	ppm	<0.5	<0.5	<0.5	1.2	1.1	<0.5	<0.5	<0.5	0.7	0.8	<0.5	<0.5
Se	ppm	<0.5	<0.5	<0.5	<0.5	<0.5	<0.5	<0.5	<0.5	<0.5	<0.5	<0.5	<0.5
Rb	ppm	75.3	62.5	110.3	70.7	91.2	262.9	323.2	111	44.7	214.1	132.2	39.1
Sr	ppm	206.2	232.1	297.8	10782.2	2897.7	1500.9	1332	1200	1474.8	539.8	427	426.2
Y	ppm	19.8	29.9	9.8	166.4	19.4	11.1	34.2	6.4	95	36.9	6.9	155.1
Zr	ppm	70.7	5.2	8.2	116.8	56.5	83.5	357.1	146.4	140.6	88	24.6	4809.1
Nb	ppm	20.9	38	41.9	2402.6	42.7	204.8	340.6	52.8	3885.3	493.9	35	157.5
Mo	ppm	<0.1	<0.1	<0.1	0.2	1.5	0.1	<0.1	0.1	12.4	28.9	1.3	<0.1
Ag	ppm	<0.1	<0.1	<0.1	<0.1	<0.1	<0.1	0.2	<0.1	0.4	<0.1	<0.1	<0.1
Cd	ppm	<0.1	<0.1	<0.1	0.4	<0.1	<0.1	0.3	<0.1	1.7	<0.1	<0.1	0.4
Sn	ppm	3	5	7	24	<1	2	2	<1	11	7	<1	3
Sb	ppm	<0.1	<0.1	<0.1	<0.1	<0.1	<0.1	<0.1	<0.1	0.1	<0.1	<0.1	<0.1
Cs	ppm	1.4	1.9	5.3	4	1.1	4.8	8.1	1.1	3.1	12.3	1.5	2.6
Ba	ppm	424	204	356	30351	8905	4220	1165	2253	1382	656	1555	100

**Table 4.2** Minor element whole rock geochemistry results continued.

Sample		G17	G18	G19	K135	JBKNR014	JBKNR015	JBKNR016	JBKNR017	MKKNR012	JBTDOR12	JBTDOR13	JBTDOR14
Description		Granite	Granite	Granite	Pegmatite	Syenite							
La	ppm	8.7	7.7	3	5805.9	122.9	72.8	209.4	40.3	1234.9	1398.7	22.9	397.5
Ce	ppm	12.6	17.1	6.3	8354.9	192.8	118.3	328.6	61	2069.5	1848.7	31.7	578.5
Pr	ppm	1.46	2.12	0.7	680.23	18.15	11.62	31.9	5.56	207.49	147.69	2.8	49.97
Nd	ppm	4.3	8.6	2.5	1802.2	56.5	36.4	99.2	16.9	609.4	378.6	7.3	141.1
Sm	ppm	1.39	3.09	0.91	149.77	7.32	4.43	12.92	2.21	61.91	32.57	0.9	17.85
Eu	ppm	0.65	0.94	0.87	31	1.95	1.34	3.72	0.63	13.23	5.67	1.24	4.37
Gd	ppm	1.8	4.55	1.03	83.98	5.43	3.12	9.14	1.58	30.98	16.66	0.78	15.24
Tb	ppm	0.46	1.04	0.27	8.3	0.75	0.43	1.34	0.23	3.97	1.79	0.15	2.66
Dy	ppm	3.16	6.14	1.76	38.53	3.86	2.33	6.88	1.16	20.15	8.87	1.03	18.72
Ho	ppm	0.66	0.89	0.28	5.71	0.73	0.43	1.31	0.25	3.57	1.19	0.19	4.54
Er	ppm	2.05	2.19	0.72	15.27	1.97	1.16	3.46	0.67	9.57	2.5	0.58	14.41
Tm	ppm	0.31	0.29	0.1	2.12	0.28	0.17	0.5	0.1	1.4	0.34	0.08	2.62
Yb	ppm	2.11	1.5	0.52	13.95	1.71	1.05	3.26	0.7	8.98	1.82	0.46	17.93
Lu	ppm	0.33	0.16	0.07	1.91	0.24	0.16	0.47	0.11	1.25	0.18	0.07	2.66
Hf	ppm	2.8	0.2	0.4	3	1	1.4	6.9	1.9	4.3	2.2	0.6	56.4
Ta	ppm	0.9	1.2	5.5	2	0.8	9.9	16	3.4	32.8	5.8	2	7.8
W	ppm	1.5	1.7	2.6	4.9	1	<0.5	<0.5	<0.5	12.6	1.3	<0.5	<0.5
Au	ppm	0.8	1	2.1	1	<0.5	<0.5	*	<0.5	41.7	3.8	1.4	<0.5
Hg	ppm	<0.01	<0.01	<0.01	<0.01	<0.01	<0.01	<0.01	<0.01	<0.01	<0.01	<0.01	<0.01
Tl	ppm	<0.1	<0.1	<0.1	0.3	<0.1	0.2	0.4	0.2	0.2	1	<0.1	0.2
Pb	ppm	10.8	12.3	15.8	67.3	7.5	2.8	6.5	2.7	134.6	6.8	10.6	11.2
Bi	ppm	3.9	17.8	7.6	2.4	<0.1	<0.1	<0.1	<0.1	93.1	1.4	0.1	0.1
Th	ppm	7.4	3.9	1.8	2544.9	14.9	6.8	4.4	3.3	843.9	362.4	7	19.7
U	ppm	18.5	2.6	10.8	6.2	2.9	5.3	0.6	2.4	19.6	8.1	1.9	25.3

**Table 4. 3** Trace element analyses for Trident Mountain syenites.

	Sample	026-1	026-2	038-1	038-2	038-3	038-4	042-1	042-2	042-3	042-4	042-5	042-6	042-7	042-8	042-10
Ba	ppm	439.00	337.00	1808.00	300.00	109.00	1285.00	2410.00	583.00	1815.00	751.00	1171.00	2562.00	1675.00	2056.00	1007.00
Be	ppm	2.00	1.00	5.00	9.00	7.00	7.00	2.00	7.00	5.00	8.00	5.00	5.00	3.00	2.00	7.00
Co	ppm	8.00	24.30	10.10	3.50	3.10	29.20	1.20	41.00	17.30	32.00	9.00	19.60	30.10	15.50	34.60
Cs	ppm	1.10	6.60	1.00	0.10	<0.1	4.10	1.60	7.80	2.40	0.20	1.40	0.40	1.10	10.20	3.40
Ga	ppm	21.00	21.70	16.00	23.70	23.80	18.80	23.00	21.90	27.00	25.60	26.90	19.80	20.70	25.20	22.80
Hf	ppm	9.70	5.30	5.40	19.50	16.70	5.00	1.90	3.90	9.30	6.00	9.10	5.70	6.30	1.70	4.40
Nb	ppm	31.10	21.70	108.10	353.80	19711.90	391.80	53.40	232.10	419.60	232.60	439.10	256.10	208.70	327.60	177.20
Rb	ppm	51.80	85.40	64.30	15.30	5.40	166.80	217.20	378.90	242.60	66.00	173.80	133.00	92.70	320.50	201.60
Sn	ppm	2.00	4.00	4.00	11.00	11.00	6.00	<1	2.00	2.00	3.00	4.00	3.00	2.00	2.00	2.00
Sr	ppm	175.30	156.90	1441.20	464.90	315.10	794.50	817.50	390.50	849.10	339.00	772.20	1367.10	1130.60	1594.30	522.20
Ta	ppm	1.20	0.80	4.30	8.50	409.70	16.90	2.00	6.50	17.40	9.80	22.60	17.10	8.50	6.40	5.60
Th	ppm	11.20	6.90	21.00	18.40	2676.10	39.00	2.90	20.20	48.70	23.50	46.80	44.20	21.20	3.30	33.50
U	ppm	3.00	1.70	3.80	1.50	62.60	2.70	1.30	2.10	9.90	4.70	0.70	2.50	4.30	0.40	1.80
V	ppm	16.00	238.00	152.00	301.00	294.00	254.00	9.00	229.00	129.00	275.00	85.00	125.00	211.00	90.00	279.00
W	ppm	<0.5	1.10	<0.5	<0.5	12.10	<0.5	2.50	<0.5	0.90	<0.5	<0.5	<0.5	<0.5	<0.5	<0.5
Zr	ppm	356.90	196.10	207.40	589.30	438.90	249.00	106.20	167.50	511.20	303.80	430.80	299.70	303.10	107.70	190.00
Y	ppm	64.70	47.30	27.60	11.00	24.60	38.50	5.00	39.70	27.50	34.50	44.30	29.70	28.40	33.90	25.40
La	ppm	38.80	21.70	114.40	26.90	197.50	197.60	28.00	69.60	93.50	72.10	192.60	178.80	119.50	449.80	83.00
Ce	ppm	88.80	51.90	196.00	52.80	539.70	345.10	45.10	144.60	168.30	153.40	337.60	281.10	206.80	715.50	154.60
Pr	ppm	11.17	6.94	19.06	5.92	50.59	35.41	4.01	15.87	16.12	16.31	30.80	23.76	18.11	61.78	14.69
Nd	ppm	47.80	30.30	62.30	20.80	153.90	119.60	11.90	58.70	51.20	57.60	92.70	70.20	59.30	188.00	49.60
Sm	ppm	10.80	7.36	8.50	3.44	19.66	15.52	1.47	10.07	7.48	8.98	12.70	8.88	8.43	20.67	7.25
Eu	ppm	2.91	2.44	2.12	0.90	4.59	3.91	0.44	2.87	1.94	2.41	2.70	2.36	2.47	4.87	2.16
Gd	ppm	11.31	8.34	6.00	2.55	10.20	10.38	1.03	8.27	5.65	7.19	9.61	6.66	6.61	12.33	5.74
Tb	ppm	1.92	1.40	0.90	0.41	1.51	1.44	0.15	1.28	0.89	1.10	1.51	1.02	1.00	1.63	0.89
Dy	ppm	11.10	8.08	4.75	2.12	7.12	7.33	0.77	6.91	4.84	6.03	8.09	5.39	5.30	7.61	4.82
Ho	ppm	2.24	1.60	0.89	0.39	1.10	1.33	0.15	1.31	0.93	1.13	1.52	0.99	1.00	1.22	0.90
Er	ppm	6.44	4.77	2.59	1.14	2.75	3.80	0.47	3.60	2.62	3.32	4.24	2.83	2.77	3.12	2.48
Tm	ppm	0.94	0.69	0.38	0.19	0.39	0.54	0.08	0.58	0.42	0.50	0.64	0.42	0.41	0.46	0.38
Yb	ppm	6.01	4.35	2.63	1.49	2.47	3.45	0.54	3.50	2.72	3.29	4.01	2.66	2.59	2.86	2.54
Lu	ppm	0.90	0.66	0.41	0.30	0.35	0.49	0.08	0.49	0.39	0.47	0.55	0.37	0.38	0.40	0.39

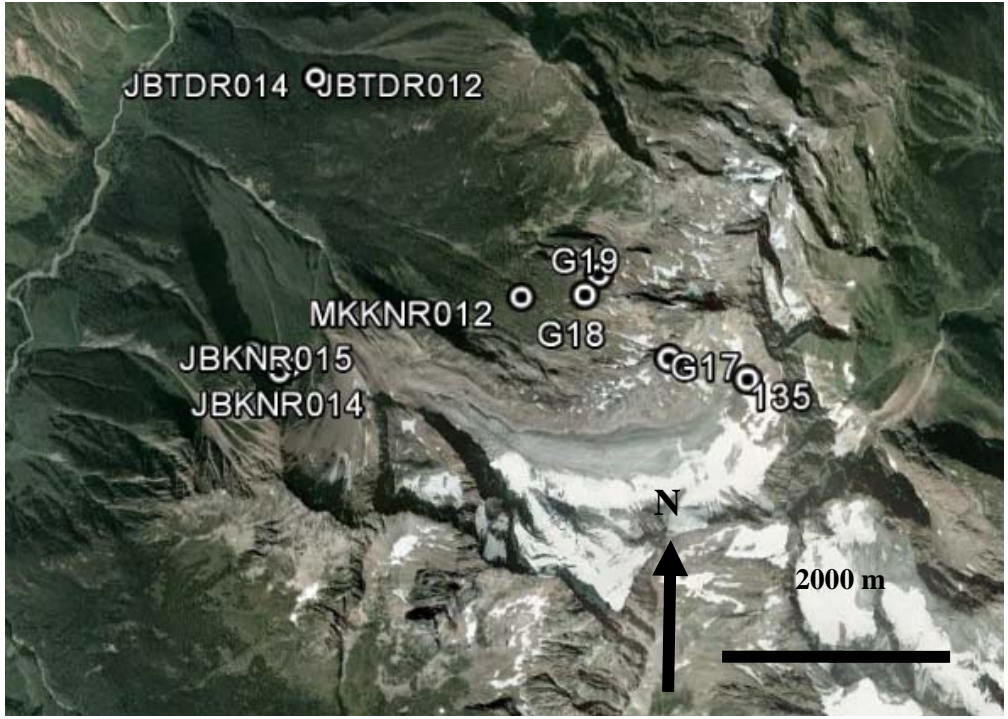
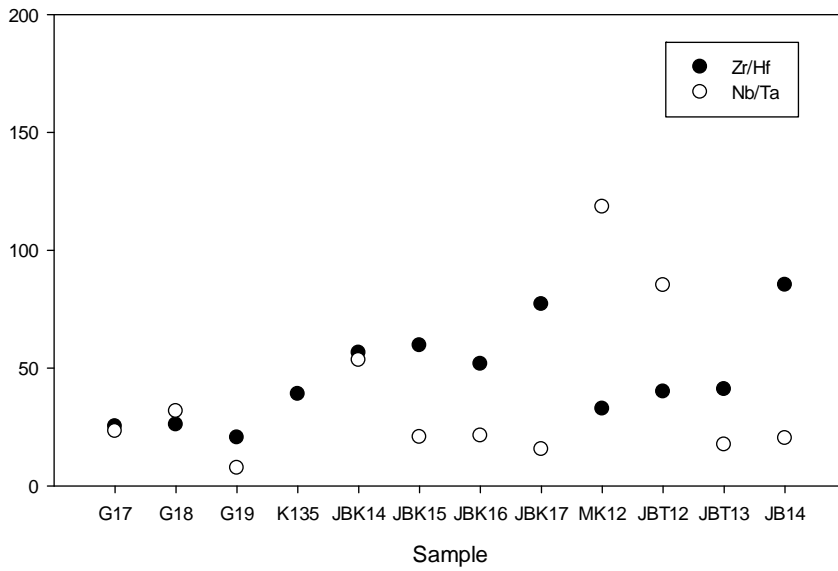
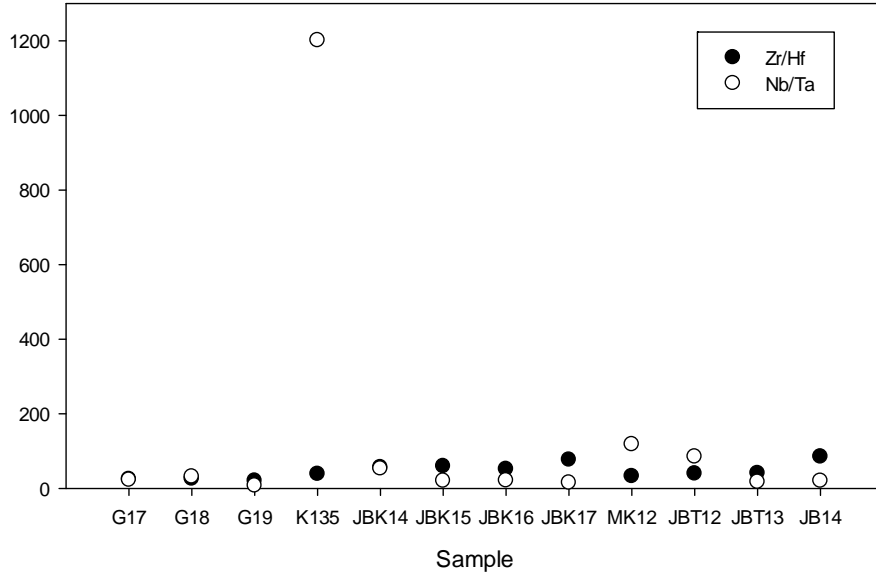
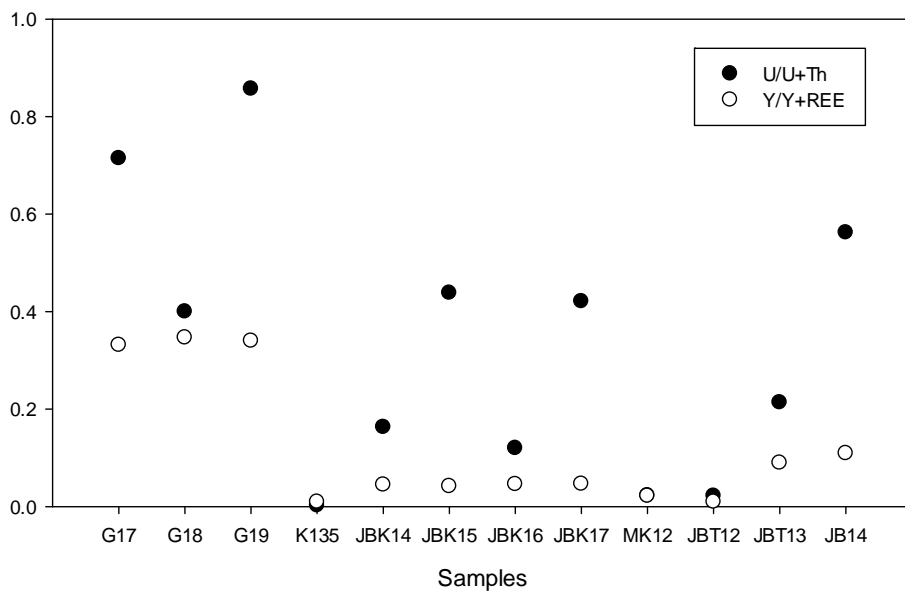


Figure 4.1 Locations of all samples used in geochemical studies.

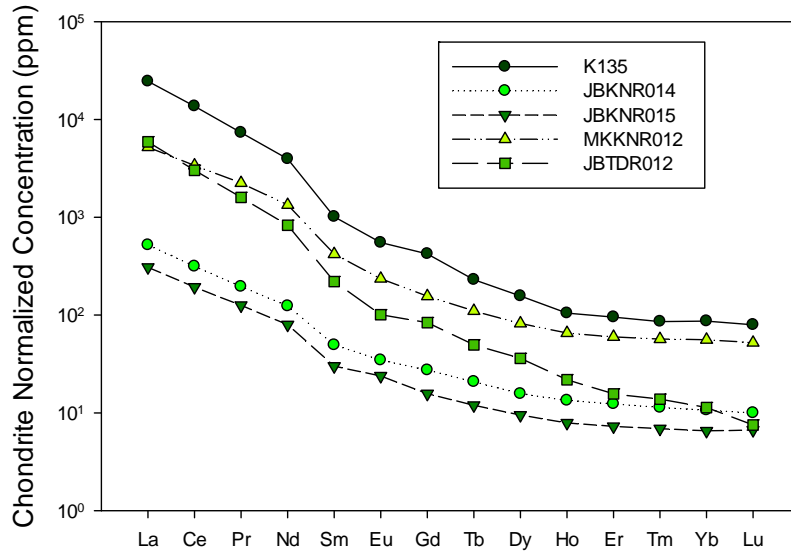


**Figure 4.2** Zr/Hf and Nb/Ta ratios. The top graph shows the entire sample set, while the axis is cut in the bottom graph to better show variation among the other samples. Syenite sample names have been shortened to contain the first three letters and final two digits to decrease sample name length.



**Figure 4.3** U/U+Th and Y/Y+REE ratios present in the samples.

### KIN Samples



### Trident Mountain Syenite

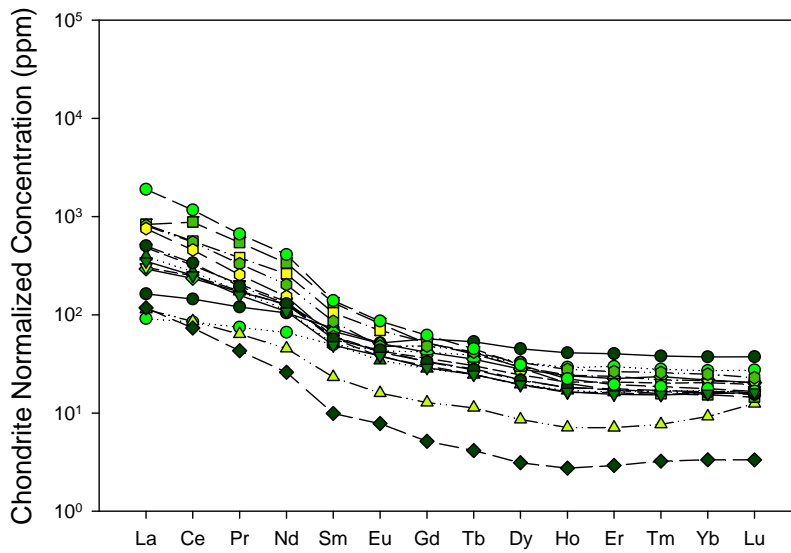


**Figure 4.4** Top: Chondrite-normalized REE values of KIN property samples (using McDonough & Sun (1995)).

Bottom: Chondrite-normalized REE values of Trident Mountain syenite samples (using McDonough & Sun (1995)).

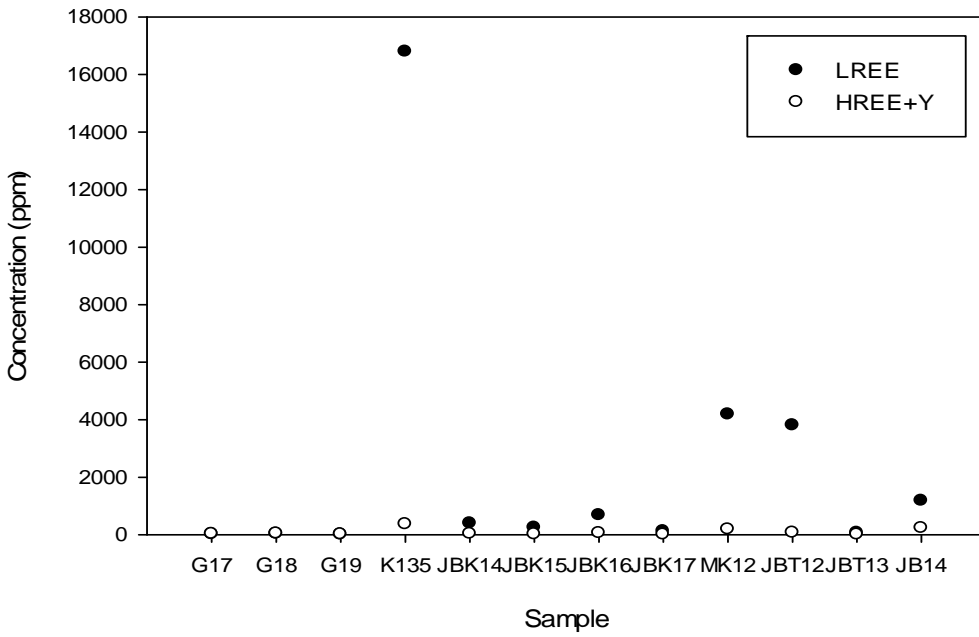


Figure 4.5 LREE and HREE+Y concentrations found in the samples.

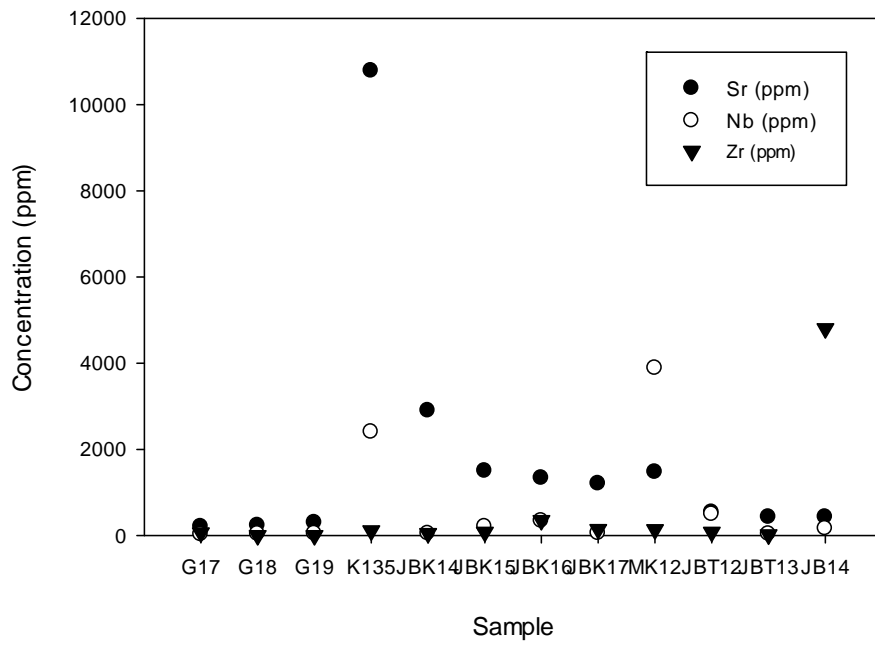
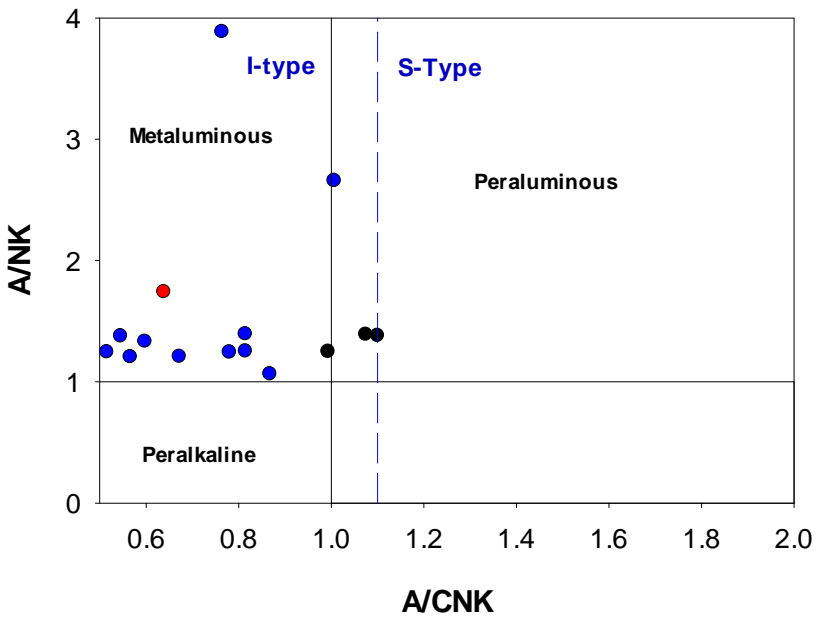
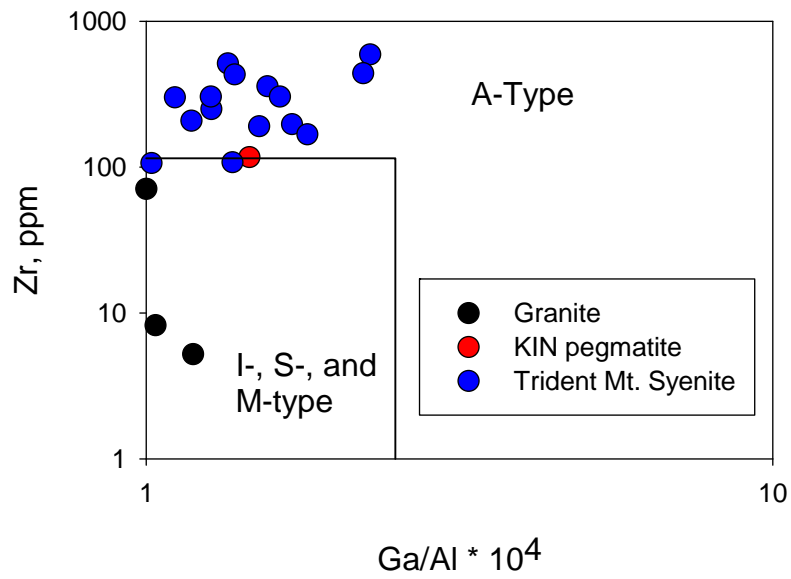


Figure 4. 6 Sr, Nb, and Zr concentrations.

Alumina Index Molar Diagram



**Figure 4.7** Granite and bulk pegmatite classification based on the alumina index molar diagram with I-type and S-type boundary added from Chappel and White in blue (2004). Granite samples are marked in black whereas the pegmatite sample is red. A/CNK is  $Al_2O_3/(CaO + Na_2O + K_2O)$  and A/NK is  $Al_2O_3/(Na_2O + K_2O)$ .



**Figure 4.8** Granite and bulk pegmatite classification (based on Whalen et al., 1989).

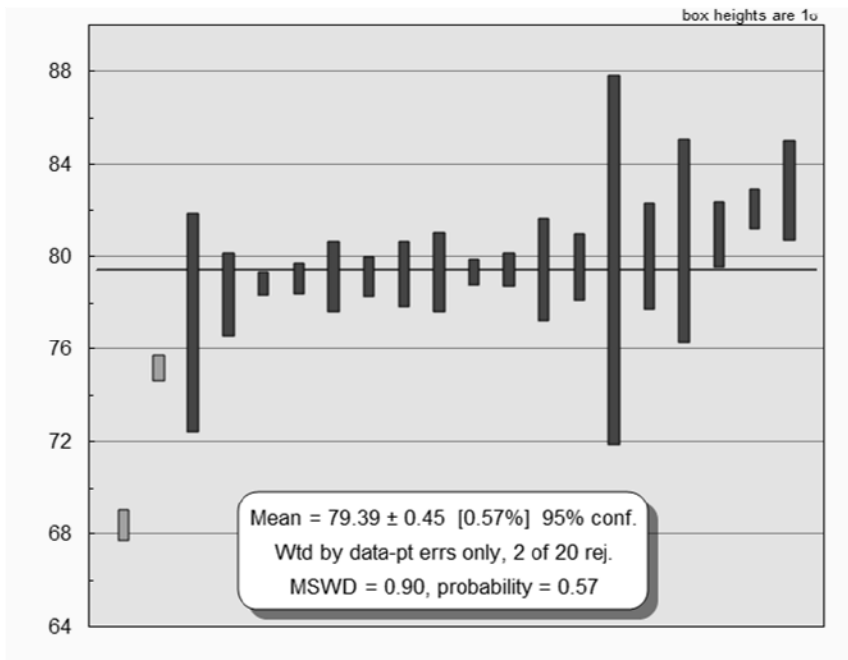
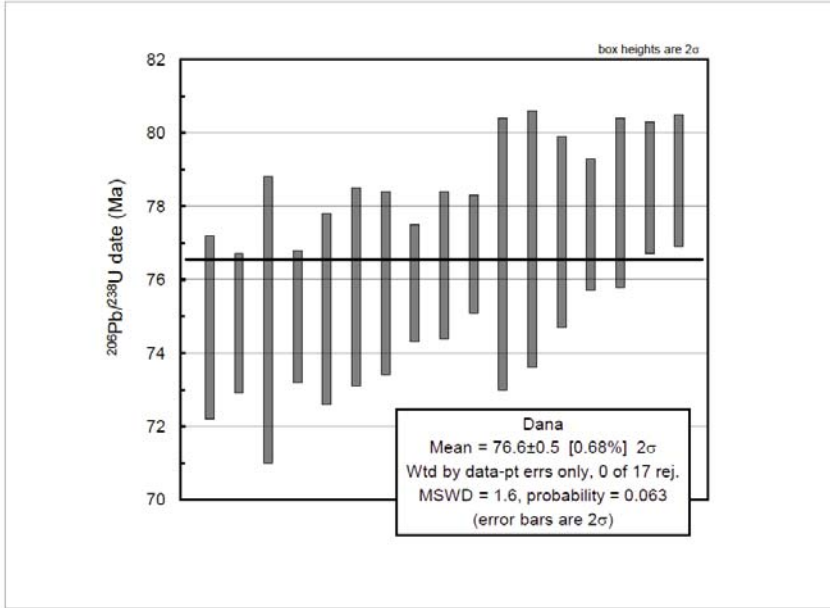


**Figure 4. 9** Top: U-Pb zircon age analyses from granite sample. Bottom: U-Pb zircon age analyses from pegmatite sample.

## 5. Discussion

### 5.1 Mineralogy Characterization and Discussion

The minerals chosen for discussion are either rare minerals, such as hyalophane, or are particularly important to this project, such as the REE- and Nb-bearing minerals.

#### 5.1.1 Hyalophane Feldspar

Barium is found in low amounts in most feldspars. BaO content higher than 5 are indicative of a barium feldspar, whereas Ba content over 80% is considered celsian (Deer et al., 2001). Hyalophane is the name used when one-third of large cation sites are filled by Ba (Deer et al., 2001). The feldspar found in intrusive rocks on the KIN property contain similar Ba/K ratios as those described within Deer et al. (2001), although there is a higher than expected level of Na (Fig. 3.1.4). The solid solution between hyalophane and celsian generally follow a path from the K to Ba end members (Deer, et al., 2001), however, the increased Na shifts the solid solution line away towards the Na-rich end member.

In these samples, hyalophane has a maximum of 17.79 wt.% BaO. Compared with the literature, this is low for hyalophane; [e.g., samples from India contain up to 28 wt.% BaO (Raith, et al., 2014)]. Minimum values of BaO in hyalophane found in a picrite sill in the Czech Republic were 27.06 wt.% BaO (Tasáryová et al., 2014). The Na enrichment [up to 3.82 wt.% Na<sub>2</sub>O as opposed to 0.46 wt.% Na<sub>2</sub>O in the Czech samples (Tasáryová et al., 2014) and 1.70 wt.% Na<sub>2</sub>O in the Indian samples (Raith et al., 2014)], is possibly the cause of the unexpected solid solution line. This enrichment may be due to hydrothermal fluids present in the rocks during metamorphism (see section 5.3.2).

### 5.1.2 Allanite

Allanite is an interesting mineral in these pegmatite localities because it occurs in both primary and secondary forms with prominent zonation elevated levels of Ti. It is also one of the most complicated minerals to understand.

The secondary allanite mineralization occurs in two main associations: 1) after monazite in a corona and 2) with columbite and aeschynite without the presence of a phosphate mineral. The first case is in the literature (e.g., Budzyń et al., 2011). It is apparent that KIN secondary allanites after monazite have elevated levels of Th (up to 7.25 wt.% ThO<sub>2</sub>) compared with Himalayan and Slovakian samples (below 0.50 wt.% ThO<sub>2</sub>). These allanite corona textures are of interest as they require specific conditions and fluid interactions in order to form (discussed further below).

The formation secondary allanite that is not associated with monazite or apatite is less clear. Under these circumstances it is associated with columbite, aeschynite, and thorite, but not with phosphate minerals (Fig. 3.32). It is not apparent which, if any, are the primary minerals and which are the secondary minerals, however, primary allanite and primary aeschynite are not commonly found together (Škoda & Novák, 2007). One hypothesis is that the original minerals were monazite and columbite and the phosphate elements were carried away by those same Ca-rich fluids, making it only appear that these associations are without a primary phosphate. Another hypothesis is the aeschynite and columbite were primary and allanite then formed with Si added from hydrothermal fluids during metamorphism. Another possibility is that hydrothermal fluids mobilized Ti to form secondary aeschynite from primary columbite and allanite (Papoutsas & Pe-Piper, 2013). However, the allanite appears secondary and there is a lack of evidence to support significant mobilization of Ti, making this theory unlikely.

Elevated Ti levels within allanite are significant, as they can be used to help determine the environment in which the grains formed. In these cases, the Ti is incorporated using a  $\text{Ti}^{4+} + \text{Fe}^{2+} = 2 \text{Al}^{3+}$  substitution, favored in relatively Fe-rich and Al-poor environments, and is indicative of an A-type aluminous rock (Vlach & Gualda, 2007). Titanium values of up to 5.03 wt.% are present in intermediate zone points within their Brazilian allanite grains used to make this determination (Vlach & Gualda, 2007). Titanium values at KIN are not elevated to the same degree, they do contain up to 4.32 wt.%  $\text{TiO}_2$  (the highest values are found within primary allanite).

### **5.1.3 Aeschynite and Euxenite**

Aeschynite and euxenite crystals are most commonly found as metamict grains (Ercit, 2005), and so it noteworthy that the grains found within these pegmatites samples are crystalline; however, it is not clear why they are. It is possible that high enough metamorphic conditions were reached to anneal the grains, creating natural crystalline grains. Experimental settings suggest that aeschynite transitions from its metamict to crystalline states at approximately 400°C (Tomašić et al., 2004).

Compositionally, the minerals are distinguished by aeschynite's preference for LREEs (most commonly Ce in this case) and Y (and HREEs) in euxenite. Aeschynite-(Y) does exist as a dimorph of euxenite-(Y), but euxenite is more common and therefore likely to be the mineral present. Crystal structure determination is necessary in order to definitely identify the minerals present.

Aeschynite and euxenite grains on the KIN property are consistently secondary and form in a variety of textures. Aeschynite in the border zone likely forms from Ti that was mobilized

from allanite due to hydrothermal fluids, although it is possible that they are primary as associations in these samples are unclear. Other aeschynite grains may form as exsolutions within allanite and euxenite grains along fractures from elements mobilized by hydrothermal fluids during metamorphism.

When comparing the aeschynite and euxenite samples found at KIN to those in the literature, it is apparent that these minerals are extremely Ta-poor with a maximum of 0.07 wt.% Ta<sub>2</sub>O<sub>5</sub> compared to the 11-14 wt.% Ta<sub>2</sub>O<sub>5</sub> at the Třebíč Pluton in the Czech Republic (Škoda & Novák, 2007). This is characteristic of all KIN samples, which have elevated levels of Nb instead. The Ti levels from the KIN samples and the Czech sample are comparable, but the Th levels are elevated seemingly randomly throughout the aeschynite and euxenite KIN samples, with a range of 1.16 to 12.61 wt.% ThO<sub>2</sub>.

#### **5.1.4 Chevkinite Group Minerals**

Chevkinite group minerals commonly contain elevated levels of Ti (maximum of 21.91 wt.% Ti present in the KIN samples). This trend is consistent with that found within allanite samples and as many of these grains are found as inclusions within allanite, this seems logical. It seems likely that these grains formed as Ti-rich pockets within the allanite at the same time.

Comparing Ti levels in chevkinite found in the literature, A-type granitic and syenitic rocks in the Graciosa Province contain up to 28.91 wt.% TiO<sub>2</sub> (Vlach & Gualda, 2007), and analyses from around the world presented by Macdonald et al. (2009) show a range of 16.87 to 18.91 wt.% TiO<sub>2</sub>. Additional samples from Mongolia show Ti levels up to 17.34 wt.% TiO<sub>2</sub> [a single perrierite-(Ce) sample is present with Ti enrichment up to 21.82 wt.% (Macdonald et al.,

2012). This elevated Ti is indicative of an A-type granite origin for the rocks, as seen in the allanite (Vlach & Gualda, 2007)

Another element of note is Th, which is more enriched within the KIN chevkinite samples (minimum of 0.94 wt.% ThO<sub>2</sub>; most samples contain over 3.00 wt.%, with a maximum of 6.00 wt.% ThO<sub>2</sub>) than in other localities internationally. Values of 3.03 wt.% ThO<sub>2</sub> can be found in the USA (Nevada and Alaska), but, most data points are below 1.50 wt.% ThO<sub>2</sub> (Macdonald et al., 2009). Additionally, Russian chevkinite samples contain Th values significantly lower than those studied here, with no values higher than 0.80 wt.% ThO<sub>2</sub> (Macdonald et al., 2012). Similar to the case of Ti, the allanite grains are also Th-rich, which likely remobilized into the chevkinite during metamorphism.

#### **5.1.5 Phosphates: Monazite and Apatite**

KIN property monazite is consistently primary and has commonly undergone a moderate to high level of substitution to form apatite and allanite in a corona (in some cases, no primary material remains). This breakdown has been described from various other localities [Western Carpathians in Slovakia (Ondrejka et al., 2012) and in the Tso Marari complex in the Himalayas (Upadhyay & Pruseth, 2012)]. In comparing these samples it is evident that they are visually very similar and contain the same minerals and texture as seen in Figure 3.31 from KIN samples. Compositionally, the monazite from the KIN property contains elevated levels of Th compared to the literature [up to almost 16.65 wt.% Th, compared to a maximum of 6.00 wt.% Th found in the Slovakian samples (Ondrejka et al., 2012) and 9.24 wt.% Th in the Himalayan samples (Ondrejka et al., 2012)]. Especially elevated Th is commonly found in samples with lower REE values, suggesting that the Th is replacing REEs in these cases, demonstrating the cheralite

substitution component. Additionally, Th is elevated to some degree consistently and this could be due to the extreme lack of fractionation within these pegmatites, (also indicated by the low levels of Ta present).

Apatite is consistently REE-depleted after monazite which is primarily due to the REEs being remobilized into the allanite. As a result, the maximum total REE values found in KIN apatite samples are rarely over 1.00 wt.% REE with most samples falling below 0.30 wt.% REE. These are similar values to those found in secondary apatite samples from Slovakia and the Himalayas (Ondrejka et al., 2012; Upadhyay & Pruseth, 2012). When compared to primary apatite samples from a nepheline syenite in South Africa, the REE levels in apatite can range significantly, with REE-poor samples containing less than 0.03 LREE apfu versus REE-rich samples with up to 0.47 LREE apfu (Liferovich & Mitchell, 2006).

Some trends are visible within the apatite sample. Strontium is lowest within the intermediate zone and increases outwards towards the border of the pegmatite. In addition, this forms a negative correlation with the amount of Ca present, with more Ca found closer to the core. The cause of this is unknown. An additional point of interest is that secondary apatite generally contains appreciable OH or Cl instead of F (London & Burt, 1982). However, all apatite in the KIN samples are secondary and consistently F-rich (Fig. 3.53).

### **5.1.6 Columbite**

Columbite group minerals from the KIN property show little variation, especially those within the main pegmatites. They show low levels of fractionation with very little Ta present. Additionally, all but one sample are ferrocolumbite in composition with low levels of Mg. Ferrocolumbite is present in a variety of forms: primary, secondary (altered after primary

columbite), secondary (after titanite) and as exsolutions, however, the compositions of these grains are still fairly homogeneous regardless.

Comparing these samples to columbite minerals from other localities suggest the low level of fractionation evidenced by the high Nb/Ta ratio is uncommon. Columbite minerals from NYF-type pegmatites in the Grenville Province show a minimum of 2.69 wt.% Ta<sub>2</sub>O<sub>5</sub> and a maximum of 14.81 wt.% Ta<sub>2</sub>O<sub>5</sub> (Ercit, 1994) and those from a the Scheibengraben pegmatite in the Czech Republic contain a minimum of 9.85 wt.% Ta<sub>2</sub>O<sub>5</sub> (Novák et al., 2003). Beyond the extreme lack of Ta, the ferrocolumbite found on the KIN property appears to have few distinguishing features.

## **5.2 Parental Magma Determination and Pegmatite Classification**

### **5.2.1 Parental Magma Determination**

A number of options were considered in attempting to determine the parental magma for the pegmatites and how they formed.

First, the undeformed I-type granites were considered, but were ruled out due to the fact that they were emplaced after the formation of the pegmatites, as evidenced by their young age of  $76.6 \pm 0.5$  Ma (the pegmatites are  $79.4 \pm 0.5$  Ma) and their apparent lack of deformation.

Furthermore, their geochemical signature is incompatible with that of the pegmatites.

Secondly the syenites which are exposed in the study area, or may be present in greater volume at depth, were considered. Based on similar geochemical signatures as the pegmatites, *e.g.*, similar A-type signatures and LREE enrichment patterns, they represent a more likely parental rock. There are several possible ways in which the pegmatites and syenites could be related:

1) The pegmatites could have been emplaced at 378 Ma (intrusion age of the Trident Mountain syenite; Pell, 1994) and the younger U-Pb zircon age obtained in this study ( $79.4 \pm 0.5$  Ma) reflects metamorphic resetting of the U-Pb isotope system of the investigated zircons. However, the simple igneous morphology and the lack of age variations across altered zircon rims and pristine cores (Appendix D.1) of the zircons used to date the pegmatites make this possibility unlikely.

2) The pegmatites formed at  $\sim 79$ Ma directly by fractionation from a buried A-type intrusion that is not presently exposed at surface and were subsequently deformed by the metamorphic event that accompanied the intrusion of undeformed granite sills. Although there are known alkaline igneous intrusions within the region, such as Trident Mountain (Pell, 1994; Millonig et al., 2012), none have igneous ages close to that of the pegmatites, making it unlikely that an A-type syenite body was emplaced so closely to the time the I-type granites intruded.

3) The pegmatites formed from partial melting of the significantly older ( $\sim 378$  Ma) syenites or hypothetical granitoid rocks associated with them, followed by syntectonic melt emplacement. Although there is a lack of measured isotopic ages for igneous units in the region around the time the pegmatites were formed, there is evidence for high-grade metamorphism ( $\sim 540$ - $700$  °C;  $\sim 6$ - $7$  kbar; Ghent et al., 1982) in the region at 72-82 Ma (Ghent & Villeneuve, 2006; Sevigny et al., 1990). During this time, the syenite could have undergone some degree of partial melting; likely mechanisms include:

a) prograde partial melting of the syenite, promoted by the presence and breakdown of primary hydrous phases and/or fluid infiltration from the surrounding host sediments, followed by syntectonic melt extraction and emplacement of the pegmatitic melts.

b) post-peak metamorphic decompression accompanied by hydration and decompressional melting of the syenite/granitoid and emplacement of melt the before the end of deformation associated with decompression.

Both mechanisms are feasible given the peak metamorphic conditions in the area and assuming a water-saturated solidus for the syenite of  $\leq 650$  °C at 5-6 kbar, similar to the water-saturated solidus of nepheline syenites from Blue Mountain, Ontario (Gittins, 1979). Temperatures needed to melt the syenite, however, even in a decompressional setting, would likely have produced voluminous melts of the meta-sedimentary host rock as well, and there is no clear evidence of this having occurred in the study area. On the other hand, no samples of the host rock were examined in detail and its history, composition, geochemistry, and state before the last metamorphic deformational event are unknown.

Ultimately, it is not clear exactly how these pegmatites formed, although partial melting of the syenite/granitoid seems the most likely scenario.

### **5.2.2 Pegmatite Classification**

Due to the uncertain origin of the pegmatites in the study area, they will be classified here first based on their geochemistry; second based on their mineralogy, and third, based on their potential origin and mineralogy. Additionally, they will also be classified based on the scheme first introduced by Černý (1991) and discussed in Chapter 1.

1. Due to their enrichment in Zr, Th, F, REE, and Nb>Ta, along with their metaluminous bulk composition, the pegmatites would be classified as NY-type family pegmatites based on their geochemistry.

2. Based on their mineralogy and following the classification scheme of Černý (1991) (from the broadest scale down), the pegmatites first belong to the rare element class of pegmatites due to their elevated levels of rare elements, specifically LREE, U, Th, and Nb>Ta. Secondly, the pegmatites belong to the rare earth element subclass of rare element (REE) pegmatites (as opposed to the Li subclass) (Table 1.1). Based on the presence of allanite, monazite, zircon, rutile, and ilmenite, they are further classified as allanite-monazite type [sometimes referred to as “allanite type” (Simmons et al., 2004) pegmatites within the REE subclass.
3. Assuming that the pegmatites indeed represent anatectic melt, formed from partial melting of an A-type syenite source, they would have to be classified as abyssal type pegmatites, specifically as members of the LREE subclass within this class, due to their enrichment in LREEs.

### **5.3 Metamorphic Conditions and Effects**

Evidence that the pegmatite bodies on the KIN property have undergone some degree of metamorphism is reflected in their mineralogy and textures.

#### **5.3.1 Evidence for Metamorphism and Effects**

Textural and mineralogical evidence, as discussed below, indicates that the allanite-bearing pegmatites in the study area were deformed shortly after their emplacement.

Foliation visible within the pegmatites, along with the poikiloblastic textures of garnet, biotite, and in some cases hornblende (Fig. 2.6) are initial indicators that the pegmatites have undergone some deformation. Additionally, the undulose extinction and boundary migration

textures of quartz also imply deformation. The latter of which specifically implies moderate metamorphic conditions following crystallization (Trouw et al., 2009). Rotational mineral textures (Fig. 2.6), suggests that there could have been synkinematic crystallization.

Minerals present within the pegmatites and their relationships with each other further imply a history of metamorphism. For example, the breakdown of monazite into a corona of apatite and allanite (Fig. 3.31) indicates a metamorphic reaction between monazite and hydrothermal fluid. Additionally, instances where secondary allanite is present with aeschynite and columbite also require the mobilization of fluids. These reactions are discussed further in the next section.

Post-magmatic metamorphic overprint of primary allanite is documented in the REE-depleted epidote rims around allanite I grains (Uher, 2009).

Although some “patchy” alteration has overprinted many of the zircon grains that were examined from the pegmatite (Appendix D), this alteration does not appear to have affected the U-Pb isotopic systematics, and it is unclear exactly what caused this alteration. More significant, however, is the fact that clear evidence was seen in CL images of some of the zircons for post-crystallization resorption and overgrowth by thin rims of metamorphic zircon (Appendix D). Unfortunately, this metamorphic zircon was not dated; however, it is presumably no younger than the 76.6 Ma granites.

### **5.3.2 Metamorphic Conditions**

The metamorphic effects described above and the conditions and mineral assemblages found within the host rocks were the primary tools used to determine what metamorphic conditions the pegmatites experienced following emplacement.

When determining what fluids were present during metamorphism, it is important to look at the secondary minerals and their textures. Monazite, and specifically the monazite breakdown into apatite and allanite that is seen at this locality, can be useful in learning about the metamorphic conditions undergone by the rocks. Although P-T conditions cannot be constrained significantly from this association, the character of the hydrothermal fluids can be determined. Monazite becomes unstable during fluid-activated overprinting (Ondrejka et al., 2012), and apatite, thorite, and allanite are formed at its expense. In this scenario, the fluids release the REEs, Th, and P from monazite while Ca, Fe, Al, Si, and F are released from local biotite and plagioclase to form coronas of apatite, thorite, and allanite around monazite (Ondrejka et al., 2012). Calcium in the fluid increases the solubility of monazite (Budzyń et al., 2011) and is then commonly incorporated into newly grown apatite. These same fluids are required for the formation of allanite and aeschynite ± euxenite with columbite, whereby the REEs are remobilized from an REE phase (likely monazite or aeschynite) and Ca, Fe, Al, Si, and F are provided by the biotite and plagioclase.

When determining the pressure and temperatures conditions, we are more limited and have focused on looking at the minerals and conditions of the host rock. Kyanite, a mineral commonly used to determine pressure and temperature conditions undergone by rocks, occurs locally within the host rock, near the pegmatite localities (specifically KIN-134 and KIN-135). This location was also interpreted to be within the kyanite zone during original mapping by Wheeler (1965). This limits the P-T conditions to low T conditions. Additionally, the host rocks have been found to be metamorphosed to amphibolite facies (Millonig, 2011), further constraining the P-T conditions to 400-600 °C and at least 300 MPa.

Returning to the breakdown of monazite, experimental conditions have confirmed this reaction occurs at a minimum of 450 MPa (up to 610 MPa) and 450-500 °C (Budzyń et al., 2011); these experiments were mostly completed at lower pressures and temperature and were noted to be highly fluid dependent, making it difficult to determine the P-T conditions based on these experiments.

Using this information, it is possible to narrow down the P-T conditions that occurred at this locality and suggest that the pegmatites and host rocks were subjected to metamorphic conditions with minimums of 450 °C, 300-400 MPa with Ca, F, Si, and Fe-rich fluids.

### **5.3.3 Potential Causes of Metamorphism**

Although it has been shown that the granite bodies found on the KIN property cannot be the parental source of the pegmatites, it is possible that they are related to the metamorphism that affected pegmatite samples. The granites are known to have intruded approximately 3 million years after the pegmatites, and the pegmatites were deformed shortly after their emplacement. These timing constraints strongly suggest that the intrusion of the granites or the mechanisms that led to this intrusion are a likely cause of metamorphism. It is difficult to determine this with any certainty without further information regarding the extent of the metamorphism and whether it these rocks have only been locally metamorphosed, or if there is, instead, a regional control and cause of metamorphism.

### **5.4 Locality Comparison**

When comparing the KIN property pegmatites to other pegmatites, it is important to first, compare them to similar allanite type pegmatites to determine what separates this locality from

other allanite type pegmatites. Next, comparing this pegmatite with other less similar NYF-type pegmatites can draw attention to how it classifies and compares to NYF pegmatites as a group. Finally, comparing these NYF-type pegmatites to LCT-type pegmatites from a similar environment will help determine what factors would lead to different pegmatite within this environment.

First, the KIN property pegmatites will be compared to very similar pegmatites found on Mt. Bisson, which is located less than 100 km NW of Mackenzie, BC in the Wolverine Metamorphic Complex within the Omenica Belt. These bodies are also described as allanite type pegmatites enriched in LREEs and classified as abyssal type (Černý & Ercit, 2005), like the KIN pegmatites. They were described as “rare earth element-mineralized pegmatites and metasomatic alkaline rocks (Halleran & Russell, 1990, 1993; Halleran, 1991) in Proterozoic [rock] (Halleran & Russell, 1996),” similar to those described in this project. Like the KIN pegmatites, those on Mt. Bisson are composed of potassium feldspar, plagioclase, and green amphibole, with titanite and apatite, and with REE allanite contents varying from 2,700 to > 35,000 ppm REE, making them mineralogically similar to those found on the KIN property. However, whereas the KIN pegmatites contain significant amounts of columbite and Nb-bearing minerals, the Mt. Bisson pegmatites do not (Halleran & Russell, 1996). These two pegmatite localities are located in similar environments and contain similar levels of REEs; the main difference is the lack of Nb-bearing minerals at this second locality. As for their formation, the Mt. Bisson pegmatites are inferred as being derived from mantle melts (Heinrich, 1966; Currie, 1976; Bell, 1987) whereas the KIN property pegmatites are likely derived from syenites. Both, however, can be considered abyssal type pegmatites (Černý & Ercit, 2005).

Next, to compare the KIN pegmatites to other NYF-type pegmatites, specifically to those found within the REL-REE subclass, we can look at the pegmatites found in South Platte, Colorado, which listed as an example of this subclass of pegmatites by Černý and Ercit (2005). These pegmatites are enriched in REEs, Y, Nb, and F with allanite, fluorite, bastnaesite, and samarskite (Simmons et al., 1987). These pegmatites are similar in that both contain large allanite grains, although those at KIN are more prevalent, and Nb-Ta oxides (samarskite in this case and columbite at KIN). Differences arise in the KIN pegmatites' lack of F, whereas it is enriched here.

Another NYF-type pegmatite locality to be compared is that in Western Transbaikalia in Russia which are described as NYF-type pegmatites with a syenite parent. These are composed primarily of potassium feldspar, albite, and minor pyroxene with biotite, magnetite, titanite, zircon, and pyrochlore accessory minerals (Ripp et al., 2013), similar to those found on the KIN property except for amphibole in the place of pyroxene and higher contents of REE- and Nb-bearing minerals, and lack of quartz. These pegmatites lack the Nb-enrichment and elevated levels of REEs described by London (2008), as being characteristic of syenite pegmatites and seen within the KIN pegmatites.

A final well studied NYF-type is the El Muerto granitic pegmatite located in Oaxaca, Mexico. Although "F" is part of the description, the label should not be taken too literally, if a pegmatite meets the other general requirements for a group, as is apparent this pegmatite which lacks F enrichment. In this case, that includes the allanite, perrierite, monazite, thorite, aeschynite, and Nb-rutile found at the locality (Prol-Ledesma, et al., 2012). These pegmatites are similar to the KIN pegmatites with regards to REE-bearing minerals present; however, the lack of F and Nb-bearing mineralogy sets them apart.

Finally, comparing the KIN pegmatites to LCT-type pegmatites found on Mt. Begbie, located 12 km south of Revelstoke, BC, can indicate why NYF-type pegmatites might appear in an area where LCT-type are also present. These pegmatites contain tourmaline and beryl and contain an S-type composition (Dixon et al., 2014). They are likely related to S-type granites that were partially melting during a local exhumation event (Dixon et al., 2014).

The pegmatites on the KIN property are mineralogically similar to other allanite-monazite and NYF-type pegmatites described in the literature. However, they do differ in some important features. The KIN pegmatites are set apart from other NYF-type pegmatites by the presence of hyalophane and Ti-rich allanite, and a bulk geochemical preference for Nb>Ta (indicating, along with other elemental ratios, that the pegmatite has low levels of fractionation). The metamorphic conditions experienced by the pegmatites also created textures and minerals that are uncommonly seen in this rock type (monazite coronas, REE-depleted apatite, crystalline aeschynite and euxenite). Finally, the location of these pegmatites within the Cordillera is unusual, as NYF-type pegmatites rarely form in compressional tectonic settings. However, by studying the other pegmatite found within the Omineca Belt such as the LCT-type pegmatites it is worth noting that a significant difference lies in their formation where the KIN property pegmatites are likely derived from partial melting of an older A-type source, the Mt. Begbie pegmatites were related to granites with an S-type signature.

## 6. Conclusions

REE- and Nb-bearing pegmatites on the KIN property are classified as rare element class pegmatites belonging to the allanite-monazite type within the REE subclass. They are additionally members of the NYF-type pegmatite family. The dykes found at four in-situ localities were divided into four different zones (border zone, wall zone, intermediate zone, and quartz core zone) based on an increase of grain size, quartz content, and iron levels within biotite towards the core while decreasing the number of major minerals present. The border zone samples contained allanite and monazite grains within plagioclase feldspar and little to no quartz; the wall zone contained coarse allanite, monazite and columbite, all within plagioclase feldspar and moderate amounts of quartz; the intermediate zone contained blockier feldspar (and hyalophane feldspar at one locality) with large grains of allanite, monazite, and columbite; the core is primarily composed of quartz with slight accessory mineralization.

The mineralogy present within the KIN pegmatites is fairly typical of that found within NYF-type pegmatites, however, the low levels of Ta present is atypical. These low Ta levels, along with the low Zr/Hf, U/U+Th and Y/Y+REE ratios, indicate a very low level of fractionation for NYF-type pegmatites. Additionally, allanite and chevkinite grains contain elevated Ti levels, which is indicative of the pegmatite being derived from an A-type granite parent rock.

The granite and syenite rocks found on this property and the local Trident Mountain property were investigated to determine whether one of the two (or a third unknown rock) was the parental source magma for the pegmatites. The geochemistry, S-type signature, and geochronology determined that the granite could not be the parent. However, the geochemistry and A-type signatures of the syenite and pegmatites creates three theories: 1) that the pegmatites

were emplaced at the same time as the Trident Mountain syenites (unlikely due to the lack of age variation within the zircons used to date the pegmatites); 2) the pegmatites formed from a hidden A-type intrusion (unlikely as there are no other A-type igneous magmatic dates during that period); or 3) the pegmatites formed from partial melting of the older syenites. This seems to match the available data the best, questions are still unanswered as to how this partial melting could have occurred without the melting of the host rock well.

Metamorphic conditions were constrained to minimums of 450 °C, 300-400 MPa with Ca, F, Si, and Fe-rich fluids.

## 7. Suggestions for Future Work

Future work on the KIN property should include complete mapping, beyond that seen during field exploration, of the granite, syenite, and pegmatite outcrops. This would likely reveal previously undiscovered pegmatite, granite, and syenite outcrops, possibly including the source of the granitic pegmatite float samples. Additional sampling of pegmatite zones, such as the core from locality KIN-134 and KIN-133, which was unable to be visited, would help complete a comprehensive data set from all zones at all known localities. Furthermore, more syenite material would be extremely beneficial, as only one thin section was available for study during this project.

Additional thin sections should be made from zones with fewer examined sections (e.g., the core at KIN-134 and KIN-135 and the wall zone at KIN-130) and petrographical and mineralogical data should be collected with the use of microscopy, SEM analyses, and EMP analyses. Data collection from all the minerals in all the sections would be the final step towards understanding the complete mineralogy present within these pegmatites.

Only one pegmatite sample was submitted for geochemical analyses, making fractionation trends difficult to ascertain. Additional geochemical analyses for each of the localities, and from each zone at each locality, would be helpful in determining relationships between these localities, variation present, and fractionation trends present between and along pegmatites. Unfortunately, the coarse nature of the pegmatites makes geochemical analyses difficult as a large amount of material is needed for each analysis, so large quantities of material would need to be collected. Additionally, only minor elemental analyses have been completed for the syenite, and major element geochemical analyses would be beneficial to determine the bulk composition of the syenite.

Finally, minerals aeschynite and euxenite are primarily found as metamict grains; however, the samples found on the KIN property appear crystalline and display pleochroism. Single-crystal analyses should be done on these uncommon grains to learn more about the crystal structure of these minerals.

## References

- ARMBRUSTER, T., BONAZZI, P., AKASAKA, M., BERMANEC, B., CHOPIN, C., GIERÉ, R., HEUSS-ASSBICHLER, S., LIEBSCHER, A., MENCHETTI, S., PAN, Y., & PASERO, M. (2006) Recommended nomenclature of epidote-group minerals. *European Journal of Mineralogy* **18**, 551–567.
- BARNES, E.M. (2010) *The Rare Element Little Nahanni pegmatite group, NWT: studies of emplacement, and magmatic evolution from geochemical and Li isotope evidence*. Doctoral Thesis, University of British Columbia, July 30<sup>th</sup>, 2010. 1-242.
- BELL, K. (1989) *Carbonatites – Genesis and evolutions*. Unwin Hyman Publishing, London, 1-618.
- BROWN, J.A. (2003) Mineralogy and Geochemistry of beryl and rare-metal-bearing granitic pegmatites in the Kootenay region of south-eastern British Columbia. Geological Fieldwork, British Columbia Geological Survey, 167–184.
- BROWN, J.A. (2012) Kin-Trident Assessment Report: 32655. *Ministry of Forest, Mines and Lands: BC Geological Survey* 1-240.
- BROWN, J. A., MILLONIG, L.J. (2010) Trident Assessment Report: 31861. *Ministry of Forest, Mines and Lands: BC Geological Survey* 1-111.
- BUDZYŃ, B., HARLOV, D.E., WILLIAMS, M.L., & JERCINOVIC, M.J. (2011). Experimental determination of stability relations between monazite, fluorapatite, allanite, and REE-epidote as a function of pressure, temperature, and fluid composition. *American Mineralogist* **96**, 1547–1567.

CARR, S.D. (1991) Three crustal zones in the thor-Odin-Pinnacles area, southern Omineca Belt, British Columbia. *Canadian Journal of Earth Sciences* **28**, 2003–2023.

CEMPÍREK, J., HOUZAR, S., & NOVÁK, M. (2008) Complexly zoned niobian titanite from hedenbergite skarn at Písek, Czech Republic, constrained by substitutions  $\text{Al}(\text{Nb,Ta})\text{Ti}_2$ ,  $\text{Al}(\text{F,OH})(\text{Ti,O})_{-1}$  and  $\text{SnTi}_{-1}$ . *Mineralogical Magazine* **72(6)**, 1293–1305.

ČERNÝ, P. (1991) Rare-element Granitic Pegmatites. Part I: Anatomy and Internal Evolution of Pegmatite Deposits. *Geoscience Canada* **18(2)**, 49–67.

ČERNÝ, P. & ERCIT, T.S. (2005) The Classification of Granitic Pegmatites Revisited. *Canadian Mineralogist* **43**, 2005–2026.

CHAPPELL, B.W., & WHITE, A.J.R. (2001) Two contrasting granite types: 25 years later! *Australian Journal of Earth Sciences* **48**, 489-499.

CROWLEY, J.L., GHENT, E.D., CARR, S.D., SIMONY, P.S., & HAMILTON, M.A. (2000) Multiple thermotectonic events in a continuous metamorphic sequence, Mica Creek area, southeastern Canadian Cordillera. *Mineralogical Society of America: Geological Materials Research* **2, 2**, 1-45.

CURRIE, K.L. (1976) The alkaline rocks of Canada. *Geological Survey of Canada. Bulletin* 239, 1-278.

DAWSON, J.B. (1980) *Kimberlites and their Xenoliths*. Springer-Verlag Berlin Heidelberg, Germany. 1-250.

DEER, W.A., HOWIE, R.A., & ZUSSMAN, J. (2001) *Rock-Forming Minerals volume 4A: Framework silicates, feldspars*, Second Edition. The Geological Society of London, The Alden Press, Oxford, England, 909–943.

DIGEL, S.G., GHENT, E.D., CARR, S.D., & SIMMONY, P.S. (1998) Early Cretaceous kyanite-sillimanite metamorphism and Paleocene sillimanite overprint near Mount Cheadle, southeastern British Columbia: geometry, geochronology, and metamorphic interpretations. *Canadian Journal of Earth Sciences* **35**, 1070-1087.

DILL, H.G. (2015) The geology of pegmatites and the CMS classification scheme. PEG 2015 Conference, Książ, Poland.

DIXON, A. (2013) *Mineralogy and the geochemistry of pegmatites on Mount Begbie, British Columbia*. Master of Science Thesis, University of British Columbia. 1-366.

DIXON, A., CEMPÍREK, J., & GROAT, L.A. (2014). Mineralogy and geochemistry of pegmatites on Mount Begbie, British Columbia. *The Canadian Mineralogist* **52**, 129-164.

ELS, F. (2014) *Canada wants 20% of global rare earth market by 2018*. Mining.com, January 8, 2014.

ERCIT, T.S. (1994) The geochemistry and crystal chemistry of columbite-group minerals from granitic pegmatites, southwestern Grenville Province, Canadian Shield. *Canadian Mineralogist* **32**, 421–438.

ERCIT, T.S. (2002) The mess that is “allanite.” *Canadian Mineralogist* **40**, 1411–1419.

ERCIT, T.S. (2004) REE-enriched granitic pegmatites. *GAC Short Course Notes: Rare-Element Geochemistry and Mineral Deposits* **17**, 175-199.

ERCIT, T.S. (2005) Identification and alteration trends of granitic-pegmatite-hosted (Y,REE,U,Th)-(Nb,Ta,Ti) oxide minerals: A statistical approach. *Canadian Mineralogist* **43**, 1291–1303.

FINGER, F., BROSKA, I., ROBERTS, M.P., & SCHERMAIER, A. (1998) Replacement of primary monazite by apatite-allanite-epidote coronas in an amphibolite facies granite gneiss from the eastern Alps. *American Mineralogist* **83**, 248–258.

GHENT, E.D., KNITTER, C.C., RAESIDE, R.P., & STOUT, M.Z. (1982) Geothermometry and geobarometry of pelitic rocks, upper kyanite and sillimanite zones, Mica Creek area, British Columbia. *The Canadian Mineralogist* **20**, 3, 295-305.

GHENT, E. & VILLENEUVE, M. (2006)  $^{40}\text{Ar}/^{39}\text{Ar}$  dates on hornblende, muscovite, and biotite from the Mica Creek area, British Columbia: regional metamorphic and tectonic implications. *Canadian Journal of Earth Science* **43**, 83-100.

GIBSON H.D., BROWN, R.L., & PARRISH, R.R. (1999) Deformation-induced inverted metamorphic field gradients: an example from the southeastern Canadian Cordillera. *Journal of Structural Geology* **21**, 751-767.

GITTINS, J. (1979) The feldspathoid alkaline rocks. *The evolution of the igneous rocks: fiftieth anniversary perspectives*. Ed. Yoder, H.S., Jr. 351-390.

HALLERAN, A.A.D. (1991) *Geological, geochemistry and origins of the Mount Bisson alkaline rocks, Munroe Creek, British Columbia Canada*. Unpublished M.Sc. thesis, University of British Columbia, Vancouver, British Columbia, 1-167.

HALLERAN, A.A.D. & RUSSEL, J.K. (1990) Geology and descriptive petrology of the Mount Bisson alkaline complex, Munroe Creek, British Columbia (97N/9E, 93O/45W, 5W). British Columbia Ministry of Energy, Mines and Petroleum Resources Paper 1990-1, 297–304.

HALLERAN, A.A.D. & RUSSELL, J.K. (1996) REE-bearing alkaline pegmatites and associated light REE-enriched fenites at Mount Bisson, British Columbia. *Economic Geology* **91**, 451–459.

HAWTHORNE, F.C., OBERTI, R., HARLOW, G.E., MARESCH, W.V., MARTIN, R.F., SCHUMACHER, J.C., & WELCH, M.D. (2012) Nomenclature of the amphibole supergroup. *American Mineralogist* **97**, 2031–2048.

HEINRICH, E.W. (1966) *The Geology of Carbonatites*. Robert E. Krieger Publishing Company, Chicago, Illinois, United States, 1-585.

HINCHEY, A.M., CARR, S.D., MCNEILL, P.D., & RAYNER, N. (2006) Paleocene-Eocene high-grade metamorphism, anatexis, and deformation in the Thor-Odin dome, Monashee complex, southeastern British Columbia. *Canadian Journal of Earth Sciences* **43**, 1341–1365.

KREMMIDAS, T. (2012) Canada's rare earth deposits can offer substantial competitive advantages. *The Canadian Business Journal* **5**, 82-87.

LIFEROVICH, R.P. & MITCHELL, R.H. (2006) Apatite-group minerals from nepheline syenite, Pilansberg alkaline complex, South Africa. *Mineralogical Magazine* **70(5)**, 463–484.

LONDON, D. (2008) Pegmatites. *Canadian Mineralogist*, Special Publication **10**, 1-347.

LONDON, D. (2014) A petrologic assessment of internal zonation in granitic pegmatites. *Lithos* **184-187**, 74-104.

LONDON, D. & BURT, D.M. (1982) Lithium aluminosilicate occurrences in pegmatites and the lithium aluminosilicate phase diagram. *American Mineralogist* **67**, 483–493.

LONDON, D. & KONTAK, D.J. (2012) Granitic Pegmatites: Scientific Wonders and Economic Bonanzas. *Elements* **8**, 257–261.

MACDONALD, F. & BELKIN, H.E. (2002) Compositional variation in minerals of the chevkinite group. *Mineralogical Magazine* **66(6)**, 1075–1098

MACDONALD, R., BELKIN, H.E., WALL, F., & BAGIŃSKI, B. (2009) Compositional variation in the chevkinite group: new data from igneous and metamorphic rocks. *Mineralogical Magazine* **73(5)**, 777–796.

MACDONALD, R., BAGIŃSKI, S.B., KARTASHOV, P., ZOZULYA, D., & DZIERŻANOWSKI, P. (2012) Chevkinite-group minerals from Russia and Mongolia: new compositional data from metasomatites and ore deposits. *Mineralogical Magazine* **76(3)**, 535–549.

MANCHERI, N.A. (2012) Chinese Monopoly in Rare Earth Elements: Supply-Demand and Industrial Applications. *China Report* **48(4)**, 449–468.

MASSEY, N.W.D., MACINTYRE, D.G., DESJARDINS, P.J., & COONEY, R.T. (2005) Geology of British Columbia, *BC Ministry of Energy, Mines and Petroleum Resources*, Geoscience Map 2005-3, (3 sheets), scale 1: 1 000 000.

MCDONOUGH, W.F. & SUN, S.-S. (1995) The composition of the Earth. *Chemical Geology* **120**, 223–253.

MILLONIG, L.J. (2011) Mineralogy of rare metal-bearing zones at the KIN and Trident properties, British Columbia. Company Report. 1-25.

MILLONIG, L.J., GERDES, A., GROAT, L.A. (2012) U-Th-Pb geochronology of meta-carbonates and meta-alkaline rocks in the southern Canadian Cordillera: A geodynamic perspective. *Lithos* **152**, 202-217.

MONGER, J. & PRICE, R. (2002) The Canadian Cordillera: Geology and tectonic evolution. *CSEG Recorder*, 17-36.

NOVÁK, M., ČERNÝ, P., & UHER, P. (2003) Extreme variation and apparent reversal of Nb-Ta fractionation in columbite-group minerals from the Scheibengraben beryl-columbite granitic pegmatite, Maršikov, Czech Republic. *European Journal of Mineralogy* **15**, 565–574.

NOVÁK, M., KADLEC, T., GADAS, P. (2013) Geological position, mineral assemblages and contamination of granitic pegmatites in the Moldanubian Zone, Czech Republic; examples from the Vlastějovice region. *Journal of Geosciences* **58**, 21-47.

NOVÁK, M., ŠKODA, R., PILIP, J., MACEK, I., VACULOVÍČ, T. (2011) Compositional trends in tourmaline from intragranitic NYF pegmatites of the Třebíč Pluton, Czech Republic: An electron microprobe, Mössbauer and LA-ICP-MS study. *The Canadian Mineralogist* **49**, 357-380.

ONDREJKA, M., UHER, P., PUTIŠ, M., BROSKA, I., BAČIK, P., KONEČNÝ, P., & SCHMIEDT, I. (2012) Two-stage breakdown of monazite by post-magmatic and metamorphic fluids: An example from the Veporic orthogneiss, Western Carpathians, Slovakia. *Lithos* **142–143**, 245–255

PAL, D.C., MISHRA, B., & HEINZ, J.B. Mineralogy and geochemistry of pegmatite-hosted Sn-, Ta-Nb-, and Zr-Hf-bearing minerals from the southeastern part of the Baster-Malkangiri pegmatite belt, Central India. *Ore Geology Reviews* **30**, 30–55.

PAPOUTSA, A.D., PE-PIPER, G. (2013) The relationship between REE-Y-Th minerals and the evolution of an A-type granite, Wentworth Pluton, Nova Scotia. *American Mineralogist* **98**, 444-432.

PELL, J. (1994) Carbonatites, Nepheline Syenites, Kimberlites and related rocks in British Columbia. Province of British Columbia, Ministry of Energy, Mines and Petroleum Resources, Bulletin **88**, 1-136

PERKINS, M.J. (1983) *Structural Geology and Stratigraphy of the Northern Big Bend of the Columbia River, Selkirk Mountains, Southeastern British Columbia*. Thesis, Carleton University, Ottawa, Canada, 1-238.

POULTON, T.P. & SIMONY, P.S. (1980) Stratigraphy, sedimentology, and regional correlation of the Horsethief Creek Group (Hadrynian, Late Cambrian) in the northern Purcell and Selkirk Mountains, British Columbia. *Canadian Journal of Earth Sciences* **17**, 1708–1724.

PROL-LEDESMA, R-M., MELGAREJO, J.C., MARTIN, R.F. (2012) The El Muerto “NYF” granitic pegmatite, Oaxaca, Mexico, and its striking enrichment in allanite-(Ce) and monazite-(Ce). *The Canadian Mineralogist* **50**, 1055-1076.

RAITH, M.M., DEVARAJU, T.C., & SPIERING, B. (2014) Paragenesis and chemical characteristics of the celsian-hyalophane-K-feldspar series and associated Ba-Cr micas in barite-bearing strata of the Mesoarchaeon Ghattihosahalli Belt, Western Dharwar Craton, South India. *Mineralogy and Petrology* **108**, 153–176.

RIPP, G.S., IZBRODIN, I.A., DOROSHKEVICH, A.G., LASTOCHKIN, E.I., RAMPILOV, M.O., SERGEEV, S.A., TRAVIN, A.V., & POSOKHOV, V.F. (2013) Chronology of the Formation of the gabbro-syenite-granite series of the Oshurkovo Pluton, Western Transbaikalia. *Petrology* **4**, 375–392.

SCAMMELL, R.J. (1993) *Mid-Cretaceous to Tertiary thermotectonic history of former mid-crustal rocks, southern Omineca Belt, Canadian Cordillera*. PhD thesis, Queen's University. 1-576.

SEVIGNY, J.H., PARRISH, R.R., & GHENT, E.D. (1989) Petrogenesis of peraluminous granite, Monashee Mountains, southeastern Canadian Cordillera. *Journal of Petrography* **30**, 557-581.

SEVIGNY, J.H., PARRISH, R.R., DONELICK, R.A. & GHENT, E.D. (1990) Northern Monashee Mountains, Omineca Crystalline Belt, British Columbia: Timing of metamorphism, anatexis, and tectonic denudation. *Geology* **18**, 103-106.

SHAW, D. (1980) A concordant uranium-lead age for zircons in the Adamand pluton, British Columbia. *In Current Research, Part C, Geological Survey of Canada*, **80-1C**, 243-246.

SIMMONS, W.B., LEE, M.T., & BREWSTER, R.H. (1987) Geochemistry and evolution of the South Platte granite-pegmatite system, Jefferson County, Colorado. *Geochimica et Cosmochimica Acta*, **51**, 455-471.

- SIMMONS, W.B., WEBBER, K.L., FALSTER, A.U., & NIZAMOFF, J.W. (2003) *Pegmatology: Pegmatite mineralogy, petrology and petrogenesis*. Rubellite Press, New Orleans, Louisiana, United States. 1-176.
- ŠKODA, R. & NOVÁK, M. (2007) Y,REE,Nb,Ta,Ti-oxide ( $AB_2O_6$ ) minerals from REL-REE euxenite-subtype pegmatites of the Třebíč Pluton, Czech Republic; substitutions and fractionation trends. *Lithos* **95**, 43–57.
- SLÁMA, J., KOŠLER, J., CONDON, D.J., CROWLEY, J.L., GERDES, A., HANCHAR, J.M., HORSTWOOD, M.S.A., MORRISH, G.A., NASDALA, L., NORBERG, N., SCHALTEGGER, U., XCHOENE, B., TUBRETT, M.N. & WHITEHOUSE, M.J. (2007) Plešovice zircon – A new natural reference material for U-Pb and Hf isotopic microanalysis. *Chemical Geology* **249**, 1-35.
- TAFTI, R., MORTENSEN, J.K., LANG, J.R., REBAGLIATI, M., & OLIVER, J.L. (2009) Jurassic U-Pb and Re-Os ages for newly discovered Xietongmen Cu-Au porphyry district, Tibet: Implications for metallogenic epochs in the southern Gangdese Belt. *Economic Geology* **104**, 127-136.
- TASÁRYOVÁ, Z., FRÝDA, J., JANOUŠEK, V., & RACEK, M. (2014) Slawsonite-celsian-hyalophane assemblage from a picrite sill (Prague Basin, Czech Republic). *American Mineralogist* **99**, 2272–2279.
- TOMAŠIĆ, N., GAJOVIĆ, A., BERMANEC, V., RAJIĆ, M. (2004) Recrystallization of metamict Nb-Ta-Ti-REE complex oxides: a coupled X-ray diffraction and Raman Spectroscopy study of Aeschynite-(Y) and Polycrase-(Y). *The Canadian Mineralogy* **42**, 1847-1857.
- THOMAS, R., DAVIDSON, P., & BEURLIN, H. (2012) The competing models of the origin and internal evolution of granitic pegmatites in the light of melt and fluid inclusion research.

*Mineralogy and Petrology* **106**, 55–73.

TROUW, R.A.J., PASSCHIER, C.W., & SIERSMA, D. (2009) *Atlas of Mylonites – and related microstructures*, 1<sup>st</sup> Edition. Springer-Verlag, Berlin, Heidelberg, Germany. 1-322.

UHER, P., ONDREJKA, M., & KONEČNÝ, P. (2009) Magmatic and post-magmatic Y-REE-Th phosphate, silicate, and Nb-Ta-REE oxide minerals in A-type metagranite: an example from the Turčok massif, the Western Carpathians, Slovakia. *Mineralogical Magazine* **73(6)**, 1009-1025.

UPADHYAY, D. & PRUSETH, K.L. (2012) Fluid-induced dissolution breakdown of monazite from Tso Moriri complex, NW Himalayas: evidence for immobility of trace element. *Contributions to Mineral Petrology* **164**, 303–316.

VLACH, S.R.F. & GUALDA, G.A.R. (2007) Allanite and chevkinite in A-type granites and syenites of the Graciosa Province, southern Brazil. *Lithos* **97**, 98–121.

WHALEN, J.B., CURRIE, K.L., & CHAPPELL, B.W. (1987) A-type granites: geochemical characteristics, discrimination and petrogenesis. *Contributions to Mineralogy and Petrography* **95**, 407-419.

WHEELER, J.O. (1965) *Big Bend Map-area, British Columbia*. Geological Survey of Canada, Paper 64-32, 1-37.

WHITE, G.V. (1989) *Industrial Minerals in British Columbia*. Ministry of Energy, Mines and Petroleum Resources, Information Circular 1989-2.

## Appendices

### Appendix A: EMPA Methods

All electron microprobe results were done on a Cameca SX-100 machine at Joint Laboratory of Electron Microscopy and Microanalyses, Department of Geological Sciences, Masaryk University, Brno, Czech Republic. Chemical compositions were analyzed using wavelength-dispersive mode.

#### A.1 Feldspar

EMPA analyses for feldspar were collected with the following conditions: excitation voltage: 15 kV; beam current: 10 nA; diameter: 5  $\mu\text{m}$ .

For the elements considered, the following standards, X-ray lines and crystals were used: albite,  $\text{NaK}_{\alpha}$ , TAP; sanidine,  $\text{SiK}_{\alpha}$ , TAP; sanidine,  $\text{AlK}_{\alpha}$ , TAP; sanidine,  $\text{KK}_{\alpha}$ , TAP; wollastonite,  $\text{CaK}_{\alpha}$ , LPET; baryte,  $\text{BaL}_{\alpha}$ , LPET; andradite,  $\text{FeK}_{\alpha}$ , LLIF;  $\text{SrSO}_4$ ,  $\text{SrL}_{\alpha}$ , TAP; fluorapatite,  $\text{PK}_{\alpha}$ , PET; Rb leucite,  $\text{RbL}_{\alpha}$ , TAP; pollucite,  $\text{CsL}_{\alpha}$ , LPET.

#### A.2 Mica, Beryl, and Bertrandite

EMPA analyses for mica minerals were collected with the following conditions: excitation voltage: 15 kV; beam current: 10 nA; diameter: 3  $\mu\text{m}$ .

For the elements considered, the following standards, X-ray lines and crystals were used: albite,  $\text{NaK}_{\alpha}$ , TAP; sanidine,  $\text{SiK}_{\alpha}$ , TAP; sanidine,  $\text{AlK}_{\alpha}$ , TAP; sanidine,  $\text{KK}_{\alpha}$ , TAP; pyrope,  $\text{MgK}_{\alpha}$ , TAP; titanite,  $\text{TiK}_{\alpha}$ , LPET; fluorapatite,  $\text{PK}_{\alpha}$ , LPET; chromite,  $\text{CrK}_{\alpha}$ , LPET; pollucite,  $\text{CsL}_{\alpha}$ , LPET; vanadinite,  $\text{ClK}_{\alpha}$ , LPET; wollastonite,  $\text{CaK}_{\alpha}$ , PET; almandine,  $\text{FeK}_{\alpha}$ , LLIF;

spessartine,  $MnK_{\alpha}$ , LLIF;  $ScVO_4$ ,  $VK_{\alpha}$ , LLIF;  $ScVO_4$ ,  $ScK_{\alpha}$ , PET; gahnite,  $ZnK_{\alpha}$ , LLIF; topaz,  $FK_{\alpha}$ , PC1;  $SrSO_4$ ,  $SK_{\alpha}$ , LPET; Rb leucite,  $RbL_{\alpha}$ , TAP.

### **A.3 Amphibole**

EMPA analyses for amphibole were collected with the following conditions: excitation voltage: 15 kV; beam current: 10 nA; diameter: 10  $\mu$ m.

For the elements considered, the following standards, X-ray lines and crystals were used: albite,  $NaK_{\alpha}$ , TAP; sanidine,  $SiK_{\alpha}$ , TAP; sanidine,  $AlK_{\alpha}$ , TAP; sanidine,  $KK_{\alpha}$ , TAP; pyrope,  $MgK_{\alpha}$ , TAP; titanite,  $TiK_{\alpha}$ , LPET; fluorapatite,  $PK_{\alpha}$ , LPET; chromite;  $CrK_{\alpha}$ , LPET; vanadinite,  $ClK_{\alpha}$ , LPET; wollastonite,  $CaK_{\alpha}$ , PET; almandine,  $FeK_{\alpha}$ , LLIF; spessartine,  $MnK_{\alpha}$ , LLIF;  $ScVO_4$ ,  $VK_{\alpha}$ , LLIF; gahnite,  $ZnK_{\alpha}$ , LLIF; topaz,  $FK_{\alpha}$ , PC1;  $SrSO_4$ ,  $SK_{\alpha}$ , LPET.

### **A.4 Garnet**

EMPA analyses for garnet were collected with the following conditions: excitation voltage: 15 kV; beam current: 20 nA; diameter: 2  $\mu$ m.

For the elements considered, the following standards, X-ray lines and crystals were used: albite,  $NaK_{\alpha}$ , TAP; sanidine,  $SiK_{\alpha}$ , TAP; sanidine,  $AlK_{\alpha}$ , TAP; sanidine,  $KK_{\alpha}$ , TAP; pyrope,  $MgK_{\alpha}$ , TAP; fluorapatite,  $PK_{\alpha}$ , LPET;  $ScVO_4$ ,  $ScK_{\alpha}$ , PET;  $ScVO_4$ ,  $VK_{\alpha}$ , LLIF; titanite,  $TiK_{\alpha}$ , LPET; chromite;  $CrK_{\alpha}$ , LPET; wollastonite,  $CaK_{\alpha}$ , PET;  $YPO_4$ ,  $YL_{\alpha}$ , TAP; almandine,  $FeK_{\alpha}$ , LLIF; spessartine,  $MnK_{\alpha}$ , LLIF; topaz,  $FK_{\alpha}$ , PC1.

## A.5 Zircon

EMPA analyses for zircon were collected with the following conditions: excitation voltage: 15 kV; beam current: 20 nA; diameter: 2  $\mu\text{m}$ .

For the elements considered, the following standards, X-ray lines and crystals were used: wollastonite,  $\text{CaK}_{\alpha}$ , PET;  $\text{LaPO}_4$ ,  $\text{LaL}_{\alpha}$ , PET;  $\text{LaPO}_4$ ,  $\text{PK}_{\alpha}$ , LPET;  $\text{CePO}_4$ ,  $\text{CeL}_{\alpha}$ , PET; brabanite,  $\text{ThM}_{\alpha}$ , LPET; U,  $\text{UM}_{\beta}$ , LPET; vanadinite,  $\text{PbM}_{\alpha}$ , LPET; zircon,  $\text{ZrL}_{\alpha}$ , TAP; zircon,  $\text{SiK}_{\alpha}$ , TAP; Hf,  $\text{HfM}_{\alpha}$ , TAP; YAG,  $\text{YL}_{\alpha}$ , TAP;  $\text{SmPO}_4$ ,  $\text{SmL}_{\alpha}$ , LLIF;  $\text{NdPO}_4$ ,  $\text{NdL}_{\beta}$ , LLIF;  $\text{Mn}_2\text{SiO}_4$ ,  $\text{MnK}_{\alpha}$ , LLIF; almandine,  $\text{FeK}_{\alpha}$ , LLIF; gahnite,  $\text{AlK}_{\alpha}$ , TAP; topaz,  $\text{FK}_{\alpha}$ , PC1;  $\text{ScVO}_4$ ,  $\text{ScK}_{\alpha}$ , PET; TiO,  $\text{TiK}_{\alpha}$ , PET; columbite Ivigtut,  $\text{NbL}_{\alpha}$ , LPET;  $\text{CrTa}_2\text{O}_6$ ,  $\text{TaM}_{\alpha}$ , LPET;  $\text{MgAl}_2\text{O}_4$ ,  $\text{MgK}_{\alpha}$ , TAP.

## A.6 Titanite

EMPA analyses for titanite were collected with the following conditions: excitation voltage: 15 kV; beam current: 20 nA; diameter: 2  $\mu\text{m}$ .

For the elements considered, the following standards, X-ray lines and crystals were used: albite,  $\text{NaK}_{\alpha}$ , TAP;  $\text{CrTa}_2\text{O}_6$ ,  $\text{TaL}_{\alpha}$ , LLIF; almandine,  $\text{FeK}_{\alpha}$ , LLIF; wollastonite,  $\text{CaK}_{\alpha}$ , PET; sanidine,  $\text{AlK}_{\alpha}$ , TAP; sanidine,  $\text{KK}_{\alpha}$ , PET;  $\text{LaPO}_4$ ,  $\text{LaL}_{\alpha}$ , PET;  $\text{CePO}_4$ ,  $\text{CeL}_{\alpha}$ , PET; titanite,  $\text{TiK}_{\alpha}$ , LPET; titanite,  $\text{SiK}_{\alpha}$ , TAP;  $\text{YPO}_4$ ,  $\text{YL}_{\alpha}$ , TAP;  $\text{PrPO}_4$ ,  $\text{PrL}_{\beta}$ , LLIF;  $\text{NdPO}_4$ ,  $\text{NdL}_{\beta}$ , LLIF;  $\text{SmPO}_4$ ,  $\text{SmL}_{\beta}$ , LLIF; Sn,  $\text{SnL}_{\alpha}$ , LPET; topaz,  $\text{FK}_{\alpha}$ , PC1; pyrope,  $\text{MgK}_{\alpha}$ , TAP; columbite Ivigtut,  $\text{NbL}_{\alpha}$ , LPET; vanadinite,  $\text{VK}_{\beta}$ , LPET; brabanite,  $\text{ThM}_{\alpha}$ , LPET;  $\text{ScVO}_4$ ,  $\text{ScK}_{\alpha}$ , PET; zircon,  $\text{ZrL}_{\alpha}$ , TAP;  $\text{GdPO}_4$ ,  $\text{GdL}_{\alpha}$ , LLIF; U,  $\text{UM}_{\beta}$ , LPET;  $\text{DyPO}_4$ ,  $\text{DyL}_{\alpha}$ , LLIF;  $\text{ErPO}_4$  modified,  $\text{ErL}_{\alpha}$ , LLIF;  $\text{YbPO}_4$ ,  $\text{YbL}_{\alpha}$ , LLIF.

## A.7 Tourmaline

EMPA analyses for tourmaline were collected with the following conditions: excitation voltage: 15 kV; beam current: 10 nA; diameter: 5  $\mu\text{m}$ .

For the elements considered, the following standards, X-ray lines and crystals were used: albite,  $\text{NaK}_\alpha$ , TAP; sanidine,  $\text{SiK}_\alpha$ , TAP; sanidine,  $\text{AlK}_\alpha$ , TAP; sanidine,  $\text{KK}_\alpha$ , TAP; pyrope,  $\text{MgK}_\alpha$ , TAP; titanite,  $\text{TiK}_\alpha$ , LPET; vanadinite,  $\text{ClK}_\alpha$ , LPET; fluorapatite,  $\text{PK}_\alpha$ , LPET; wollastonite,  $\text{CaK}_\alpha$ , PET; almandine,  $\text{FeK}_\alpha$ , LLIF; spessartine,  $\text{MnK}_\alpha$ , LLIF;  $\text{ScVO}_4$ ,  $\text{VK}_\alpha$ , LLIF; gahnite,  $\text{ZnK}_\alpha$ , LLIF; topaz,  $\text{FK}_\alpha$ , PC1.

## A.8 Epidote Group Minerals

EMPA analyses for the epidote group minerals were collected with the following conditions: excitation voltage: 15 kV; beam current: 20 nA; diameter: 3  $\mu\text{m}$ .

For the elements considered, the following standards, X-ray lines and crystals were used: albite,  $\text{NaK}_\alpha$ , TAP; almandine,  $\text{FeK}_\alpha$ , LLIF; spessartine,  $\text{MnK}_\alpha$ , LLIF;  $\text{NdPO}_4$ ,  $\text{NdL}_\beta$ , LLIF;  $\text{PrPO}_4$ ,  $\text{PrL}_\beta$ , LLIF;  $\text{LaPO}_4$ ,  $\text{LaL}_\alpha$ , PET;  $\text{CePO}_4$ ,  $\text{CeL}_\alpha$ , PET;  $\text{TiO}$ ,  $\text{TiK}_\alpha$ , PET; sanidine,  $\text{SiK}_\alpha$ , TAP; sanidine,  $\text{AlK}_\alpha$ , TAP; sanidine,  $\text{KK}_\alpha$ , LPET;  $\text{YPO}_4$ ,  $\text{YL}_\alpha$ , TAP;  $\text{SmPO}_4$ ,  $\text{SmL}_\beta$ , LLIF;  $\text{GdPO}_4$  modified,  $\text{GdL}_\beta$ , LLIF;  $\text{CePO}_4$ ,  $\text{CeL}_\alpha$ , PET;  $\text{DyPO}_4$  modified,  $\text{DyL}_\beta$ , LLIF;  $\text{ErPO}_4$  modified,  $\text{ErL}_\alpha$ , LLIF; wollastonite,  $\text{CaK}_\alpha$ , LPET; vanadinite,  $\text{ClK}_\alpha$ , LPET; vanadinite,  $\text{VK}_\beta$ , LPET; vanadinite,  $\text{PbM}_\alpha$ , LPET; brabanite,  $\text{ThM}_\alpha$ , LPET; U,  $\text{UM}_\beta$ , LPET; topaz,  $\text{FK}_\alpha$ , PC1;  $\text{Mg}_2\text{SiO}_4$ ,  $\text{MgK}_\alpha$ , TAP; zircon,  $\text{ZrL}_\alpha$ , TAP; Sn,  $\text{SnL}_\alpha$ , LPET;  $\text{ScVO}_4$ ,  $\text{ScK}_\alpha$ , PET; fluorapatite,  $\text{PK}_\alpha$ , LPET; chromite,  $\text{CrK}_\alpha$ , PET;  $\text{SrSO}_4$ ,  $\text{SrL}_\alpha$ , TAP;  $\text{TbPO}_4$ ,  $\text{TbL}_\alpha$ , LLIF;  $\text{HoPO}_4$ ,  $\text{HoL}_\beta$ , LLIF;  $\text{YbPO}_4$ ,  $\text{YbL}_\alpha$ , LLIF;  $\text{TmPO}_4$ ,  $\text{TmL}_\alpha$ , LLIF;  $\text{EuPO}_4$ ,  $\text{EuL}_\beta$ , LLIF.

## A.9 Chevkinite Group Minerals

EMPA analyses for chevkinite group minerals were collected with the following conditions: excitation voltage: 15 kV; beam current: 20 nA; diameter: 2  $\mu\text{m}$ .

For the elements considered, the following standards, X-ray lines and crystals were used: albite,  $\text{NaK}_{\alpha}$ , TAP; almandine,  $\text{FeK}_{\alpha}$ , LLIF; spessartine,  $\text{MnK}_{\alpha}$ , LLIF;  $\text{NdPO}_4$ ,  $\text{NdL}_{\beta}$ , LLIF;  $\text{PrPO}_4$ ,  $\text{PrL}_{\beta}$ , LLIF;  $\text{TiO}$ ,  $\text{TiK}_{\alpha}$ , PET;  $\text{LaPO}_4$ ,  $\text{LaL}_{\alpha}$ , PET,  $\text{CePO}_4$ ,  $\text{CeL}_{\alpha}$ , PET; sanidine,  $\text{SiK}_{\alpha}$ , TAP; sanidine,  $\text{AlK}_{\alpha}$ , TAP; sanidine,  $\text{KK}_{\alpha}$ , LPET;  $\text{YPO}_4$  modified,  $\text{YL}_{\alpha}$ , TAP;  $\text{SmPO}_4$ ,  $\text{SmL}_{\beta}$ , LLIF;  $\text{DyPO}_4$ ,  $\text{DyL}_{\beta}$ , LLIF;  $\text{GdPO}_4$  modified,  $\text{GdL}_{\beta}$ , LLIF;  $\text{ErPO}_4$  modified,  $\text{ErL}_{\alpha}$ , LLIF; wollastonite,  $\text{CaK}_{\alpha}$ , LPET; columbite Ivigtut,  $\text{NbL}_{\alpha}$ , LPET; vanadinite,  $\text{ClK}_{\alpha}$ , LPET; vanadinite,  $\text{PbM}_{\alpha}$ , LPET; U,  $\text{UM}_{\beta}$ , LPET; topaz,  $\text{FK}_{\alpha}$ , PC1;  $\text{Mg}_2\text{SiO}_4$ ,  $\text{MgK}_{\alpha}$ , TAP; zircon,  $\text{ZrL}_{\alpha}$ , TAP; Sn,  $\text{SnL}_{\alpha}$ , LPET;  $\text{ScVO}_4$ ,  $\text{ScK}_{\alpha}$ , PET;  $\text{SrSO}_4$ ,  $\text{SrL}_{\alpha}$ , TAP;  $\text{TbPO}_4$ ,  $\text{TbL}_{\alpha}$ , LLIF;  $\text{HoPO}_4$ ,  $\text{HoL}_{\beta}$ , LLIF;  $\text{YbPO}_4$ ,  $\text{YbL}_{\alpha}$ , LLIF;  $\text{TmPO}_4$ ,  $\text{TmL}_{\alpha}$ , LLIF;  $\text{CrTa}_2\text{O}_6$ ,  $\text{TaM}_{\alpha}$ , TAP; barite,  $\text{BaL}_{\alpha}$ , LLIF.

## A.10 Monazite and Thorite

EMPA analyses for monazite were collected with the following conditions: excitation voltage: 15 kV; beam current: 20 nA; diameter: 3  $\mu\text{m}$ .

For the elements considered, the following standards, X-ray lines and crystals were used: albite,  $\text{NaK}_{\alpha}$ , TAP;  $\text{YPO}_4$ ,  $\text{YL}_{\alpha}$ , TAP; sanidine,  $\text{SiK}_{\alpha}$ , TAP, fluorapatite,  $\text{PK}_{\alpha}$ , PET; fluorapatite,  $\text{CaK}_{\alpha}$ , LPET;  $\text{SrSO}_4$ ,  $\text{SrL}_{\alpha}$ , TAP;  $\text{PrPO}_4$ ,  $\text{PrL}_{\beta}$ , LLIF;  $\text{NdPO}_4$ ,  $\text{NdL}_{\beta}$ , LLIF;  $\text{SmPO}_4$ ,  $\text{SmL}_{\alpha}$ , LLIF;  $\text{LaPO}_4$ ,  $\text{LaL}_{\alpha}$ , LPET,  $\text{CePO}_4$ ,  $\text{CeL}_{\alpha}$ , LPET;  $\text{EuPO}_4$ ,  $\text{EuL}_{\beta}$ , LLIF;  $\text{GdPO}_4$  modified,  $\text{GdL}_{\beta}$ , LLIF;  $\text{DyPO}_4$  modified,  $\text{DyL}_{\alpha}$ , LLIF;  $\text{ErPO}_4$  modified,  $\text{ErL}_{\alpha}$ , LLIF; U,  $\text{UM}_{\beta}$ , LPET; brabanite,  $\text{ThM}_{\alpha}$ , LPET; vanadinite,  $\text{PbM}_{\alpha}$ , LPET; lammerite,  $\text{AsL}_{\alpha}$ , TAP; almandine,  $\text{FeK}_{\alpha}$ , LLIF;  $\text{TiO}$ ,  $\text{TiK}_{\alpha}$ , PET; zircon,  $\text{ZrL}_{\alpha}$ , TAP;  $\text{ScVO}_4$ ,  $\text{ScK}_{\alpha}$ , LPET.

### A.11 Apatite

EMPA analyses for apatite were collected with the following conditions: excitation voltage: 15 kV; beam current: 10 nA; diameter: 7  $\mu\text{m}$ .

For the elements considered, the following standards, X-ray lines and crystals were used: albite,  $\text{NaK}_{\alpha}$ , TAP;  $\text{SrSO}_4$ ,  $\text{SrL}_{\alpha}$ , TAP;  $\text{SrSO}_4$ ,  $\text{SrL}_{\alpha}$ , PET; sanidine,  $\text{AlK}_{\alpha}$ , TAP; spessartine,  $\text{MnK}_{\alpha}$ , LLIF; spessartine,  $\text{SiK}_{\alpha}$ , TAP;  $\text{YPO}_4$ ,  $\text{YL}_{\alpha}$ , TAP;  $\text{Mg}_2\text{SiO}_4$ ,  $\text{MgK}_{\alpha}$ , TAP; fluorapatite,  $\text{PK}_{\alpha}$ , PET; fluorapatite,  $\text{CaK}_{\alpha}$ , LPET; almandine,  $\text{FeK}_{\alpha}$ , LLIF; topaz,  $\text{FK}_{\alpha}$ , PC1; brabanite,  $\text{ThM}_{\alpha}$ , LPET; baryte,  $\text{BaL}_{\alpha}$ , LPET; vanadinite,  $\text{ClK}_{\alpha}$ , LPET;  $\text{CePO}_4$ ,  $\text{CeL}_{\alpha}$ , PET;  $\text{NdPO}_4$ ,  $\text{NdL}_{\beta}$ , LLIF;  $\text{LaPO}_4$ ,  $\text{LaL}_{\alpha}$ , LPET.

### A.12 Columbite

EMPA analyses for columbite were collected with the following conditions: excitation voltage: 15 kV; beam current: 20 nA; diameter: 8  $\mu\text{m}$ .

For the elements considered, the following standards, X-ray lines and crystals were used: albite,  $\text{NaK}_{\alpha}$ , TAP;  $\text{CrTa}_2\text{O}_6$ ,  $\text{TaM}_{\alpha}$ , TAP; gahnite,  $\text{AlK}_{\alpha}$ , TAP; gahnite,  $\text{ZnK}_{\alpha}$ , LLIF;  $\text{YPO}_4$ ,  $\text{YL}_{\alpha}$ , TAP;  $\text{MgAl}_2\text{O}_4$ ,  $\text{MgK}_{\alpha}$ , TAP; columbite Ivigtut,  $\text{NbL}_{\alpha}$ , LPET; columbite Ivigtut,  $\text{FeK}_{\alpha}$ , LLIF; vanadinite,  $\text{PbM}_{\beta}$ , LPET; U,  $\text{UM}_{\beta}$ , LPET; brabanite,  $\text{ThM}_{\alpha}$ , LPET; sanidine,  $\text{SiK}_{\alpha}$ , LPET;  $\text{TiO}$ ,  $\text{TiK}_{\alpha}$ , PET; titanite,  $\text{CaK}_{\beta}$ , PET;  $\text{Mn}_2\text{SiO}_4$ ,  $\text{MnK}_{\alpha}$ , LLIF; W,  $\text{WL}_{\alpha}$ , LLIF; zircon,  $\text{ZrL}_{\alpha}$ , TAP; Sn,  $\text{SnL}_{\alpha}$ , PET; Bi,  $\text{BiM}_{\beta}$ , PET; Sb,  $\text{SbL}_{\beta}$ , PET;  $\text{ScVO}_4$ ,  $\text{ScK}_{\alpha}$ , LLIF; topaz,  $\text{FK}_{\alpha}$ , PC1.

### **A.13 Rutile and Ilmenite-Pyrophanite**

EMPA analyses for apatite were collected with the following conditions: excitation voltage: 15 kV; beam current: 20 nA; diameter: 2  $\mu\text{m}$ .

For the elements considered, the following standards, X-ray lines and crystals were used: columbite ivigtut,  $\text{Nb}L_{\alpha}$ , LPET; columbite ivigtut,  $\text{Fe}K_{\alpha}$ , LLIF;  $\text{Mn}_2\text{SiO}_4$ ,  $\text{Mn}K_{\alpha}$ , LLIF; W,  $WL_{\alpha}$ , LLIF;  $\text{CrTa}_2\text{O}_6$ ,  $\text{Ta}L_{\alpha}$ , LLIF; wollastonite,  $\text{Ca}K_{\alpha}$ , PET; titanite,  $\text{Si}K_{\alpha}$ , TAP; sanidine,  $\text{Al}K_{\alpha}$ , TAP; chromite,  $\text{Cr}K_{\alpha}$ , LPET; Sn,  $\text{Sn}L_{\alpha}$ , LPET; pyrope,  $\text{Mg}K_{\alpha}$ , TAP; vanadinite,  $\text{V}K_{\beta}$ , LPET;  $\text{ScVO}_4$ ,  $\text{Sc}K_{\alpha}$ , PET; zircon,  $\text{Zr}L_{\alpha}$ , TAP; gahnite,  $\text{Zn}K_{\alpha}$ , LLIF.

### **A.14 Aeschynite, Nioboeschynite, Euxenite, and Fersmite**

EMPA analyses for these REE-bearing oxide minerals were collected with the following conditions: excitation voltage: 15 kV; beam current: 20 nA; diameter: 2  $\mu\text{m}$ .

For the elements considered, the following standards, X-ray lines and crystals were used: albite,  $\text{Na}K_{\alpha}$ , TAP; almandine,  $\text{Fe}K_{\alpha}$ , LLIF; TiO,  $\text{Ti}K_{\alpha}$ , PET; titanite,  $\text{Ca}K_{\alpha}$ , PET; sanidine,  $\text{Si}K_{\alpha}$ , LPET; sanidine,  $\text{Al}K_{\alpha}$ , TAP; sanidine,  $\text{K}K_{\alpha}$ , PET;  $\text{LaPO}_4$ ,  $\text{La}L_{\alpha}$ , PET;  $\text{LaPO}_4$ ,  $\text{P}K_{\alpha}$ , LPET;  $\text{CePO}_4$ ,  $\text{Ce}L_{\alpha}$ , PET;  $\text{YPO}_4$ ,  $\text{Y}L_{\alpha}$ , TAP;  $\text{CrTa}_2\text{O}_6$ ,  $\text{Ta}M_{\alpha}$ , TAP;  $\text{Mn}_2\text{SiO}_4$ ,  $\text{Mn}K_{\alpha}$ , LLIF;  $\text{PrPO}_4$ ,  $\text{Pr}L_{\beta}$ , LLIF;  $\text{NdPO}_4$ ,  $\text{Nd}L_{\beta}$ , LLIF;  $\text{SmPO}_4$ ,  $\text{Sm}L_{\alpha}$ , LLIF; columbite Ivigtut,  $\text{Nb}L_{\alpha}$ , LPET; topaz,  $\text{F}K_{\alpha}$ , PC1; pyrope,  $\text{Mg}K_{\alpha}$ , TAP; U,  $\text{U}M_{\beta}$ , LPET; brabanite,  $\text{Th}M_{\alpha}$ , LPET;  $\text{ScVO}_4$ ,  $\text{Sc}K_{\alpha}$ , PET; zircon,  $\text{Zr}L_{\alpha}$ , TAP;  $\text{GdPO}_4$  modified,  $\text{Gd}L_{\alpha}$ , LLIF;  $\text{DyPO}_4$  modified,  $\text{Dy}L_{\beta}$ , LLIF;  $\text{ErPO}_4$  modified,  $\text{Er}L_{\alpha}$ , LLIF; fluorapatite,  $\text{P}K_{\alpha}$ , PET; lammerite,  $\text{As}L_{\alpha}$ , TAP;  $\text{TbPO}_4$ ,  $\text{Tb}L_{\alpha}$ , LLIF;  $\text{HoPO}_4$  modified,  $\text{Ho}L_{\beta}$ , LLIF;  $\text{YbPO}_4$ ,  $\text{Yb}L_{\alpha}$ , LLIF; W,  $WL_{\alpha}$ , LLIF; vanadinite,  $\text{Pb}M_{\beta}$ , LPET; Bi,  $\text{Bi}M_{\beta}$ , LPET.

## A.15 Lanthanite

EMPA analyses for lanthanite were collected with the following conditions: excitation voltage: 15 kV; beam current: 10 nA; diameter: 5  $\mu\text{m}$ .

For the elements considered, the following standards, X-ray lines and crystals were used: albite,  $\text{NaK}_{\alpha}$ , TAP;  $\text{YPO}_4$  modified,  $\text{YL}_{\alpha}$ , TAP; sanidine,  $\text{SiK}_{\alpha}$ , TAP;  $\text{SrSO}_4$ ,  $\text{SrL}_{\alpha}$ , TAP;  $\text{SrSO}_4$ ,  $\text{SK}_{\alpha}$ , LPET;  $\text{LaPO}_4$ ,  $\text{LaL}_{\alpha}$ , PET;  $\text{CePO}_4$ ,  $\text{CeL}_{\alpha}$ , PET; fluorapatite,  $\text{PK}_{\alpha}$ , PET; fluorapatite,  $\text{CaK}_{\alpha}$ , LPET; barite,  $\text{BaL}_{\alpha}$ , LLIF;  $\text{PrPO}_4$ ,  $\text{PrL}_{\beta}$ , LLIF;  $\text{NdPO}_4$ ,  $\text{NdL}_{\beta}$ , LLIF;  $\text{SmPO}_4$  modified,  $\text{SmL}_{\beta}$ , LLIF;  $\text{EuPO}_4$ ,  $\text{EuL}_{\beta}$ , LLIF;  $\text{GdPO}_4$  modified,  $\text{GdL}_{\beta}$ , LLIF;  $\text{DyPO}_4$  modified,  $\text{DyL}_{\alpha}$ , LLIF;  $\text{ErPO}_4$  modified,  $\text{ErL}_{\alpha}$ , LLIF; U,  $\text{UM}_{\beta}$ , LPET; brabanite,  $\text{ThM}_{\alpha}$ , LPET; vanadinite,  $\text{PbM}_{\alpha}$ , LPET; lammerite,  $\text{AsL}_{\alpha}$ , TAP; almandine,  $\text{FeK}_{\alpha}$ , LLIF;  $\text{TiO}$ ,  $\text{TiK}_{\alpha}$ , PET; zircon,  $\text{ZrL}_{\alpha}$ , TAP;  $\text{ScVO}_4$ ,  $\text{ScK}_{\alpha}$ , LPET; topaz,  $\text{FK}_{\alpha}$ , PC1; gahnite,  $\text{AlK}_{\alpha}$ , TAP.

## Appendix B: EMPA Results

### B.1: Feldspar

ab: albite

hy: hyalophane

k-spar: potassium feldspar

#### Appendix B.1: EMPA analyses of feldspar

Mineral	ab	ab	hy	hy	hy	hy	ab
Point	101 / 1 .	102 / 1 .	38 / 1 .	39 / 1 .	40 / 1 .	41 / 1 .	42 / 1 .
Thin Section	KIN134-2	KIN134-2	kin 130A				
SiO <sub>2</sub> (wt.%)	60.40	61.35	51.07	50.19	50.36	49.94	63.34
Al <sub>2</sub> O <sub>3</sub>	24.85	24.49	23.02	23.63	23.55	23.25	21.39
FeO	0.07	0.03	0.00	0.00	0.00	0.04	0.05
CaO	4.98	4.73	0.05	0.10	0.16	0.11	0.28
SrO	2.65	2.28	3.32	3.75	4.28	3.01	5.33
BaO	0.16	0.14	15.42	15.49	14.74	16.67	0.49
Na <sub>2</sub> O	7.91	8.00	2.51	2.48	2.81	2.25	9.10
K <sub>2</sub> O	0.24	0.32	5.27	4.83	4.35	4.92	0.13
Rb <sub>2</sub> O	0.13	0.18	0.00	0.01	0.00	0.00	0.13
Total	101.39	101.53	100.66	100.47	100.26	100.19	100.25
Si (apfu)	3.365	3.399	3.265	3.216	3.223	3.227	3.575
Al	1.632	1.599	1.735	1.784	1.776	1.771	1.423
Fe <sup>2+</sup>	0.003	0.001	0.000	0.000	0.000	0.002	0.002
Ca	0.297	0.281	0.003	0.007	0.011	0.007	0.017
Sr	0.086	0.073	0.123	0.139	0.159	0.113	0.174
Ba	0.004	0.003	0.386	0.389	0.370	0.422	0.011
Na	0.854	0.859	0.311	0.308	0.349	0.282	0.996
K	0.017	0.023	0.430	0.395	0.355	0.405	0.010
Rb	0.005	0.007	0.000	0.000	0.000	0.000	0.005

\*Note: feldspar formula was calculated on the basis of cation sum = 5

Elements sought but not found (or below detection limit): P, Rb, Cs (average detection limits of 360 ppm, 1338 ppm, and 431 ppm respectively)

**Appendix B.1:** EMPA analyses of feldspar

Mineral	hy	ab	hy	hy	hy	hy	hy
Point	43 / 1 .	17 / 1 .	25 / 1 .	26 / 1 .	27 / 1 .	28 / 1 .	29 / 1 .
Thin Section	kin 130A	G17a	130b	130b	130b	130b	130b
SiO <sub>2</sub> (wt.%)	52.01	67.28	51.76	53.31	52.04	50.50	54.13
Al <sub>2</sub> O <sub>3</sub>	23.37	21.36	23.39	23.79	23.73	23.71	23.46
FeO	0.04	0.01	0.00	0.00	0.00	0.00	0.00
CaO	0.16	1.67	0.04	0.35	0.24	0.06	0.34
SrO	4.65	0.00	3.37	4.62	4.48	2.65	4.71
BaO	12.98	0.00	15.30	11.98	13.81	17.79	11.07
Na <sub>2</sub> O	3.13	10.86	2.63	3.67	3.16	2.04	3.83
K <sub>2</sub> O	4.38	0.16	5.01	3.90	4.17	5.45	4.08
Rb <sub>2</sub> O	0.02	0.09	0.00	0.04	0.02	0.00	0.05
Total	100.74	101.46	101.51	101.66	101.72	102.21	101.68
Si (apfu)	3.267	3.637	3.262	3.277	3.250	3.219	3.308
Al	1.730	1.361	1.738	1.723	1.747	1.781	1.690
Fe <sup>2+</sup>	0.002	0.000	0.000	0.000	0.000	0.000	0.000
Ca	0.011	0.097	0.003	0.023	0.016	0.004	0.022
Sr	0.169	0.000	0.123	0.165	0.162	0.098	0.167
Ba	0.319	0.000	0.378	0.288	0.338	0.444	0.265
Na	0.382	1.138	0.322	0.437	0.383	0.252	0.453
K	0.351	0.011	0.403	0.306	0.332	0.443	0.318
Rb	0.001	0.003	0.000	0.002	0.001	0.000	0.002

**Appendix B.1:** EMPA analyses of feldspar

Mineral	hy	ab	ab	ab	ab	ab	ab
Point	30 / 1 .	31 / 1 .	32 / 1 .	33 / 1 .	34 / 1 .	39 / 1 .	40 / 1 .
Thin Section	130b						
SiO <sub>2</sub> (wt.%)	52.73	58.88	59.15	60.64	60.36	58.26	59.73
Al <sub>2</sub> O <sub>3</sub>	23.86	25.00	24.58	24.03	23.97	25.24	24.48
FeO	0.01	0.00	0.00	0.00	0.03	0.01	0.00
CaO	0.16	3.83	3.74	3.40	3.38	4.57	3.69
SrO	4.19	5.22	4.88	4.22	4.06	4.64	4.60
BaO	13.66	0.97	0.82	0.85	0.70	0.72	0.84
Na <sub>2</sub> O	3.14	7.28	7.48	8.02	7.99	7.02	7.71
K <sub>2</sub> O	4.50	0.38	0.37	0.36	0.37	0.34	0.36
Rb <sub>2</sub> O	0.01	0.01	0.00	0.01	0.00	0.00	0.01
Total	102.26	101.59	101.03	101.57	100.90	100.84	101.42
Si (apfu)	3.261	3.332	3.356	3.408	3.404	3.309	3.371
Al	1.739	1.667	1.644	1.591	1.593	1.689	1.628
Fe <sup>2+</sup>	0.000	0.000	0.000	0.000	0.001	0.000	0.000
Ca	0.011	0.232	0.227	0.205	0.204	0.278	0.223
Sr	0.150	0.171	0.161	0.138	0.133	0.153	0.151
Ba	0.331	0.022	0.018	0.019	0.015	0.016	0.019
Na	0.376	0.798	0.823	0.874	0.873	0.773	0.844
K	0.355	0.027	0.027	0.025	0.027	0.025	0.026
Rb	0.000	0.000	0.000	0.000	0.000	0.000	0.000

**Appendix B.1:** EMPA analyses of feldspar

Mineral	ab						
Point	55 / 1 .	65 / 1 .	66 / 1 .	79 / 1 .	80 / 1 .	30 / 1 .	31 / 1 .
Thin Section	Rad 2a	Rad 2a	Rad 2a	134-4	134-4	133C	133C
SiO <sub>2</sub> (wt.%)	61.62	61.49	61.17	59.32	59.32	60.01	60.54
Al <sub>2</sub> O <sub>3</sub>	23.45	24.20	23.89	24.17	24.16	24.98	24.82
FeO	0.01	0.00	0.02	0.02	0.03	0.01	0.02
CaO	4.88	5.59	5.28	5.00	4.95	5.68	5.44
SrO	0.49	0.62	0.48	2.04	2.04	2.01	2.17
BaO	0.18	0.12	0.14	0.15	0.13	0.09	0.06
Na <sub>2</sub> O	8.57	8.50	8.38	7.80	7.99	7.78	7.67
K <sub>2</sub> O	0.25	0.16	0.22	0.37	0.29	0.13	0.14
Rb <sub>2</sub> O	0.10	0.08	0.12	0.10	0.06	0.00	0.02
Total	99.55	100.79	99.73	98.95	98.97	100.70	100.92
Si (apfu)	3.451	3.415	3.422	3.378	3.377	3.354	3.370
Al	1.548	1.584	1.576	1.622	1.621	1.646	1.628
Fe <sup>2+</sup>	0.000	0.000	0.001	0.001	0.001	0.000	0.001
Ca	0.293	0.333	0.316	0.305	0.302	0.340	0.324
Sr	0.016	0.020	0.016	0.067	0.067	0.065	0.070
Ba	0.004	0.003	0.003	0.003	0.003	0.002	0.001
Na	0.930	0.916	0.909	0.861	0.881	0.843	0.828
K	0.018	0.011	0.016	0.027	0.021	0.009	0.010
Rb	0.004	0.003	0.004	0.003	0.002	0.000	0.001

**Appendix B.1:** EMPA analyses of feldspar

Mineral	ab	K-spar	K-spar	ab	ab
Point	32 / 1 .	8 / 1 .	9 / 1 .	10 / 1 .	11 / 1 .
Thin Section	133C	Pegm1	Pegm1	Pegm1	Pegm1
SiO <sub>2</sub> (wt.%)	60.55	65.96	65.65	68.26	67.62
Al <sub>2</sub> O <sub>3</sub>	24.93	18.62	18.63	20.68	20.82
FeO	0.03	0.02	0.02	0.01	0.01
CaO	5.62	0.00	0.00	1.06	1.21
SrO	2.11	0.00	0.00	0.00	0.00
BaO	0.01	0.06	0.09	0.00	0.00
Na <sub>2</sub> O	7.82	1.26	0.94	11.43	11.14
K <sub>2</sub> O	0.17	15.43	15.48	0.14	0.28
Rb <sub>2</sub> O	0.00	0.00	0.00	0.05	0.04
Total	101.24	101.43	100.86	101.67	101.21
Si (apfu)	3.365	3.749	3.745	3.683	3.666
Al	1.633	1.247	1.253	1.315	1.330
Fe <sup>2+</sup>	0.001	0.001	0.001	0.000	0.000
Ca	0.335	0.000	0.000	0.061	0.070
Sr	0.068	0.000	0.000	0.000	0.000
Ba	0.000	0.001	0.002	0.000	0.000
Na	0.842	0.139	0.104	1.195	1.171
K	0.012	1.119	1.126	0.010	0.019
Rb	0.000	0.000	0.000	0.002	0.001

## B.2: Micas

bt: biotite

ms: muscovite

chl: chlorite

### Appendix B.2: EMPA analyses of micas

Mineral	bt						
Point	65 / 1 .	67 / 1 .	85 / 1 .	86 / 1 .	91 / 1 .	92 / 1 .	98 / 1 .
Thin Section	KIN133D	KIN133D	KIN134-2	KIN134-2	KIN134-2	KIN134-2	KIN134-2
SiO <sub>2</sub> (wt.%)	37.45	37.48	36.42	36.11	35.47	36.24	36.41
TiO <sub>2</sub>	2.44	2.19	2.70	3.02	2.66	2.92	2.57
Al <sub>2</sub> O <sub>3</sub>	14.18	14.42	15.42	16.27	15.79	16.07	16.08
V <sub>2</sub> O <sub>3</sub>	0.08	0.03	0.02	0.05	0.03	0.07	0.01
Cr <sub>2</sub> O <sub>3</sub>	0.02	0.02	0.04	0.02	0.03	0.04	0.01
FeO	16.68	16.77	17.01	16.84	18.03	17.78	17.97
MgO	13.51	13.51	12.10	11.17	11.19	11.19	11.47
CaO	0.02	0.03	0.02	0.00	0.00	0.01	0.02
MnO	0.29	0.29	0.47	0.47	0.35	0.32	0.25
ZnO	0.22	0.27	0.07	0.06	0.13	0.20	0.20
Na <sub>2</sub> O	0.25	0.18	0.13	0.13	0.13	0.14	0.11
K <sub>2</sub> O	8.01	8.33	8.60	8.78	8.71	8.68	8.73
F	1.43	1.52	1.06	0.90	0.94	0.88	0.94
Cl	0.02	0.04	0.02	0.01	0.01	0.01	0.02
H <sub>2</sub> O*	3.23	3.19	3.38	3.45	3.39	3.48	3.46
-(O=F,Cl)	0.60	0.65	0.45	0.38	0.40	0.38	0.40
Total	98.42	98.93	97.90	97.67	97.26	98.40	98.64
Si (apfu)	2.868	2.864	2.810	2.787	2.772	2.787	2.795
Ti	0.141	0.126	0.157	0.175	0.156	0.169	0.148
Al	1.280	1.299	1.402	1.480	1.454	1.456	1.455
V	0.005	0.002	0.001	0.003	0.002	0.004	0.001
Cr	0.001	0.001	0.002	0.001	0.002	0.002	0.001
Mg	1.543	1.539	1.391	1.285	1.303	1.283	1.312
Ca	0.002	0.003	0.001	0.000	0.000	0.001	0.002
Mn	0.019	0.019	0.031	0.031	0.023	0.021	0.017
Fe	1.069	1.071	1.098	1.087	1.178	1.143	1.153
Zn	0.012	0.015	0.004	0.003	0.007	0.011	0.011
Na	0.037	0.027	0.019	0.019	0.019	0.021	0.016
K	0.783	0.812	0.847	0.864	0.868	0.852	0.855
F	0.345	0.367	0.259	0.220	0.233	0.215	0.228
Cl	0.002	0.005	0.003	0.002	0.001	0.002	0.003
OH	1.652	1.628	1.738	1.778	1.766	1.783	1.769
vac.	0.076	0.078	0.108	0.150	0.108	0.136	0.119
O	10.000	10.000	10.000	10.000	10.000	10.000	10.000

\*Note: mica formula calculation based on O=11

Elements sought but not found (or below detection limit): P, Zn, S (average detection limits of 357 ppm, 977 ppm, and 284 ppm respectively)

**Appendix B.2:** EMPA analyses of micas

Mineral	bt	ms	ms	ms	ms	bt	bt
Point	100 / 1 .	14 / 1 .	15 / 1 .	16 / 1 .	35 / 1 .	59 / 1 .	60 / 1 .
Thin Section	KIN134-2	G17a	G17a	G17a	130b	Rad 2a	Rad 2a
SiO <sub>2</sub> (wt.%)	37.15	45.65	47.16	47.16	45.74	37.00	36.41
TiO <sub>2</sub>	2.56	0.03	0.19	0.14	0.06	2.46	2.45
Al <sub>2</sub> O <sub>3</sub>	16.10	33.83	33.98	33.75	35.40	17.48	17.81
V <sub>2</sub> O <sub>3</sub>	0.03	0.00	0.00	0.05	0.00	0.04	0.06
Cr <sub>2</sub> O <sub>3</sub>	0.01	0.00	0.02	0.00	0.02	0.01	0.04
FeO	17.52	3.15	2.15	2.28	0.93	13.66	14.11
MgO	11.58	1.59	0.99	1.07	0.22	11.93	11.73
CaO	0.00	0.00	0.04	0.02	0.03	0.02	0.02
MnO	0.34	0.04	0.00	0.03	0.00	0.62	0.58
ZnO	0.29	0.00	0.01	0.04	0.00	0.07	0.10
Na <sub>2</sub> O	0.12	0.39	0.55	0.43	0.63	0.16	0.23
K <sub>2</sub> O	8.91	10.61	10.40	10.63	8.39	8.68	8.36
F	0.99	0.22	0.20	0.20	0.07	2.34	2.42
Cl	0.02	0.07	0.02	0.01	0.00	0.02	0.02
H <sub>2</sub> O*	3.48	4.33	4.41	4.40	4.36	2.81	2.76
-(O=F,Cl)	0.42	0.11	0.09	0.08	0.03	0.99	1.02
Total	99.52	100.00	100.20	100.30	95.87	98.28	98.13
Si (apfu)	2.821	3.074	3.140	3.143	3.120	2.824	2.790
Ti	0.146	0.001	0.010	0.007	0.003	0.141	0.141
Al	1.441	2.685	2.666	2.651	2.846	1.572	1.609
V	0.002	0.000	0.000	0.003	0.000	0.002	0.004
Cr	0.001	0.000	0.001	0.000	0.001	0.001	0.002
Mg	1.311	0.160	0.099	0.107	0.022	1.357	1.340
Ca	0.000	0.000	0.003	0.002	0.002	0.001	0.002
Mn	0.022	0.002	0.000	0.002	0.000	0.040	0.038
Fe	1.112	0.177	0.120	0.127	0.053	0.872	0.904
Zn	0.016	0.000	0.001	0.002	0.000	0.004	0.006
Na	0.017	0.050	0.071	0.055	0.083	0.024	0.035
K	0.863	0.912	0.883	0.904	0.730	0.845	0.817
F	0.237	0.047	0.041	0.042	0.014	0.565	0.587
Cl	0.002	0.007	0.002	0.001	0.000	0.002	0.002
OH	1.761	1.946	1.957	1.957	1.986	1.432	1.410
vac.	0.145	0.900	0.964	0.960	0.955	0.192	0.172
O	10.000	10.000	10.000	10.000	10.000	10.000	10.000

Appendix B.2: EMPA analyses of micas

Mineral	ms	bt	bt	ms	bt	bt	bt
Point	61 / 1 .	62 / 1 .	72 / 1 .	73 / 1 .	77 / 1 .	11 / 1 .	21 / 1 .
Thin Section	Rad 2a	Rad 2a	Rad 2a	Rad 2a	134-4	133C	133C
SiO <sub>2</sub> (wt.%)	43.06	35.93	36.59	43.68	36.18	38.56	38.87
TiO <sub>2</sub>	1.34	2.39	2.37	1.26	2.33	1.41	1.19
Al <sub>2</sub> O <sub>3</sub>	31.34	16.83	17.42	31.13	16.43	15.52	15.80
V <sub>2</sub> O <sub>3</sub>	0.00	0.04	0.05	0.02	0.07	0.00	0.03
Cr <sub>2</sub> O <sub>3</sub>	0.02	0.00	0.02	0.00	0.04	0.02	0.02
FeO	1.82	14.17	13.89	1.62	17.87	12.44	12.73
MgO	1.84	12.28	11.55	1.86	10.19	15.66	15.70
CaO	0.00	0.00	0.00	0.02	0.00	0.00	0.00
MnO	0.05	0.52	0.59	0.00	0.50	0.34	0.32
ZnO	0.07	0.12	0.18	0.00	0.13	0.36	0.34
Na <sub>2</sub> O	0.58	0.18	0.21	0.56	0.04	0.22	0.22
K <sub>2</sub> O	8.77	8.34	8.34	8.74	8.74	8.36	8.49
F	0.68	2.49	2.21	0.64	0.97	1.93	1.92
Cl	0.00	0.05	0.03	0.00	0.01	0.02	0.02
H <sub>2</sub> O*	3.87	2.66	2.83	3.91	3.39	3.07	3.11
-(O=F,Cl)	0.29	1.06	0.94	0.27	0.41	0.82	0.81
Total	93.72	97.05	97.21	93.71	97.29	98.71	99.55
Si (apfu)	3.074	2.795	2.822	3.108	2.816	2.895	2.895
Ti	0.072	0.140	0.137	0.067	0.137	0.080	0.066
Al	2.637	1.542	1.584	2.611	1.508	1.373	1.387
V	0.000	0.002	0.003	0.001	0.004	0.000	0.002
Cr	0.001	0.000	0.001	0.000	0.002	0.001	0.001
Mg	0.196	1.424	1.328	0.198	1.182	1.752	1.743
Ca	0.000	0.000	0.000	0.001	0.000	0.000	0.000
Mn	0.003	0.034	0.038	0.000	0.033	0.021	0.020
Fe	0.109	0.922	0.896	0.097	1.163	0.781	0.793
Zn	0.004	0.007	0.010	0.000	0.007	0.020	0.018
Na	0.081	0.027	0.031	0.078	0.007	0.032	0.031
K	0.798	0.827	0.821	0.793	0.868	0.801	0.806
F	0.154	0.612	0.539	0.144	0.239	0.458	0.451
Cl	0.000	0.007	0.004	0.000	0.002	0.003	0.002
OH	1.846	1.382	1.458	1.856	1.760	1.539	1.547
vac.	0.909	0.141	0.190	0.918	0.154	0.097	0.093
O	10.000	10.000	10.000	10.000	10.000	10.000	10.000

Appendix B.2: EMPA analyses of micas

Mineral	bt	ms	ms	bt	bt	bt	bt
Point	22 / 1 .	12 / 1 .	13 / 1 .	63 / 1 .	64 / 1 .	65 / 1 .	66 / 1 .
Thin Section	133C	Pegm1	Pegm1	135C	135C	135C	135C
SiO <sub>2</sub> (wt.%)	37.94	46.90	46.87	31.77	31.91	31.54	33.76
TiO <sub>2</sub>	1.30	0.71	0.63	4.78	4.79	4.66	3.73
Al <sub>2</sub> O <sub>3</sub>	15.25	32.16	32.58	13.95	13.80	13.48	13.43
V <sub>2</sub> O <sub>3</sub>	0.00	0.00	0.00	0.02	0.06	0.09	0.06
Cr <sub>2</sub> O <sub>3</sub>	0.04	0.00	0.01	0.03	0.03	0.02	0.03
FeO	12.60	3.32	3.29	19.72	19.51	19.73	19.78
MgO	15.51	1.03	1.00	8.32	8.26	8.25	9.79
CaO	0.04	0.01	0.02	0.01	0.00	0.02	0.02
MnO	0.34	0.02	0.07	0.75	0.69	0.76	0.74
ZnO	0.37	0.04	0.03	0.12	0.06	0.05	0.09
Na <sub>2</sub> O	0.19	0.49	0.44	0.10	0.10	0.10	0.17
K <sub>2</sub> O	8.75	10.71	10.73	4.99	4.83	5.13	6.26
F	1.86	0.55	0.54	1.33	1.35	1.35	1.43
Cl	0.02	0.01	0.02	0.02	0.02	0.03	0.03
H <sub>2</sub> O*	3.06	4.19	4.20	2.86	2.83	2.80	2.93
-(O=F,Cl)	0.79	0.23	0.23	0.56	0.57	0.57	0.61
Total	98.05	100.37	100.67	89.32	88.81	88.55	92.85
Si (apfu)	2.881	3.157	3.145	2.730	2.754	2.743	2.803
Ti	0.074	0.036	0.032	0.309	0.311	0.305	0.233
Al	1.364	2.551	2.577	1.412	1.404	1.382	1.314
V	0.000	0.000	0.000	0.001	0.004	0.006	0.004
Cr	0.002	0.000	0.001	0.002	0.002	0.001	0.002
Mg	1.756	0.104	0.100	1.066	1.062	1.070	1.212
Ca	0.003	0.001	0.002	0.001	0.000	0.001	0.002
Mn	0.022	0.001	0.004	0.055	0.051	0.056	0.052
Fe	0.800	0.187	0.184	1.417	1.408	1.435	1.374
Zn	0.021	0.002	0.001	0.007	0.004	0.003	0.005
Na	0.027	0.064	0.058	0.017	0.017	0.017	0.028
K	0.848	0.920	0.919	0.547	0.532	0.569	0.663
F	0.446	0.117	0.115	0.361	0.368	0.371	0.374
Cl	0.003	0.001	0.003	0.002	0.003	0.005	0.004
OH	1.550	1.882	1.882	1.637	1.629	1.624	1.622
vac.	0.100	0.963	0.957	0.007	0.004	0.003	0.005
O	10.000	10.000	10.000	10.030	10.045	10.036	10.044

Appendix B.2: EMPA analyses of micas

Mineral	bt	bt	chl	chl	chl	chl
Point	67 / 1 .	68 / 1 .	22 / 1 .	23 / 1 .	13 / 1 .	78 / 1 .
Thin Section	135C	135C	kin 136	kin 136	G17a	134-4
SiO <sub>2</sub> (wt.%)	32.13	29.52	22.90	23.53	23.26	25.25
TiO <sub>2</sub>	3.23	3.35	0.11	0.01	0.05	0.08
Al <sub>2</sub> O <sub>3</sub>	13.08	12.43	21.62	22.23	21.67	22.04
V <sub>2</sub> O <sub>3</sub>	0.06	0.06	0.00	0.00	0.00	0.06
Cr <sub>2</sub> O <sub>3</sub>	0.04	0.01	0.00	0.01	0.02	0.03
FeO	20.97	24.86	34.30	34.52	33.24	28.02
MgO	9.55	8.82	5.80	6.96	5.67	9.84
CaO	0.03	0.00	0.02	0.01	0.07	0.04
MnO	0.72	0.67	1.29	0.96	1.04	1.89
ZnO	0.04	0.07	0.06	0.02	0.02	0.03
Na <sub>2</sub> O	0.16	0.07	0.03	0.00	0.01	0.01
K <sub>2</sub> O	6.12	5.36	0.00	0.03	0.00	0.01
F	1.45	1.22	0.00	0.00	0.00	0.02
Cl	0.00	0.03	0.10	0.03	0.08	0.00
H <sub>2</sub> O*	2.85	2.90	10.40	10.77	10.30	10.92
-(O=F,Cl)	0.61	0.52	0.02	0.01	0.02	0.01
Total	92.96	99.40	96.67	99.07	95.44	98.24
Si (apfu)	2.727	2.541	2.633	2.620	2.703	2.771
Ti	0.206	0.217	0.010	0.001	0.004	0.006
Al	1.309	1.261	2.930	2.916	2.967	2.851
V	0.004	0.004	0.000	0.000	0.000	0.005
Cr	0.002	0.001	0.000	0.001	0.002	0.002
Mg	1.209	1.132	0.995	1.156	0.981	1.609
Ca	0.002	0.000	0.002	0.001	0.009	0.005
Mn	0.052	0.049	0.126	0.090	0.102	0.176
Fe	1.489	1.789	3.299	3.214	3.230	2.572
Zn	0.002	0.004	0.005	0.001	0.002	0.002
Na	0.027	0.012	0.008	0.000	0.002	0.001
K	0.663	0.589	0.000	0.005	0.000	0.002
F	0.388	0.333	0.000	0.000	0.000	0.008
Cl	0.000	0.005	0.019	0.005	0.016	0.001
OH	1.612	1.663	7.981	7.995	7.984	7.991
vac.	-0.121	-0.611	0.007	0.003	0.010	0.007
O	10.000	10.000	10.112	10.082	10.193	10.208

### B.3: Amphibole

mg-hlb: magnesiohornblende

#### Appendix B.3: EMPA analyses of amphiboles

Mineral	mg-hlb						
Point	55 / 1 .	56 / 1 .	57 / 1 .	58 / 1 .	59 / 1 .	60 / 1 .	63 / 1 .
Thin section	KIN133D						
SiO <sub>2</sub> (wt.%)	48.07	48.73	47.82	48.17	47.59	48.45	47.82
TiO <sub>2</sub>	0.53	0.48	0.56	0.50	0.56	0.46	0.61
Al <sub>2</sub> O <sub>3</sub>	7.15	6.69	7.37	6.95	6.89	6.73	7.43
Fe <sub>2</sub> O <sub>3</sub> *	0.00	0.00	0.00	0.00	0.00	0.00	0.00
FeO*	16.35	16.24	16.15	15.92	16.10	16.14	15.63
V <sub>2</sub> O <sub>3</sub>	0.02	0.02	0.06	0.08	0.10	0.02	0.09
Cr <sub>2</sub> O <sub>3</sub>	0.06	0.02	0.01	0.05	0.06	0.04	0.04
MnO	0.87	0.91	0.81	0.83	0.74	0.69	0.83
MgO	11.68	11.94	11.45	11.82	11.66	12.05	12.05
CaO	11.53	11.23	11.71	11.44	11.70	11.70	11.38
Na <sub>2</sub> O	0.99	0.83	1.06	1.14	1.04	0.95	0.93
K <sub>2</sub> O	0.50	0.40	0.52	0.53	0.54	0.46	0.44
F	0.65	0.61	0.66	0.70	0.70	0.69	0.60
Cl	0.01	0.02	0.01	0.00	0.01	0.00	0.00
H <sub>2</sub> O*	1.74	1.76	1.72	1.71	1.69	1.72	1.77
-(O=F,Cl)	-0.02	-0.02	-0.02	-0.02	-0.02	-0.02	-0.02
Total	100.13	99.89	99.90	99.83	99.38	100.10	99.61
<sup>T</sup> Si (apfu)	7.039	7.105	7.046	7.078	7.052	7.091	6.995
<sup>T</sup> Al	0.961	0.895	0.954	0.922	0.948	0.909	1.005
<sup>C</sup> Al	0.273	0.255	0.325	0.282	0.256	0.252	0.277
<sup>T</sup> Ti	0.000	0.000	0.000	0.000	0.000	0.000	0.000
Ti	0.058	0.053	0.062	0.055	0.063	0.051	0.067
Fe <sup>3+</sup>	0.000	0.000	0.000	0.000	0.000	0.000	0.000
V	0.002	0.002	0.007	0.009	0.012	0.002	0.011
Cr	0.007	0.002	0.001	0.006	0.007	0.005	0.004
<sup>C</sup> Mg	2.550	2.595	2.514	2.588	2.575	2.630	2.627
<sup>C</sup> Fe <sup>2+</sup>	2.003	1.980	1.990	1.957	1.996	1.975	1.912
<sup>C</sup> Mn <sup>2+</sup>	0.107	0.113	0.100	0.104	0.093	0.085	0.102
<sup>C</sup> Ca	0.000	0.000	0.000	0.000	0.000	0.000	0.000
<sup>B</sup> Mg	0.000	0.000	0.000	0.000	0.000	0.000	0.000
<sup>B</sup> Fe <sup>2+</sup>	0.000	0.000	0.000	0.000	0.000	0.000	0.000
<sup>B</sup> Mn <sup>2+</sup>	0.000	0.000	0.000	0.000	0.000	0.000	0.000
<sup>B</sup> Ca	1.809	1.754	1.849	1.800	1.857	1.835	1.783
<sup>B</sup> Na	0.191	0.235	0.151	0.200	0.143	0.165	0.217
<sup>A</sup> Ca	0.000	0.000	0.000	0.000	0.000	0.000	0.000
<sup>A</sup> Na	0.089	0.000	0.152	0.125	0.156	0.104	0.048
<sup>A</sup> K	0.093	0.073	0.098	0.099	0.102	0.086	0.081
<sup>W</sup> F	0.301	0.280	0.307	0.325	0.329	0.317	0.277
<sup>W</sup> Cl	0.003	0.005	0.003	0.000	0.003	0.000	0.000
<sup>W</sup> OH	1.696	1.714	1.690	1.675	1.668	1.683	1.723
<sup>W</sup> O	-0.285	-0.356	-0.200	-0.245	-0.216	-0.261	-0.333
O <sup>2-</sup>	22.000	22.000	22.000	22.000	22.000	22.000	22.000

\*Note: amphibole formula based cation sum = 13

Elements sought but not found (or below detection limit): P, Zn, Ni (detection limits of 359 ppm, 1539 ppm, and 662 ppm respectively)

Appendix B.3: EMPA analyses of amphiboles

Mineral	mg-hlb	mg-hlb	mg-hlb	mg-hlb	mg-hlb	mg-hlb	mg-hlb
Point	64 / 1 .	66 / 1 .	53 / 1 .	54 / 1 .	55 / 1 .	56 / 1 .	4 / 1 .
Thin section	KIN133D	KIN133D	135C	135C	135C	135C	130b-2
SiO <sub>2</sub> (wt.%)	48.04	49.15	49.15	49.15	49.15	49.15	52.08
TiO <sub>2</sub>	0.52	0.51	0.51	0.51	0.51	0.51	0.24
Al <sub>2</sub> O <sub>3</sub>	6.74	6.65	6.65	6.65	6.65	6.65	5.02
Fe <sub>2</sub> O <sub>3</sub> *	0.00	0.00	0.00	0.00	0.00	0.00	0.00
FeO*	15.71	15.00	15.00	15.00	15.00	15.00	11.47
V <sub>2</sub> O <sub>3</sub>	0.03	0.04	0.04	0.04	0.04	0.04	0.05
Cr <sub>2</sub> O <sub>3</sub>	0.04	0.00	0.00	0.00	0.00	0.00	0.04
MnO	0.78	0.94	0.94	0.94	0.94	0.94	1.00
MgO	12.21	12.84	12.84	12.84	12.84	12.84	15.69
CaO	11.42	11.20	11.20	11.20	11.20	11.20	11.96
Na <sub>2</sub> O	1.01	1.01	1.01	1.01	1.01	1.01	0.73
K <sub>2</sub> O	0.43	0.34	0.34	0.34	0.34	0.34	0.23
F	0.63	0.63	0.63	0.63	0.63	0.63	0.00
Cl	0.00	0.00	0.00	0.00	0.00	0.00	0.00
H <sub>2</sub> O*	1.74	1.78	1.78	1.78	1.78	1.78	2.12
-(O=F,Cl)	-0.02	-0.02	-0.02	-0.02	-0.02	-0.02	0.00
Total	99.29	100.07	100.07	100.07	100.07	100.07	89.49
<sup>T</sup> Si (apfu)	7.062	7.109	7.109	7.109	7.109	7.109	7.354
<sup>T</sup> Al	0.938	0.891	0.891	0.891	0.891	0.891	0.646
<sup>L</sup> Al	0.231	0.242	0.242	0.242	0.242	0.242	0.188
<sup>T</sup> Ti	0.000	0.000	0.000	0.000	0.000	0.000	0.000
Ti	0.057	0.056	0.056	0.056	0.056	0.056	0.025
Fe <sup>3+</sup>	0.000	0.000	0.000	0.000	0.000	0.000	0.000
V	0.004	0.005	0.005	0.005	0.005	0.005	0.005
Cr	0.005	0.000	0.000	0.000	0.000	0.000	0.004
<sup>L</sup> Mg	2.676	2.769	2.769	2.769	2.769	2.769	3.303
<sup>C</sup> Fe <sup>2+</sup>	1.932	1.814	1.814	1.814	1.814	1.814	1.355
<sup>C</sup> Mn <sup>2+</sup>	0.097	0.115	0.115	0.115	0.115	0.115	0.120
<sup>L</sup> Ca	0.000	0.000	0.000	0.000	0.000	0.000	0.000
<sup>B</sup> Mg	0.000	0.000	0.000	0.000	0.000	0.000	0.000
<sup>B</sup> Fe <sup>2+</sup>	0.000	0.000	0.000	0.000	0.000	0.000	0.000
<sup>B</sup> Mn <sup>2+</sup>	0.000	0.000	0.000	0.000	0.000	0.000	0.000
<sup>B</sup> Ca	1.798	1.735	1.735	1.735	1.735	1.735	1.809
<sup>B</sup> Na	0.202	0.265	0.265	0.265	0.265	0.265	0.191
<sup>A</sup> Ca	0.000	0.000	0.000	0.000	0.000	0.000	0.000
<sup>A</sup> Na	0.087	0.019	0.019	0.019	0.019	0.019	0.008
<sup>A</sup> K	0.080	0.062	0.062	0.062	0.062	0.062	0.041
<sup>w</sup> F	0.292	0.287	0.287	0.287	0.287	0.287	0.000
<sup>w</sup> Cl	0.000	0.000	0.000	0.000	0.000	0.000	0.000
<sup>w</sup> OH	1.708	1.713	1.713	1.713	1.713	1.713	2.000
<sup>w</sup> O	-0.310	-0.358	-0.358	-0.358	-0.358	-0.358	-0.234
O <sup>2-</sup>	22.000	22.000	22.000	22.000	22.000	22.000	22.000

Appendix B.3: EMPA analyses of amphiboles

Mineral	mg-hlb	mg-hlb	mg-hlb	mg-hlb	mg-hlb	mg-hlb
Point	5 / 1 .	6 / 1 .	9 / 1 .	52 / 1 .	53 / 1 .	55 / 1 .
Thin section	130b-2	130b-2	130b-2	135a	135a	135a
SiO <sub>2</sub> (wt.%)	53.25	52.89	52.12	47.67	49.66	48.36
TiO <sub>2</sub>	0.11	0.18	0.29	0.50	0.33	0.45
Al <sub>2</sub> O <sub>3</sub>	3.62	4.34	4.28	7.13	5.30	5.86
Fe <sub>2</sub> O <sub>3</sub> *	0.00	0.00	0.00	0.00	0.00	0.00
FeO*	11.29	11.42	13.63	17.40	17.11	17.46
V <sub>2</sub> O <sub>3</sub>	0.03	0.00	0.03	0.02	0.05	0.06
Cr <sub>2</sub> O <sub>3</sub>	0.03	0.03	0.03	0.02	0.04	0.04
MnO	0.91	0.97	1.46	1.00	0.98	1.18
MgO	16.73	15.88	14.47	10.80	11.68	11.46
CaO	11.88	11.95	11.50	11.72	11.47	11.41
Na <sub>2</sub> O	0.55	0.61	0.61	1.16	0.82	0.99
K <sub>2</sub> O	0.16	0.23	0.20	0.59	0.40	0.49
F	0.00	0.00	0.00	0.00	0.00	0.00
Cl	0.00	0.00	0.00	0.00	0.00	0.00
H <sub>2</sub> O*	2.14	2.13	2.11	2.03	2.05	2.04
-(O=F,Cl)	0.00	0.00	0.00	0.00	0.00	0.00
Total	89.69	89.39	87.43	82.85	83.15	82.58
<sup>T</sup> Si (apfu)	7.459	7.457	7.394	7.044	7.271	7.114
<sup>T</sup> Al	0.541	0.543	0.606	0.956	0.729	0.886
<sup>L</sup> Al	0.056	0.178	0.110	0.286	0.186	0.130
<sup>T</sup> Ti	0.000	0.000	0.000	0.000	0.000	0.000
Ti	0.012	0.019	0.031	0.055	0.037	0.050
Fe <sup>3+</sup>	0.000	0.000	0.000	0.000	0.000	0.000
V	0.003	0.000	0.003	0.002	0.006	0.007
Cr	0.003	0.003	0.003	0.002	0.005	0.005
<sup>L</sup> Mg	3.495	3.338	3.060	2.379	2.550	2.513
<sup>C</sup> Fe <sup>2+</sup>	1.322	1.346	1.617	2.150	2.095	2.149
<sup>C</sup> Mn <sup>2+</sup>	0.108	0.115	0.176	0.125	0.121	0.147
<sup>L</sup> Ca	0.000	0.000	0.000	0.000	0.000	0.000
<sup>B</sup> Mg	0.000	0.000	0.000	0.000	0.000	0.000
<sup>B</sup> Fe <sup>2+</sup>	0.000	0.000	0.000	0.000	0.000	0.000
<sup>B</sup> Mn <sup>2+</sup>	0.000	0.000	0.000	0.000	0.000	0.000
<sup>B</sup> Ca	1.782	1.804	1.748	1.856	1.800	1.798
<sup>B</sup> Na	0.149	0.166	0.169	0.144	0.200	0.202
<sup>A</sup> Ca	0.000	0.000	0.000	0.000	0.000	0.000
<sup>A</sup> Na	0.000	0.000	0.000	0.189	0.032	0.081
<sup>A</sup> K	0.029	0.042	0.037	0.111	0.075	0.093
<sup>W</sup> F	0.000	0.000	0.000	0.000	0.000	0.000
<sup>W</sup> Cl	0.000	0.000	0.000	0.000	0.000	0.000
<sup>W</sup> OH	2.000	2.000	2.000	2.000	2.000	2.000
<sup>W</sup> O	-0.327	-0.233	-0.329	-0.176	-0.236	-0.309
O <sup>2-</sup>	22.000	22.000	22.000	22.000	22.000	22.000

## B.4: Garnet

### Appendix B.4: EMPA analyses of garnets

Point	33 / 1 .	34 / 1 .	35 / 1 .	36 / 1 .	37 / 1 .	38 / 1 .	47 / 1 .
Thin Section	KIN133D						
SiO <sub>2</sub> (wt.%)	36.67	36.42	37.30	36.83	36.77	36.94	37.15
Al <sub>2</sub> O <sub>3</sub>	20.39	20.36	20.58	20.55	20.47	20.30	20.36
Cr <sub>2</sub> O <sub>3</sub>	0.06	0.02	0.03	0.02	0.08	0.08	0.07
TiO <sub>2</sub>	0.27	0.05	0.05	0.04	0.15	0.22	0.11
MgO	2.14	1.94	1.94	1.76	1.92	1.96	1.57
CaO	7.74	9.07	9.18	8.99	8.99	8.26	9.83
MnO	9.41	9.05	9.14	9.07	9.21	9.54	9.40
Fe <sub>2</sub> O <sub>3</sub> *	2.59	3.45	1.91	2.74	2.69	2.26	2.19
FeO*	22.98	22.38	21.89	22.74	22.26	22.49	21.44
Na <sub>2</sub> O	0.04	0.02	0.00	0.00	0.01	0.04	0.03
Total	99.97	99.68	100.31	100.31	100.19	100.06	100.22
Si (apfu)	2.944	2.929	2.973	2.945	2.943	2.962	2.970
Al	1.929	1.929	1.933	1.936	1.931	1.918	1.919
Cr	0.004	0.001	0.002	0.001	0.005	0.005	0.004
Ti	0.016	0.003	0.003	0.002	0.009	0.013	0.006
Mg	0.256	0.232	0.230	0.210	0.229	0.235	0.187
Ca	0.666	0.782	0.784	0.770	0.771	0.709	0.842
Mn	0.640	0.617	0.617	0.614	0.624	0.648	0.636
Fe <sup>3+</sup>	0.157	0.209	0.115	0.165	0.162	0.136	0.132
Fe <sup>2+</sup>	1.386	1.296	1.345	1.356	1.328	1.372	1.301
Na	0.006	0.003	0.000	0.000	0.002	0.006	0.005

\*Note: Garnet formula are based on cation sum = 8

Elements sought but not found (or below detection limit): P, Sc, K, and V (detection limits of 205 ppm, 228 ppm, 356 ppm, and 259 ppm respectively)

**Appendix B.4:** EMPA analyses of garnets

Point	48 / 1 .	49 / 1 .	61 / 1 .	62 / 1 .	99 / 1 .	1 / 1 .	2 / 1 .
Thin Section	KIN133D	KIN133D	KIN133D	KIN133D	KIN134-2	130b-2	130b-2
SiO <sub>2</sub> (wt.%)	36.34	37.22	36.82	36.54	37.42	37.87	37.29
Al <sub>2</sub> O <sub>3</sub>	20.40	20.38	20.37	20.35	20.90	21.12	21.01
Cr <sub>2</sub> O <sub>3</sub>	0.09	0.07	0.00	0.00	0.01	0.07	0.08
TiO <sub>2</sub>	0.08	0.03	0.13	0.18	0.03	0.03	0.05
MgO	1.54	1.72	2.09	1.99	1.94	1.63	1.67
CaO	9.89	9.49	7.65	8.30	10.05	10.71	7.13
MnO	10.12	9.33	9.47	9.27	7.79	13.01	18.82
Fe <sub>2</sub> O <sub>3</sub> *	3.53	2.01	2.14	3.04	1.75	0.75	1.29
FeO*	20.88	21.69	22.97	22.88	22.06	16.11	14.64
Na <sub>2</sub> O	0.03	0.00	0.00	0.03	0.02	0.02	0.01
Total	99.74	100.16	99.76	99.87	100.43	100.67	100.90
Si (apfu)	2.924	2.976	2.961	2.936	2.969	2.993	2.970
Al	1.935	1.921	1.931	1.927	1.954	1.968	1.973
Cr	0.006	0.004	0.000	0.000	0.001	0.005	0.005
Ti	0.005	0.002	0.008	0.011	0.002	0.002	0.003
Mg	0.185	0.205	0.251	0.239	0.229	0.192	0.198
Ca	0.853	0.813	0.659	0.714	0.854	0.907	0.609
Mn	0.690	0.632	0.645	0.631	0.524	0.871	1.270
Fe <sup>3+</sup>	0.214	0.121	0.129	0.184	0.104	0.045	0.077
Fe <sup>2+</sup>	1.191	1.329	1.415	1.354	1.359	1.020	0.898
Na	0.005	0.000	0.000	0.005	0.004	0.002	0.001

**Appendix B.4:** EMPA analyses of garnets

Point	3 / 1 .	10 / 1 .	11 / 1 .	50 / 1 .	51 / 1 .	54 / 1 .	75 / 1 .
Thin Section	130b-2	G17a	G17a	135a	135a	135a	134-4
SiO <sub>2</sub> (wt.%)	37.91	36.88	37.05	37.15	36.97	37.26	37.39
Al <sub>2</sub> O <sub>3</sub>	20.98	20.95	21.00	20.45	20.42	20.68	20.86
Cr <sub>2</sub> O <sub>3</sub>	0.09	0.00	0.00	0.06	0.11	0.08	0.01
TiO <sub>2</sub>	0.05	0.02	0.00	0.07	0.05	0.00	0.05
MgO	1.82	1.94	1.93	1.30	1.25	1.45	1.83
CaO	7.00	1.08	0.87	8.26	8.78	8.56	8.86
MnO	16.61	6.83	8.47	11.34	11.33	11.30	9.08
Fe <sub>2</sub> O <sub>3</sub> *	0.35	0.16	0.27	1.08	1.30	1.20	1.13
FeO*	16.51	32.47	31.31	21.02	20.49	20.62	21.85
Na <sub>2</sub> O	0.03	0.03	0.03	0.01	0.00	0.01	0.04
Total	101.06	100.36	100.72	99.82	99.55	100.11	100.12
Si (apfu)	3.008	2.988	2.992	2.993	2.985	2.986	2.983
Al	1.962	2.001	1.999	1.941	1.943	1.954	1.961
Cr	0.006	0.000	0.000	0.004	0.007	0.005	0.001
Ti	0.003	0.001	0.000	0.004	0.003	0.000	0.003
Mg	0.215	0.234	0.233	0.156	0.150	0.173	0.217
Ca	0.595	0.094	0.075	0.713	0.760	0.735	0.757
Mn	1.116	0.469	0.579	0.774	0.775	0.767	0.614
Fe <sup>3+</sup>	0.021	0.010	0.017	0.065	0.079	0.073	0.068
Fe <sup>2+</sup>	1.075	2.190	2.098	1.351	1.305	1.310	1.390
Na	0.005	0.005	0.005	0.002	0.000	0.001	0.006

**Appendix B.4:** EMPA analyses of garnets

Point	76 / 1 .	84 / 1 .	86 / 1 .	8 / 1 .	9 / 1 .	10 / 1 .	59 / 1 .
Thin Section	134-4	134-4	134-4	133C	133C	133C	135C
SiO <sub>2</sub> (wt.%)	37.18	36.40	37.07	38.04	38.01	37.94	37.76
Al <sub>2</sub> O <sub>3</sub>	20.90	20.33	21.02	21.12	21.34	21.50	20.73
Cr <sub>2</sub> O <sub>3</sub>	0.01	0.02	0.00	0.01	0.00	0.01	0.03
TiO <sub>2</sub>	0.04	0.11	0.02	0.03	0.01	0.02	0.07
MgO	1.77	1.06	1.82	2.62	2.65	2.98	1.46
CaO	10.24	12.05	10.93	7.72	8.08	8.06	7.36
MnO	7.40	9.26	7.10	11.52	11.22	10.62	13.79
Fe <sub>2</sub> O <sub>3</sub> *	1.37	2.33	1.76	0.05	0.80	0.95	0.25
FeO*	21.99	18.94	21.38	19.40	19.74	19.83	19.47
Na <sub>2</sub> O	0.00	0.02	0.02	0.00	0.00	0.00	0.00
Total	99.70	98.42	99.59	100.52	101.16	101.07	100.73
Si (apfu)	2.971	2.952	2.959	3.009	2.988	2.977	3.012
Al	1.968	1.943	1.977	1.969	1.976	1.988	1.949
Cr	0.000	0.001	0.000	0.001	0.000	0.001	0.002
Ti	0.002	0.007	0.001	0.002	0.001	0.001	0.004
Mg	0.211	0.128	0.216	0.308	0.311	0.349	0.173
Ca	0.877	1.047	0.935	0.655	0.680	0.677	0.629
Mn	0.501	0.636	0.480	0.772	0.747	0.706	0.932
Fe <sup>3+</sup>	0.082	0.142	0.106	0.003	0.047	0.056	0.015
Fe <sup>2+</sup>	1.387	1.143	1.322	1.281	1.250	1.245	1.284
Na	0.000	0.003	0.004	0.000	0.000	0.000	0.000

**Appendix B.4:** EMPA analyses of garnets

Point	60 / 1 .	61 / 1 .	62 / 1 .	1 / 1 .	2 / 1 .
Thin Section	135C	135C	135C	Pegm1	Pegm1
SiO <sub>2</sub> (wt.%)	37.80	37.37	37.79	37.02	36.87
Al <sub>2</sub> O <sub>3</sub>	20.64	20.71	20.86	20.95	20.74
Cr <sub>2</sub> O <sub>3</sub>	0.03	0.03	0.03	0.00	0.00
TiO <sub>2</sub>	0.18	0.09	0.03	0.03	0.02
MgO	1.43	1.44	1.47	1.06	0.85
CaO	7.31	7.56	7.81	0.88	0.74
MnO	13.81	13.54	13.32	9.03	9.37
Fe <sub>2</sub> O <sub>3</sub> *	0.80	0.89	0.17	0.00	0.00
FeO*	20.04	19.47	19.22	31.94	31.90
Na <sub>2</sub> O	0.04	0.03	0.01	0.02	0.00
Total	101.38	100.40	100.61	101.99	102.52
Si (apfu)	3.002	2.993	3.012	3.001	3.009
Al	1.931	1.955	1.960	2.002	1.994
Cr	0.002	0.002	0.002	0.000	0.000
Ti	0.011	0.005	0.002	0.002	0.001
Mg	0.169	0.172	0.175	0.128	0.104
Ca	0.622	0.649	0.667	0.077	0.065
Mn	0.929	0.918	0.899	0.620	0.647
Fe <sup>3+</sup>	0.048	0.053	0.010	0.000	0.000
Fe <sup>2+</sup>	1.283	1.250	1.271	2.165	2.177
Na	0.006	0.004	0.002	0.002	0.000

## B.5: Zircon

### Appendix B.5: EMPA analyses of zircon

Point	30 / 1 .	31 / 1 .	67 / 1 .	68 / 1 .	63 / 1 .	64 / 1 .	83 / 1 .
Thin Section	kin 136	kin 136	135a	135a	Rad 2a	Rad 2a	134-4
P <sub>2</sub> O <sub>5</sub> (wt.%)	0.01	0.00	0.00	0.00	0.09	0.01	0.00
SiO <sub>2</sub>	32.28	32.30	32.84	32.88	31.83	32.30	31.78
ZrO <sub>2</sub>	63.86	64.85	64.94	65.83	63.56	64.00	63.15
HfO <sub>2</sub>	2.28	1.82	2.40	1.67	0.98	0.75	0.88
ThO <sub>2</sub>	0.52	0.16	0.01	0.00	0.04	0.00	0.02
UO <sub>2</sub>	0.03	0.05	0.02	0.00	0.09	0.00	0.04
FeO	0.02	0.00	0.00	0.07	0.00	0.00	0.12
Y <sub>2</sub> O <sub>3</sub>	0.43	0.08	0.00	0.00	0.07	0.00	0.00
La <sub>2</sub> O <sub>3</sub>	0.00	0.03	0.00	0.02	0.06	0.00	0.03
Total	99.52	99.39	101.24	102.41	99.71	101.17	101.20
P (apfu)	0.000	0.000	0.000	0.000	0.002	0.000	0.000
Si	1.000	1.000	1.000	1.000	0.998	1.000	1.000
Zr	0.965	0.979	0.964	0.976	0.971	0.966	0.969
Hf	0.020	0.016	0.021	0.014	0.009	0.007	0.008
Th	0.004	0.001	0.000	0.000	0.000	0.000	0.000
U	0.000	0.000	0.000	0.000	0.001	0.000	0.000
Fe <sup>2+</sup>	0.000	0.000	0.000	0.002	0.000	0.000	0.003
Y	0.007	0.001	0.000	0.000	0.001	0.000	0.000
La	0.000	0.000	0.000	0.000	0.001	0.000	0.000

\*Note: Zircon formula based on Si = 1

Elements sought but not found (or below detection limit): Ca, Pb, Sm, Nd, Mn, Al, Sc, Ti, Nb, and Mg (average detection limits of 331 ppm, 787 ppm, 726 ppm, 1284 ppm, 417 ppm, 160 ppm, 307 ppm, 727 ppm, and 162 ppm respectively)

**Appendix B.5:** EMPA analyses of zircon

Point	85 / 1 .	29 / 1 .	22 / 1 .
Thin Section	134-4	133C	Pegm1
P <sub>2</sub> O <sub>5</sub> (wt.%)	0.00	0.00	0.18
SiO <sub>2</sub>	31.84	32.85	28.95
ZrO <sub>2</sub>	64.26	66.19	53.70
HfO <sub>2</sub>	0.60	1.33	2.63
ThO <sub>2</sub>	0.01	0.04	0.02
UO <sub>2</sub>	0.00	0.03	0.42
FeO	0.12	0.01	0.00
Y <sub>2</sub> O <sub>3</sub>	0.00	0.00	0.00
La <sub>2</sub> O <sub>3</sub>	0.07	0.00	0.00
Total	102.86	107.50	94.03
P (apfu)	0.000	0.000	0.005
Si	1.000	1.000	0.995
Zr	0.984	0.982	0.900
Hf	0.005	0.012	0.026
Th	0.000	0.000	0.000
U	0.000	0.000	0.003
Fe <sup>2+</sup>	0.003	0.000	0.000
Y	0.000	0.000	0.000
La	0.001	0.000	0.000

## B.6: Titanite

### Appendix B.6: EMPA analyses of titanite

Point	41 / 1 .	45 / 1 .	46 / 1 .	44 / 1 .	57 / 1 .	58 / 1 .
Thin Section	KIN133D	KIN133D	KIN133D	KIN133D	135C	135C
Nb <sub>2</sub> O <sub>5</sub> (wt.%)	3.84	2.35	2.93	4.26	4.22	4.43
Ta <sub>2</sub> O <sub>5</sub>	0.08	0.09	0.02	0.14	0.05	0.05
SiO <sub>2</sub>	29.63	29.89	30.43	29.70	30.63	30.55
TiO <sub>2</sub>	33.68	34.41	34.40	33.08	31.47	31.50
ZrO <sub>2</sub>	0.00	0.02	0.00	0.00	0.06	0.05
SnO <sub>2</sub>	0.29	0.38	0.32	0.34	0.19	0.19
Al <sub>2</sub> O <sub>3</sub>	2.86	3.12	3.29	2.53	3.12	3.17
Y <sub>2</sub> O <sub>3</sub>	0.03	0.18	0.00	0.04	0.00	0.00
Ce <sub>2</sub> O <sub>3</sub>	0.13	0.15	0.00	0.25	0.06	0.11
Pr <sub>2</sub> O <sub>3</sub>	0.01	0.03	0.00	0.06	0.02	0.00
Nd <sub>2</sub> O <sub>3</sub>	0.20	0.27	0.04	0.29	0.10	0.10
Sm <sub>2</sub> O <sub>3</sub>	0.02	0.13	0.16	0.13	0.00	0.09
Gd <sub>2</sub> O <sub>3</sub>	0.04	0.09	0.07	0.12	0.06	0.03
Dy <sub>2</sub> O <sub>3</sub>	0.12	0.19	0.04	0.18	0.10	0.08
Er <sub>2</sub> O <sub>3</sub>	0.07	0.00	0.00	0.01	0.00	0.00
Yb <sub>2</sub> O <sub>3</sub>	0.10	0.00	0.04	0.06	0.00	0.00
CaO	27.65	27.82	28.06	26.94	28.03	27.78
Fe <sub>2</sub> O <sub>3</sub> *	1.20	0.57	0.57	1.54	0.87	0.87
FeO*	1.08	0.51	0.51	1.39	0.78	0.78
Na <sub>2</sub> O	0.12	0.06	0.05	0.19	0.06	0.05
F	0.68	0.74	0.74	0.57	0.66	0.65
H <sub>2</sub> O*	0.20	0.15	0.34	1.52	0.08	0.17
-O=F	-0.29	-0.31	-0.31	-0.24	-0.28	-0.27
Total	100.72	100.35	101.21	101.77	99.52	99.67

\*Note: Titanite formula based on tetrahedral M-site = 2

Elements sought but not found (or below detection limit): K, La, Sn, Mg, and Th (average detections limits of 351 ppm, 666 ppm, 364 ppm, 158 ppm, and 562 ppm respectively)

**Appendix B.6:** EMPA analyses of titanite

Point	41 / 1 .	45 / 1 .	46 / 1 .	44 / 1 .	57 / 1 .	58 / 1 .
Thin Section	KIN133D	KIN133D	KIN133D	KIN133D	135C	135C
Nb (apfu)	0.057	0.035	0.043	0.063	0.063	0.066
Ta	0.001	0.001	0.000	0.001	0.000	0.000
Si	0.969	0.977	0.980	0.975	1.009	1.005
Ti	0.829	0.847	0.833	0.817	0.780	0.779
Zr	0.000	0.000	0.000	0.000	0.001	0.001
Sn	0.004	0.005	0.004	0.004	0.003	0.003
Al	0.110	0.120	0.125	0.098	0.121	0.123
Y	0.000	0.003	0.000	0.001	0.000	0.000
Ce	0.002	0.002	0.000	0.003	0.001	0.001
Pr	0.000	0.000	0.000	0.001	0.000	0.000
Nd	0.002	0.003	0.000	0.003	0.001	0.001
Sm	0.000	0.001	0.002	0.001	0.000	0.001
Gd	0.000	0.001	0.001	0.001	0.001	0.000
Dy	0.001	0.002	0.000	0.002	0.001	0.001
Er	0.001	0.000	0.000	0.000	0.000	0.000
Yb	0.001	0.000	0.000	0.001	0.000	0.000
Ca	0.969	0.975	0.968	0.948	0.990	0.979
Fe <sup>3+</sup>	0.030	0.014	0.014	0.038	0.022	0.022
Fe <sup>2+</sup>	0.030	0.014	0.014	0.038	0.022	0.022
Na	0.008	0.004	0.003	0.012	0.004	0.003
F	0.071	0.077	0.075	0.059	0.069	0.068
OH	0.044	0.032	0.072	0.333	0.018	0.037

## B.7: Beryl+Bertrandite

### Appendix B.7: EMPA analyses of Beryl+Bertrandite

Mineral	bert	beryl	Mineral	bert	beryl
Point	8 / 1 .	49 / 1 .	Point	8 / 1 .	49 / 1 .
Thin Section	130b-2	kin 130A	Thin Section	130b-2	kin 130A
SiO <sub>2</sub> (wt.%)	51.60	66.84	Si	1.946	6.019
TiO <sub>2</sub>	0.01	0.03	Ti	0.000	0.002
Al <sub>2</sub> O <sub>3</sub>	0.75	17.42	Al	0.033	1.848
MgO	0.13	0.25	Mg	0.007	0.033
FeO	0.40	1.23	Fe	0.012	0.092
CaO	0.05	0.00	Ca	0.002	0.000
Na <sub>2</sub> O	0.02	0.80	Na	0.001	0.140
K <sub>2</sub> O	0.01	0.04	K	0.000	0.005
F	0.04	0.00	F	0.005	0.000
Cl	0.01	0.01	Cl	0.001	0.002
-(O=F,Cl)	0.02	0.00	vac	5.000	
Total	53.04	86.69	O	3.963	15.020

\*Note: formula calculation based on 18 anions

Elements sought but not found (or below detection limit): P, Zn, S

## B.8: Tourmaline

### Appendix B.8: EMPA analyses of Tourmaline

Point	50 / 1 .	51 / 1 .	52 / 1 .	53 / 1 .	54 / 1 .	56 / 1 .	57 / 1 .	58 / 1 .
Thin section	Rad 2a							
SiO <sub>2</sub> (wt.%)	36.13	35.29	35.50	35.80	36.26	36.10	35.87	36.14
TiO <sub>2</sub>	0.71	0.84	0.88	0.87	0.71	0.70	0.70	0.62
B <sub>2</sub> O <sub>3</sub>	10.60	10.46	10.50	10.49	10.60	10.53	10.54	10.60
Al <sub>2</sub> O <sub>3</sub>	32.47	32.11	32.20	31.85	32.35	31.99	32.26	32.50
FeO*	5.30	5.30	5.30	5.30	5.30	5.30	5.30	5.30
ZnO	0.21	0.21	0.21	0.21	0.21	0.21	0.21	0.21
MnO	0.12	0.12	0.12	0.12	0.12	0.12	0.12	0.12
MgO	7.95	7.95	7.95	7.95	7.95	7.95	7.95	7.95
CaO	1.06	1.06	1.06	1.06	1.06	1.06	1.06	1.06
Na <sub>2</sub> O	2.29	2.29	2.29	2.29	2.29	2.29	2.29	2.29
K <sub>2</sub> O	0.05	0.05	0.05	0.05	0.05	0.05	0.05	0.05
F	0.93	0.93	0.93	0.93	0.93	0.93	0.93	0.93
Cl	0.01	0.01	0.00	0.00	0.00	0.00	0.00	0.00
H <sub>2</sub> O*	2.84	2.86	2.84	2.80	2.82	2.78	2.83	2.85
-(O=F,Cl)	-0.44	-0.44	-0.44	-0.44	-0.44	-0.44	-0.44	-0.44
Total	100.23	99.01	99.39	99.26	100.22	99.61	99.69	100.16
T Si (apfu)	5.925	5.862	5.875	5.932	5.947	5.956	5.915	5.928
T Al	0.075	0.138	0.125	0.068	0.053	0.044	0.085	0.072
B	3.000	3.000	3.000	3.000	3.000	3.000	3.000	3.000
Z Al	6.000	6.000	6.000	6.000	6.000	6.000	6.000	6.000
Y Al	0.200	0.148	0.154	0.153	0.198	0.177	0.183	0.210
Y Ti	0.088	0.104	0.110	0.108	0.088	0.087	0.087	0.077
Y Fe <sup>2+</sup>	0.727	0.737	0.734	0.735	0.727	0.732	0.731	0.727
Y Zn	0.025	0.025	0.025	0.025	0.025	0.025	0.025	0.025
Y Mn	0.016	0.016	0.016	0.016	0.016	0.016	0.016	0.016
Y Mg	1.943	1.969	1.961	1.964	1.943	1.955	1.954	1.944
X Ca	0.187	0.189	0.189	0.189	0.187	0.188	0.188	0.187
X Na	0.727	0.737	0.734	0.735	0.727	0.732	0.731	0.727
X K	0.010	0.010	0.010	0.010	0.010	0.010	0.010	0.010
X vac	0.076	0.064	0.068	0.067	0.076	0.071	0.071	0.076
W F	0.480	0.486	0.484	0.485	0.480	0.483	0.482	0.480
W Cl	0.004	0.003	0.000	0.001	0.000	0.000	0.000	0.000
W OH	0.104	0.166	0.137	0.092	0.087	0.061	0.112	0.117
W O	0.412	0.345	0.379	0.423	0.434	0.457	0.406	0.403

\*Note: formula calculation based on cation sum = 13

Elements sought but not found (or below detection limit): Cr, P, and V (average detection limits of 279 ppm, 307 ppm, and 486 ppm respectively)

Appendix B.8: EMPA analyses of Tourmaline

Point	3 / 1 .	4 / 1 .	5 / 1 .	6 / 1 .	7 / 1 .	14 / 1 .
Thin section	Pegm1	Pegm1	Pegm1	Pegm1	Pegm1	Pegm1
SiO <sub>2</sub> (wt.%)	35.14	35.72	35.86	35.72	35.97	35.29
TiO <sub>2</sub>	0.83	0.76	0.59	0.67	0.78	0.68
B <sub>2</sub> O <sub>3</sub>	10.63	10.63	10.63	10.63	10.63	10.63
Al <sub>2</sub> O <sub>3</sub>	32.03	32.08	31.85	32.23	32.31	32.46
FeO*	12.01	11.80	10.89	10.71	10.39	10.63
ZnO	0.10	0.09	0.14	0.11	0.07	0.19
MnO	0.10	0.09	0.08	0.07	0.08	0.10
MgO	3.60	3.83	4.42	4.34	4.43	4.50
CaO	0.20	0.22	0.24	0.23	0.23	0.26
Na <sub>2</sub> O	2.56	2.56	2.48	2.57	2.66	2.59
K <sub>2</sub> O	0.07	0.05	0.05	0.10	0.07	0.09
F	0.54	0.54	0.61	0.59	0.60	0.60
Cl	0.01	0.01	0.01	0.00	0.00	0.00
H <sub>2</sub> O*	3.01	3.02	3.01	2.94	2.87	3.05
-(O=F,Cl)	-0.26	-0.26	-0.29	-0.28	-0.28	-0.28
Total	100.56	101.13	100.60	100.65	100.80	100.79
T Si (apfu)	5.917	5.965	5.995	5.968	5.993	5.890
T Al	0.083	0.035	0.005	0.032	0.007	0.110
B	4.000	5.000	6.000	7.000	8.000	9.000
Z Al	6.000	6.000	6.000	6.000	6.000	6.000
Y Al	0.274	0.278	0.270	0.314	0.336	0.275
Y Ti	0.105	0.096	0.074	0.084	0.098	0.085
Y Fe <sup>2+</sup>	1.691	1.647	1.522	1.496	1.447	1.484
Y Zn	0.013	0.011	0.017	0.014	0.009	0.023
Y Mn	0.014	0.012	0.012	0.010	0.011	0.014
Y Mg	0.903	0.954	1.101	1.081	1.100	1.120
X Ca	0.035	0.040	0.044	0.041	0.041	0.047
X Na	0.836	0.827	0.804	0.832	0.860	0.839
X K	0.014	0.011	0.011	0.021	0.015	0.018
X vac	0.115	0.122	0.141	0.105	0.084	0.095
W F	0.289	0.285	0.324	0.312	0.316	0.315
W Cl	0.001	0.001	0.003	0.000	0.000	0.000
W OH	0.385	0.360	0.354	0.278	0.194	0.399
W O	0.325	0.353	0.320	0.410	0.490	0.286

## B.9: Epidote Group Minerals

Allanite type described further in chapter 3

**Appendix B.9:** EMPA analyses of Epidote Group Minerals

Allanite type	III	III	III	III	III	III	III
Thin Section	KIN133D	KIN133D	KIN133D	KIN133D	KIN133D	KIN133D	KIN134-2
Point	1 / 1 .	2 / 1 .	26 / 1 .	51 / 1 .	52 / 1 .	53 / 1 .	78 / 1 .
P <sub>2</sub> O <sub>5</sub> (wt.%)	0.05	0.05	0.00	0.01	0.00	0.02	0.03
SiO <sub>2</sub>	31.49	32.59	30.90	31.53	32.69	31.32	31.75
TiO <sub>2</sub>	1.19	1.91	2.99	0.93	0.65	1.22	0.88
SnO <sub>2</sub>	0.04	0.03	0.03	0.02	0.02	0.01	0.00
Al <sub>2</sub> O <sub>3</sub>	14.02	15.09	12.73	16.29	17.47	15.57	15.78
Fe <sub>2</sub> O <sub>3</sub> *	6.40	14.50	2.20	1.72	8.16	1.40	2.90
FeO*	9.19	0.00	12.31	11.79	5.32	12.85	10.68
ThO <sub>2</sub>	1.06	3.82	1.17	4.91	3.38	2.92	1.49
UO <sub>2</sub>	0.00	0.11	0.00	0.14	0.08	0.08	0.01
Y <sub>2</sub> O <sub>3</sub>	0.05	0.02	0.02	0.03	0.06	0.05	0.05
La <sub>2</sub> O <sub>3</sub>	8.24	5.79	8.52	5.23	4.97	6.06	8.50
Ce <sub>2</sub> O <sub>3</sub>	12.34	9.30	11.87	8.12	7.86	9.35	11.60
Pr <sub>2</sub> O <sub>3</sub>	0.84	0.61	0.92	0.52	0.55	0.61	0.91
Nd <sub>2</sub> O <sub>3</sub>	2.55	2.16	2.39	1.83	1.79	2.07	2.47
Sm <sub>2</sub> O <sub>3</sub>	0.04	0.07	0.08	0.03	0.08	0.05	0.12
Gd <sub>2</sub> O <sub>3</sub>	0.05	0.06	0.03	0.12	0.07	0.00	0.10
Dy <sub>2</sub> O <sub>3</sub>	0.00	0.00	0.00	0.00	0.00	0.00	0.00
Ho <sub>2</sub> O <sub>3</sub>	0.00	0.00	0.00	0.05	0.00	0.16	0.03
Er <sub>2</sub> O <sub>3</sub>	0.00	0.05	0.00	0.00	0.01	0.00	0.00
Yb <sub>2</sub> O <sub>3</sub>	0.00	0.00	0.00	0.00	0.04	0.03	0.03
MgO	0.83	0.82	1.37	0.64	0.57	0.55	1.13
CaO	9.47	9.34	9.48	11.87	12.06	11.30	10.50
MnO	1.21	0.83	0.89	1.29	1.18	1.52	0.73
SrO	1.06	0.52	1.03	0.96	0.91	0.97	0.17
PbO	0.01	0.04	0.00	0.04	0.06	0.04	0.04
Na <sub>2</sub> O	0.04	0.09	0.06	0.01	0.03	0.01	0.05
F	0.02	0.07	0.05	0.04	0.05	0.04	0.03
Cl	0.00	0.01	0.01	0.02	0.02	0.00	0.01
H <sub>2</sub> O*	1.56	1.81	1.50	1.53	1.57	1.53	1.56
Total	101.76	99.68	100.53	99.65	99.65	99.73	101.55

\*Note: formula calculation based on Si=3

Appendix B.9: EMPA analyses of Epidote Group Minerals

Allanite type	III	III	III	III	III	III	III
Thin Section	KIN133D	KIN133D	KIN133D	KIN133D	KIN133D	KIN133D	KIN134-2
Point	1 / 1 .	2 / 1 .	26 / 1 .	51 / 1 .	52 / 1 .	53 / 1 .	78 / 1 .
P (apfu)	0.004	0.004	0.000	0.000	0.000	0.002	0.003
Si	2.996	2.996	3.000	3.000	3.000	2.998	2.997
Ti	0.085	0.132	0.218	0.066	0.045	0.087	0.063
Sn	0.002	0.001	0.001	0.001	0.001	0.000	0.000
Al	1.572	1.635	1.457	1.827	1.890	1.757	1.756
Fe <sup>3+</sup>	0.459	1.003	0.161	0.123	0.564	0.101	0.206
Fe <sup>2+</sup>	0.731	0.000	0.999	0.938	0.408	1.029	0.844
Th	0.023	0.080	0.026	0.106	0.071	0.064	0.032
U	0.000	0.002	0.000	0.003	0.002	0.002	0.000
Y	0.002	0.001	0.001	0.002	0.003	0.003	0.003
La	0.289	0.196	0.305	0.184	0.168	0.214	0.296
Ce	0.430	0.313	0.422	0.283	0.264	0.328	0.401
Pr	0.029	0.020	0.033	0.018	0.018	0.021	0.031
Nd	0.087	0.071	0.083	0.062	0.059	0.071	0.083
Sm	0.001	0.002	0.003	0.001	0.002	0.002	0.004
Gd	0.002	0.002	0.001	0.004	0.002	0.000	0.003
Tb	0.000	0.000	0.000	0.000	0.000	0.000	0.000
Dy	0.000	0.000	0.000	0.000	0.000	0.000	0.000
Ho	0.000	0.000	0.000	0.001	0.000	0.005	0.001
Er	0.000	0.001	0.000	0.000	0.000	0.000	0.000
Yb	0.000	0.000	0.000	0.000	0.001	0.001	0.001
Mg	0.118	0.113	0.198	0.091	0.078	0.079	0.158
Ca	0.966	0.920	0.986	1.210	1.186	1.159	1.062
Mn	0.098	0.065	0.073	0.104	0.091	0.123	0.058
Sr	0.059	0.028	0.058	0.053	0.049	0.054	0.010
Pb	0.000	0.001	0.000	0.001	0.001	0.001	0.001
Na	0.007	0.016	0.011	0.002	0.005	0.003	0.009
F	0.006	0.021	0.014	0.012	0.016	0.012	0.009
Cl	0.000	0.002	0.001	0.003	0.002	0.000	0.002
OH	0.988	1.108	0.970	0.971	0.964	0.974	0.980

**Appendix B.9:** EMPA analyses of Epidote Group Minerals

Allanite type	III						
Thin Section	KIN134-2	KIN134-2	KIN134-2	KIN134-2	KIN134-2	KIN134-2	kin 130A
Point	79 / 1 .	80 / 1 .	81 / 1 .	82 / 1 .	83 / 1 .	84 / 1 .	32 / 1 .
P <sub>2</sub> O <sub>5</sub> (wt.%)	0.00	0.02	0.02	0.02	0.02	0.03	0.03
SiO <sub>2</sub>	31.24	31.63	33.05	34.56	34.02	31.93	31.19
TiO <sub>2</sub>	1.33	1.20	0.37	0.19	0.30	0.07	2.79
SnO <sub>2</sub>	0.04	0.02	0.01	0.01	0.02	0.03	0.03
Al <sub>2</sub> O <sub>3</sub>	14.54	15.30	19.72	21.61	21.24	18.51	11.76
Fe <sub>2</sub> O <sub>3</sub> *	2.24	2.95	0.64	5.15	1.68	0.00	6.64
FeO*	12.02	11.01	11.00	5.12	8.65	11.83	8.72
ThO <sub>2</sub>	0.48	1.00	1.02	1.04	1.06	1.51	0.85
UO <sub>2</sub>	0.00	0.01	0.00	0.07	0.01	0.14	0.02
Y <sub>2</sub> O <sub>3</sub>	0.00	0.00	0.00	0.09	0.00	0.09	0.07
La <sub>2</sub> O <sub>3</sub>	11.15	9.83	5.60	5.20	5.12	7.75	6.82
Ce <sub>2</sub> O <sub>3</sub>	12.66	11.83	7.96	7.14	7.19	10.82	11.46
Pr <sub>2</sub> O <sub>3</sub>	0.73	0.70	0.59	0.55	0.43	0.70	0.97
Nd <sub>2</sub> O <sub>3</sub>	1.62	1.47	1.53	1.27	1.53	2.20	2.87
Sm <sub>2</sub> O <sub>3</sub>	0.00	0.11	0.02	0.01	0.08	0.01	0.28
Gd <sub>2</sub> O <sub>3</sub>	0.00	0.08	0.00	0.00	0.00	0.05	0.15
Dy <sub>2</sub> O <sub>3</sub>	0.00	0.00	0.00	0.00	0.00	0.00	0.40
Ho <sub>2</sub> O <sub>3</sub>	0.02	0.01	0.00	0.00	0.01	0.02	0.00
Er <sub>2</sub> O <sub>3</sub>	0.00	0.00	0.00	0.00	0.00	0.01	0.00
Yb <sub>2</sub> O <sub>3</sub>	0.02	0.01	0.05	0.00	0.03	0.01	0.04
MgO	1.19	0.99	0.33	0.55	0.45	0.81	1.01
CaO	9.43	10.49	13.89	15.35	15.06	10.85	8.41
MnO	0.73	0.64	0.92	0.51	0.64	1.05	3.90
SrO	0.39	0.41	1.94	0.57	1.49	0.11	1.56
PbO	0.00	0.02	0.00	0.02	0.01	0.02	0.00
Na <sub>2</sub> O	0.06	0.05	0.01	0.01	0.03	0.11	0.09
F	0.00	0.02	0.07	0.06	0.03	0.03	-0.01
Cl	0.01	0.00	0.01	0.01	0.00	0.00	0.02
H <sub>2</sub> O*	1.55	1.56	1.59	1.67	1.67	1.57	1.56
Total	101.44	101.34	100.31	100.76	100.76	100.23	101.62

Appendix B.9: EMPA analyses of Epidote Group Minerals

Allanite type	III						
Thin Section	KIN134-2	KIN134-2	KIN134-2	KIN134-2	KIN134-2	KIN134-2	kin 130A
Point	79 / 1 .	80 / 1 .	81 / 1 .	82 / 1 .	83 / 1 .	84 / 1 .	32 / 1 .
P (apfu)	0.000	0.002	0.002	0.001	0.001	0.003	0.003
Si	3.000	2.998	2.998	2.999	2.999	2.997	2.997
Ti	0.096	0.085	0.025	0.012	0.020	0.005	0.202
Sn	0.001	0.001	0.001	0.000	0.001	0.001	0.001
Al	1.645	1.709	2.109	2.211	2.207	2.048	1.332
Fe <sup>3+</sup>	0.162	0.210	0.044	0.336	0.112	0.000	0.480
Fe <sup>2+</sup>	0.965	0.873	0.835	0.372	0.638	0.928	0.701
Th	0.010	0.022	0.021	0.021	0.021	0.032	0.018
U	0.000	0.000	0.000	0.001	0.000	0.003	0.000
Y	0.000	0.000	0.000	0.004	0.000	0.004	0.004
La	0.395	0.344	0.187	0.166	0.166	0.268	0.242
Ce	0.445	0.411	0.264	0.227	0.232	0.372	0.403
Pr	0.026	0.024	0.020	0.017	0.014	0.024	0.034
Nd	0.056	0.050	0.049	0.039	0.048	0.074	0.098
Sm	0.000	0.003	0.001	0.000	0.002	0.000	0.009
Gd	0.000	0.002	0.000	0.000	0.000	0.001	0.005
Tb	0.000	0.000	0.000	0.000	0.000	0.000	0.000
Dy	0.000	0.000	0.000	0.000	0.000	0.000	0.012
Ho	0.001	0.000	0.000	0.000	0.000	0.001	0.000
Er	0.000	0.000	0.000	0.000	0.000	0.000	0.000
Yb	0.001	0.000	0.001	0.000	0.001	0.000	0.001
Mg	0.170	0.139	0.045	0.071	0.060	0.113	0.145
Ca	0.970	1.066	1.350	1.427	1.422	1.091	0.866
Mn	0.059	0.052	0.070	0.037	0.048	0.083	0.317
Sr	0.022	0.022	0.102	0.029	0.076	0.006	0.087
Pb	0.000	0.000	0.000	0.001	0.000	0.000	0.000
Na	0.011	0.009	0.001	0.002	0.006	0.020	0.017
F	0.001	0.007	0.019	0.015	0.008	0.008	-0.002
Cl	0.001	0.000	0.001	0.001	0.000	0.000	0.003
OH	0.995	0.985	0.960	0.967	0.984	0.985	0.998

**Appendix B.9:** EMPA analyses of Epidote Group Minerals

Allanite type	III						
Thin Section	kin 130A	130b	130b	130b	130b	Rad 2a	Rad 2a
Point	33 / 1 .	41 / 1 .	42 / 1 .	44 / 1 .	45 / 1 .	67 / 1 .	68 / 1 .
P <sub>2</sub> O <sub>5</sub> (wt.%)	0.01	0.03	0.04	0.05	0.09	0.05	0.03
SiO <sub>2</sub>	31.15	32.83	32.70	33.02	32.72	33.65	33.28
TiO <sub>2</sub>	2.08	0.02	0.13	0.32	0.10	0.12	0.12
SnO <sub>2</sub>	0.02	0.00	0.03	0.00	0.01	0.01	0.01
Al <sub>2</sub> O <sub>3</sub>	13.59	20.50	20.28	20.67	20.47	22.22	21.44
Fe <sub>2</sub> O <sub>3</sub> *	3.49	8.78	6.97	8.62	9.41	0.50	0.98
FeO*	10.51	0.00	2.82	0.00	0.00	7.49	7.19
ThO <sub>2</sub>	1.06	3.88	2.20	7.25	5.28	0.20	0.21
UO <sub>2</sub>	0.00	0.07	0.04	0.16	0.07	0.00	0.00
Y <sub>2</sub> O <sub>3</sub>	0.09	0.28	0.27	0.41	0.30	0.88	0.43
La <sub>2</sub> O <sub>3</sub>	6.41	2.64	1.86	1.18	2.02	1.83	2.29
Ce <sub>2</sub> O <sub>3</sub>	10.70	6.72	8.03	3.45	5.20	6.68	8.04
Pr <sub>2</sub> O <sub>3</sub>	0.95	0.77	1.28	0.53	0.76	1.15	1.10
Nd <sub>2</sub> O <sub>3</sub>	2.69	3.07	4.91	1.73	2.33	4.98	5.50
Sm <sub>2</sub> O <sub>3</sub>	0.20	0.22	0.63	0.26	0.28	0.82	0.92
Gd <sub>2</sub> O <sub>3</sub>	0.00	0.19	0.28	0.15	0.10	0.68	0.59
Dy <sub>2</sub> O <sub>3</sub>	0.28	0.00	0.05	0.03	0.02	0.14	0.10
Ho <sub>2</sub> O <sub>3</sub>	0.06	0.00	0.00	0.07	0.00	0.02	0.02
Er <sub>2</sub> O <sub>3</sub>	0.00	0.00	0.01	0.00	0.00	0.06	0.00
Yb <sub>2</sub> O <sub>3</sub>	0.03	0.00	0.01	0.02	0.07	0.00	0.02
MgO	0.96	0.63	0.45	0.53	0.51	0.75	0.86
CaO	9.38	10.80	10.79	8.54	9.80	13.63	13.13
MnO	3.25	0.82	1.38	0.93	0.83	1.30	0.94
SrO	1.95	0.73	1.05	1.09	0.81	0.27	0.46
PbO	0.03	0.67	0.36	0.43	0.90	0.01	0.02
Na <sub>2</sub> O	0.01	0.12	0.04	0.22	0.14	0.06	0.01
F	-0.02	-0.03	-0.02	0.01	0.00	0.00	
Cl	0.00	0.14	0.08	0.20	0.23	0.01	0.01
H <sub>2</sub> O*	1.57	2.11	1.62	3.23	2.39	1.68	1.66
Total	100.44	95.98	98.28	93.10	94.84	99.18	99.36

Appendix B.9: EMPA analyses of Epidote Group Minerals

Allanite type	III						
Thin Section	kin 130A	130b	130b	130b	130b	Rad 2a	Rad 2a
Point	33 / 1 .	41 / 1 .	42 / 1 .	44 / 1 .	45 / 1 .	67 / 1 .	68 / 1 .
P (apfu)	0.000	0.003	0.003	0.004	0.007	0.004	0.002
Si	3.000	2.997	2.997	2.996	2.993	2.996	2.998
Ti	0.150	0.001	0.009	0.022	0.007	0.008	0.008
Sn	0.001	0.000	0.001	0.000	0.000	0.000	0.000
Al	1.542	2.206	2.191	2.211	2.207	2.332	2.276
Fe <sup>3+</sup>	0.253	0.603	0.481	0.588	0.648	0.034	0.067
Fe <sup>2+</sup>	0.846	0.000	0.216	0.000	0.000	0.557	0.542
Th	0.023	0.081	0.046	0.150	0.110	0.004	0.004
U	0.000	0.001	0.001	0.003	0.001	0.000	0.000
Y	0.005	0.014	0.013	0.020	0.015	0.042	0.020
La	0.228	0.089	0.063	0.039	0.068	0.060	0.076
Ce	0.377	0.225	0.269	0.115	0.174	0.218	0.265
Pr	0.033	0.026	0.043	0.017	0.025	0.037	0.036
Nd	0.093	0.100	0.161	0.056	0.076	0.158	0.177
Sm	0.007	0.007	0.020	0.008	0.009	0.025	0.028
Gd	0.000	0.006	0.009	0.004	0.003	0.020	0.017
Tb	0.000	0.000	0.000	0.000	0.000	0.000	0.000
Dy	0.009	0.000	0.001	0.001	0.000	0.004	0.003
Ho	0.002	0.000	0.000	0.002	0.000	0.001	0.001
Er	0.000	0.000	0.000	0.000	0.000	0.002	0.000
Yb	0.001	0.000	0.000	0.000	0.002	0.000	0.000
Mg	0.137	0.086	0.061	0.072	0.069	0.100	0.116
Ca	0.967	1.057	1.059	0.830	0.960	1.300	1.267
Mn	0.265	0.063	0.107	0.071	0.064	0.098	0.072
Sr	0.109	0.039	0.056	0.057	0.043	0.014	0.024
Pb	0.001	0.017	0.009	0.011	0.022	0.000	0.001
Na	0.002	0.021	0.007	0.039	0.025	0.011	0.002
F	-0.005	-0.008	-0.006	0.004	0.001	0.000	0.000
Cl	0.000	0.021	0.013	0.030	0.035	0.002	0.002
OH	1.009	1.285	0.987	1.956	1.458	0.997	0.996

**Appendix B.9:** EMPA analyses of Epidote Group Minerals

Allanite type	III	III	III	III	III	III	III
Thin Section	134-4	134-4	133C	133C	133C	133C	133C
Point	81 / 1 .	82 / 1 .	1 / 1 .	14 / 1 .	18 / 1 .	19 / 1 .	20 / 1 .
P <sub>2</sub> O <sub>5</sub> (wt.%)	0.00	0.03	0.06	0.02	0.00	0.01	0.06
SiO <sub>2</sub>	33.70	34.27	32.34	32.64	31.85	34.16	34.16
TiO <sub>2</sub>	0.17	0.12	0.77	0.81	0.38	0.03	0.04
SnO <sub>2</sub>	0.02	0.00	0.02	0.02	0.01	0.00	0.01
Al <sub>2</sub> O <sub>3</sub>	22.69	23.12	17.21	17.91	17.48	21.56	21.46
Fe <sub>2</sub> O <sub>3</sub> *	0.00	0.45	5.81	5.96	2.42	3.91	9.40
FeO*	8.12	7.85	5.69	4.29	8.20	4.88	0.00
ThO <sub>2</sub>	1.36	1.24	0.32	3.32	0.67	1.46	3.45
UO <sub>2</sub>	0.04	0.03	0.00	0.08	0.01	0.09	0.17
Y <sub>2</sub> O <sub>3</sub>	0.00	0.00	0.00	0.03	0.00	0.08	0.01
La <sub>2</sub> O <sub>3</sub>	4.24	4.23	7.84	4.37	9.53	5.14	4.03
Ce <sub>2</sub> O <sub>3</sub>	6.11	5.82	12.68	10.90	12.44	8.04	6.57
Pr <sub>2</sub> O <sub>3</sub>	0.45	0.40	0.77	1.17	0.73	0.64	0.64
Nd <sub>2</sub> O <sub>3</sub>	1.27	1.18	1.76	2.76	1.95	1.73	1.58
Sm <sub>2</sub> O <sub>3</sub>	0.03	0.01	0.00	0.19	0.04	0.09	0.05
Gd <sub>2</sub> O <sub>3</sub>	0.01	0.16	0.02	0.10	0.00	0.11	0.06
Dy <sub>2</sub> O <sub>3</sub>	0.00	0.09	0.00	0.00	0.00	0.00	0.03
Ho <sub>2</sub> O <sub>3</sub>	0.00	0.05	0.00	0.01	0.00	0.00	0.05
Er <sub>2</sub> O <sub>3</sub>	0.00	0.00	0.00	0.00	0.00	0.03	0.00
Yb <sub>2</sub> O <sub>3</sub>	0.02	0.00	0.00	0.00	0.03	0.01	0.01
MgO	0.50	0.50	0.95	1.41	1.47	0.70	0.69
CaO	15.94	16.41	10.66	10.72	9.90	13.87	12.22
MnO	0.45	0.37	1.34	1.43	1.05	1.91	0.81
SrO	1.22	0.68	0.75	0.75	0.57	0.64	0.68
PbO	0.00	0.00	0.00	0.04	0.01	0.06	0.04
Na <sub>2</sub> O	0.02	0.02	0.04	0.09	0.06	0.00	0.18
F	0.00	0.00	0.02	0.01	0.02	-0.02	0.06
Cl	0.00	0.00	0.00	0.03	0.01	0.01	0.09
H <sub>2</sub> O*	1.57	1.71	1.60	1.60	1.57	1.72	2.05
Total	97.92	98.71	100.66	100.69	100.41	100.87	98.59

**Appendix B.9:** EMPA analyses of Epidote Group Minerals

Allanite type	III	III	III	III	III	III	III
Thin Section	134-4	134-4	133C	133C	133C	133C	133C
Point	81 / 1 .	82 / 1 .	1 / 1 .	14 / 1 .	18 / 1 .	19 / 1 .	20 / 1 .
P (apfu)	0.000	0.002	0.005	0.002	0.000	0.001	0.004
Si	3.000	2.998	2.995	2.998	3.000	2.999	2.996
Ti	0.011	0.008	0.054	0.056	0.027	0.002	0.003
Sn	0.001	0.000	0.001	0.001	0.000	0.000	0.000
Al	2.381	2.384	1.878	1.939	1.941	2.231	2.218
Fe <sup>3+</sup>	0.000	0.029	0.405	0.412	0.171	0.259	0.620
Fe <sup>2+</sup>	0.604	0.574	0.441	0.329	0.646	0.358	0.000
Th	0.028	0.025	0.007	0.069	0.014	0.029	0.069
U	0.001	0.001	0.000	0.002	0.000	0.002	0.003
Y	0.000	0.000	0.000	0.001	0.000	0.004	0.001
La	0.139	0.136	0.268	0.148	0.331	0.167	0.130
Ce	0.199	0.186	0.430	0.366	0.429	0.259	0.211
Pr	0.014	0.013	0.026	0.039	0.025	0.020	0.021
Nd	0.040	0.037	0.058	0.090	0.066	0.054	0.049
Sm	0.001	0.000	0.000	0.006	0.001	0.003	0.001
Gd	0.000	0.005	0.001	0.003	0.000	0.003	0.002
Tb	0.000	0.000	0.000	0.000	0.000	0.000	0.000
Dy	0.000	0.003	0.000	0.000	0.000	0.000	0.001
Ho	0.000	0.001	0.000	0.000	0.000	0.000	0.001
Er	0.000	0.000	0.000	0.000	0.000	0.001	0.000
Yb	0.001	0.000	0.000	0.000	0.001	0.000	0.000
Mg	0.066	0.065	0.132	0.193	0.206	0.092	0.091
Ca	1.521	1.538	1.058	1.055	0.999	1.305	1.148
Mn	0.034	0.027	0.105	0.111	0.083	0.142	0.060
Sr	0.063	0.034	0.040	0.040	0.031	0.033	0.034
Pb	0.000	0.000	0.000	0.001	0.000	0.001	0.001
Na	0.004	0.003	0.007	0.017	0.010	0.000	0.030
F	0.000	0.000	0.006	0.004	0.005	-0.006	0.018
Cl	0.000	0.000	0.000	0.004	0.001	0.001	0.013
OH	0.930	0.999	0.988	0.983	0.989	1.010	1.198

**Appendix B.9:** EMPA analyses of Epidote Group Minerals

Allanite type	III	III	I	I	I	I	II
Thin Section	133C	133C	135a	135a	135a	135a	135a
Point	27 / 1 .	28 / 1 .	46 / 1 .	47 / 1 .	56 / 1 .	57 / 1 .	59 / 1 .
P <sub>2</sub> O <sub>5</sub> (wt.%)	0.03	0.03	0.00	0.01	0.00	0.03	0.00
SiO <sub>2</sub>	32.09	32.57	31.39	31.37	30.56	30.52	33.29
TiO <sub>2</sub>	1.23	0.58	1.97	2.12	3.00	2.85	0.32
SnO <sub>2</sub>	0.02	0.00	0.02	0.05	0.02	0.03	0.03
Al <sub>2</sub> O <sub>3</sub>	15.88	17.85	12.78	12.45	9.97	10.16	18.27
Fe <sub>2</sub> O <sub>3</sub> *	6.13	4.58	9.23	10.42	10.23	10.36	7.82
FeO*	5.27	5.63	6.72	5.89	7.69	7.47	5.14
ThO <sub>2</sub>	2.18	1.69	1.33	0.76	1.10	1.14	1.52
UO <sub>2</sub>	0.06	0.04	0.00	0.00	0.00	0.00	0.00
Y <sub>2</sub> O <sub>3</sub>	0.00	0.00	0.10	0.09	0.08	0.09	0.08
La <sub>2</sub> O <sub>3</sub>	6.88	6.74	7.39	7.75	7.77	7.67	5.72
Ce <sub>2</sub> O <sub>3</sub>	12.63	12.93	10.27	10.48	10.78	10.78	7.95
Pr <sub>2</sub> O <sub>3</sub>	0.83	0.95	0.64	0.59	0.71	0.70	0.50
Nd <sub>2</sub> O <sub>3</sub>	1.99	2.30	2.04	1.80	2.26	2.25	1.80
Sm <sub>2</sub> O <sub>3</sub>	0.00	0.02	0.12	0.00	0.05	0.12	0.08
Gd <sub>2</sub> O <sub>3</sub>	0.06	0.00	0.11	0.01	0.16	0.03	0.10
Dy <sub>2</sub> O <sub>3</sub>	0.00	0.00	0.00	0.00	0.00	0.00	0.00
Ho <sub>2</sub> O <sub>3</sub>	0.02	0.00	0.04	0.09	0.00	0.00	0.03
Er <sub>2</sub> O <sub>3</sub>	0.03	0.00	0.00	0.00	0.00	0.00	0.03
Yb <sub>2</sub> O <sub>3</sub>	0.00	0.02	0.07	0.03	0.00	0.03	0.00
MgO	1.61	1.41	0.59	0.56	0.74	0.66	0.25
CaO	10.17	10.85	9.61	9.47	8.57	8.51	13.54
MnO	1.86	1.10	2.28	2.24	2.51	2.57	0.83
SrO	0.23	0.36	2.22	2.41	2.10	2.11	1.61
PbO	0.01	0.05	0.08	0.04	0.01	0.05	0.03
Na <sub>2</sub> O	0.09	0.08	0.00	0.03	0.02	0.03	0.00
F	0.07	0.03	0.02	0.04	0.03	0.02	-0.03
Cl	0.01	0.01	0.00	0.00	0.01	0.00	0.00
H <sub>2</sub> O*	1.53	1.60	1.55	1.53	1.50	1.51	1.69
Total	100.90	101.42	100.56	100.24	99.86	99.70	100.60

Appendix B.9: EMPA analyses of Epidote Group Minerals

Allanite type	III	III	I	I	I	I	II
Thin Section	133C	133C	135a	135a	135a	135a	135a
Point	27 / 1 .	28 / 1 .	46 / 1 .	47 / 1 .	56 / 1 .	57 / 1 .	59 / 1 .
P (apfu)	0.002	0.002	0.000	0.000	0.000	0.002	0.000
Si	2.998	2.998	3.000	3.000	3.000	2.998	3.000
Ti	0.086	0.040	0.141	0.152	0.222	0.211	0.022
Sn	0.001	0.000	0.001	0.002	0.001	0.001	0.001
Al	1.749	1.936	1.440	1.404	1.153	1.176	1.940
Fe <sup>3+</sup>	0.431	0.318	0.664	0.749	0.756	0.766	0.530
Fe <sup>2+</sup>	0.411	0.434	0.537	0.471	0.632	0.614	0.387
Th	0.046	0.035	0.029	0.017	0.025	0.026	0.031
U	0.001	0.001	0.000	0.000	0.000	0.000	0.000
Y	0.000	0.000	0.005	0.005	0.004	0.004	0.004
La	0.237	0.229	0.261	0.273	0.281	0.278	0.190
Ce	0.432	0.436	0.359	0.367	0.387	0.387	0.262
Pr	0.028	0.032	0.022	0.020	0.025	0.025	0.017
Nd	0.066	0.076	0.070	0.061	0.079	0.079	0.058
Sm	0.000	0.001	0.004	0.000	0.002	0.004	0.002
Gd	0.002	0.000	0.003	0.000	0.005	0.001	0.003
Tb	0.000	0.000	0.000	0.000	0.000	0.000	0.000
Dy	0.000	0.000	0.000	0.000	0.000	0.000	0.000
Ho	0.001	0.000	0.001	0.003	0.000	0.000	0.001
Er	0.001	0.000	0.000	0.000	0.000	0.000	0.001
Yb	0.000	0.001	0.002	0.001	0.000	0.001	0.000
Mg	0.224	0.193	0.083	0.079	0.108	0.097	0.033
Ca	1.018	1.070	0.984	0.971	0.902	0.896	1.307
Mn	0.147	0.086	0.185	0.181	0.208	0.214	0.064
Sr	0.013	0.019	0.123	0.133	0.119	0.120	0.084
Pb	0.000	0.001	0.002	0.001	0.000	0.001	0.001
Na	0.016	0.014	0.000	0.005	0.004	0.006	0.000
F	0.021	0.009	0.007	0.013	0.008	0.006	-0.008
Cl	0.001	0.001	0.000	0.000	0.001	0.000	0.001
OH	0.956	0.980	0.985	0.973	0.981	0.988	1.015

Appendix B.9: EMPA analyses of Epidote Group Minerals

Allanite type	I	I	I	I	I	I	I
Thin Section	135a						
Point	64 / 1 .	65 / 1 .	66 / 1 .	69 / 1 .	70 / 1 .	71 / 1 .	72 / 1 .
P <sub>2</sub> O <sub>5</sub> (wt.%)	0.02	0.00	0.02	0.01	0.03	0.03	0.00
SiO <sub>2</sub>	31.28	30.93	31.04	30.65	30.80	30.80	30.07
TiO <sub>2</sub>	2.29	2.75	2.55	2.66	2.43	2.21	3.29
SnO <sub>2</sub>	0.03	0.02	0.04	0.03	0.04	0.06	0.03
Al <sub>2</sub> O <sub>3</sub>	11.87	11.53	10.86	9.87	11.43	11.77	9.66
Fe <sub>2</sub> O <sub>3</sub> *	10.88	8.83	11.51	11.79	8.69	8.14	7.69
FeO*	6.13	7.40	6.02	6.87	8.45	8.80	9.79
ThO <sub>2</sub>	1.15	0.89	1.22	1.23	1.19	1.41	0.89
UO <sub>2</sub>	0.00	0.00	0.03	0.00	0.00	0.00	0.02
Y <sub>2</sub> O <sub>3</sub>	0.10	0.08	0.07	0.07	0.05	0.10	0.01
La <sub>2</sub> O <sub>3</sub>	7.61	8.63	8.00	7.63	7.91	7.61	9.05
Ce <sub>2</sub> O <sub>3</sub>	10.29	11.10	10.46	10.58	10.32	10.31	11.69
Pr <sub>2</sub> O <sub>3</sub>	0.67	0.61	0.76	0.64	0.61	0.59	0.71
Nd <sub>2</sub> O <sub>3</sub>	1.75	1.99	2.03	2.23	2.03	1.87	1.73
Sm <sub>2</sub> O <sub>3</sub>	0.04	0.05	0.05	0.16	0.05	0.01	0.00
Gd <sub>2</sub> O <sub>3</sub>	0.19	0.00	0.00	0.07	0.10	0.12	0.07
Dy <sub>2</sub> O <sub>3</sub>	0.00	0.00	0.09	0.03	0.00	0.01	0.00
Ho <sub>2</sub> O <sub>3</sub>	0.00	0.00	0.09	0.00	0.00	0.06	0.00
Er <sub>2</sub> O <sub>3</sub>	0.00	0.00	0.00	0.00	0.01	0.00	0.00
Yb <sub>2</sub> O <sub>3</sub>	0.00	0.00	0.00	0.01	0.02	0.07	0.00
MgO	0.59	0.76	0.64	0.65	0.66	0.57	0.71
CaO	9.32	9.39	8.82	8.45	8.96	8.97	7.92
MnO	2.26	1.66	2.45	2.68	2.41	2.49	2.97
SrO	2.36	1.75	2.30	2.23	2.21	2.46	1.75
PbO	0.05	0.04	0.00	0.04	0.02	0.06	0.04
Na <sub>2</sub> O	0.00	0.02	0.00	0.04	0.00	0.02	0.02
F	0.05	0.03	0.02	0.03	0.03	0.01	0.02
Cl	0.01	0.00	0.00	0.01	0.00	0.01	0.01
H <sub>2</sub> O*	1.51	1.51	1.53	1.50	1.51	1.53	1.48
Total	100.44	99.96	100.60	100.15	99.94	100.07	99.59

**Appendix B.9:** EMPA analyses of Epidote Group Minerals

Allanite type	I	I	I	I	I	I	I
Thin Section	135a						
Point	64 / 1 .	65 / 1 .	66 / 1 .	69 / 1 .	70 / 1 .	71 / 1 .	72 / 1 .
P (apfu)	0.002	0.000	0.001	0.001	0.002	0.002	0.000
Si	2.998	3.000	2.999	2.999	2.998	2.998	3.000
Ti	0.165	0.201	0.185	0.196	0.178	0.162	0.247
Sn	0.001	0.001	0.002	0.001	0.002	0.002	0.001
Al	1.341	1.317	1.236	1.138	1.312	1.350	1.136
Fe <sup>3+</sup>	0.785	0.644	0.837	0.868	0.636	0.596	0.577
Fe <sup>2+</sup>	0.491	0.600	0.486	0.562	0.688	0.716	0.817
Th	0.025	0.020	0.027	0.027	0.026	0.031	0.020
U	0.000	0.000	0.001	0.000	0.000	0.000	0.000
Y	0.005	0.004	0.004	0.004	0.003	0.005	0.001
La	0.269	0.309	0.285	0.275	0.284	0.273	0.333
Ce	0.361	0.394	0.370	0.379	0.368	0.367	0.427
Pr	0.023	0.022	0.027	0.023	0.021	0.021	0.026
Nd	0.060	0.069	0.070	0.078	0.070	0.065	0.062
Sm	0.001	0.002	0.002	0.005	0.002	0.000	0.000
Gd	0.006	0.000	0.000	0.002	0.003	0.004	0.002
Tb	0.000	0.000	0.000	0.000	0.000	0.000	0.000
Dy	0.000	0.000	0.003	0.001	0.000	0.000	0.000
Ho	0.000	0.000	0.003	0.000	0.000	0.002	0.000
Er	0.000	0.000	0.000	0.000	0.000	0.000	0.000
Yb	0.000	0.000	0.000	0.000	0.001	0.002	0.000
Mg	0.084	0.110	0.091	0.095	0.095	0.082	0.105
Ca	0.957	0.976	0.913	0.886	0.934	0.935	0.846
Mn	0.183	0.137	0.201	0.222	0.198	0.205	0.251
Sr	0.131	0.098	0.129	0.127	0.125	0.139	0.101
Pb	0.001	0.001	0.000	0.001	0.000	0.001	0.001
Na	0.001	0.004	0.001	0.007	0.000	0.004	0.003
F	0.015	0.010	0.007	0.008	0.008	0.002	0.007
Cl	0.001	0.001	0.000	0.002	0.000	0.001	0.001
OH	0.967	0.978	0.986	0.980	0.983	0.993	0.984

**Appendix B.9:** EMPA analyses of Epidote Group Minerals

Allanite type	I	I	I	I	I	I	I
Thin Section	135a						
Point	64 / 1 .	65 / 1 .	66 / 1 .	69 / 1 .	70 / 1 .	71 / 1 .	72 / 1 .
P (apfu)	0.002	0.000	0.001	0.001	0.002	0.002	0.000
Si	2.998	3.000	2.999	2.999	2.998	2.998	3.000
Ti	0.165	0.201	0.185	0.196	0.178	0.162	0.247
Sn	0.001	0.001	0.002	0.001	0.002	0.002	0.001
Al	1.341	1.317	1.236	1.138	1.312	1.350	1.136
Fe <sup>3+</sup>	0.785	0.644	0.837	0.868	0.636	0.596	0.577
Fe <sup>2+</sup>	0.491	0.600	0.486	0.562	0.688	0.716	0.817
Th	0.025	0.020	0.027	0.027	0.026	0.031	0.020
U	0.000	0.000	0.001	0.000	0.000	0.000	0.000
Y	0.005	0.004	0.004	0.004	0.003	0.005	0.001
La	0.269	0.309	0.285	0.275	0.284	0.273	0.333
Ce	0.361	0.394	0.370	0.379	0.368	0.367	0.427
Pr	0.023	0.022	0.027	0.023	0.021	0.021	0.026
Nd	0.060	0.069	0.070	0.078	0.070	0.065	0.062
Sm	0.001	0.002	0.002	0.005	0.002	0.000	0.000
Gd	0.006	0.000	0.000	0.002	0.003	0.004	0.002
Tb	0.000	0.000	0.000	0.000	0.000	0.000	0.000
Dy	0.000	0.000	0.003	0.001	0.000	0.000	0.000
Ho	0.000	0.000	0.003	0.000	0.000	0.002	0.000
Er	0.000	0.000	0.000	0.000	0.000	0.000	0.000
Yb	0.000	0.000	0.000	0.000	0.001	0.002	0.000
Mg	0.084	0.110	0.091	0.095	0.095	0.082	0.105
Ca	0.957	0.976	0.913	0.886	0.934	0.935	0.846
Mn	0.183	0.137	0.201	0.222	0.198	0.205	0.251
Sr	0.131	0.098	0.129	0.127	0.125	0.139	0.101
Pb	0.001	0.001	0.000	0.001	0.000	0.001	0.001
Na	0.001	0.004	0.001	0.007	0.000	0.004	0.003
F	0.015	0.010	0.007	0.008	0.008	0.002	0.007
Cl	0.001	0.001	0.000	0.002	0.000	0.001	0.001
OH	0.967	0.978	0.986	0.980	0.983	0.993	0.984

Appendix B.9: EMPA analyses of Epidote Group Minerals

Allanite type	I	I	I	I	I	I	I
Thin Section	135a	135a	135a	135a	135a	135C	135C
Point	73 / 1 .	74 / 1 .	75 / 1 .	76 / 1 .	77 / 1 .	45 / 1 .	46 / 1 .
P <sub>2</sub> O <sub>5</sub> (wt.%)	0.03	0.00	0.01	0.02	0.01	0.03	0.01
SiO <sub>2</sub>	31.75	31.93	30.97	31.25	30.24	30.55	30.38
TiO <sub>2</sub>	1.83	1.80	2.68	2.29	3.52	4.05	3.61
SnO <sub>2</sub>	0.04	0.05	0.02	0.03	0.02	0.02	0.03
Al <sub>2</sub> O <sub>3</sub>	14.61	14.09	12.00	12.23	8.96	9.34	9.31
Fe <sub>2</sub> O <sub>3</sub> *	6.19	9.01	8.48	9.56	9.87	9.02	9.54
FeO*	8.01	5.90	7.05	6.67	8.38	8.50	8.27
ThO <sub>2</sub>	1.44	1.55	1.40	1.20	0.73	0.75	0.85
UO <sub>2</sub>	0.00	0.00	0.00	0.00	0.01	0.01	0.00
Y <sub>2</sub> O <sub>3</sub>	0.11	0.07	0.02	0.08	0.02	0.02	0.02
La <sub>2</sub> O <sub>3</sub>	7.33	7.23	8.50	8.27	9.87	9.06	9.43
Ce <sub>2</sub> O <sub>3</sub>	9.78	9.92	11.07	10.60	11.45	11.62	11.68
Pr <sub>2</sub> O <sub>3</sub>	0.63	0.65	0.78	0.65	0.62	0.75	0.60
Nd <sub>2</sub> O <sub>3</sub>	2.14	1.91	1.89	1.83	1.54	1.85	1.61
Sm <sub>2</sub> O <sub>3</sub>	0.16	0.09	0.03	0.00	0.00	0.00	0.00
Gd <sub>2</sub> O <sub>3</sub>	0.11	0.03	0.10	0.03	0.04	0.00	0.02
Dy <sub>2</sub> O <sub>3</sub>	0.03	0.00	0.00	0.00	0.00	0.00	0.00
Ho <sub>2</sub> O <sub>3</sub>	0.00	0.01	0.00	0.03	0.00	0.00	0.04
Er <sub>2</sub> O <sub>3</sub>	0.00	0.00	0.00	0.00	0.00	0.00	0.00
Yb <sub>2</sub> O <sub>3</sub>	0.02	0.02	0.04	0.07	0.00	0.02	0.02
MgO	0.68	0.67	0.66	0.64	0.72	1.06	0.94
CaO	10.54	10.46	9.06	9.40	8.00	8.20	7.94
MnO	1.69	1.81	2.06	2.19	2.89	2.17	2.42
SrO	1.71	1.80	1.81	1.83	1.57	1.62	1.77
PbO	0.02	0.03	0.04	0.04	0.03	0.02	0.02
Na <sub>2</sub> O	0.00	0.03	0.01	0.00	0.03	0.00	0.02
F	0.02	0.02	0.05	0.04	0.05	0.01	0.01
Cl	0.00	0.01	0.01	0.00	0.00	0.00	0.01
H <sub>2</sub> O*	1.57	1.57	1.50	1.52	1.46	1.52	1.50
Total	100.43	100.64	100.23	100.47	100.04	100.20	100.09

Appendix B.9: EMPA analyses of Epidote Group Minerals

Allanite type	I	I	I	I	I	I	I
Thin Section	135a	135a	135a	135a	135a	135C	135C
Point	73 / 1 .	74 / 1 .	75 / 1 .	76 / 1 .	77 / 1 .	45 / 1 .	46 / 1 .
P (apfu)	0.002	0.000	0.001	0.001	0.001	0.002	0.001
Si	2.998	3.000	2.999	2.999	2.999	2.998	2.999
Ti	0.130	0.127	0.195	0.165	0.263	0.299	0.268
Sn	0.002	0.002	0.001	0.001	0.001	0.001	0.001
Al	1.626	1.560	1.369	1.383	1.047	1.080	1.083
Fe <sup>3+</sup>	0.440	0.637	0.618	0.690	0.737	0.666	0.709
Fe <sup>2+</sup>	0.633	0.463	0.571	0.535	0.695	0.698	0.683
Th	0.031	0.033	0.031	0.026	0.016	0.155	0.138
U	0.000	0.000	0.000	0.000	0.000	0.017	0.019
Y	0.005	0.003	0.001	0.004	0.001	0.000	0.000
La	0.255	0.251	0.303	0.293	0.361	0.001	0.001
Ce	0.338	0.341	0.393	0.372	0.416	0.328	0.343
Pr	0.022	0.022	0.027	0.023	0.022	0.417	0.422
Nd	0.072	0.064	0.065	0.063	0.055	0.027	0.022
Sm	0.005	0.003	0.001	0.000	0.000	0.065	0.057
Gd	0.003	0.001	0.003	0.001	0.001	0.000	0.000
Tb	0.000	0.000	0.000	0.000	0.000	0.000	0.001
Dy	0.001	0.000	0.000	0.000	0.000	0.000	0.000
Ho	0.000	0.000	0.000	0.001	0.000	0.000	0.000
Er	0.000	0.000	0.000	0.000	0.000	0.000	0.001
Yb	0.001	0.001	0.001	0.002	0.000	0.000	0.000
Mg	0.096	0.094	0.096	0.091	0.106	1.364	1.392
Ca	1.066	1.053	0.941	0.967	0.850	0.001	0.001
Mn	0.135	0.144	0.169	0.178	0.243	0.862	0.840
Sr	0.094	0.098	0.102	0.102	0.090	0.180	0.202
Pb	0.001	0.001	0.001	0.001	0.001	0.000	0.000
Na	0.001	0.005	0.001	0.000	0.006	0.000	0.000
F	0.006	0.007	0.015	0.012	0.015	0.000	0.000
Cl	0.000	0.001	0.001	0.000	0.001	0.003	0.005
OH	0.986	0.984	0.968	0.975	0.969	0.000	0.001

Appendix B.9: EMPA analyses of Epidote Group Minerals

Allanite type	I	I	I	I	I	II	II
Thin Section	135C	135C	135C	135C	135C	135C	KIN133D
Point	47 / 1 .	48 / 1 .	49 / 1 .	50 / 1 .	51 / 1 .	52 / 1 .	54 / 1 .
P <sub>2</sub> O <sub>5</sub> (wt.%)	0.00	0.00	0.02	0.02	0.07	0.02	0.04
SiO <sub>2</sub>	30.82	30.31	30.62	32.28	31.88	33.06	35.90
TiO <sub>2</sub>	3.93	3.40	4.33	1.19	1.51	1.18	2.09
SnO <sub>2</sub>	0.02	0.01	0.03	0.03	0.01	0.01	0.04
Al <sub>2</sub> O <sub>3</sub>	9.55	9.07	10.24	16.01	17.00	17.38	14.64
Fe <sub>2</sub> O <sub>3</sub> *	9.79	9.41	6.84	8.43	8.03	13.18	13.92
FeO*	7.47	9.00	8.73	4.98	6.25	1.41	0.00
ThO <sub>2</sub>	0.89	0.90	0.90	1.32	5.49	4.66	5.20
UO <sub>2</sub>	0.03	0.00	0.00	0.04	0.09	0.07	0.10
Y <sub>2</sub> O <sub>3</sub>	0.02	0.00	0.01	0.04	0.04	0.06	0.06
La <sub>2</sub> O <sub>3</sub>	9.33	9.18	9.10	7.04	5.13	5.18	4.69
Ce <sub>2</sub> O <sub>3</sub>	11.31	11.70	11.56	9.43	7.28	7.32	7.56
Pr <sub>2</sub> O <sub>3</sub>	0.72	0.87	0.66	0.74	0.37	0.45	0.33
Nd <sub>2</sub> O <sub>3</sub>	1.52	1.60	1.67	1.75	1.40	1.40	1.75
Sm <sub>2</sub> O <sub>3</sub>	0.00	0.00	0.00	0.00	0.04	0.03	0.07
Gd <sub>2</sub> O <sub>3</sub>	0.05	0.11	0.00	0.08	0.09	0.09	0.11
Dy <sub>2</sub> O <sub>3</sub>	0.00	0.00	0.03	0.01	0.00	0.00	0.00
Ho <sub>2</sub> O <sub>3</sub>	0.10	0.11	0.00	0.02	0.00	0.00	0.05
Er <sub>2</sub> O <sub>3</sub>	0.00	0.00	0.00	0.00	0.00	0.06	0.00
Yb <sub>2</sub> O <sub>3</sub>	0.03	0.03	0.01	0.00	0.02	0.03	0.03
MgO	1.15	0.86	1.24	0.81	0.63	0.59	0.38
CaO	8.46	8.02	8.29	10.82	8.67	9.38	7.03
MnO	2.01	2.54	2.01	1.16	0.91	0.95	1.24
SrO	1.90	1.59	1.99	2.18	1.65	1.81	0.63
PbO	0.05	0.02	0.05	0.05	0.12	0.04	0.07
Na <sub>2</sub> O	0.03	0.02	0.06	0.00	0.17	0.17	0.07
F	0.03	-0.02	0.02	0.00	0.02	0.02	0.05
Cl	0.00	0.00	0.00	0.01	0.02	0.01	0.00
H <sub>2</sub> O*	1.51	1.53	1.52	1.61	1.57	1.63	5.68
Total	100.71	100.26	99.93	100.04	98.46	100.21	101.71

Appendix B.9: EMPA analyses of Epidote Group Minerals

Allanite type	I	I	I	I	I	II	II
Thin Section	135C	135C	135C	135C	135C	135C	KIN133D
Point	47 / 1 .	48 / 1 .	49 / 1 .	50 / 1 .	51 / 1 .	52 / 1 .	54 / 1 .
P (apfu)	0.000	0.000	0.001	0.001	0.006	0.002	0.003
Si	3.000	3.000	2.999	2.999	2.994	2.998	2.997
Ti	0.288	0.253	0.319	0.083	0.107	0.080	0.131
Sn	0.001	0.000	0.001	0.001	0.000	0.000	0.001
Al	1.096	1.058	1.182	1.752	1.882	1.857	1.440
Fe <sup>3+</sup>	0.717	0.701	0.504	0.589	0.568	0.900	0.875
Fe <sup>2+</sup>	0.608	0.745	0.715	0.387	0.491	0.107	0.000
Th	0.166	0.127	0.181	0.113	0.088	0.080	0.047
U	0.020	0.020	0.020	0.028	0.117	0.096	0.099
Y	0.001	0.000	0.000	0.001	0.002	0.001	0.002
La	0.001	0.000	0.001	0.002	0.002	0.003	0.003
Ce	0.335	0.335	0.329	0.241	0.178	0.173	0.145
Pr	0.403	0.424	0.415	0.321	0.250	0.243	0.231
Nd	0.026	0.032	0.024	0.025	0.013	0.015	0.010
Sm	0.053	0.057	0.058	0.058	0.047	0.045	0.052
Gd	0.000	0.000	0.000	0.000	0.001	0.001	0.002
Tb	0.002	0.004	0.000	0.003	0.003	0.003	0.003
Dy	0.000	0.000	0.000	0.000	0.000	0.000	0.000
Ho	0.000	0.000	0.001	0.000	0.000	0.000	0.000
Er	0.003	0.003	0.000	0.001	0.000	0.000	0.001
Yb	0.000	0.000	0.000	0.000	0.000	0.002	0.000
Mg	1.325	1.445	1.218	0.976	1.059	1.007	0.875
Ca	0.001	0.001	0.000	0.000	0.000	0.001	0.001
Mn	0.882	0.850	0.870	1.077	0.872	0.911	0.629
Sr	0.166	0.213	0.167	0.091	0.072	0.073	0.087
Pb	0.000	0.000	0.000	0.000	0.000	0.000	0.000
Na	0.001	0.001	0.001	0.001	0.003	0.001	0.002
F	0.000	0.000	0.000	0.000	0.000	0.000	0.000
Cl	0.009	-0.006	0.005	-0.001	0.005	0.005	0.014
OH	0.000	0.000	0.000	0.002	0.003	0.002	0.000

Appendix B.9: EMPA analyses of Epidote Group Minerals

Allanite type	II	II	II	II	II	II
Thin Section	kin 130A	133C	130b	135a	135a	135a
Point	34 / 1 .	15 / 1 .	43 / 1 .	48 / 1 .	49 / 1 .	58 / 1 .
P <sub>2</sub> O <sub>5</sub> (wt.%)	0.02	0.17	0.06	0.02	0.00	0.01
SiO <sub>2</sub>	34.27	35.98	33.89	34.66	37.40	34.85
TiO <sub>2</sub>	0.22	0.26	0.35	2.28	1.92	2.68
SnO <sub>2</sub>	0.00	0.00	0.01	0.03	0.05	0.06
Al <sub>2</sub> O <sub>3</sub>	22.12	16.81	20.35	12.63	13.34	11.62
Fe <sub>2</sub> O <sub>3</sub> *	8.15	12.28	8.72	16.36	13.95	16.16
FeO*	0.00	0.00	0.00	0.00	0.00	0.00
ThO <sub>2</sub>	4.18	11.54	7.41	2.80	2.54	2.77
UO <sub>2</sub>	0.02	0.37	0.14	0.00	0.01	0.01
Y <sub>2</sub> O <sub>3</sub>	0.16	0.04	0.38	0.10	0.08	0.10
La <sub>2</sub> O <sub>3</sub>	3.55	1.59	1.22	5.70	5.47	6.14
Ce <sub>2</sub> O <sub>3</sub>	5.87	3.29	3.58	8.24	7.81	8.53
Pr <sub>2</sub> O <sub>3</sub>	0.48	0.45	0.49	0.34	0.36	0.41
Nd <sub>2</sub> O <sub>3</sub>	1.46	1.09	1.64	1.69	1.57	1.90
Sm <sub>2</sub> O <sub>3</sub>	0.14	0.18	0.24	0.12	0.13	0.04
Gd <sub>2</sub> O <sub>3</sub>	0.04	0.04	0.16	0.11	0.09	0.04
Dy <sub>2</sub> O <sub>3</sub>	0.00	0.00	0.04	0.05	0.00	0.00
Ho <sub>2</sub> O <sub>3</sub>	0.00	0.00	0.03	0.03	0.04	0.00
Er <sub>2</sub> O <sub>3</sub>	0.09	0.00	0.00	0.00	0.00	0.00
Yb <sub>2</sub> O <sub>3</sub>	0.01	0.02	0.03	0.01	0.00	0.00
MgO	0.61	0.32	0.40	0.48	0.45	0.54
CaO	11.55	5.41	8.78	7.54	7.81	7.50
MnO	0.93	0.91	1.03	1.80	1.62	1.62
SrO	1.31	0.39	1.04	1.56	1.50	2.01
PbO	0.07	0.04	0.73	0.10	0.04	0.05
Na <sub>2</sub> O	0.15	0.13	0.17	0.08	0.07	0.11
F	0.03	-0.03	0.02	-0.02	-0.01	0.01
Cl	0.07	0.30	0.13	0.01	0.01	0.01
H <sub>2</sub> O*	2.36	7.06	3.90	4.52	7.18	4.87
Total	97.85	98.63	94.98	101.24	103.42	102.04

Appendix B.9: EMPA analyses of Epidote Group Minerals

Allanite type	II	II	II	II	II	II
Thin Section	kin 130A	133C	130b	135a	135a	135a
Point	34 / 1 .	15 / 1 .	43 / 1 .	48 / 1 .	49 / 1 .	58 / 1 .
P (apfu)	0.010	0.003	0.004	0.029	0.024	0.034
Si	2.990	0.000	0.000	0.000	0.000	0.000
Ti	0.247	0.000	0.000	0.000	0.000	0.000
Sn	0.003	0.000	0.000	0.000	0.000	0.000
Al	1.482	0.154	0.109	0.205	0.175	0.202
Fe <sup>3+</sup>	0.000	0.154	0.109	0.205	0.175	0.202
Fe <sup>2+</sup>	1.916	0.008	0.010	0.012	0.011	0.013
Th	0.062	0.000	0.003	0.001	0.001	0.001
U	0.084	0.010	0.008	0.035	0.034	0.038
Y	0.001	0.020	0.022	0.050	0.048	0.052
La	0.007	0.003	0.003	0.002	0.002	0.003
Ce	0.195	0.006	0.010	0.010	0.009	0.011
Pr	0.316	0.001	0.001	0.001	0.001	0.000
Nd	0.020	0.000	0.001	0.001	0.000	0.000
Sm	0.070	0.000	0.000	0.000	0.000	0.000
Gd	0.005	0.000	0.000	0.000	0.000	0.000
Tb	0.003	0.000	0.000	0.000	0.000	0.000
Dy	0.000	0.000	0.000	0.000	0.000	0.000
Ho	0.000	0.000	0.000	0.000	0.000	0.000
Er	0.001	0.096	0.157	0.134	0.139	0.134
Yb	0.000	0.013	0.015	0.025	0.023	0.023
Mg	1.916	0.001	0.000	0.000	0.000	0.000
Ca	0.000	0.004	0.010	0.015	0.014	0.019
Mn	0.757	0.000	0.000	0.000	0.000	0.000
Sr	0.153	0.000	0.003	0.000	0.000	0.000
Pb	0.000	0.000	0.000	0.000	0.000	0.000
Na	0.000	-0.001	0.001	-0.001	0.000	0.001
F	0.000	2.129	2.171	2.148	2.211	2.142
Cl	0.058	4.990	5.312	5.198	4.820	5.171
OH	0.002	5.412	5.444	5.476	5.371	5.553

## B.10: Chevkinite Group Minerals

### Appendix B.10: EMPA analyses of Chevkinite Group Minerals

Mineral	Chevkinite						
Point	3 / 1 .	4 / 1 .	12 / 1 .	13 / 1 .	14 / 1 .	15 / 1 .	16 / 1 .
Thin section	KIN133D						
Nb <sub>2</sub> O <sub>5</sub> (wt.%)	2.70	1.96	3.42	3.34	2.61	2.69	2.73
P <sub>2</sub> O <sub>5</sub>	0.00	0.02	0.08	0.01	0.02	0.01	0.02
SiO <sub>2</sub>	19.25	18.56	19.95	19.60	19.17	19.40	19.68
TiO <sub>2</sub>	17.25	16.62	18.58	17.19	16.79	16.73	17.20
ZrO <sub>2</sub>	0.38	0.03	0.47	0.37	0.30	0.25	0.39
SnO <sub>2</sub>	0.01	0.06	0.03	0.07	0.00	0.02	0.03
Al <sub>2</sub> O <sub>3</sub>	0.24	0.13	0.53	0.33	0.16	0.20	0.19
Fe <sub>2</sub> O <sub>3</sub> *	3.31	3.15	8.37	4.21	3.83	3.62	3.05
FeO*	7.15	8.17	1.66	6.31	5.93	6.00	6.85
ThO <sub>2</sub>	2.07	0.94	4.05	2.44	3.76	3.59	2.03
UO <sub>2</sub>	0.05	0.01	0.13	0.03	0.03	0.05	0.03
Y <sub>2</sub> O <sub>3</sub>	0.12	0.05	0.12	0.12	0.12	0.12	0.13
La <sub>2</sub> O <sub>3</sub>	14.99	15.96	12.57	14.28	14.41	14.75	14.66
Ce <sub>2</sub> O <sub>3</sub>	20.98	23.75	18.96	20.31	20.77	20.82	21.18
Pr <sub>2</sub> O <sub>3</sub>	1.46	1.83	1.41	1.45	1.55	1.50	1.63
Nd <sub>2</sub> O <sub>3</sub>	3.87	4.71	3.49	4.01	3.84	3.88	3.95
Sm <sub>2</sub> O <sub>3</sub>	0.04	0.12	0.08	0.14	0.11	0.09	0.09
Gd <sub>2</sub> O <sub>3</sub>	0.11	0.04	0.13	0.16	0.00	0.13	0.13
Dy <sub>2</sub> O <sub>3</sub>	0.00	0.00	0.00	0.00	0.25	0.16	0.05
Ho <sub>2</sub> O <sub>3</sub>	0.04	0.09	0.02	0.02	0.02	0.02	0.10
Er <sub>2</sub> O <sub>3</sub>	0.00	0.00	0.00	0.00	0.00	0.00	0.01
Yb <sub>2</sub> O <sub>3</sub>	0.00	0.03	0.00	0.00	0.00	0.00	0.07
MgO	0.21	0.26	0.19	0.25	0.22	0.21	0.22
CaO	2.51	1.31	2.02	2.41	2.05	1.98	2.52
MnO	1.21	0.89	0.91	0.79	2.22	2.24	1.64
SrO	1.69	0.42	1.30	1.58	1.50	1.40	1.60
PbO	0.09	0.06	0.22	0.15	0.07	0.13	0.07
Na <sub>2</sub> O	0.00	0.00	0.05	0.00	0.00	0.00	0.00
Total	99.72	99.17	98.76	99.61	99.75	100.04	100.28

\*Note: formula calculation based on BCTD = 9

Elements sought but not found (or below detection limit): Cl, F, K, Sc, and Ba (average detection limits of 184 ppm, 335 ppm, 172 ppm, 364 ppm, and 945 respectively)

**Appendix B.10:** EMPA analyses of Chevkinite Group Minerals

Mineral	Chevkinite						
Point	3 / 1 .	4 / 1 .	12 / 1 .	13 / 1 .	14 / 1 .	15 / 1 .	16 / 1 .
Thin section	KIN133D						
Nb (apfu)	0.252	0.187	0.308	0.308	0.244	0.252	0.253
P	0.000	0.003	0.013	0.001	0.003	0.001	0.003
Si	3.962	3.930	3.977	3.997	3.978	4.012	4.022
Ti	2.670	2.647	2.786	2.638	2.620	2.601	2.643
Zr	0.038	0.003	0.045	0.036	0.030	0.026	0.038
Sn	0.001	0.005	0.003	0.006	0.000	0.002	0.003
Al	0.059	0.032	0.124	0.079	0.039	0.049	0.045
Fe <sup>3+</sup>	0.512	0.502	1.255	0.646	0.598	0.563	0.469
Fe <sup>2+</sup>	1.230	1.447	0.278	1.077	1.029	1.038	1.171
Th	0.097	0.045	0.184	0.113	0.178	0.169	0.094
U	0.002	0.000	0.006	0.001	0.001	0.002	0.001
Y	0.013	0.006	0.013	0.013	0.013	0.013	0.014
La	1.138	1.247	0.924	1.074	1.103	1.125	1.105
Ce	1.580	1.842	1.384	1.516	1.577	1.576	1.585
Pr	0.110	0.141	0.102	0.108	0.117	0.113	0.121
Nd	0.284	0.356	0.248	0.292	0.284	0.286	0.289
Sm	0.003	0.008	0.005	0.010	0.008	0.006	0.007
Gd	0.007	0.003	0.009	0.011	0.000	0.009	0.009
Dy	0.000	0.000	0.000	0.000	0.017	0.011	0.003
Ho	0.003	0.006	0.001	0.001	0.001	0.001	0.006
Er	0.000	0.000	0.000	0.000	0.000	0.000	0.001
Yb	0.000	0.002	0.000	0.000	0.000	0.000	0.004
Mg	0.066	0.082	0.057	0.077	0.069	0.064	0.068
Ca	0.554	0.298	0.432	0.526	0.456	0.439	0.552
Mn	0.210	0.160	0.154	0.136	0.389	0.393	0.284
Sr	0.202	0.052	0.151	0.186	0.180	0.167	0.190
Pb	0.005	0.003	0.012	0.008	0.004	0.007	0.004
Na	0.000	0.000	0.019	0.001	0.000	0.000	0.000

**Appendix B.10:** EMPA analyses of Chevkinite Group Minerals

Mineral	Chevkinite						
Point	17 / 1 .	19 / 1 .	20 / 1 .	21 / 1 .	22 / 1 .	23 / 1 .	24 / 1 .
Thin section	KIN133D						
Nb <sub>2</sub> O <sub>5</sub> (wt.%)	3.17	3.85	2.77	2.90	2.68	2.52	2.50
P <sub>2</sub> O <sub>5</sub>	0.03	0.11	0.04	0.00	0.03	0.00	0.00
SiO <sub>2</sub>	19.50	19.11	19.27	19.67	19.13	19.57	19.82
TiO <sub>2</sub>	19.85	21.91	16.80	17.01	16.83	17.26	17.64
ZrO <sub>2</sub>	0.15	0.38	0.22	0.33	0.25	0.32	0.33
SnO <sub>2</sub>	0.02	0.02	0.01	0.01	0.00	0.00	0.01
Al <sub>2</sub> O <sub>3</sub>	0.30	0.52	0.31	0.30	0.31	0.15	0.14
Fe <sub>2</sub> O <sub>3</sub> *	4.03	5.29	3.50	3.58	4.53	2.97	4.01
FeO*	3.93	1.82	7.24	6.42	6.03	6.61	5.45
ThO <sub>2</sub>	4.72	5.16	3.67	2.24	4.35	2.76	1.98
UO <sub>2</sub>	0.05	0.23	0.07	0.02	0.05	0.03	0.02
Y <sub>2</sub> O <sub>3</sub>	0.12	0.11	0.09	0.13	0.13	0.12	0.14
La <sub>2</sub> O <sub>3</sub>	12.39	11.04	14.75	14.28	14.22	14.80	14.39
Ce <sub>2</sub> O <sub>3</sub>	19.16	17.95	20.66	20.94	20.42	21.37	20.98
Pr <sub>2</sub> O <sub>3</sub>	1.43	1.37	1.42	1.57	1.48	1.36	1.58
Nd <sub>2</sub> O <sub>3</sub>	3.66	3.50	3.81	3.90	3.69	4.05	4.02
Sm <sub>2</sub> O <sub>3</sub>	0.12	0.13	0.14	0.18	0.12	0.13	0.24
Gd <sub>2</sub> O <sub>3</sub>	0.04	0.15	0.16	0.13	0.12	0.10	0.11
Dy <sub>2</sub> O <sub>3</sub>	0.00	0.00	0.00	0.00	0.00	0.10	0.26
Ho <sub>2</sub> O <sub>3</sub>	0.04	0.00	0.00	0.03	0.03	0.00	0.09
Er <sub>2</sub> O <sub>3</sub>	0.00	0.00	0.03	0.00	0.00	0.05	0.04
Yb <sub>2</sub> O <sub>3</sub>	0.00	0.05	0.07	0.00	0.00	0.02	0.10
MgO	0.15	0.12	0.22	0.18	0.19	0.22	0.26
CaO	1.54	1.43	2.19	2.54	2.04	2.13	2.47
MnO	1.09	0.98	1.10	1.52	1.44	1.99	2.19
SrO	1.13	1.15	1.45	1.57	1.44	1.59	1.56
PbO	0.13	0.25	0.07	0.09	0.07	0.09	0.06
Na <sub>2</sub> O	0.02	0.22	0.00	0.00	0.00	0.00	0.01
Total	96.77	96.88	100.10	99.54	99.58	100.33	100.44

**Appendix B.10:** EMPA analyses of Chevkinite Group Minerals

Mineral	Chevkinite						
Point	17 / 1 .	19 / 1 .	20 / 1 .	21 / 1 .	22 / 1 .	23 / 1 .	24 / 1 .
Thin section	KIN133D						
Nb (apfu)	0.294	0.350	0.258	0.269	0.251	0.234	0.229
P	0.006	0.018	0.007	0.000	0.005	0.000	0.001
Si	4.009	3.846	3.976	4.032	3.960	4.020	4.020
Ti	3.069	3.316	2.608	2.623	2.621	2.668	2.691
Zr	0.015	0.037	0.022	0.033	0.025	0.032	0.032
Sn	0.002	0.001	0.000	0.001	0.000	0.000	0.001
Al	0.072	0.122	0.075	0.073	0.076	0.037	0.034
Fe <sup>3+</sup>	0.624	0.801	0.543	0.551	0.705	0.460	0.613
Fe <sup>2+</sup>	0.676	0.307	1.250	1.100	1.044	1.136	0.925
Th	0.221	0.236	0.173	0.105	0.205	0.129	0.091
U	0.002	0.010	0.003	0.001	0.002	0.001	0.001
Y	0.013	0.012	0.009	0.015	0.015	0.013	0.015
La	0.940	0.819	1.122	1.080	1.085	1.122	1.077
Ce	1.442	1.322	1.561	1.571	1.548	1.607	1.558
Pr	0.107	0.100	0.107	0.117	0.112	0.102	0.117
Nd	0.268	0.252	0.280	0.286	0.272	0.297	0.292
Sm	0.008	0.009	0.010	0.013	0.008	0.009	0.017
Gd	0.003	0.010	0.011	0.009	0.009	0.007	0.007
Dy	0.000	0.000	0.000	0.000	0.000	0.006	0.017
Ho	0.002	0.000	0.000	0.002	0.002	0.000	0.006
Er	0.000	0.000	0.002	0.000	0.000	0.003	0.003
Yb	0.000	0.003	0.005	0.000	0.000	0.001	0.006
Mg	0.045	0.035	0.067	0.055	0.059	0.067	0.077
Ca	0.340	0.307	0.484	0.557	0.453	0.469	0.537
Mn	0.189	0.166	0.193	0.263	0.253	0.346	0.377
Sr	0.135	0.134	0.173	0.186	0.173	0.189	0.184
Pb	0.007	0.013	0.004	0.005	0.004	0.005	0.003
Na	0.008	0.085	0.001	0.000	0.000	0.000	0.005

**Appendix B.10:** EMPA analyses of Chevkinite Group Minerals

Mineral	Chevkinite	Chevkinite	Chevkinite	Perrierite	Perrierite	Perrierite	Perrierite
Point	94 / 1 .	60 / 1 .	61 / 1 .	33 / 1 .	34 / 1 .	35 / 1 .	36 / 1 .
Thin section	KIN134-2	135a	135a	135C	135C	135C	135C
Nb <sub>2</sub> O <sub>5</sub> (wt.%)	1.28	4.32	4.25	5.18	3.98	4.46	3.61
P <sub>2</sub> O <sub>5</sub>	0.04	0.01	0.02	0.02	0.02	0.03	0.01
SiO <sub>2</sub>	19.53	19.57	19.40	19.30	19.44	19.54	19.61
TiO <sub>2</sub>	17.43	14.29	14.32	14.13	15.50	15.15	16.08
ZrO <sub>2</sub>	0.06	0.14	0.15	0.42	0.38	0.52	0.52
SnO <sub>2</sub>	0.02	0.07	0.05	0.12	0.14	0.14	0.17
Al <sub>2</sub> O <sub>3</sub>	0.75	0.53	0.41	0.29	0.30	0.35	0.40
Fe <sub>2</sub> O <sub>3</sub> *	1.93	0.50	0.98	0.00	0.92	0.78	1.22
FeO*	8.25	9.51	9.19	9.59	8.82	8.84	8.30
ThO <sub>2</sub>	2.25	4.62	3.29	4.87	5.01	4.75	4.65
UO <sub>2</sub>	0.03	0.02	0.03	0.02	0.05	0.05	0.00
Y <sub>2</sub> O <sub>3</sub>	0.04	0.12	0.14	0.18	0.22	0.19	0.17
La <sub>2</sub> O <sub>3</sub>	17.73	15.31	15.56	12.94	12.96	12.27	12.61
Ce <sub>2</sub> O <sub>3</sub>	22.36	19.54	20.27	18.19	18.22	17.99	18.05
Pr <sub>2</sub> O <sub>3</sub>	1.42	1.27	1.38	1.35	1.24	1.36	1.26
Nd <sub>2</sub> O <sub>3</sub>	3.50	3.51	3.74	3.71	3.55	3.76	3.50
Sm <sub>2</sub> O <sub>3</sub>	0.05	0.00	0.19	0.20	0.11	0.15	0.08
Gd <sub>2</sub> O <sub>3</sub>	0.12	0.22	0.11	0.16	0.16	0.03	0.18
Dy <sub>2</sub> O <sub>3</sub>	0.00	0.00	0.09	0.00	0.00	0.04	0.00
Ho <sub>2</sub> O <sub>3</sub>	0.07	0.02	0.00	0.00	0.00	0.04	0.05
Er <sub>2</sub> O <sub>3</sub>	0.00	0.02	0.00	0.15	0.03	0.00	0.02
Yb <sub>2</sub> O <sub>3</sub>	0.00	0.07	0.00	0.03	0.06	0.03	0.04
MgO	0.48	0.26	0.24	0.19	0.28	0.23	0.31
CaO	1.78	1.97	1.96	2.19	2.26	2.50	2.46
MnO	0.41	0.95	1.06	0.87	0.77	0.84	0.68
SrO	0.53	2.15	1.60	3.55	3.56	3.87	4.15
PbO	0.05	0.18	0.12	0.18	0.20	0.23	0.22
Na <sub>2</sub> O	0.00	0.00	0.00	0.00	0.00	0.00	0.00
Total	100.14	99.14	98.56	97.83	98.20	98.16	98.33

**Appendix B.10:** EMPA analyses of Chevkinite Group Minerals

Mineral	Chevkinite	Chevkinite	Chevkinite	Perrierite	Perrierite	Perrierite	Perrierite
Point	94 / 1 .	60 / 1 .	61 / 1 .	33 / 1 .	34 / 1 .	35 / 1 .	36 / 1 .
Thin section	KIN134-2	135a	135a	135C	135C	135C	135C
Nb (apfu)	0.119	0.413	0.408	0.503	0.380	0.425	0.342
P	0.007	0.002	0.004	0.004	0.003	0.005	0.001
Si	4.033	4.145	4.122	4.144	4.103	4.115	4.102
Ti	2.706	2.275	2.289	2.282	2.461	2.400	2.529
Zr	0.006	0.014	0.015	0.044	0.039	0.054	0.053
Sn	0.002	0.006	0.004	0.010	0.012	0.012	0.014
Al	0.183	0.132	0.103	0.074	0.074	0.087	0.097
Fe <sup>3+</sup>	0.300	0.079	0.157	0.000	0.147	0.123	0.192
Fe <sup>2+</sup>	1.425	1.684	1.632	1.722	1.557	1.557	1.451
Th	0.106	0.223	0.159	0.238	0.240	0.228	0.221
U	0.001	0.001	0.001	0.001	0.002	0.002	0.000
Y	0.004	0.014	0.016	0.020	0.025	0.021	0.019
La	1.350	1.196	1.219	1.025	1.009	0.953	0.973
Ce	1.690	1.515	1.577	1.430	1.408	1.387	1.382
Pr	0.107	0.098	0.107	0.106	0.095	0.104	0.096
Nd	0.258	0.265	0.284	0.284	0.268	0.283	0.261
Sm	0.003	0.000	0.014	0.015	0.008	0.011	0.005
Gd	0.008	0.015	0.008	0.012	0.011	0.002	0.012
Dy	0.000	0.000	0.006	0.000	0.000	0.003	0.000
Ho	0.005	0.001	0.000	0.000	0.000	0.003	0.003
Er	0.000	0.001	0.000	0.010	0.002	0.000	0.001
Yb	0.000	0.004	0.000	0.002	0.004	0.002	0.003
Mg	0.148	0.080	0.075	0.060	0.087	0.073	0.098
Ca	0.394	0.447	0.447	0.504	0.510	0.563	0.552
Mn	0.071	0.170	0.191	0.158	0.138	0.150	0.120
Sr	0.063	0.263	0.197	0.442	0.436	0.472	0.503
Pb	0.003	0.010	0.007	0.011	0.012	0.013	0.012
Na	0.000	0.000	0.000	0.000	0.000	0.000	0.000

**Appendix B.10:** EMPA analyses of Chevkinite Group Minerals

Mineral	Chevkinite	Chevkinite	Chevkinite	Perrierite	Perrierite	Perrierite	Perrierite
Point	37 / 1 .	38 / 1 .	39 / 1 .	40 / 1 .	41 / 1 .	42 / 1 .	43 / 1 .
Thin section	135C						
Nb <sub>2</sub> O <sub>5</sub> (wt.%)	2.85	2.39	3.74	4.68	4.73	5.25	4.94
P <sub>2</sub> O <sub>5</sub>	0.00	0.00	0.03	0.06	0.02	0.05	0.04
SiO <sub>2</sub>	19.28	19.41	19.23	19.09	19.74	19.76	19.62
TiO <sub>2</sub>	15.78	15.83	14.88	14.34	14.91	14.46	16.01
ZrO <sub>2</sub>	0.12	0.07	0.12	0.20	0.56	0.46	0.34
SnO <sub>2</sub>	0.17	0.15	0.04	0.06	0.14	0.15	0.11
Al <sub>2</sub> O <sub>3</sub>	0.14	0.17	0.26	0.32	0.33	0.36	0.34
Fe <sub>2</sub> O <sub>3</sub> *	1.49	0.72	0.83	0.00	1.49	1.11	0.00
FeO*	8.82	9.15	9.40	9.89	8.40	8.83	6.35
ThO <sub>2</sub>	2.11	2.25	3.24	4.43	4.58	4.58	5.92
UO <sub>2</sub>	0.00	0.00	0.04	0.04	0.03	0.04	0.01
Y <sub>2</sub> O <sub>3</sub>	0.09	0.07	0.20	0.24	0.17	0.25	0.22
La <sub>2</sub> O <sub>3</sub>	14.90	14.68	14.25	12.77	12.37	12.37	10.68
Ce <sub>2</sub> O <sub>3</sub>	21.29	21.68	20.87	19.69	18.17	17.94	16.86
Pr <sub>2</sub> O <sub>3</sub>	1.55	1.49	1.51	1.56	1.32	1.36	1.22
Nd <sub>2</sub> O <sub>3</sub>	4.29	4.46	4.26	4.50	3.63	3.68	3.56
Sm <sub>2</sub> O <sub>3</sub>	0.14	0.25	0.19	0.26	0.19	0.23	0.25
Gd <sub>2</sub> O <sub>3</sub>	0.05	0.10	0.18	0.20	0.06	0.22	0.07
Dy <sub>2</sub> O <sub>3</sub>	0.00	0.00	0.00	0.03	0.00	0.01	0.13
Ho <sub>2</sub> O <sub>3</sub>	0.00	0.00	0.00	0.05	0.00	0.00	0.02
Er <sub>2</sub> O <sub>3</sub>	0.00	0.00	0.02	0.02	0.00	0.04	0.01
Yb <sub>2</sub> O <sub>3</sub>	0.03	0.07	0.03	0.07	0.02	0.03	0.00
MgO	0.28	0.28	0.30	0.36	0.26	0.27	0.17
CaO	1.23	1.26	1.57	1.51	2.50	2.47	2.64
MnO	0.79	0.90	0.85	0.76	0.75	0.68	1.02
SrO	2.88	2.45	2.30	3.28	3.82	3.74	3.06
PbO	0.06	0.05	0.14	0.13	0.19	0.24	0.11
Na <sub>2</sub> O	0.00	0.00	0.00	0.00	0.00	0.00	0.01
Total	98.35	97.92	98.50	98.58	98.40	98.57	93.71

**Appendix B.10:** EMPA analyses of Chevkinite Group Minerals

Mineral	Chevkinite	Chevkinite	Chevkinite	Perrierite	Perrierite	Perrierite	Perrierite
Point	37 / 1 .	38 / 1 .	39 / 1 .	40 / 1 .	41 / 1 .	42 / 1 .	43 / 1 .
Thin section	135C						
Nb (apfu)	0.274	0.231	0.361	0.453	0.448	0.498	0.491
P	0.000	0.000	0.005	0.011	0.003	0.009	0.007
Si	4.101	4.152	4.103	4.092	4.133	4.141	4.311
Ti	2.525	2.548	2.389	2.311	2.348	2.279	2.646
Zr	0.012	0.007	0.013	0.021	0.057	0.046	0.037
Sn	0.014	0.013	0.003	0.005	0.012	0.012	0.010
Al	0.035	0.044	0.066	0.081	0.081	0.088	0.087
Fe <sup>3+</sup>	0.238	0.116	0.134	0.000	0.235	0.175	0.000
Fe <sup>2+</sup>	1.569	1.638	1.678	1.773	1.470	1.547	1.167
Th	0.102	0.109	0.157	0.216	0.218	0.218	0.296
U	0.000	0.000	0.002	0.002	0.001	0.002	0.000
Y	0.010	0.008	0.023	0.028	0.019	0.027	0.026
La	1.169	1.158	1.121	1.009	0.955	0.956	0.865
Ce	1.659	1.698	1.631	1.545	1.393	1.376	1.356
Pr	0.120	0.116	0.118	0.122	0.101	0.104	0.098
Nd	0.326	0.340	0.325	0.344	0.272	0.275	0.279
Sm	0.010	0.019	0.014	0.019	0.014	0.016	0.019
Gd	0.004	0.007	0.013	0.014	0.004	0.015	0.005
Dy	0.000	0.000	0.000	0.002	0.000	0.000	0.009
Ho	0.000	0.000	0.000	0.003	0.000	0.000	0.001
Er	0.000	0.000	0.001	0.002	0.000	0.003	0.001
Yb	0.002	0.004	0.002	0.005	0.001	0.002	0.000
Mg	0.088	0.088	0.095	0.115	0.081	0.084	0.055
Ca	0.280	0.289	0.359	0.347	0.560	0.553	0.622
Mn	0.143	0.163	0.153	0.139	0.132	0.120	0.189
Sr	0.355	0.304	0.284	0.408	0.463	0.454	0.389
Pb	0.003	0.003	0.008	0.007	0.011	0.014	0.006
Na	0.000	0.000	0.000	0.000	0.000	0.000	0.006

## B.11: Monazite and Thorite

Mnz: monazite

Thr: thorite

### Appendix B.11: EMPA analyses of Monazite and Thorite

Mineral	Mnz	Mnz	Mnz	Mnz	Mnz	Mnz	Mnz	Mnz
Point	7 / 1 .	8 / 1 .	9 / 1 .	11 / 1 .	70 / 1 .	71 / 1 .	72 / 1 .	73 / 1 .
Thin Section	KIN133D	KIN133D	KIN133D	KIN133D	KIN134-2	KIN134-2	KIN134-2	KIN134-2
P <sub>2</sub> O <sub>5</sub> (wt.%)	15.66	24.16	29.04	24.99	24.65	27.16	26.98	27.36
SiO <sub>2</sub>	8.72	3.77	0.95	2.70	3.95	1.95	2.16	2.24
TiO <sub>2</sub>	0.03	0.00	0.16	0.07	0.00	0.00	0.00	0.01
ZrO <sub>2</sub>	0.00	0.00	0.00	0.00	0.00	0.00	0.00	0.00
ThO <sub>2</sub>	37.69	16.65	3.99	10.69	15.97	7.56	8.99	9.43
UO <sub>2</sub>	0.49	0.20	0.06	0.17	0.24	0.08	0.14	0.15
Sc <sub>2</sub> O <sub>3</sub>	0.02	0.00	0.03	0.02	0.02	0.02	0.02	0.02
Y <sub>2</sub> O <sub>3</sub>	0.09	0.17	0.00	0.05	0.05	0.05	0.09	0.00
La <sub>2</sub> O <sub>3</sub>	13.90	20.62	26.33	23.10	21.40	20.78	19.86	22.91
Ce <sub>2</sub> O <sub>3</sub>	18.06	26.46	32.06	29.14	27.37	31.75	31.20	30.77
Pr <sub>2</sub> O <sub>3</sub>	1.21	2.10	2.13	2.00	1.97	2.49	2.58	2.11
Nd <sub>2</sub> O <sub>3</sub>	3.63	5.34	5.36	5.17	5.30	6.81	7.08	5.54
Sm <sub>2</sub> O <sub>3</sub>	0.30	0.44	0.18	0.38	0.35	0.53	0.46	0.45
Eu <sub>2</sub> O <sub>3</sub>	0.12	0.14	0.07	0.04	0.04	0.07	0.17	0.02
Gd <sub>2</sub> O <sub>3</sub>	0.15	0.21	0.06	0.06	0.00	0.24	0.15	0.06
Dy <sub>2</sub> O <sub>3</sub>	0.11	0.06	0.00	0.08	0.05	0.10	0.05	0.01
Er <sub>2</sub> O <sub>3</sub>	0.00	0.03	0.00	0.00	0.02	0.00	0.02	0.01
CaO	0.08	0.12	0.03	0.08	0.08	0.18	0.15	0.09
SrO	0.10	0.13	0.00	0.05	0.09	0.17	0.17	0.11
PbO	0.14	0.08	0.05	0.06	0.08	0.04	0.05	0.00
Total	100.51	100.67	100.50	98.82	101.62	100.02	100.33	101.30

\*Note: formula calculation based on cation sum = 2

Elements sought but not found (or below detection limit): Fe, Na, As, S (average detection limits of 788 ppm, 307 ppm, 395 ppm, and 292 ppm respectively)

**Appendix B.11:** EMPA analyses of Monazite and Thorite

Mineral	Mnz	Mnz	Mnz	Mnz	Mnz	Mnz	Mnz	Mnz
Point	7 / 1 .	8 / 1 .	9 / 1 .	11 / 1 .	70 / 1 .	71 / 1 .	72 / 1 .	73 / 1 .
Thin Section	KIN133D	KIN133D	KIN133D	KIN133D	KIN134-2	KIN134-2	KIN134-2	KIN134-2
P (apfu)	0.594	0.841	0.966	0.872	0.845	0.920	0.915	0.919
Si	0.390	0.155	0.037	0.111	0.160	0.078	0.086	0.089
Ti	0.001	0.000	0.005	0.002	0.000	0.000	0.000	0.000
Zr	0.000	0.000	0.000	0.000	0.000	0.000	0.000	0.000
Th	0.384	0.156	0.036	0.100	0.147	0.069	0.082	0.085
U	0.005	0.002	0.001	0.002	0.002	0.001	0.001	0.001
Sc	0.001	0.000	0.001	0.001	0.001	0.001	0.001	0.001
Y	0.002	0.004	0.000	0.001	0.001	0.001	0.002	0.000
La	0.230	0.313	0.382	0.351	0.320	0.307	0.293	0.335
Ce	0.296	0.398	0.461	0.440	0.406	0.465	0.458	0.447
Pr	0.020	0.031	0.030	0.030	0.029	0.036	0.038	0.031
Nd	0.058	0.078	0.075	0.076	0.077	0.097	0.101	0.079
Sm	0.005	0.006	0.002	0.005	0.005	0.007	0.006	0.006
Eu	0.002	0.002	0.001	0.000	0.001	0.001	0.002	0.000
Gd	0.002	0.003	0.001	0.001	0.000	0.003	0.002	0.001
Dy	0.002	0.001	0.000	0.001	0.001	0.001	0.001	0.000
Er	0.000	0.000	0.000	0.000	0.000	0.000	0.000	0.000
Ca	0.004	0.005	0.001	0.003	0.003	0.008	0.006	0.004
Sr	0.003	0.003	0.000	0.001	0.002	0.004	0.004	0.003
Pb	0.002	0.001	0.001	0.001	0.001	0.000	0.001	0.000

**Appendix B.11:** EMPA analyses of Monazite and Thorite

Mineral	Mnz	Mnz	Mnz	Mnz	Mnz	Mnz
Point	97 / 1 .	24 / 1 .	28 / 1 .	69 / 1 .	16 / 1 .	15 / 1 .
Thin Section	KIN134-2	kin 136	kin 136	Rad 2a	133C	Pegm1
P <sub>2</sub> O <sub>5</sub> (wt.%)	29.49	30.74	31.03	14.92	27.80	30.69
SiO <sub>2</sub>	0.72	0.35	0.15	37.62	1.85	0.61
TiO <sub>2</sub>	0.02	0.01	0.02	0.04	0.00	0.03
ZrO <sub>2</sub>	0.00	0.00	0.00	0.12	0.37	0.00
ThO <sub>2</sub>	6.70	7.72	7.80	0.52	7.73	15.71
UO <sub>2</sub>	0.63	0.81	0.39	0.02	0.14	2.00
Sc <sub>2</sub> O <sub>3</sub>	0.00	0.02	0.02	1.02	0.02	0.00
Y <sub>2</sub> O <sub>3</sub>	0.33	1.07	0.66	0.59	0.06	2.60
La <sub>2</sub> O <sub>3</sub>	22.13	21.70	21.61	3.83	23.24	11.84
Ce <sub>2</sub> O <sub>3</sub>	30.16	28.32	29.06	13.44	31.43	22.11
Pr <sub>2</sub> O <sub>3</sub>	2.33	2.00	2.15	2.22	2.16	2.23
Nd <sub>2</sub> O <sub>3</sub>	6.27	5.37	5.70	11.22	5.70	6.55
Sm <sub>2</sub> O <sub>3</sub>	0.56	0.57	0.45	2.86	0.30	1.87
Eu <sub>2</sub> O <sub>3</sub>	0.10	0.15	0.14	0.49	0.12	0.02
Gd <sub>2</sub> O <sub>3</sub>	0.32	0.42	0.26	1.72	0.08	1.75
Dy <sub>2</sub> O <sub>3</sub>	0.06	0.29	0.21	0.36	0.07	0.92
Er <sub>2</sub> O <sub>3</sub>	0.04	0.08	0.06	0.04	0.00	0.09
CaO	1.12	1.51	1.67	1.70	0.11	3.31
SrO	0.01	0.00	0.00	0.05	0.11	0.00
PbO	0.05	0.03	0.02	0.01	0.04	0.06
Total	101.07	101.16	101.39	94.14	101.33	102.41

**Appendix B.11:** EMPA analyses of Monazite and Thorite

Mineral	Mnz	Mnz	Mnz	Mnz	Mnz	Mnz
Point	97 / 1 .	24 / 1 .	28 / 1 .	69 / 1 .	16 / 1 .	15 / 1 .
Thin Section	KIN134-2	kin 136	kin 136	Rad 2a	133C	Pegm1
P (apfu)	0.971	1.000	1.005	0.373	0.932	0.985
Si	0.028	0.013	0.006	1.112	0.073	0.023
Ti	0.001	0.000	0.001	0.001	0.000	0.001
Zr	0.000	0.000	0.000	0.002	0.000	0.000
Th	0.059	0.067	0.068	0.003	0.070	0.136
U	0.005	0.007	0.003	0.000	0.001	0.017
Sc	0.000	0.001	0.001	0.026	0.001	0.000
Y	0.007	0.022	0.013	0.009	0.001	0.052
La	0.317	0.308	0.305	0.042	0.339	0.166
Ce	0.429	0.398	0.407	0.145	0.456	0.307
Pr	0.033	0.028	0.030	0.024	0.031	0.031
Nd	0.087	0.074	0.078	0.118	0.081	0.089
Sm	0.007	0.008	0.006	0.029	0.004	0.024
Eu	0.001	0.002	0.002	0.005	0.002	0.000
Gd	0.004	0.005	0.003	0.017	0.001	0.022
Dy	0.001	0.004	0.003	0.003	0.001	0.011
Er	0.000	0.001	0.001	0.000	0.000	0.001
Ca	0.047	0.062	0.068	0.054	0.005	0.135
Sr	0.000	0.000	0.000	0.001	0.003	0.000
Pb	0.001	0.000	0.000	0.000	0.000	0.001

**Appendix B.11:** EMPA analyses of Monazite and Thorite

Mineral	Thr	Thr	Thr		Thr	Thr	Thr
Point	96 / 1 .	51 / 1 .	7 / 1 .		96 / 1 .	51 / 1 .	7 / 1 .
Thin Section	KIN134-2	kin 130A	133C		KIN134-2	kin 130A	133C
P <sub>2</sub> O <sub>5</sub> (wt.%)	1.57	0.30	0.02	P (apfu)	0.068	0.013	0.001
SiO <sub>2</sub>	17.80	18.00	18.70	Si	0.912	0.956	0.985
TiO <sub>2</sub>	0.02	0.03	0.03	Ti	0.001	0.001	0.001
ZrO <sub>2</sub>	0.00	0.00	0.00	Zr	0.000	0.000	0.000
ThO <sub>2</sub>	77.46	80.40	78.61	Th	0.903	0.972	0.943
UO <sub>2</sub>	0.92	1.07	2.05	U	0.010	0.013	0.024
Sc <sub>2</sub> O <sub>3</sub>	0.02	0.04	0.03	Sc	0.001	0.002	0.001
Y <sub>2</sub> O <sub>3</sub>	0.00	0.01	0.05	Y	0.000	0.000	0.001
La <sub>2</sub> O <sub>3</sub>	1.05	0.15	0.01	La	0.020	0.003	0.000
Ce <sub>2</sub> O <sub>3</sub>	1.73	0.30	0.00	Ce	0.032	0.006	0.000
Pr <sub>2</sub> O <sub>3</sub>	0.20	0.11	0.01	Pr	0.004	0.002	0.000
Nd <sub>2</sub> O <sub>3</sub>	0.59	0.00	0.00	Nd	0.011	0.000	0.000
Sm <sub>2</sub> O <sub>3</sub>	0.00	0.04	0.04	Sm	0.000	0.001	0.001
Eu <sub>2</sub> O <sub>3</sub>	0.00	0.00	0.00	Eu	0.000	0.000	0.000
Gd <sub>2</sub> O <sub>3</sub>	0.12	0.01	0.02	Gd	0.002	0.000	0.000
Dy <sub>2</sub> O <sub>3</sub>	0.00	0.05	0.00	Dy	0.000	0.001	0.000
Er <sub>2</sub> O <sub>3</sub>	0.00	0.00	0.01	Er	0.000	0.000	0.000
CaO	0.00	0.00	0.10	Ca	0.000	0.000	0.006
SrO	0.00	0.00	0.00	Sr	0.000	0.000	0.000
PbO	0.30	0.33	0.23	Pb	0.004	0.005	0.003
Total	102.10	101.07	100.26				

## B.11: Apatite

### Appendix B.12: EMPA analyses of apatite

Point	36 / 1 .	37 / 1 .	5 / 1 .	6 / 1 .	87 / 1 .	88 / 1 .	70 / 1 .
Thin section	kin 130A	kin 130A	KIN133D	KIN133D	KIN134-2	KIN134-2	Rad 2a
P <sub>2</sub> O <sub>5</sub> (wt.%)	41.26	41.51	41.43	42.10	41.65	41.54	39.39
SiO <sub>2</sub>	0.12	0.12	0.04	0.08	0.15	0.26	0.38
Al <sub>2</sub> O <sub>3</sub>	0.05	0.00	0.05	0.03	0.03	0.03	0.00
ThO <sub>2</sub>	0.00	0.02	0.00	0.00	0.04	0.03	0.02
Y <sub>2</sub> O <sub>3</sub>	0.00	0.00	0.00	0.00	0.00	0.00	0.23
La <sub>2</sub> O <sub>3</sub>	0.00	0.06	0.04	0.06	0.00	0.10	0.00
Ce <sub>2</sub> O <sub>3</sub>	0.00	0.09	0.00	0.15	0.12	0.29	0.25
Nd <sub>2</sub> O <sub>3</sub>	0.17	0.07	0.14	0.00	0.05	0.07	0.26
SO <sub>2</sub>	0.00	0.02	0.00	0.00	0.00	0.00	0.18
MgO	0.04	0.05	0.01	0.00	0.01	0.02	0.02
CaO	54.54	54.61	53.81	52.95	54.32	53.85	53.98
MnO	0.21	0.24	0.08	0.05	0.08	0.10	0.29
SrO	1.35	1.42	1.51	2.07	0.65	1.04	0.57
FeO	0.04	0.04	0.04	0.02	0.03	0.13	0.07
Na <sub>2</sub> O	0.02	0.03	0.00	0.02	0.00	0.00	0.07
F	3.72	3.95	3.77	3.73	3.92	3.89	3.47
Cl	0.05	0.06	0.05	0.08	0.03	0.13	0.00
-O=F	-1.58	-1.68	-1.60	-1.59	-1.66	-1.67	-1.46
Total	99.99	100.59	99.37	99.75	99.42	99.80	97.81
P (apfu)	2.952	2.957	2.989	3.038	2.994	2.988	2.877
Si	0.010	0.010	0.003	0.007	0.013	0.022	0.033
Al	0.005	0.000	0.005	0.003	0.003	0.003	0.000
Th	0.000	0.000	0.000	0.000	0.001	0.001	0.000
La	0.000	0.002	0.001	0.002	0.000	0.003	0.000
Ce	0.000	0.003	0.000	0.005	0.004	0.009	0.008
Nd	0.005	0.002	0.004	0.000	0.002	0.002	0.008
S	0.000	0.001	0.000	0.000	0.000	0.000	0.015
Mg	0.005	0.006	0.001	0.000	0.001	0.003	0.003
Ca	4.938	4.925	4.913	4.835	4.943	4.902	4.990
Mn	0.015	0.017	0.005	0.004	0.006	0.007	0.021
Sr	0.066	0.069	0.075	0.102	0.032	0.051	0.029
Fe <sup>2+</sup>	0.003	0.003	0.003	0.002	0.002	0.009	0.005
Na	0.002	0.004	0.001	0.003	0.000	0.000	0.011
F	0.995	1.051	1.017	1.004	1.053	1.045	0.947
Cl	0.008	0.009	0.008	0.011	0.004	0.018	0.000

\*Note: formula calculation based on cation sum = 8

Appendix B.12: EMPA analyses of apatite

Point	71 / 1 .	6 / 1 .	69 / 1 .	70 / 1 .
Thin section	Rad 2a	133C	135C	135C
P <sub>2</sub> O <sub>5</sub> (wt.%)	41.14	41.68	40.43	40.80
SiO <sub>2</sub>	0.06	0.47	0.16	0.18
Al <sub>2</sub> O <sub>3</sub>	0.06	0.03	0.00	0.00
ThO <sub>2</sub>	0.01	0.04	0.05	0.01
Y <sub>2</sub> O <sub>3</sub>	0.04	0.00	0.00	0.00
La <sub>2</sub> O <sub>3</sub>	0.04	0.31	0.00	0.08
Ce <sub>2</sub> O <sub>3</sub>	0.02	0.55	0.11	0.02
Nd <sub>2</sub> O <sub>3</sub>	0.09	0.21	0.04	0.12
SO <sub>2</sub>	0.04	0.05	0.00	0.00
MgO	0.03	0.01	0.00	0.01
CaO	54.50	52.28	52.32	52.71
MnO	0.30	0.23	0.12	0.15
SrO	0.41	4.09	4.10	3.95
FeO	0.12	0.04	0.03	0.04
Na <sub>2</sub> O	0.04	0.06	0.00	0.00
F	3.82	3.78	3.95	3.74
Cl	0.02	0.01	0.02	0.02
-O=F	-1.61	-1.60	-1.67	-1.58
Total	99.13	102.24	99.66	100.26
P (apfu)	2.959	2.972	2.943	2.948
Si	0.005	0.040	0.013	0.016
Al	0.006	0.003	0.000	0.000
Th	0.000	0.001	0.001	0.000
La	0.001	0.010	0.000	0.002
Ce	0.001	0.017	0.003	0.001
Nd	0.003	0.006	0.001	0.004
S	0.004	0.004	0.000	0.000
Mg	0.004	0.002	0.001	0.001
Ca	4.961	4.718	4.822	4.819
Mn	0.022	0.017	0.009	0.011
Sr	0.020	0.200	0.204	0.195
Fe <sup>2+</sup>	0.008	0.003	0.002	0.003
Na	0.007	0.009	0.000	0.000
F	1.026	1.007	1.075	1.009
Cl	0.003	0.002	0.003	0.003

## B.13: Columbite

### Appendix B.13: EMPA analyses of columbite

Point	27 / 1 .	29 / 1 .	30 / 1 .	31 / 1 .	32 / 1 .	68 / 1 .	69 / 1 .
Thin Section	KIN133D						
WO <sub>3</sub> (wt.%)	0.50	0.25	0.35	0.17	0.29	0.23	0.22
Nb <sub>2</sub> O <sub>5</sub>	76.42	76.61	76.69	76.83	76.26	77.20	77.07
Ta <sub>2</sub> O <sub>5</sub>	0.12	0.12	0.14	0.15	0.08	0.16	0.14
SiO <sub>2</sub>	0.02	0.02	0.03	0.01	0.00	0.04	0.04
TiO <sub>2</sub>	2.63	2.21	2.31	2.02	2.15	1.87	1.97
ZrO <sub>2</sub>	0.00	0.00	0.00	0.00	0.00	0.00	0.00
SnO <sub>2</sub>	0.13	0.10	0.04	0.03	0.05	0.03	0.00
ThO <sub>2</sub>	0.00	0.00	0.00	0.00	0.00	0.00	0.00
UO <sub>2</sub>	0.02	0.00	0.00	0.03	0.00	0.00	0.00
Al <sub>2</sub> O <sub>3</sub>	0.04	0.03	0.03	0.03	0.00	0.00	0.00
Sc <sub>2</sub> O <sub>3</sub>	0.01	0.00	0.03	0.00	0.03	0.00	0.03
Fe <sub>2</sub> O <sub>3</sub> *	1.65	2.53	1.84	2.63	2.73	2.03	1.91
FeO*	13.65	14.35	14.86	14.35	14.32	14.74	15.18
Y <sub>2</sub> O <sub>3</sub>	0.00	0.00	0.00	0.00	0.00	0.00	0.00
MgO	0.59	0.87	0.90	0.90	0.88	0.85	0.91
CaO	0.23	0.06	0.00	0.20	0.15	0.04	0.00
MnO	5.15	3.64	3.52	3.36	3.40	3.63	3.18
ZnO	0.02	0.09	0.03	0.07	0.00	0.09	0.05
PbO	0.00	0.00	0.00	0.00	0.01	0.05	0.01
Na <sub>2</sub> O	0.04	0.00	0.02	0.00	0.00	0.00	0.03
Total	101.12	100.67	100.62	100.54	100.09	100.77	100.56
W (apfu)	0.007	0.003	0.005	0.002	0.004	0.003	0.003
Nb	1.887	1.894	1.899	1.901	1.895	1.912	1.910
Ta	0.002	0.002	0.002	0.002	0.001	0.002	0.002
Si	0.001	0.001	0.002	0.001	0.000	0.002	0.002
Ti	0.108	0.091	0.095	0.083	0.089	0.077	0.081
Zr	0.000	0.000	0.000	0.000	0.000	0.000	0.000
Sn	0.003	0.002	0.001	0.001	0.001	0.001	0.000
Th	0.000	0.000	0.000	0.000	0.000	0.000	0.000
U	0.000	0.000	0.000	0.000	0.000	0.000	0.000
Al	0.003	0.002	0.002	0.002	0.000	0.000	0.000
Sc	0.000	0.000	0.001	0.000	0.001	0.000	0.002
Fe <sup>3+</sup>	0.068	0.104	0.076	0.108	0.113	0.084	0.079
Fe <sup>2+</sup>	0.623	0.656	0.681	0.657	0.658	0.675	0.696
Y	0.000	0.000	0.000	0.000	0.000	0.000	0.000
Mg	0.048	0.071	0.073	0.073	0.072	0.069	0.075
Ca	0.014	0.003	0.000	0.011	0.009	0.002	0.000
Mn	0.238	0.169	0.163	0.156	0.158	0.169	0.148
Zn	0.001	0.004	0.001	0.003	0.000	0.003	0.002
Pb	0.000	0.000	0.000	0.000	0.000	0.001	0.000
Na	0.004	0.000	0.002	0.000	0.000	0.000	0.003

\*Note: formula calculation based on cation sum = 3

Elements sought but not found (or below detection limit): Zn (average detection limit of 952 ppm)

Appendix B.13: EMPA analyses of columbite

Point	76 / 1 .	77 / 1 .	89 / 1 .	90 / 1 .	27 / 1 .	29 / 1 .	44 / 1 .
Thin Section	KIN134-2	KIN134-2	KIN134-2	KIN134-2	kin 136	kin 136	kin 130A
WO <sub>3</sub> (wt.%)	0.22	0.18	0.12	0.25	0.29	0.29	0.24
Nb <sub>2</sub> O <sub>5</sub>	77.07	77.37	77.86	77.94	74.32	72.78	78.00
Ta <sub>2</sub> O <sub>5</sub>	0.05	0.06	0.02	0.06	0.87	1.66	0.00
SiO <sub>2</sub>	0.01	0.01	0.02	0.02	0.04	0.02	0.02
TiO <sub>2</sub>	1.20	1.90	1.32	1.12	3.83	4.66	1.52
ZrO <sub>2</sub>	0.00	0.00	0.00	0.00	0.00	0.00	0.00
SnO <sub>2</sub>	0.07	0.00	0.01	0.03	0.04	0.02	0.07
ThO <sub>2</sub>	0.00	0.00	0.00	0.00	0.00	0.00	0.00
UO <sub>2</sub>	0.04	0.03	0.00	0.00	0.10	0.06	0.00
Al <sub>2</sub> O <sub>3</sub>	0.01	0.01	0.01	0.00	0.52	0.05	0.00
Sc <sub>2</sub> O <sub>3</sub>	0.00	0.01	0.04	0.07	0.07	0.06	0.00
Fe <sub>2</sub> O <sub>3</sub> *	1.67	2.49	1.97	2.06	3.48	3.35	0.99
FeO*	15.08	15.21	15.22	12.83	15.92	17.45	13.15
Y <sub>2</sub> O <sub>3</sub>	0.00	0.00	0.00	0.00	0.00	0.00	0.00
MgO	0.59	0.94	0.77	0.68	0.66	0.39	1.25
CaO	0.04	0.02	0.06	0.07	0.03	0.05	0.06
MnO	3.97	2.88	3.35	6.07	1.25	0.27	5.11
ZnO	0.04	0.03	0.11	0.00	0.00	0.01	0.19
PbO	0.05	0.05	0.05	0.00	0.00	0.00	0.01
Na <sub>2</sub> O	0.04	0.01	0.00	0.05	0.01	0.00	0.02
Total	100.01	100.93	100.74	101.03	101.08	100.78	100.57
W (apfu)	0.003	0.003	0.002	0.004	0.004	0.004	0.003
Nb	1.934	1.909	1.932	1.931	1.815	1.793	1.936
Ta	0.001	0.001	0.000	0.001	0.013	0.025	0.000
Si	0.001	0.000	0.001	0.001	0.002	0.001	0.001
Ti	0.050	0.078	0.055	0.046	0.156	0.191	0.063
Zr	0.000	0.000	0.000	0.000	0.000	0.000	0.000
Sn	0.002	0.000	0.000	0.001	0.001	0.000	0.001
Th	0.000	0.000	0.000	0.000	0.000	0.000	0.000
U	0.000	0.000	0.000	0.000	0.001	0.001	0.000
Al	0.001	0.000	0.001	0.000	0.033	0.003	0.000
Sc	0.000	0.000	0.002	0.003	0.003	0.003	0.000
Fe <sup>3+</sup>	0.070	0.102	0.081	0.085	0.141	0.137	0.041
Fe <sup>2+</sup>	0.700	0.694	0.699	0.588	0.719	0.795	0.604
Y	0.000	0.000	0.000	0.000	0.000	0.000	0.000
Mg	0.049	0.077	0.063	0.055	0.053	0.032	0.102
Ca	0.003	0.001	0.003	0.004	0.002	0.003	0.004
Mn	0.186	0.133	0.156	0.282	0.057	0.012	0.238
Zn	0.001	0.001	0.005	0.000	0.000	0.000	0.008
Pb	0.001	0.001	0.001	0.000	0.000	0.000	0.000
Na	0.004	0.001	0.000	0.005	0.001	0.000	0.003

Appendix B.13: EMPA analyses of columbite

Point	45 / 1.	52 / 1.	53 / 1.	54 / 1.	55 / 1.	56 / 1.	57 / 1.
Thin Section	kin 130A						
WO <sub>3</sub> (wt.%)	0.16	0.25	0.30	0.12	0.01	0.27	0.20
Nb <sub>2</sub> O <sub>5</sub>	77.87	72.81	72.58	78.41	78.36	77.25	75.46
Ta <sub>2</sub> O <sub>5</sub>	0.00	0.06	0.00	0.00	0.01	0.03	0.00
SiO <sub>2</sub>	0.04	0.04	0.06	0.04	0.04	0.02	0.05
TiO <sub>2</sub>	1.48	3.87	4.02	1.07	1.27	1.28	2.26
ZrO <sub>2</sub>	0.00	0.00	0.00	0.00	0.00	0.00	0.00
SnO <sub>2</sub>	0.02	0.01	0.05	0.00	0.04	0.06	0.05
ThO <sub>2</sub>	0.00	0.00	0.00	0.00	0.00	0.00	0.00
UO <sub>2</sub>	0.00	0.05	0.07	0.00	0.00	0.01	0.02
Al <sub>2</sub> O <sub>3</sub>	0.00	0.00	0.00	0.02	0.00	0.00	0.00
Sc <sub>2</sub> O <sub>3</sub>	0.03	0.05	0.02	0.00	0.01	0.03	0.02
Fe <sub>2</sub> O <sub>3</sub> *	1.15	0.00	0.00	0.96	1.37	1.19	1.39
FeO*	12.97	12.30	11.99	13.77	13.47	12.89	12.92
Y <sub>2</sub> O <sub>3</sub>	0.00	0.00	0.00	0.00	0.00	0.00	0.00
MgO	1.26	0.29	0.38	1.20	1.16	0.54	0.30
CaO	0.15	0.89	1.14	0.10	0.17	0.00	0.22
MnO	5.09	5.21	5.20	4.60	4.72	6.56	6.06
ZnO	0.07	0.06	0.00	0.10	0.10	0.01	0.00
PbO	0.00	0.02	0.03	0.00	0.00	0.01	0.02
Na <sub>2</sub> O	0.04	0.00	0.02	0.00	0.02	0.03	0.02
Total	100.22	95.90	95.88	100.31	100.63	100.09	98.86
W (apfu)	0.002	0.004	0.004	0.002	0.000	0.004	0.003
Nb	1.936	1.894	1.884	1.953	1.942	1.938	1.909
Ta	0.000	0.001	0.000	0.000	0.000	0.000	0.000
Si	0.002	0.003	0.004	0.002	0.002	0.001	0.003
Ti	0.061	0.168	0.174	0.044	0.052	0.053	0.095
Zr	0.000	0.000	0.000	0.000	0.000	0.000	0.000
Sn	0.000	0.000	0.001	0.000	0.001	0.001	0.001
Th	0.000	0.000	0.000	0.000	0.000	0.000	0.000
U	0.000	0.001	0.001	0.000	0.000	0.000	0.000
Al	0.000	0.000	0.000	0.001	0.000	0.000	0.000
Sc	0.001	0.002	0.001	0.000	0.000	0.001	0.001
Fe <sup>3+</sup>	0.048	0.000	0.000	0.040	0.057	0.050	0.058
Fe <sup>2+</sup>	0.597	0.592	0.576	0.634	0.617	0.598	0.605
Y	0.000	0.000	0.000	0.000	0.000	0.000	0.000
Mg	0.103	0.025	0.033	0.099	0.095	0.045	0.025
Ca	0.009	0.055	0.070	0.006	0.010	0.000	0.013
Mn	0.237	0.254	0.253	0.215	0.219	0.308	0.287
Zn	0.003	0.002	0.000	0.004	0.004	0.000	0.000
Pb	0.000	0.000	0.000	0.000	0.000	0.000	0.000
Na	0.005	0.000	0.002	0.000	0.002	0.003	0.002

Appendix B.13: EMPA analyses of columbite

Point	18 / 1 .	19 / 1 .	20 / 1 .	21 / 1 .	62 / 1 .	63 / 1 .	5 / 1 .
Thin Section	130b	130b	130b	130b	135a	135a	133C
WO <sub>3</sub> (wt.%)	0.34	0.32	0.46	0.31	0.21	0.11	0.12
Nb <sub>2</sub> O <sub>5</sub>	77.22	77.28	77.23	77.05	76.07	76.23	77.21
Ta <sub>2</sub> O <sub>5</sub>	0.07	0.01	0.04	0.02	0.07	0.02	0.22
SiO <sub>2</sub>	0.01	0.02	0.04	0.02	0.03	0.02	0.03
TiO <sub>2</sub>	1.65	1.77	1.75	1.72	1.87	1.89	1.13
ZrO <sub>2</sub>	0.08	0.08	0.10	0.10	0.13	0.13	0.06
SnO <sub>2</sub>	0.00	0.07	0.14	0.00	0.04	0.03	0.02
ThO <sub>2</sub>	0.03	0.00	0.00	0.03	0.02	0.01	0.00
UO <sub>2</sub>	0.00	0.02	0.04	0.02	0.02	0.02	0.03
Al <sub>2</sub> O <sub>3</sub>	0.00	0.00	0.00	0.00	0.20	0.01	0.02
Sc <sub>2</sub> O <sub>3</sub>	0.00	0.00	0.01	0.00	0.03	0.00	0.00
Fe <sub>2</sub> O <sub>3</sub> *	1.96	2.54	1.34	2.40	1.64	0.62	1.12
FeO*	13.08	12.59	13.54	12.87	14.29	12.81	9.55
Y <sub>2</sub> O <sub>3</sub>	0.18	0.18	0.24	0.24	0.06	0.25	0.08
MgO	1.11	1.13	1.13	1.10	0.64	0.31	0.52
CaO	0.24	0.30	0.18	0.24	0.01	0.09	0.19
MnO	4.65	4.76	4.65	4.54	4.33	6.90	9.69
ZnO	0.11	0.17	0.11	0.14	0.07	0.00	0.02
PbO	0.03	0.00	0.00	0.06	0.04	0.00	0.00
Na <sub>2</sub> O	0.02	0.00	0.00	0.00	0.00	0.00	0.06
Total	100.59	101.07	100.98	100.64	99.68	99.47	100.02
W (apfu)	0.005	0.005	0.007	0.004	0.003	0.002	0.002
Nb	1.914	1.903	1.912	1.907	1.908	1.927	1.940
Ta	0.001	0.000	0.001	0.000	0.001	0.000	0.003
Si	0.001	0.001	0.002	0.001	0.001	0.001	0.002
Ti	0.068	0.073	0.072	0.071	0.078	0.079	0.047
Zr	0.002	0.002	0.003	0.003	0.003	0.004	0.002
Sn	0.000	0.002	0.003	0.000	0.001	0.001	0.000
Th	0.000	0.000	0.000	0.000	0.000	0.000	0.000
U	0.000	0.000	0.001	0.000	0.000	0.000	0.000
Al	0.000	0.000	0.000	0.000	0.013	0.000	0.001
Sc	0.000	0.000	0.000	0.000	0.001	0.000	0.000
Fe <sup>3+</sup>	0.081	0.104	0.055	0.099	0.069	0.026	0.047
Fe <sup>2+</sup>	0.600	0.573	0.620	0.589	0.663	0.599	0.444
Y	0.005	0.005	0.007	0.007	0.002	0.007	0.002
Mg	0.090	0.092	0.092	0.090	0.053	0.026	0.043
Ca	0.014	0.018	0.010	0.014	0.000	0.005	0.011
Mn	0.216	0.219	0.216	0.211	0.203	0.327	0.456
Zn	0.004	0.007	0.005	0.006	0.003	0.000	0.001
Pb	0.000	0.000	0.000	0.001	0.001	0.000	0.000
Na	0.003	0.000	0.000	0.000	0.000	0.000	0.006

Appendix B.13: EMPA analyses of columbite

Point	12 / 1.	23 / 1.	24 / 1.	16 / 1.	17 / 1.	18 / 1.	21 / 1.
Thin Section	133C	133C	133C	Pegm1	Pegm1	Pegm1	Pegm1
WO <sub>3</sub> (wt.%)	0.05	0.04	0.09	0.80	0.54	0.65	0.91
Nb <sub>2</sub> O <sub>5</sub>	76.97	77.88	77.58	72.98	71.83	73.40	73.25
Ta <sub>2</sub> O <sub>5</sub>	0.27	0.12	0.06	2.55	4.07	2.85	5.05
SiO <sub>2</sub>	0.03	0.03	0.05	0.03	0.23	0.07	0.02
TiO <sub>2</sub>	1.41	1.16	1.03	2.08	1.93	2.08	1.25
ZrO <sub>2</sub>	0.06	0.07	0.02	0.26	0.02	0.10	0.01
SnO <sub>2</sub>	0.05	0.00	0.00	0.00	0.08	0.17	0.00
ThO <sub>2</sub>	0.00	0.03	0.03	0.02	0.33	0.00	0.00
UO <sub>2</sub>	0.02	0.07	0.00	0.11	0.10	0.07	0.02
Al <sub>2</sub> O <sub>3</sub>	0.00	0.02	0.00	0.01	0.41	0.08	0.04
Sc <sub>2</sub> O <sub>3</sub>	0.01	0.00	0.00	0.14	0.19	0.18	0.12
Fe <sub>2</sub> O <sub>3</sub> *	1.41	0.97	2.87	3.78	2.69	4.53	0.29
FeO*	13.47	11.63	10.42	15.75	15.86	15.26	15.13
Y <sub>2</sub> O <sub>3</sub>	0.07	0.09	0.06	0.07	0.09	0.05	0.15
MgO	1.09	0.71	0.84	0.34	0.30	0.31	0.09
CaO	0.00	0.04	0.47	0.00	0.00	0.17	0.11
MnO	4.76	7.60	7.06	2.46	2.21	2.47	5.14
ZnO	0.12	0.12	0.10	0.05	0.08	0.06	0.00
PbO	0.00	0.02	0.07	0.06	0.06	0.05	0.06
Na <sub>2</sub> O	0.01	0.05	0.04	0.01	0.00	0.00	0.00
Total	99.70	100.55	100.48	101.24	100.69	102.23	101.61
W (apfu)	0.001	0.001	0.001	0.011	0.008	0.009	0.013
Nb	1.930	1.944	1.925	1.822	1.808	1.810	1.860
Ta	0.004	0.002	0.001	0.038	0.062	0.042	0.077
Si	0.002	0.002	0.003	0.001	0.013	0.004	0.001
Ti	0.059	0.048	0.042	0.086	0.081	0.085	0.053
Zr	0.002	0.002	0.001	0.007	0.001	0.003	0.000
Sn	0.001	0.000	0.000	0.000	0.002	0.004	0.000
Th	0.000	0.000	0.000	0.000	0.004	0.000	0.000
U	0.000	0.001	0.000	0.001	0.001	0.001	0.000
Al	0.000	0.001	0.000	0.001	0.027	0.005	0.003
Sc	0.000	0.000	0.000	0.006	0.009	0.009	0.006
Fe <sup>3+</sup>	0.059	0.040	0.119	0.157	0.113	0.186	0.012
Fe <sup>2+</sup>	0.625	0.537	0.478	0.727	0.739	0.696	0.711
Y	0.002	0.003	0.002	0.002	0.003	0.001	0.004
Mg	0.090	0.059	0.069	0.028	0.025	0.025	0.008
Ca	0.000	0.002	0.027	0.000	0.000	0.010	0.006
Mn	0.224	0.356	0.328	0.115	0.104	0.114	0.245
Zn	0.005	0.005	0.004	0.002	0.003	0.002	0.000
Pb	0.000	0.000	0.001	0.001	0.001	0.001	0.001
Na	0.001	0.005	0.004	0.001	0.000	0.000	0.000

Appendix B.13: EMPA analyses of columbite

Point	23 / 1 .	24 / 1 .	25 / 1 .	26 / 1 .
Thin Section	Pegm1	Pegm1	Pegm1	Pegm1
WO <sub>3</sub> (wt.%)	0.81	0.59	1.01	0.99
Nb <sub>2</sub> O <sub>5</sub>	62.56	61.39	72.47	72.23
Ta <sub>2</sub> O <sub>5</sub>	13.40	12.01	5.54	5.92
SiO <sub>2</sub>	0.03	0.19	0.13	0.03
TiO <sub>2</sub>	3.56	2.07	1.85	2.01
ZrO <sub>2</sub>	0.70	0.29	0.16	0.14
SnO <sub>2</sub>	0.04	0.00	0.00	0.13
ThO <sub>2</sub>	0.00	0.02	0.01	0.00
UO <sub>2</sub>	0.23	0.05	0.06	0.00
Al <sub>2</sub> O <sub>3</sub>	1.07	3.33	0.21	0.04
Sc <sub>2</sub> O <sub>3</sub>	0.28	0.21	0.10	0.13
Fe <sub>2</sub> O <sub>3</sub> *	1.50	7.57	1.87	0.59
FeO*	16.13	10.66	16.74	17.93
Y <sub>2</sub> O <sub>3</sub>	0.10	0.06	0.02	0.01
MgO	0.32	0.33	0.30	0.27
CaO	0.00	0.00	0.38	0.03
MnO	1.84	1.96	2.12	2.21
ZnO	0.00	0.05	0.04	0.01
PbO	0.10	0.02	0.01	0.04
Na <sub>2</sub> O	0.01	0.08	0.00	0.00
Total	103.00	100.30	102.91	102.80
W (apfu)	0.012	0.009	0.014	0.014
Nb	1.597	1.545	1.804	1.814
Ta	0.206	0.182	0.083	0.089
Si	0.002	0.011	0.007	0.002
Ti	0.151	0.087	0.077	0.084
Zr	0.019	0.008	0.004	0.004
Sn	0.001	0.000	0.000	0.003
Th	0.000	0.000	0.000	0.000
U	0.003	0.001	0.001	0.000
Al	0.071	0.218	0.013	0.003
Sc	0.014	0.010	0.005	0.006
Fe <sup>3+</sup>	0.064	0.317	0.077	0.025
Fe <sup>2+</sup>	0.762	0.497	0.771	0.833
Y	0.003	0.002	0.001	0.000
Mg	0.027	0.027	0.024	0.022
Ca	0.000	0.000	0.022	0.002
Mn	0.088	0.092	0.099	0.104
Zn	0.000	0.002	0.002	0.001
Pb	0.002	0.000	0.000	0.001
Na	0.001	0.009	0.000	0.000

## B.14: Oxides

Ilm: Ilmenite

Pyr: Pyrophanite

Nb-Rt: Nb-rich rutile

### Appendix B.14: EMPA analyses of oxides

Mineral	Ilm	Ilm	Pyr	Nb-Rt	Nb-Rt	Nb-Rt
Point	18 / 1 .	40 / 1 .	71 / 1 .	25 / 1 .	26 / 1 .	74 / 1 .
Thin Section	KIN133D	KIN133D	133C	kin 136	kin 136	Rad 2a
WO <sub>3</sub> (wt.%)	0.00	0.01	0.00	0.04	0.00	0.08
Nb <sub>2</sub> O <sub>5</sub>	0.65	0.59	0.75	24.02	24.48	22.04
Ta <sub>2</sub> O <sub>5</sub>	0.00	0.03	0.05	1.12	1.20	0.04
SiO <sub>2</sub>	0.03	0.19	0.05	0.03	0.02	0.07
TiO <sub>2</sub>	53.10	51.89	52.41	65.40	65.45	69.74
ZrO <sub>2</sub>	0.00	0.00	0.00	0.04	0.03	0.02
Al <sub>2</sub> O <sub>3</sub>	0.02	0.29	0.00	0.36	0.31	0.20
V <sub>2</sub> O <sub>3</sub>	0.00	0.08	0.00	0.34	0.25	0.41
Cr <sub>2</sub> O <sub>3</sub>	0.00	0.03	0.00	0.05	0.07	0.10
Fe <sub>2</sub> O <sub>3</sub> *	0.00	0.73	0.00	4.15	3.62	4.17
FeO*	38.54	40.17	18.17	4.24	4.66	3.52
MgO	0.05	0.04	0.00	0.05	0.05	0.03
CaO	0.00	0.04	0.02	0.00	0.00	0.02
MnO	8.55	7.18	28.06	0.04	0.02	0.03
ZnO	0.05	0.00	0.03	0.00	0.02	0.06
SnO	0.02	0.01	0.01	0.02	0.04	0.09
Total	101.00	101.28	99.54	99.91	100.22	100.62
W (apfu)	0.000	0.000	0.000	0.000	0.000	0.000
Nb	0.007	0.007	0.009	0.160	0.163	0.143
Ta	0.000	0.000	0.000	0.004	0.005	0.000
Si	0.001	0.005	0.001	0.000	0.000	0.001
Ti	1.000	0.973	1.000	0.724	0.724	0.756
Zr	0.000	0.000	0.000	0.000	0.000	0.000
Al	0.001	0.009	0.000	0.006	0.005	0.003
V	0.000	0.002	0.000	0.004	0.003	0.005
Cr	0.000	0.001	0.000	0.001	0.001	0.001
Fe <sup>3+</sup>	0.000	0.014	0.000	0.046	0.040	0.045
Fe <sup>2+</sup>	0.807	0.837	0.386	0.052	0.057	0.042
Mg	0.002	0.002	0.000	0.001	0.001	0.001
Ca	0.000	0.001	0.000	0.000	0.000	0.000
Mn	0.181	0.151	0.603	0.001	0.000	0.000
Zn	0.001	0.000	0.000	0.000	0.000	0.001
Sn	0.000	0.000	0.000	0.000	0.000	0.001

\*Note: formula calculation based on cation sum = 2

Elements sought but not found (or below detection limit): W, Sn, Sc, Zn (detection limits of 1741 ppm, 364 ppm, 170 ppm, and 824 ppm respectively)

## B.15: Aeschnite, Niobaeschnite, Euxenite, and Fersmite

Aesch: Aeschnite

NAesch: Niobaeschnite

Eux: Euxenite

Ferg: Fergusonite

### Appendix B.15: EMPA analyses of Aeschnite, Niobaeschnite, Euxenite, and Fersmite

Mineral	Aesch	Aesch	NAesch	NAesch	Aesch	Aesch
Point	25 / 1 .	28 / 1 .	74 / 1 .	75 / 1 .	93 / 1 .	103 / 1 .
Thin Section	KIN133D	KIN133D	KIN134-2	KIN134-2	KIN134-2	KIN133D
WO <sub>3</sub> (wt.%)	0.08	0.14	0.26	0.10	0.15	0.19
P <sub>2</sub> O <sub>5</sub>	0.02	0.02	0.03	0.01	0.03	0.00
Nb <sub>2</sub> O <sub>5</sub>	26.75	30.17	49.87	49.98	30.38	31.43
Ta <sub>2</sub> O <sub>5</sub>	0.00	0.00	0.00	0.00	0.00	0.00
SiO <sub>2</sub>	0.02	0.02	0.05	0.07	0.07	0.03
TiO <sub>2</sub>	27.28	25.33	14.84	14.03	24.94	22.57
ZrO <sub>2</sub>	0.08	0.00	0.00	0.00	0.00	0.00
ThO <sub>2</sub>	8.35	8.97	5.21	4.89	10.66	6.48
UO <sub>2</sub>	0.23	0.14	0.31	0.56	0.17	0.09
Al <sub>2</sub> O <sub>3</sub>	0.00	0.00	0.00	0.00	0.00	0.00
Y <sub>2</sub> O <sub>3</sub>	0.42	1.25	0.57	0.74	0.82	1.61
La <sub>2</sub> O <sub>3</sub>	6.43	3.68	3.30	2.72	4.96	2.97
Ce <sub>2</sub> O <sub>3</sub>	17.31	13.82	9.79	8.90	14.35	14.17
Pr <sub>2</sub> O <sub>3</sub>	2.01	1.93	1.19	1.20	1.89	2.32
Nd <sub>2</sub> O <sub>3</sub>	6.01	7.41	4.08	4.17	5.87	9.16
Sm <sub>2</sub> O <sub>3</sub>	0.73	1.18	0.61	0.70	0.89	1.69
Gd <sub>2</sub> O <sub>3</sub>	0.09	0.59	0.29	0.38	0.41	0.83
Tb <sub>2</sub> O <sub>3</sub>	0.00	0.04	0.02	0.00	0.00	0.07
Dy <sub>2</sub> O <sub>3</sub>	0.07	0.48	0.13	0.08	0.16	0.46
Ho <sub>2</sub> O <sub>3</sub>	0.00	0.00	0.00	0.00	0.00	0.00
Er <sub>2</sub> O <sub>3</sub>	0.04	0.12	0.05	0.05	0.09	0.13
Yb <sub>2</sub> O <sub>3</sub>	0.04	0.04	0.07	0.05	0.05	0.08
Bi <sub>2</sub> O <sub>3</sub>	0.24	0.12	0.17	0.10	0.22	0.15
Fe <sub>2</sub> O <sub>3</sub> *	0.34	0.26	0.54	0.55	0.31	0.24
FeO*	0.31	0.23	0.48	0.50	0.28	0.22
MgO	0.00	0.00	0.00	0.00	0.00	0.00
CaO	1.33	2.19	7.08	7.45	2.03	1.73
MnO	0.00	0.00	0.00	0.00	0.00	0.00
PbO	0.02	0.01	0.00	0.05	0.04	0.07
Na <sub>2</sub> O	0.01	0.00	0.00	0.01	0.00	0.00
K <sub>2</sub> O	0.00	0.00	0.00	0.00	0.00	0.00
F	0.03	0.00	0.00	0.00	0.02	0.10
Total	89.94	89.19	93.77	92.40	88.17	90.36

\*Note: formula calculation based on cation sum = 3

Elements sought but not found (or below detection limit): Sc, As, W (average detection limits of 222 ppm, 443 ppm, and 1683 ppm respectively)

**Appendix B.15:** EMPA analyses of Aeschynite, Nioboaschynite, Euxenite, and Fersmite

Mineral	Aesch	Aesch	NAesch	NAesch	Aesch	Aesch
Point	25 / 1 .	28 / 1 .	74 / 1 .	75 / 1 .	93 / 1 .	103 / 1 .
Thin Section	KIN133D	KIN133D	KIN134-2	KIN134-2	KIN134-2	KIN133D
W (apfu)	0.001	0.002	0.004	0.001	0.002	0.003
P	0.001	0.001	0.001	0.000	0.001	0.000
Nb	0.747	0.841	1.338	1.357	0.851	0.902
Ta	0.000	0.000	0.000	0.000	0.000	0.000
Si	0.001	0.001	0.003	0.004	0.005	0.002
Ti	1.267	1.175	0.663	0.634	1.162	1.078
Zr	0.002	0.000	0.000	0.000	0.000	0.000
Th	0.117	0.126	0.070	0.067	0.150	0.094
U	0.003	0.002	0.004	0.008	0.002	0.001
Al	0.000	0.000	0.000	0.000	0.000	0.000
Y	0.014	0.041	0.018	0.023	0.027	0.054
La	0.146	0.084	0.072	0.060	0.113	0.070
Ce	0.391	0.312	0.213	0.196	0.325	0.329
Pr	0.045	0.043	0.026	0.026	0.043	0.054
Nd	0.133	0.163	0.087	0.089	0.130	0.208
Sm	0.016	0.025	0.013	0.014	0.019	0.037
Gd	0.002	0.012	0.006	0.008	0.008	0.017
Tb	0.000	0.001	0.000	0.000	0.000	0.001
Dy	0.001	0.010	0.002	0.002	0.003	0.009
Ho	0.000	0.000	0.000	0.000	0.000	0.000
Er	0.001	0.002	0.001	0.001	0.002	0.003
Yb	0.001	0.001	0.001	0.001	0.001	0.001
Bi	0.004	0.002	0.003	0.001	0.003	0.003
Fe <sup>3+</sup>	0.016	0.012	0.024	0.025	0.014	0.012
Fe <sup>2+</sup>	0.016	0.012	0.024	0.025	0.014	0.012
Mg	0.000	0.000	0.000	0.000	0.000	0.000
Ca	0.088	0.145	0.450	0.479	0.135	0.118
Mn	0.000	0.000	0.000	0.000	0.000	0.000
Pb	0.000	0.000	0.000	0.001	0.001	0.001
Na	0.001	0.000	0.000	0.002	0.000	0.000
K	0.000	0.000	0.000	0.000	0.000	0.000
F	0.007	0.000	0.000	0.000	0.004	0.020

**Appendix B.15:** EMPA analyses of Aeschynite, Nioboaeschynite, Euxenite, and Fersmite

Mineral	Eux	Eux	Eux	Eux	Eux	Eux
Point	104 / 1 .	46 / 1 .	47 / 1 .	48 / 1 .	58 / 1 .	59 / 1 .
Thin Section	KIN133D	kin 130A				
WO <sub>3</sub> (wt.%)	0.54	0.47	0.39	0.28	0.53	0.36
P <sub>2</sub> O <sub>5</sub>	0.00	0.04	0.05	0.03	0.08	0.04
Nb <sub>2</sub> O <sub>5</sub>	41.94	38.51	39.52	39.61	34.59	49.22
Ta <sub>2</sub> O <sub>5</sub>	0.50	0.04	0.07	0.05	0.00	0.03
SiO <sub>2</sub>	0.04	0.08	0.06	0.06	1.79	0.05
TiO <sub>2</sub>	19.94	21.13	20.17	20.20	19.87	15.65
ZrO <sub>2</sub>	0.14	0.00	0.00	0.00	0.00	0.00
ThO <sub>2</sub>	1.16	6.56	7.28	7.56	5.23	3.63
UO <sub>2</sub>	0.91	0.49	0.58	0.54	0.79	0.66
Al <sub>2</sub> O <sub>3</sub>	0.00	0.00	0.00	0.00	0.20	0.00
Y <sub>2</sub> O <sub>3</sub>	16.94	17.53	15.03	14.63	15.51	13.28
La <sub>2</sub> O <sub>3</sub>	0.00	0.00	0.00	0.01	0.00	0.00
Ce <sub>2</sub> O <sub>3</sub>	0.22	0.17	0.35	0.40	0.64	0.15
Pr <sub>2</sub> O <sub>3</sub>	0.11	0.06	0.10	0.25	0.20	0.11
Nd <sub>2</sub> O <sub>3</sub>	1.48	1.28	1.76	2.06	0.94	0.75
Sm <sub>2</sub> O <sub>3</sub>	1.37	0.93	1.10	1.16	0.86	0.75
Gd <sub>2</sub> O <sub>3</sub>	3.15	2.13	2.08	2.28	2.24	2.05
Tb <sub>2</sub> O <sub>3</sub>	0.50	0.26	0.27	0.29	0.28	0.31
Dy <sub>2</sub> O <sub>3</sub>	3.48	2.63	2.33	2.20	2.37	2.59
Ho <sub>2</sub> O <sub>3</sub>	0.50	0.54	0.37	0.47	0.47	0.40
Er <sub>2</sub> O <sub>3</sub>	1.54	1.79	1.50	1.47	1.62	1.55
Yb <sub>2</sub> O <sub>3</sub>	0.78	1.31	1.06	1.03	1.04	0.81
Bi <sub>2</sub> O <sub>3</sub>	0.05	0.00	0.00	0.00	0.02	0.01
Fe <sub>2</sub> O <sub>3</sub> *	0.59	0.00	0.00	0.00	2.13	0.00
FeO*	0.68	0.36	0.33	0.26	1.92	0.34
MgO	0.00	0.01	0.00	0.00	0.04	0.00
CaO	2.21	1.55	2.28	2.44	1.26	4.98
MnO	0.21	0.26	0.29	0.24	1.23	0.41
PbO	0.00	0.00	0.03	0.00	0.00	0.00
Na <sub>2</sub> O	0.00	0.02	0.02	0.02	0.02	0.00
K <sub>2</sub> O	0.00	0.00	0.00	0.01	0.00	0.00
F	0.07	0.02	0.00	0.00	0.00	0.00
Total	98.04	91.95	90.08	90.27	90.61	94.84

**Appendix B.15:** EMPA analyses of Aeschynite, Nioboaschynite, Euxenite, and Fersmite

Mineral	Eux	Eux	Eux	Eux	Eux	Eux
Point	104 / 1 .	46 / 1 .	47 / 1 .	48 / 1 .	58 / 1 .	59 / 1 .
Thin Section	KIN133D	kin 130A				
W (apfu)	0.008	0.007	0.006	0.004	0.008	0.005
P	0.000	0.002	0.002	0.002	0.004	0.002
Nb	1.109	1.038	1.079	1.077	0.937	1.301
Ta	0.008	0.001	0.001	0.001	0.000	0.001
Si	0.002	0.005	0.004	0.004	0.107	0.003
Ti	0.877	0.947	0.916	0.914	0.896	0.688
Zr	0.004	0.000	0.000	0.000	0.000	0.000
Th	0.015	0.089	0.100	0.104	0.071	0.048
U	0.012	0.006	0.008	0.007	0.011	0.009
Al	0.000	0.000	0.000	0.000	0.014	0.000
Y	0.527	0.556	0.483	0.468	0.495	0.413
La	0.000	0.000	0.000	0.000	0.000	0.000
Ce	0.005	0.004	0.008	0.009	0.014	0.003
Pr	0.002	0.001	0.002	0.006	0.004	0.002
Nd	0.031	0.027	0.038	0.044	0.020	0.016
Sm	0.028	0.019	0.023	0.024	0.018	0.015
Gd	0.061	0.042	0.042	0.046	0.044	0.040
Tb	0.010	0.005	0.005	0.006	0.005	0.006
Dy	0.066	0.050	0.045	0.043	0.046	0.049
Ho	0.009	0.010	0.007	0.009	0.009	0.007
Er	0.028	0.034	0.028	0.028	0.030	0.029
Yb	0.014	0.024	0.020	0.019	0.019	0.014
Bi	0.001	0.000	0.000	0.000	0.000	0.000
Fe <sup>3+</sup>	0.026	0.000	0.000	0.000	0.096	0.000
Fe <sup>2+</sup>	0.033	0.018	0.017	0.013	0.096	0.016
Mg	0.000	0.001	0.000	0.000	0.003	0.000
Ca	0.138	0.099	0.147	0.157	0.081	0.312
Mn	0.010	0.013	0.015	0.012	0.062	0.020
Pb	0.000	0.000	0.000	0.000	0.000	0.000
Na	0.000	0.002	0.002	0.003	0.003	0.000
K	0.000	0.000	0.000	0.001	0.000	0.000
F	0.014	0.003	0.000	0.000	0.000	0.000

**Appendix B.15:** EMPA analyses of Aeschnite, Nioboaeschnite, Euxenite, and Fersmite

Mineral	Eux	Eux	Eux	Eux	Eux	Eux
Point	60 / 1 .	61 / 1 .	62 / 1 .	63 / 1 .	64 / 1 .	23 / 1 .
Thin Section	kin 130A	130b				
WO <sub>3</sub> (wt.%)	0.53	0.44	0.48	0.45	0.56	0.32
P <sub>2</sub> O <sub>5</sub>	0.04	0.05	0.06	0.03	0.06	0.03
Nb <sub>2</sub> O <sub>5</sub>	41.00	39.95	40.92	40.14	39.41	51.16
Ta <sub>2</sub> O <sub>5</sub>	0.05	0.07	0.05	0.03	0.01	0.04
SiO <sub>2</sub>	0.04	0.03	0.05	0.04	0.05	0.05
TiO <sub>2</sub>	20.05	20.50	19.83	20.13	20.58	16.80
ZrO <sub>2</sub>	0.00	0.00	0.00	0.00	0.00	0.00
ThO <sub>2</sub>	4.01	4.24	4.05	3.93	4.60	3.41
UO <sub>2</sub>	0.59	0.55	0.52	0.55	0.57	0.39
Al <sub>2</sub> O <sub>3</sub>	0.00	0.00	0.00	0.00	0.00	0.00
Y <sub>2</sub> O <sub>3</sub>	17.36	17.85	16.91	17.52	17.62	13.10
La <sub>2</sub> O <sub>3</sub>	0.00	0.00	0.00	0.00	0.00	0.04
Ce <sub>2</sub> O <sub>3</sub>	0.10	0.09	0.04	0.13	0.18	0.60
Pr <sub>2</sub> O <sub>3</sub>	0.15	0.00	0.05	0.02	0.07	0.24
Nd <sub>2</sub> O <sub>3</sub>	0.93	1.09	0.86	0.93	0.88	1.24
Sm <sub>2</sub> O <sub>3</sub>	1.07	1.08	1.00	1.09	0.99	0.83
Gd <sub>2</sub> O <sub>3</sub>	2.27	2.54	2.54	2.73	2.53	1.89
Tb <sub>2</sub> O <sub>3</sub>	0.35	0.36	0.34	0.40	0.36	0.26
Dy <sub>2</sub> O <sub>3</sub>	2.81	2.85	2.88	2.78	3.03	2.06
Ho <sub>2</sub> O <sub>3</sub>	0.53	0.46	0.38	0.48	0.45	0.27
Er <sub>2</sub> O <sub>3</sub>	1.80	1.77	1.75	1.73	1.82	1.41
Yb <sub>2</sub> O <sub>3</sub>	1.24	1.27	1.15	1.26	1.22	0.81
Bi <sub>2</sub> O <sub>3</sub>	0.00	0.00	0.00	0.04	0.03	0.00
Fe <sub>2</sub> O <sub>3</sub> *	0.00	0.00	0.00	0.00	0.00	0.00
FeO*	0.19	0.19	0.16	0.16	0.14	0.40
MgO	0.00	0.00	0.00	0.00	0.00	0.02
CaO	2.03	1.87	2.03	1.83	1.72	4.89
MnO	0.27	0.19	0.24	0.23	0.25	0.49
PbO	0.00	0.03	0.00	0.01	0.00	0.00
Na <sub>2</sub> O	0.01	0.01	0.03	0.01	0.01	0.02
K <sub>2</sub> O	0.00	0.01	0.01	0.00	0.00	0.00
F	0.00	0.01	0.00	0.00	0.00	0.25
Total	93.60	93.44	92.45	92.90	92.68	98.03

**Appendix B.15:** EMPA analyses of Aeschynite, Nioboaeschynite, Euxenite, and Fersmite

Mineral	Eux	Eux	Eux	Eux	Eux	Eux
Point	60 / 1 .	61 / 1 .	62 / 1 .	63 / 1 .	64 / 1 .	23 / 1 .
Thin Section	kin 130A	130b				
W (apfu)	0.008	0.007	0.007	0.007	0.009	0.005
P	0.002	0.002	0.003	0.001	0.003	0.001
Nb	1.104	1.075	1.113	1.090	1.068	1.308
Ta	0.001	0.001	0.001	0.000	0.000	0.001
Si	0.002	0.002	0.003	0.002	0.003	0.003
Ti	0.898	0.918	0.897	0.910	0.927	0.715
Zr	0.000	0.000	0.000	0.000	0.000	0.000
Th	0.054	0.057	0.056	0.054	0.063	0.044
U	0.008	0.007	0.007	0.007	0.008	0.005
Al	0.000	0.000	0.000	0.000	0.000	0.000
Y	0.550	0.566	0.541	0.560	0.562	0.394
La	0.000	0.000	0.000	0.000	0.000	0.001
Ce	0.002	0.002	0.001	0.003	0.004	0.012
Pr	0.003	0.000	0.001	0.000	0.002	0.005
Nd	0.020	0.023	0.018	0.020	0.019	0.025
Sm	0.022	0.022	0.021	0.023	0.020	0.016
Gd	0.045	0.050	0.051	0.054	0.050	0.035
Tb	0.007	0.007	0.007	0.008	0.007	0.005
Dy	0.054	0.055	0.056	0.054	0.058	0.038
Ho	0.010	0.009	0.007	0.009	0.008	0.005
Er	0.034	0.033	0.033	0.033	0.034	0.025
Yb	0.022	0.023	0.021	0.023	0.022	0.014
Bi	0.000	0.000	0.000	0.001	0.000	0.000
Fe <sup>3+</sup>	0.000	0.000	0.000	0.000	0.000	0.000
Fe <sup>2+</sup>	0.009	0.009	0.008	0.008	0.007	0.019
Mg	0.000	0.000	0.000	0.000	0.000	0.002
Ca	0.130	0.119	0.131	0.118	0.111	0.296
Mn	0.014	0.010	0.012	0.012	0.012	0.023
Pb	0.000	0.001	0.000	0.000	0.000	0.000
Na	0.002	0.001	0.004	0.001	0.002	0.002
K	0.000	0.001	0.001	0.000	0.000	0.000
F	0.000	0.002	0.000	0.001	0.000	0.044

**Appendix B.15:** EMPA analyses of Aeschnite, Nioboaeschnite, Euxenite, and Fersmite

Mineral	Eux	Eux	Eux	Eux	Aesch	Aesch
Point	24 / 1 .	36 / 1 .	37 / 1 .	38 / 1 .	2 / 1 .	3 / 1 .
Thin Section	130b	130b	130b	130b	133C	133C
WO <sub>3</sub> (wt.%)	0.43	0.53	0.42	0.47	0.16	0.07
P <sub>2</sub> O <sub>5</sub>	0.07	0.04	0.06	0.07	0.01	0.01
Nb <sub>2</sub> O <sub>5</sub>	41.38	40.96	38.13	40.85	47.16	49.20
Ta <sub>2</sub> O <sub>5</sub>	0.04	0.07	0.00	0.03	0.00	0.00
SiO <sub>2</sub>	0.04	0.08	1.25	0.04	0.09	0.08
TiO <sub>2</sub>	22.17	21.94	21.33	22.17	15.08	14.38
ZrO <sub>2</sub>	0.00	0.00	0.00	0.00	0.00	0.01
ThO <sub>2</sub>	5.36	6.11	5.64	6.40	3.18	3.91
UO <sub>2</sub>	0.57	0.74	0.65	0.75	0.37	0.29
Al <sub>2</sub> O <sub>3</sub>	0.00	0.00	0.13	0.00	0.00	0.00
Y <sub>2</sub> O <sub>3</sub>	17.22	16.73	15.62	17.05	0.24	0.18
La <sub>2</sub> O <sub>3</sub>	0.00	0.00	0.00	0.00	5.27	6.21
Ce <sub>2</sub> O <sub>3</sub>	0.50	0.42	0.42	0.35	13.84	12.62
Pr <sub>2</sub> O <sub>3</sub>	0.11	0.13	0.14	0.19	1.54	1.05
Nd <sub>2</sub> O <sub>3</sub>	1.37	1.09	1.24	1.18	4.36	3.10
Sm <sub>2</sub> O <sub>3</sub>	0.99	0.77	0.78	0.83	0.60	0.45
Gd <sub>2</sub> O <sub>3</sub>	2.40	2.40	2.18	2.37	0.18	0.06
Tb <sub>2</sub> O <sub>3</sub>	0.34	0.35	0.27	0.32	0.01	0.00
Dy <sub>2</sub> O <sub>3</sub>	2.73	2.77	2.43	2.68	0.19	0.03
Ho <sub>2</sub> O <sub>3</sub>	0.48	0.42	0.47	0.48	0.00	0.00
Er <sub>2</sub> O <sub>3</sub>	1.79	1.77	1.69	1.88	0.00	0.00
Yb <sub>2</sub> O <sub>3</sub>	1.16	1.11	1.09	1.11	0.00	0.06
Bi <sub>2</sub> O <sub>3</sub>	0.03	0.01	0.03	0.00	0.30	0.21
Fe <sub>2</sub> O <sub>3</sub> *	0.17	0.16	1.49	0.14	0.76	0.28
FeO*	0.15	0.15	1.34	0.13	0.69	0.75
MgO	0.00	0.00	0.02	0.00	0.01	0.02
CaO	2.16	2.34	1.80	2.22	5.18	5.79
MnO	0.23	0.22	0.85	0.21	0.00	0.00
PbO	0.00	0.02	0.00	0.00	0.12	0.00
Na <sub>2</sub> O	0.01	0.03	0.09	0.04	0.00	0.00
K <sub>2</sub> O	0.01	0.01	0.00	0.00	0.00	0.00
F	0.24	0.23	0.18	0.21	0.00	0.00
Total	96.78	95.50	94.10	95.76	96.20	95.34

**Appendix B.15:** EMPA analyses of Aeschynite, Nioboaeschnite, Euxenite, and Fersmite

Mineral	Eux	Eux	Eux	Eux	Aesch	Aesch
Point	24 / 1 .	36 / 1 .	37 / 1 .	38 / 1 .	2 / 1 .	3 / 1 .
Thin Section	130b	130b	130b	130b	133C	133C
W (apfu)	0.006	0.008	0.006	0.007	0.002	0.001
P	0.003	0.002	0.003	0.004	0.000	0.000
Nb	1.065	1.061	0.993	1.054	1.293	1.341
Ta	0.001	0.001	0.000	0.000	0.000	0.000
Si	0.003	0.004	0.072	0.002	0.006	0.005
Ti	0.949	0.946	0.924	0.952	0.688	0.652
Zr	0.000	0.000	0.000	0.000	0.000	0.000
Th	0.069	0.080	0.074	0.083	0.044	0.054
U	0.007	0.009	0.008	0.010	0.005	0.004
Al	0.000	0.000	0.009	0.000	0.000	0.000
Y	0.522	0.510	0.479	0.518	0.008	0.006
La	0.000	0.000	0.000	0.000	0.118	0.138
Ce	0.010	0.009	0.009	0.007	0.307	0.279
Pr	0.002	0.003	0.003	0.004	0.034	0.023
Nd	0.028	0.022	0.025	0.024	0.095	0.067
Sm	0.019	0.015	0.015	0.016	0.012	0.009
Gd	0.045	0.046	0.042	0.045	0.004	0.001
Tb	0.006	0.007	0.005	0.006	0.000	0.000
Dy	0.050	0.051	0.045	0.049	0.004	0.001
Ho	0.009	0.008	0.009	0.009	0.000	0.000
Er	0.032	0.032	0.031	0.034	0.000	0.000
Yb	0.020	0.019	0.019	0.019	0.000	0.001
Bi	0.000	0.000	0.000	0.000	0.005	0.003
Fe <sup>3+</sup>	0.007	0.007	0.065	0.006	0.035	0.013
Fe <sup>2+</sup>	0.007	0.007	0.065	0.006	0.035	0.038
Mg	0.000	0.000	0.001	0.000	0.001	0.002
Ca	0.131	0.144	0.111	0.136	0.336	0.374
Mn	0.011	0.011	0.042	0.010	0.000	0.000
Pb	0.000	0.000	0.000	0.000	0.002	0.000
Na	0.001	0.004	0.010	0.004	0.000	0.000
K	0.001	0.001	0.000	0.000	0.000	0.000
F	0.042	0.041	0.033	0.037	0.000	0.000

**Appendix B.15:** EMPA analyses of Aeschynite, Nioboaeschynite, Euxenite, and Fersmite

Mineral	Aesch	Aesch	Aesch	Aesch	Aesch	Fersmite
Point	4 / 1 .	13 / 1 .	25 / 1 .	26 / 1 .	44 / 1 .	22 / 1 .
Thin Section	133C	133C	133C	133C	135C	130b
WO <sub>3</sub> (wt.%)	0.02	0.09	0.05	0.04	0.21	0.06
P <sub>2</sub> O <sub>5</sub>	0.01	0.02	0.00	0.01	0.01	0.03
Nb <sub>2</sub> O <sub>5</sub>	35.32	42.52	48.19	53.10	36.33	70.04
Ta <sub>2</sub> O <sub>5</sub>	0.07	0.44	0.21	0.00	0.00	0.00
SiO <sub>2</sub>	0.37	0.07	0.05	0.04	0.47	0.03
TiO <sub>2</sub>	21.17	19.14	16.34	14.12	20.37	6.47
ZrO <sub>2</sub>	0.00	0.00	0.00	0.00	0.51	0.00
ThO <sub>2</sub>	12.61	11.41	6.77	8.13	5.18	1.34
UO <sub>2</sub>	1.50	2.99	0.85	0.13	0.11	0.14
Al <sub>2</sub> O <sub>3</sub>	0.00	0.00	0.00	0.00	0.00	0.01
Y <sub>2</sub> O <sub>3</sub>	0.80	0.60	0.27	0.02	1.78	5.01
La <sub>2</sub> O <sub>3</sub>	1.78	0.97	2.81	3.23	4.30	0.00
Ce <sub>2</sub> O <sub>3</sub>	8.99	7.19	10.44	7.81	14.65	0.34
Pr <sub>2</sub> O <sub>3</sub>	1.28	1.27	1.13	0.66	2.02	0.12
Nd <sub>2</sub> O <sub>3</sub>	4.79	4.72	3.77	1.60	6.82	0.61
Sm <sub>2</sub> O <sub>3</sub>	0.91	0.89	0.60	0.22	1.24	0.30
Gd <sub>2</sub> O <sub>3</sub>	0.35	0.38	0.13	0.00	0.78	0.70
Tb <sub>2</sub> O <sub>3</sub>	0.05	0.01	0.01	0.00	0.06	0.10
Dy <sub>2</sub> O <sub>3</sub>	0.09	0.22	0.04	0.00	0.40	0.84
Ho <sub>2</sub> O <sub>3</sub>	0.02	0.00	0.04	0.00	0.00	0.06
Er <sub>2</sub> O <sub>3</sub>	0.11	0.06	0.01	0.03	0.18	0.53
Yb <sub>2</sub> O <sub>3</sub>	0.04	0.00	0.01	0.00	0.08	0.38
Bi <sub>2</sub> O <sub>3</sub>	0.09	0.14	0.12	0.11	0.16	0.01
Fe <sub>2</sub> O <sub>3</sub> *	0.43	0.35	0.27	0.22	0.58	0.00
FeO*	0.39	0.32	0.25	0.20	0.52	0.34
MgO	0.01	0.00	0.00	0.00	0.00	0.01
CaO	4.87	6.47	7.10	8.85	2.36	11.69
MnO	0.40	0.03	0.01	0.01	0.01	0.45
PbO	0.00	0.03	0.01	0.02	0.01	0.01
Na <sub>2</sub> O	0.05	0.02	0.01	0.00	0.02	0.01
K <sub>2</sub> O	0.00	0.01	0.00	0.01	0.01	0.01
F	0.00	0.00	0.00	0.00	0.00	0.23
Total	83.91	88.98	92.77	90.47	94.06	98.86

**Appendix B.15:** EMPA analyses of Aeschynite, Nioboaschynite, Euxenite, and Fersmite

Mineral	Aesch	Aesch	Aesch	Aesch	Aesch	Fersmite
Point	4 / 1 .	13 / 1 .	25 / 1 .	26 / 1 .	44 / 1 .	22 / 1 .
Thin Section	133C	133C	133C	133C	135C	130b
W (apfu)	0.000	0.001	0.001	0.001	0.003	0.001
P	0.001	0.001	0.000	0.000	0.000	0.001
Nb	0.986	1.143	1.285	1.405	1.009	1.753
Ta	0.001	0.007	0.003	0.000	0.000	0.000
Si	0.023	0.004	0.003	0.002	0.029	0.002
Ti	0.983	0.856	0.725	0.622	0.942	0.269
Zr	0.000	0.000	0.000	0.000	0.015	0.000
Th	0.177	0.154	0.091	0.108	0.072	0.017
U	0.021	0.040	0.011	0.002	0.001	0.002
Al	0.000	0.000	0.000	0.000	0.000	0.000
Y	0.026	0.019	0.008	0.001	0.058	0.148
La	0.040	0.021	0.061	0.070	0.097	0.000
Ce	0.203	0.157	0.225	0.167	0.330	0.007
Pr	0.029	0.027	0.024	0.014	0.045	0.002
Nd	0.106	0.100	0.079	0.033	0.150	0.012
Sm	0.019	0.018	0.012	0.004	0.026	0.006
Gd	0.007	0.008	0.002	0.000	0.016	0.013
Tb	0.001	0.000	0.000	0.000	0.001	0.002
Dy	0.002	0.004	0.001	0.000	0.008	0.015
Ho	0.000	0.000	0.001	0.000	0.000	0.001
Er	0.002	0.001	0.000	0.000	0.003	0.009
Yb	0.001	0.000	0.000	0.000	0.001	0.006
Bi	0.001	0.002	0.002	0.002	0.003	0.000
Fe <sup>3+</sup>	0.020	0.016	0.012	0.010	0.027	0.000
Fe <sup>2+</sup>	0.020	0.016	0.012	0.010	0.027	0.016
Mg	0.001	0.000	0.000	0.000	0.000	0.001
Ca	0.322	0.412	0.448	0.555	0.155	0.694
Mn	0.021	0.002	0.000	0.000	0.000	0.021
Pb	0.000	0.000	0.000	0.000	0.000	0.000
Na	0.006	0.002	0.001	0.000	0.002	0.001
K	0.000	0.000	0.000	0.001	0.001	0.000
F	0.000	0.000	0.000	0.000	0.000	0.040

**Appendix B.15:** EMPA analyses of Aeschnynite, Nioboaeschnynite, Euxenite, and Fersmite

Mineral	Ferg	Ferg	Eux	Eux
Point	20 / 1 .	21 / 1 .	19 / 1 .	20 / 1 .
Thin Section	kin 136	kin 136	Pegm1	Pegm1
WO <sub>3</sub> (wt.%)	0.88	0.20	1.41	1.48
P <sub>2</sub> O <sub>5</sub>	0.06	0.06	0.05	0.05
Nb <sub>2</sub> O <sub>5</sub>	47.54	51.45	30.26	32.35
Ta <sub>2</sub> O <sub>5</sub>	0.81	0.65	3.00	2.88
SiO <sub>2</sub>	0.04	5.84	0.06	0.06
TiO <sub>2</sub>	0.32	0.78	23.28	22.71
ZrO <sub>2</sub>	0.00	0.00	0.00	0.00
ThO <sub>2</sub>	3.98	6.21	1.01	0.72
UO <sub>2</sub>	2.83	4.39	13.01	11.98
Al <sub>2</sub> O <sub>3</sub>	0.00	0.92	0.00	0.00
Y <sub>2</sub> O <sub>3</sub>	25.26	4.91	15.78	15.25
La <sub>2</sub> O <sub>3</sub>	0.00	0.25	0.00	0.00
Ce <sub>2</sub> O <sub>3</sub>	0.23	0.79	0.15	0.18
Pr <sub>2</sub> O <sub>3</sub>	0.00	0.07	0.06	0.05
Nd <sub>2</sub> O <sub>3</sub>	0.68	0.28	0.41	0.32
Sm <sub>2</sub> O <sub>3</sub>	0.49	0.13	0.60	0.47
Gd <sub>2</sub> O <sub>3</sub>	2.32	0.68	1.99	1.45
Tb <sub>2</sub> O <sub>3</sub>	0.45	0.06	0.35	0.25
Dy <sub>2</sub> O <sub>3</sub>	3.97	1.22	2.86	2.54
Ho <sub>2</sub> O <sub>3</sub>	0.94	0.24	0.34	0.41
Er <sub>2</sub> O <sub>3</sub>	3.14	0.94	1.54	1.46
Yb <sub>2</sub> O <sub>3</sub>	2.56	0.72	1.59	1.51
Bi <sub>2</sub> O <sub>3</sub>	0.00	0.05	0.00	0.02
Fe <sub>2</sub> O <sub>3</sub> *	0.26	3.11	0.85	0.85
FeO*	0.23	2.80	3.80	4.80
MgO	0.00	0.03	0.70	1.32
CaO	0.88	4.51	0.00	0.02
MnO	0.05	1.18	0.10	0.40
PbO	0.02	0.07	0.00	0.07
Na <sub>2</sub> O	0.03	0.29	0.18	0.17
K <sub>2</sub> O	0.02	0.23	0.05	0.06
F	0.03	0.51	0.39	0.40
Total	97.70	92.78	102.80	103.49

**Appendix B.15:** EMPA analyses of Aeschynite, Nioboaeschynite, Euxenite, and Fersmite

Mineral	Ferg	Ferg	Eux	Eux
Point	20 / 1 .	21 / 1 .	19 / 1 .	20 / 1 .
Thin Section	kin 136	kin 136	Pegm1	Pegm1
W (apfu)	0.011	0.003	0.014	0.014
P	0.002	0.002	0.002	0.002
Nb	0.994	1.132	0.528	0.548
Ta	0.010	0.009	0.031	0.029
Si	0.002	0.284	0.002	0.002
Ti	0.011	0.029	0.675	0.640
Zr	0.000	0.000	0.000	0.000
Th	0.042	0.069	0.009	0.006
U	0.029	0.048	0.112	0.100
Al	0.000	0.053	0.000	0.000
Y	0.622	0.127	0.324	0.304
La	0.000	0.004	0.000	0.000
Ce	0.004	0.014	0.002	0.003
Pr	0.000	0.001	0.001	0.001
Nd	0.011	0.005	0.006	0.004
Sm	0.008	0.002	0.008	0.006
Gd	0.036	0.011	0.025	0.018
Tb	0.007	0.001	0.004	0.003
Dy	0.059	0.019	0.036	0.031
Ho	0.014	0.004	0.004	0.005
Er	0.046	0.014	0.019	0.017
Yb	0.036	0.011	0.019	0.017
Bi	0.000	0.001	0.000	0.000
Fe <sup>3+</sup>	0.009	0.114	0.123	0.150
Fe <sup>2+</sup>	0.009	0.114	0.123	0.150
Mg	0.000	0.002	0.040	0.073
Ca	0.044	0.235	0.000	0.001
Mn	0.002	0.049	0.003	0.013
Pb	0.000	0.001	0.000	0.001
Na	0.003	0.028	0.013	0.012
K	0.001	0.014	0.002	0.003
F	0.000	0.000	0.000	0.000

## B.16: Lanthanite

### Appendix B.16: EMPA analyses of Lanthanite

Point	7 / 1 .		7 / 1 .
Thin section	130b-2		130b-2
SO <sub>3</sub> (wt.%)	0.13	S (apfu)	0.009
SiO <sub>2</sub>	0.25	Si	0.023
TiO <sub>2</sub>	0.06	Ti	0.004
Al <sub>2</sub> O <sub>3</sub>	1.81	Al	0.197
Y <sub>2</sub> O <sub>3</sub>	0.34	Y	0.017
La <sub>2</sub> O <sub>3</sub>	15.81	La	0.539
Ce <sub>2</sub> O <sub>3</sub>	24.53	Ce	0.830
Pr <sub>2</sub> O <sub>3</sub>	1.86	Pr	0.063
Nd <sub>2</sub> O <sub>3</sub>	5.68	Nd	0.187
Sm <sub>2</sub> O <sub>3</sub>	0.61	Sm	0.019
Eu <sub>2</sub> O <sub>3</sub>	0.11	Eu	0.003
Gd <sub>2</sub> O <sub>3</sub>	0.22	Gd	0.007
Dy <sub>2</sub> O <sub>3</sub>	0.12	Dy	0.003
CaO	0.87	Ca	0.086
FeO	0.11	Fe <sup>2+</sup> (tot)	0.009
F	0.38	F	0.111
CO <sub>2</sub>	23.78	C	3.000
H <sub>2</sub> O*	25.96	OH	16.000
Total	102.70		

\*Note: formula calculation based on cation sum = 1

Elements sought but not found (or below detection limit): Na, Ba, Er, U, Th, Pb, As, Fe, Zr, and Sc

## **Appendix C: Full Petrographic Descriptions**

While the majority of the petrography is described in Chapter 2, this appendix serves as the “extended” version of that chapter. Some information is repeated, some is expanded upon, and some is new.

### **C.1 Pegmatites**

#### **C.1.1 Border Zone**

Rocks with the characteristics of pegmatite border zones were observed and sampled from localities KIN-133, KIN-134. The border zone is fine-grained, heterogeneous, with plagioclase and little quartz.

#### **KIN-133**

The border zone rock sample from locality KIN-133 is composed primarily of primary phlogopite (15%) with secondary almandine (10%), allanite-(Ce) (3%), ferrocolumbite (3%), and aeschynite-(Ce) (3%) within oligoclase feldspar(40%) with little quartz. Fluorapatite, monazite-(Ce), thorite, and zircon are also present in minor amounts. Thin sections KIN-133a and KIN-133c are from this zone, and minerals in the latter were analyzed by EMP.

This zone is characterized by common phlogopite and secondary almandine with a poikiloblastic texture in feldspar scattered throughout the zone. A few phlogopite grains approach a subhedral shape, but the majority of the minerals present are anhedral. Within this matrix, groups of rarer minerals are found in association. This association is commonly secondary allanite-(Ce) after monazite-(Ce) with secondary fluorapatite and thorite in association with

ferrocolumbite and aeschynite. These minerals are never found in isolation and can be seen as two general types:

1) Secondary allanite-(Ce), fluorapatite, and thorite after monazite-(Ce) with a corona texture (Fig. C.1.1). These coronas are seen separately from other rare minerals associations.

2) Secondary allanite-(Ce) with secondary aeschynite-(Ce) found with columbite and thorite (Fig. C.1.2). It is unclear what this second association formed from. These associations may contain monazite-(Ce) and fluorapatite, whereby the allanite would be secondary after both aeschynite-(Ce) and monazite-(Ce), but this is not always the case. This second association is often much larger than the coronas, however both types feature anhedral minerals.

In hand sample, this zone is characterized by concentrations of dark minerals, primarily phlogopite, within light, cream-colored feldspar (Fig. C.1.3). Minerals within this zone do not grow as large as those in other zones, with an approximate maximum of 0.2 cm length for the phlogopite and allanite grains.

#### **KIN-134**

Clinzoesite (20%) with almandine (25%) within oligoclase feldspar (15%) makes up the majority of the border zone in the pegmatite at locality KIN-134. Columbite, rutile, thorite, and zircon are also present in minor amounts. This zone is seen in thin section KIN-134-4, which was analyzed by EMP.

Almandine occurs as primary, anhedral grains up to 0.0 mm in size and in garnet clusters up to 1.0 cm in size. These groups are generally surrounded by secondary anhedral clinzoesite that forms grains up to 0.5 cm in size (Fig. C.1.4). Phlogopite is found within the clinzoesite,

but generally separate from the almandine, as eu- to subhedral-, primary grains up to 0.0 cm in length, commonly associated with other phlogopite grains.

Columbite with rutile is found scattered throughout the clinozoisite groups, as is thorite. Zircon does not seem to be associated with any other mineral and is found within the feldspar as individual crystals.

### **C.1.2 Wall Zone**

Wall zone samples were collected from KIN-130, KIN-133 and KIN-135 localities and float sample RAD1. The samples in all instances look very similar and are described together below. Pegmatitic wall zones are characterized by being coarse grained with quartz, plagioclase, microcline, and some mica (Simmons et al., 2012). Samples from locality KIN-130 have not been analyzed; however, they appear similar to other wall zone samples in hand sample.

The wall zone is the darkest of the zones present, with large amounts of magnesiohornblende (25%) and ferriallanite-(Ce) (15%) within quartz (15%), and little feldspar. Secondary almandine (6%) after primary phlogopite and annite (9%) are the most common accessory minerals, with small amounts of fluorapatite, monazite-(Ce), chevkinite-(Ce), aeschynite-(Ce), ferrocolumbite, anandite (mica), ilmenite, Nb-rich rutile, iron oxides, pyrite, sphalerite, thorite, titanite, and zircon making up the remaining mineralogy. Thin sections KIN-133b, KIN-133d, KIN-133e, KIN-135a, KIN-135c, and Rad 1 are from this zone and sections KIN-133d, KIN-135a, and KIN-135c were analyzed with the EMP.

Both primary and secondary allanite are present in this zone, with primary ferriallanite-(Ce) in samples 135a and 135c and secondary allanite-(Ce) after monazite-(Ce) in samples KIN-133b, KIN-133d, KIN-133e, and Rad 1. These secondary grains are up to 0.3 cm in size,

anhedral, and are often associated with other REE-bearing phases such as secondary chevkinite-(Ce) and aeschynite-(Ce). The cores commonly contain some remaining monazite-(Ce) and secondary fluorapatite with thorite. Primary allanite occurs as large (up to 1.5 cm) eu- to subhedral ferriallanite-(Ce) grains with similar zoning to that of the secondary allanite, with darker REE-rich zones near the center of the grains and lighter REE-depleted rims.

The oxide minerals are often associated with each other and with the REE-bearing phases. Columbite and ilmenite occur as an- to subhedral primary grains while the other phases occur as secondary minerals. In KIN-133d, aeschynite-(Ce) occurs as an exsolution texture within ilmenite (Fig. C.1.5).

In some parts of this zone, a poikiloblastic texture is visible within the phlogopite, almandine, and magnesiohornblende grains. Sample KIN-133b in particular shows this texture (Fig. C.1.6) with a “nest” shape around the allanite grain. Additionally, graphic granite textures with intergrowths of quartz and feldspar are also visible within this zone (Fig. C.1.7).

In hand sample, this zone is the darkest of the zones and is characterized by its dark green and red/brown color and large, “blocky” grains (Fig. C.1.8). Allanite crystals up to 5 cm in size have been found within this zone. Iron oxide minerals are prevalent throughout, and are responsible for the rusty red color.

### **C.1.3 Intermediate Zone**

Intermediate zone samples were collected from the KIN-130, KIN-134, KIN-135, KIN-136, and Rad 2 localities. Intermediate pegmatite zones are characterized by a medium-grained texture with microcline, quartz, sodic plagioclase, and minor mica.

## **KIN-130**

The intermediate zone at locality KIN-130 is composed of quartz (30%), albite, and hylophane feldspar (50%). Secondary allanite-(Ce) (7%) and primary ferrocolumbite (8%) are the next most common minerals, while the additional mineralogy is present as the accessory minerals fluorapatite, thorite, fersmite, euxenite-(Y), molybdenite, garnet, phlogopite, amphibole, and seccicite after albite. Thin sections 130, 130a, 130b, and 130b-1 are from the intermediate zone, with samples 130a and 130b being analyzed with the EMP.

The quartz and feldspar matrix is composed of large anhedral grains up to 1.0 cm in size. Feldspar is more prevalent than quartz by an approximate ratio of 2:3 and is composed of approximately equal amounts of albite and hylophane.

The allanite-(Ce) grains are large (up to 1.0 cm in thin section), eu- to subhedral, with zoning seen as dark red in the core and a lighter, rusty red towards the edges (Fig. C.1.9), and higher REE contents in the darker allanite. The allanite crystals are secondary after monazite-(Ce) with small grains of monazite remaining within the allanite.

The ferrocolumbite grains are primary, euhedral, and associated with secondary euxenite-(Y) within fractures and fersmite grains as exsolution products (Fig. C.1.10).

The garnet is likely almandine and is secondary after phlogopite. These minerals, along with the amphibole (likely magnesiohornblende) were only seen in one thin section, sample KIN-130.

Sample 130b-1 however, appears different and may represent a contact between zones. It contains significantly higher amounts of garnet (35%) and phlogopite (25%) with approximately 40% feldspar. It is classified as an intermediate-zone sample due to the fact that it contains a

feldspar-rich appearance in part and because it contains the Ba-rich feldspar, hylophane, which is only seen in the intermediate zone.

In hand sample, this zone can be identified by its light cream color with large, dark, and often euhedral crystals of allanite (up to 5.0 cm) and columbite (up to 0.0 cm).

#### **KIN-134**

The intermediate zone at locality KIN-134 is composed primarily of monazite-(Ce) (15%), allanite-(Ce) (20%), and phlogopite (10%) within oligoclase (20%) with quartz (15%). Fluorapatite, almandine, ferrocolumbite, chevkinite-(Ce), aeschynite-(Ce), thorite, and zircon make up the remaining mineralogy of the zone. This zone is found in samples KIN-134-1, KIN-134-2, and KIN-134-3, of which sample KIN-134-2 was analyzed using EMP.

The defining characteristic of this zone is the extremely prevalent secondary allanite-(Ce) after primary monazite-(Ce) with apatite and thorite. The associations can form corona textures, although they are not always present and the minerals form in less defined associations. The allanite grains can grow to be large eu- to subhedral crystals. There is quite a lot of variation in grain appearance; however some do form elongate crystals that appear euhedral. Ferrocolumbite, chevkinite-(Ce), and aeschynite-(Ce) form within these grains as primary minerals, although primary and secondary relationships are unclear.

Primary phlogopite in rare cases has undergone replacement to form almandine in this zone. The phlogopite is subhedral and can grow up to 0.2 cm in size.

In hand sample, this zone appears as a cream (feldspar) background with dark, moderately sized mineralization up to 1.0cm in size. These minerals are primarily garnet

(clusters) and biotite, appearing as red and black crystals in the cream-colored sample (Fig. C.1.11).

### **KIN-135**

The zone in this locality is primarily composed of albite and hylophane feldspar (75%) with smaller amounts of quartz (15%), almandine garnet, biotite, and monazite-(Ce). The small grains of biotite are scattered throughout the primarily feldspar matrix. The additional accessory minerals (garnet and monazite) are found within these isolated biotite grains. This zone is represented by thin section KIN-135b.

In hand sample, this zone is very similar to the intermediate zone seen at locality KIN-130, and it is predominately cream in color, with feldspar and quartz grains up to 1.0 cm in size, and smaller minor minerals. It is shown with wall zone and quartz core contacts in Fig. C.1.1C.

### **KIN-136**

The intermediate zone at this locality contains muscovite (35%) within albite feldspar (55%). Almandine, monazite-(Ce), ferrocolumbite, Nb-rich rutile, euxenite-(Y), and zircon are also present.

The majority of the sample is subhedral muscovite up to 0.75 cm in size within anhedral albite (65%) up to 0.50 cm in size. The accessory minerals present generally occur as isolated grains within this matrix. Monazite-(Ce) is the most prevalent of these and makes up approximately 7% of the section. Ferrocolumbite is found as exsolutions within Nb-rich rutile, which is occasionally associated with monazite-(Ce) (Fig. C.1.13). Euxenite-(Y) occurs as a small grain within a partially replaced garnet (Fig. C.1.14).

## **Rad 2**

The intermediate zone in sample Rad 2 is composed primarily of oligoclase feldspar (75%) with quartz (10%). Phlogopite, muscovite, apatite, allanite-(Ce), monazite-(Ce), pyrite, and tourmaline are present as accessory minerals. This zone is seen in thin sections Rad 2a and Rad 2b, and section Rad 2a was analyzed by EMP.

The accessory minerals at this locality generally occur as solitary grains scattered in the feldspar and quartz, however mica growth along veins is visible in sample Rad 2a (Fig. C.1.15). These samples contain the only tourmaline present in the syenitic pegmatite bodies, with dravite grains up to 0.0 mm in length (Fig. C.1.15). These sections are highly sericitized and interesting intergrowths of muscovite and quartz are present (Fig. C.1.16).

### **C.1.4 Core Zone**

Quartz core samples were collected from the KIN-130, KIN-134, KIN-135, and Rad 2 localities. Pegmatite cores are identified by their very high levels of quartz.

#### **KIN-130**

The quartz core is composed of approximately 95% quartz with magnesiohornblende, almandine/spessartine, pyrite, wurtzite, lanthanite-(Ce), and potentially bertrandite. The accessory minerals occur as secondary mineralization within the primary amphibole grains (Fig. C.1.17), and constitute the remaining 5% of the rock, with amphibole making up approximately 75% of that 5%. This zone is found in thin section KIN-130b-2, which was analyzed using EMP.

The quartz grains are large, up to 0.0 cm in size with migratory boundaries (Fig. C.1.18) and undulose extinction. While this feature is common in quartz across the zones, it is particularly apparent here due to its abundance and the large quartz grains present.

The magnesiohornblende grains form a “kite” shape that clearly demonstrates their 124°/56° cleavage planes (Fig. C.1.19) and can attain 1.0 cm in size. These grains are partially replaced to form the garnet, pyrite, wurtzite, lanthanite-(Ce), and bertrandite as small secondary minerals present in the sample.

In hand sample, the core appears blue/gray with small green amphibole grains up to 3 mm in size and is distinguished based on its high quartz content.

#### **KIN-134**

No samples were taken from the quartz core of pegmatite 2, however photographic evidence shows a high percentage of coarse-grained quartz occurring with red garnet, likely almandine (Fig. C.1.20). In the figure below, the contact between the core and the intermediate zone is visible.

#### **KIN-135**

The core from sample KIN-135 is composed primarily of quartz (80%) with visible, euhedral grains of allanite up to 1.5 cm long with muscovite up to 0.5 cm in length.

#### **Rad 2**

The core in sample Rad 2 (as seen in sample Rad 2c) is composed primarily of quartz (85%) with plagioclase, apatite, allanite, aeschynite, pyrite, and zircon in minor amounts.

Apatite and allanite occur as medium-sized grains, up to 4.0 mm in size, and are associated with each other within the quartz (Fig. C.1.21). Small aeschynite-(Ce) grains are found within the allanite-(Ce), and these minerals, with apatite, are likely secondary after monazite, however no primary material remains. Secondary feldspar “fills” the gaps between the quartz grains.

In hand sample, this sample appears dark and is composed primarily of quartz with allanite, apatite, and feldspar grains.

## **C.2 Granitic Pegmatite**

Granitic pegmatite was only found in one float sample on the KIN-property, PGM with thin section PGM 1. This sample is finer-grained than the syenite pegmatite samples, with quartz and feldspar grains (which make up the majority of the sample) attaining approximately 1.0 mm.

This sample is composed primarily of albite and K-feldspar (80%) and quartz (10%). The remaining mineralogy is composed of monazite-(Ce), ferrocolumbite, euxenite-(Y), almandine, muscovite, schorl, pyrite, and zircon.

The garnet and tourmaline are both primary and the tourmaline is up to 1.0 mm in length. Accessory minerals usually occur as individual grains, however they can also appear in small associations (Fig. C.C.1) within the feldspar and quartz.

## **C.3 Granite**

As seen in thin sections G17a (analyzed by EMP), G17b, G18, and G19, the granite on the KIN-property is extremely coarse-grained with muscovite grains up to 10 cm in size. It is primarily composed of quartz (25%), albite (35%), and muscovite (20%) with accessory

almandine. Fluorapatite, bismuthinite, chalcopyrite, monazite, xenotime, sericite, chlorite, bismuthinite, chalcopyrite, pyrite, iron oxide, and zircon are all present in small quantities.

The quartz, albite, and muscovite grains are anhedral and relatively similar in size, with albite grains being the largest on average (up to 1.0 cm in size).

The almandine occurs as highly replaced subhedral grains that contain chlorite, muscovite, and xenotime (C.3.1) in sample G17a. Primary monazite-(Ce) occurs in samples G17b, G18, and G19 with secondary apatite and xenotime-(Yb).

#### **C.4 Syenite**

Syenite was found during the company exploration, with one thin section, JBTDR018, being passed onto UBC. The sample is composed of approximately 50% ferriallanite, 30% feldspar, and 20% biotite. Monazite, apatite, and muscovite make up the accessory mineralogy. The sample is coarse grained with ferriallanite grains up to 0.0 cm in length and biotite up to 1.0cm in length within the thin section. It is also heavily altered, with secondary iron oxides coloring the sample.

The ferriallanite is secondary after monazite with apatite and forms large, elongate, and often twinned specimens (Fig. C.4.1). Biotite and muscovite commonly occur as subhedral grains along the edges of the allanite grains.

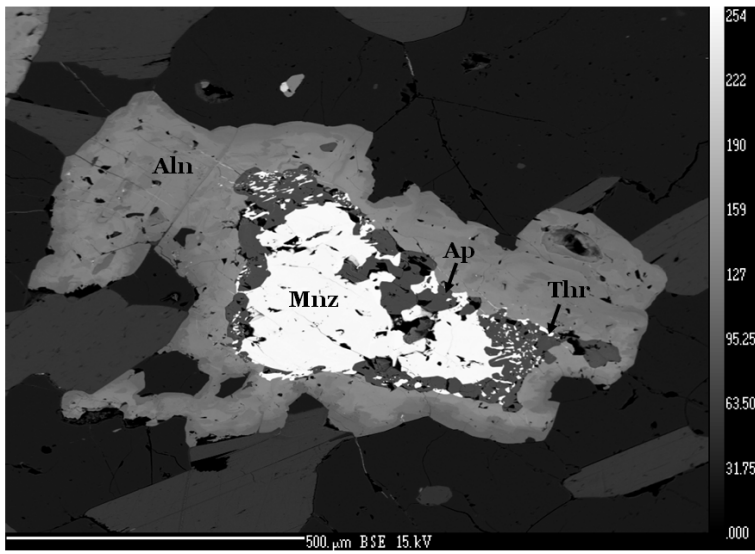


**Figure C.1.1** Primary monazite breaks down to form secondary fluorapatite, thorite, and allanite-(Ce) in a corona in sample KIN-133c.

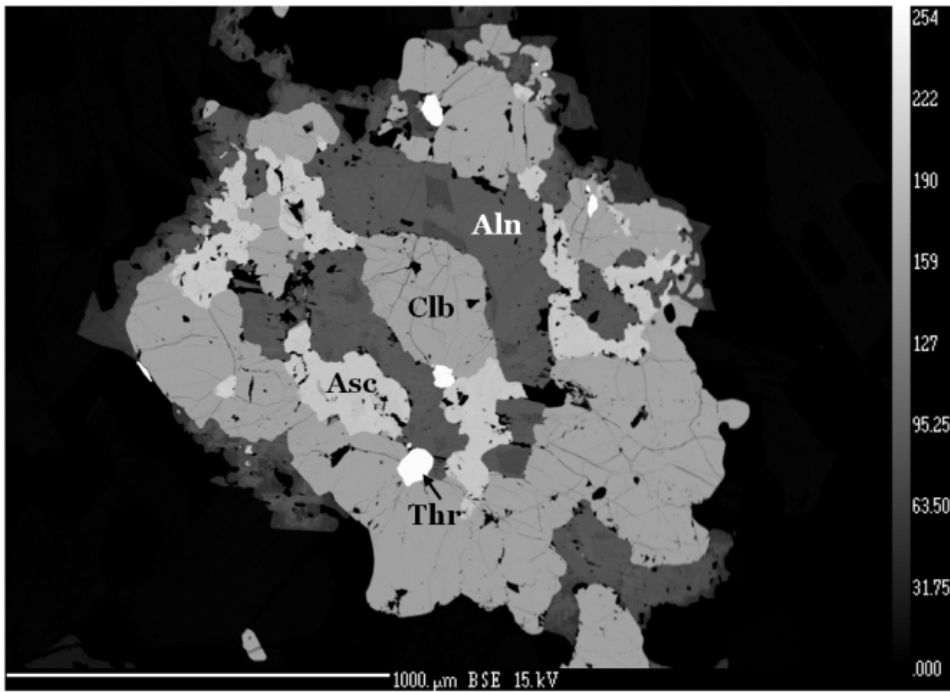


**Figure C.1.2** Primary aeschynite-(Ce) and ferrocolumbite with secondary allanite-(Ce) with thorite in sample KIN-133c.



**Figure C.1.3** Border zone sample from locality KIN-133.

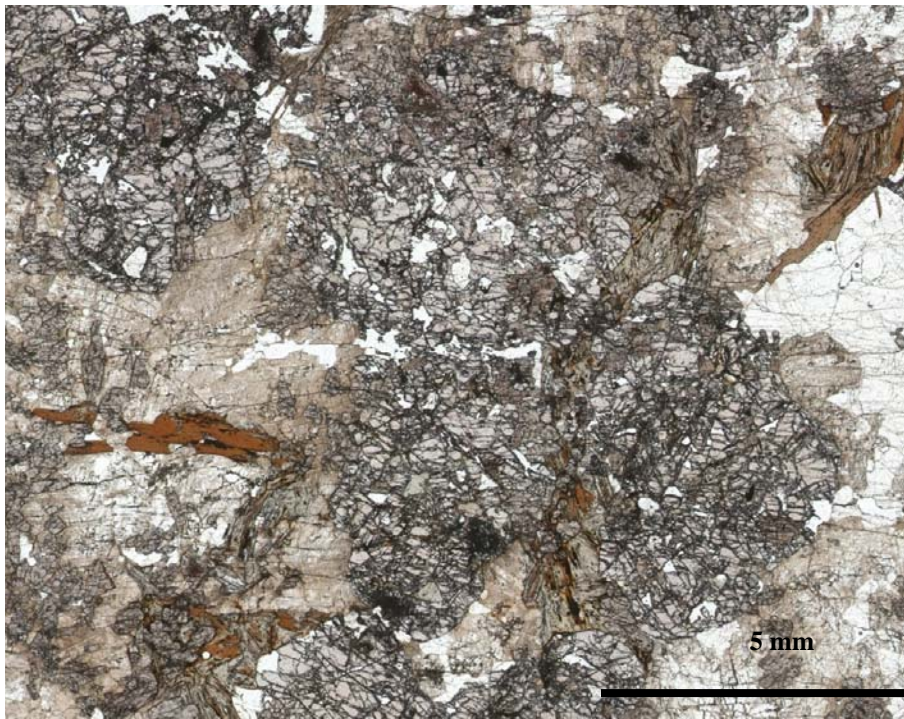


**Figure C.1.4** Garnet clusters surrounded by clinozoisite with phlogopite in sample KIN-134-4.

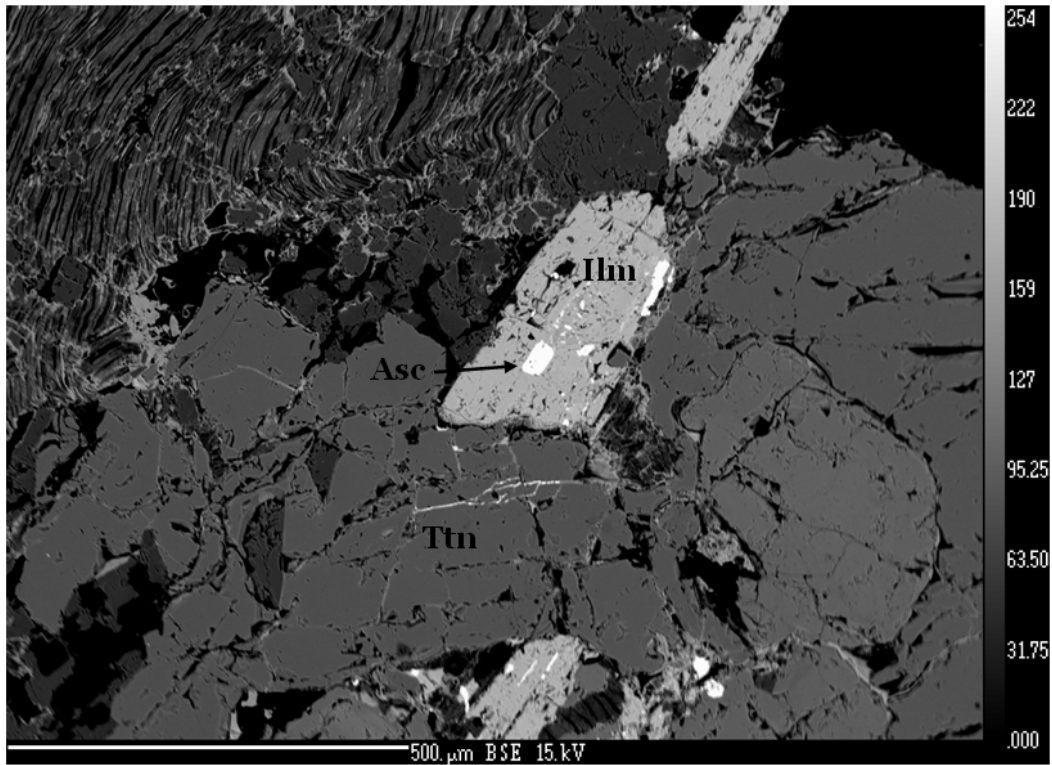


**Figure C.1.5** Exsolution of aeschynite-(Ce) within ilmenite in sample KIN-133d.

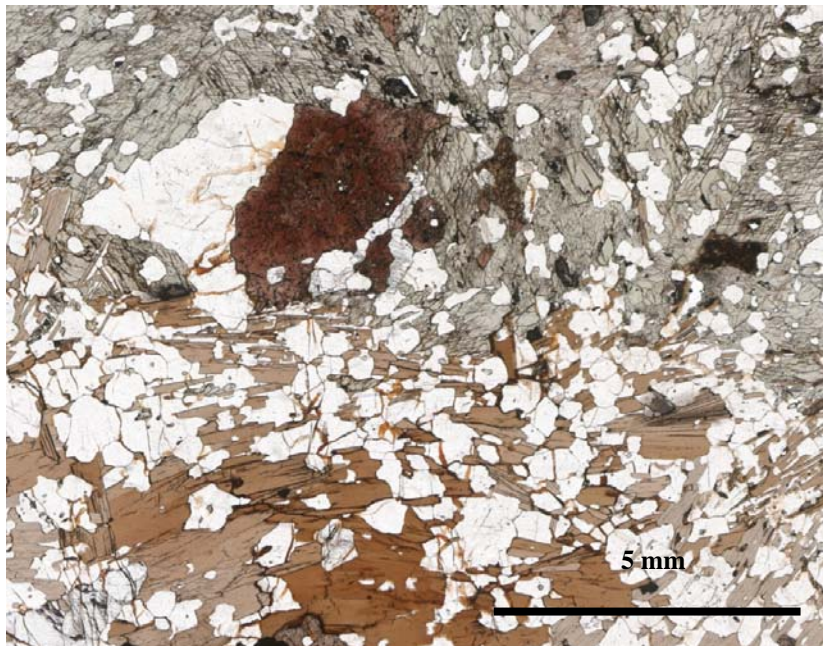


**Figure C.1.6** Poikiloblastic texture of amphibole and phlogopite within sample KIN-133b.

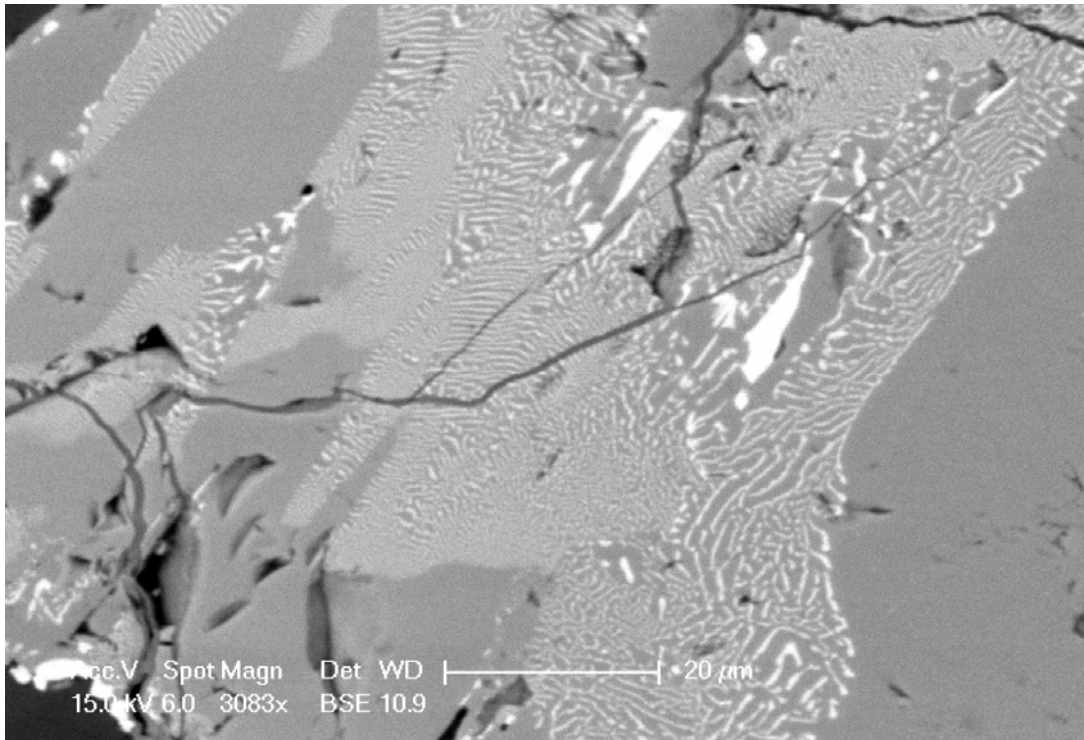


**Figure C.1.7** Graphic granite textures of quartz and feldspar within sample KIN-133d.



**Fig. C.1.8** Wall zone thin section blanks(left to right are samples KIN-133e, KIN-135a, Rad 1, KIN-133b, and KIN133d) to show texture and appearance, as well as similarities between this zone at the different localities.

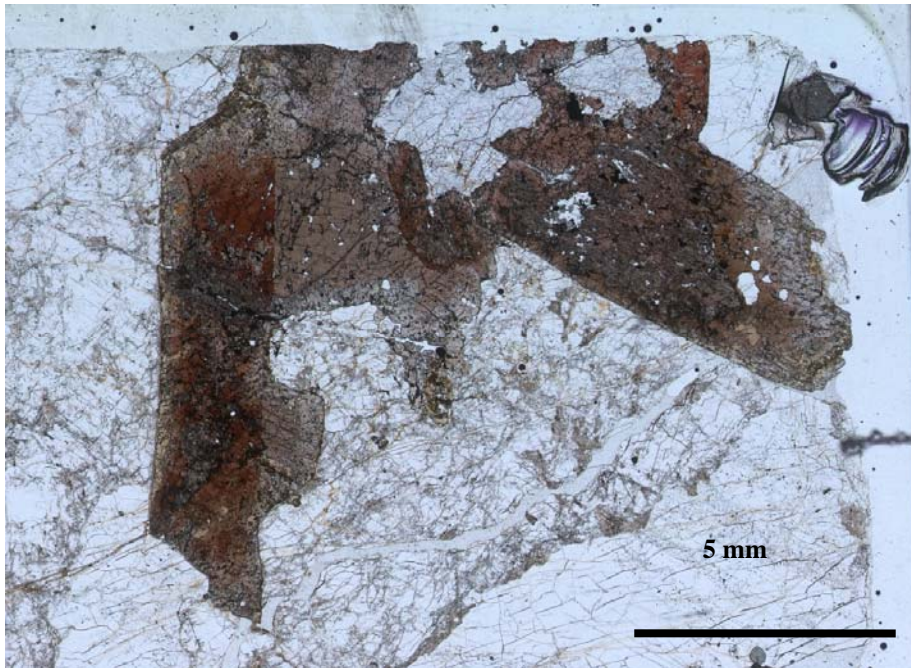


**Figure C.1.9** Secondary zoned allanite grains in the intermediate zone in sample KIN-130a.

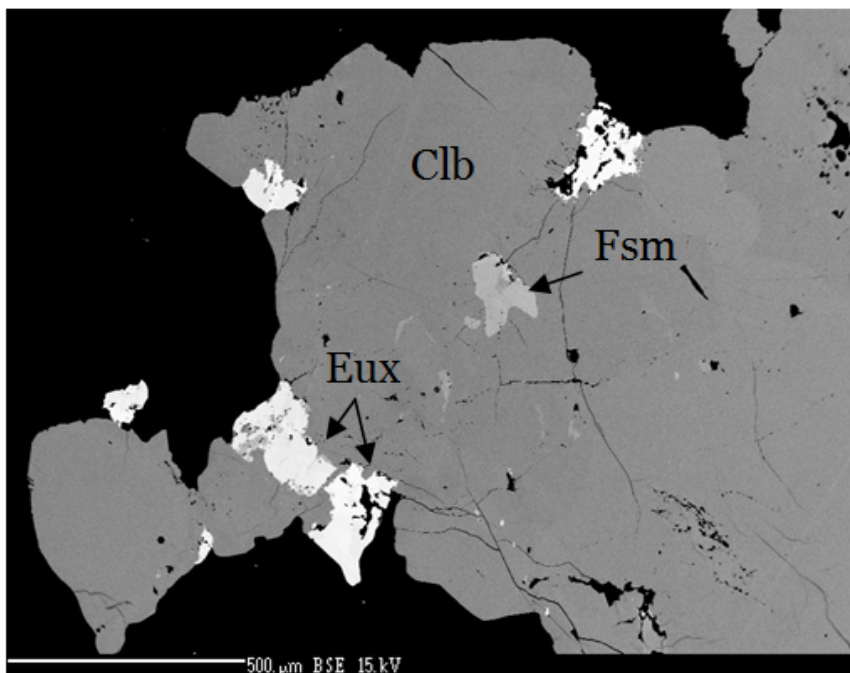


**Figure C.1.10** Primary columbite with euxenite-(Y) in fractures and fersmite as an exsolution product in section KIN-130b.



**Figure C.1.11** Hand sample from the intermediate zone at locality KIN-134.



**Figure C.1.12** Intermediate zone (middle yellow/cream rocks) in contact with wall zone (dark, coarse grained rock) and core at locality KIN-135.

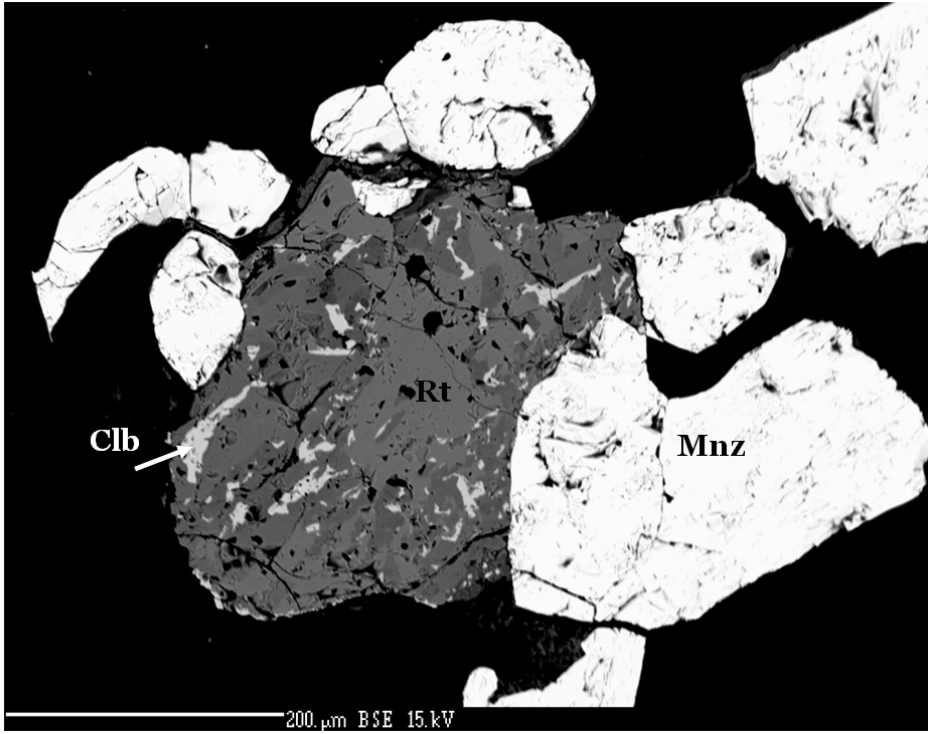


**Figure C.1.13** Columbite exsolution within rutile with monazite from KIN-136.

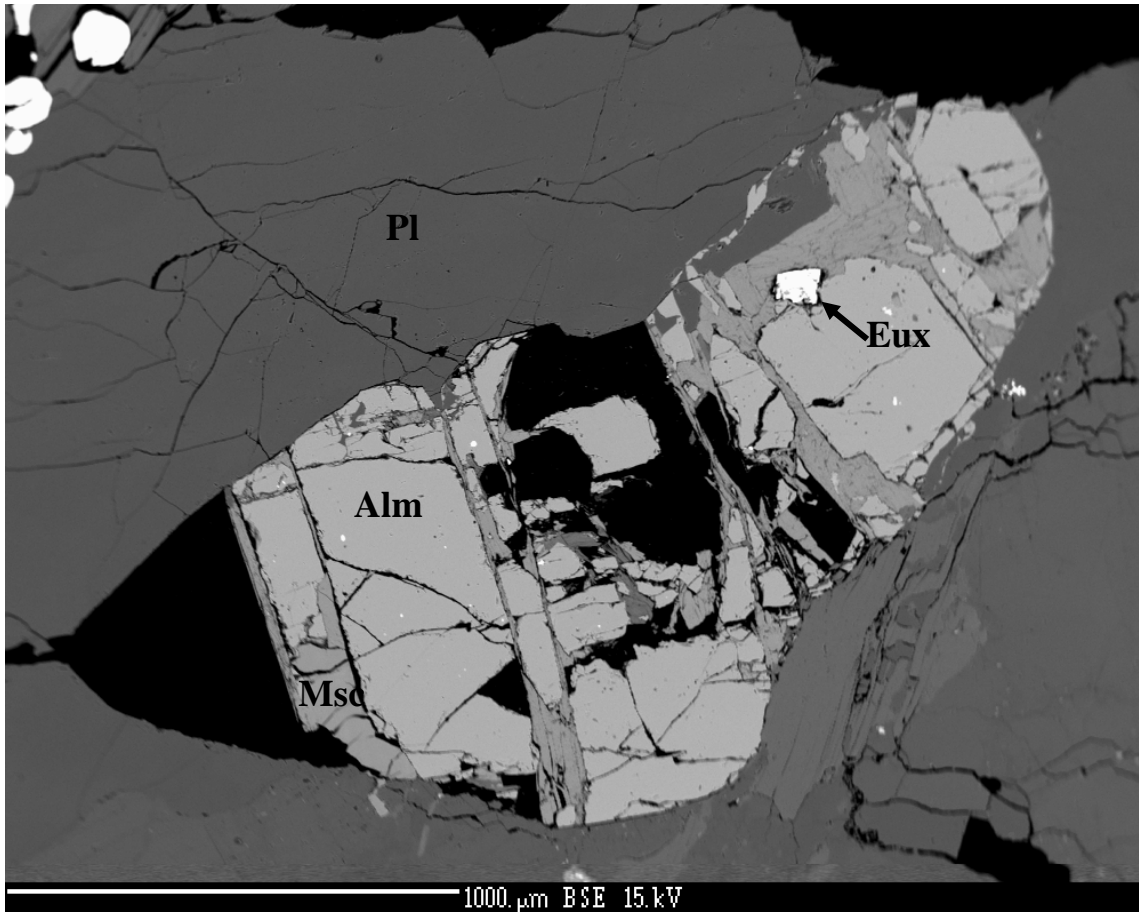


**Figure C.1.14:** Euxenite grain within partially replaced (by muscovite) almandine in sample KIN-136.

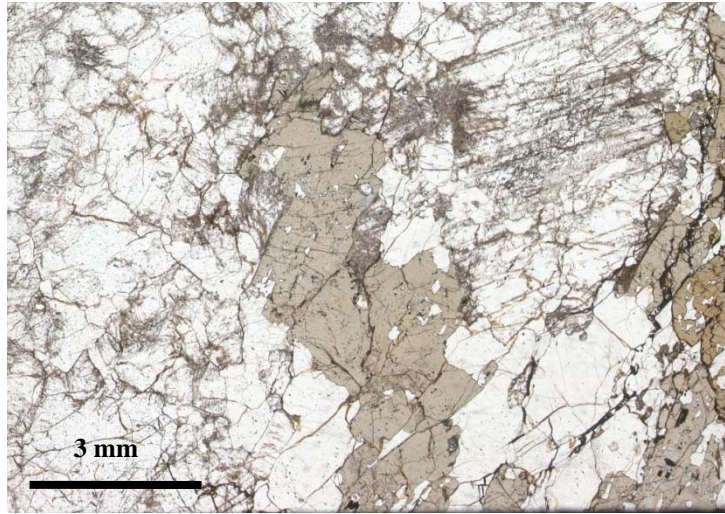


**Figure C.1.15** Images from thin section Rad 2a showing mica (phlogopite and muscovite) in vein (left) and tourmaline (right).

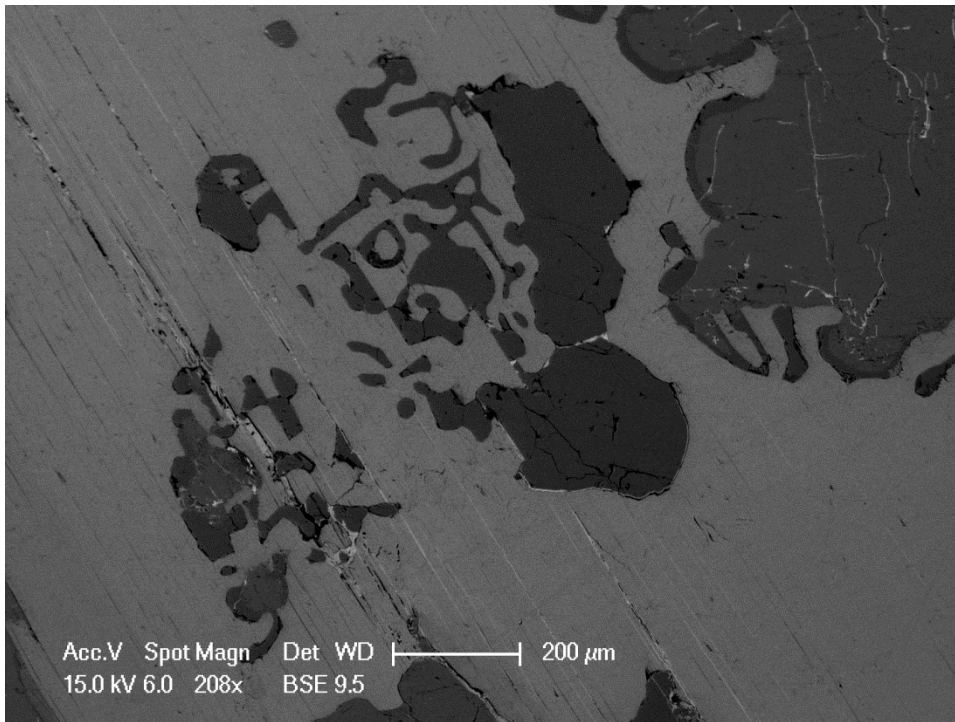


**Figure C.1.16** Intergrowths of muscovite and quartz within thin section Rad 2b.

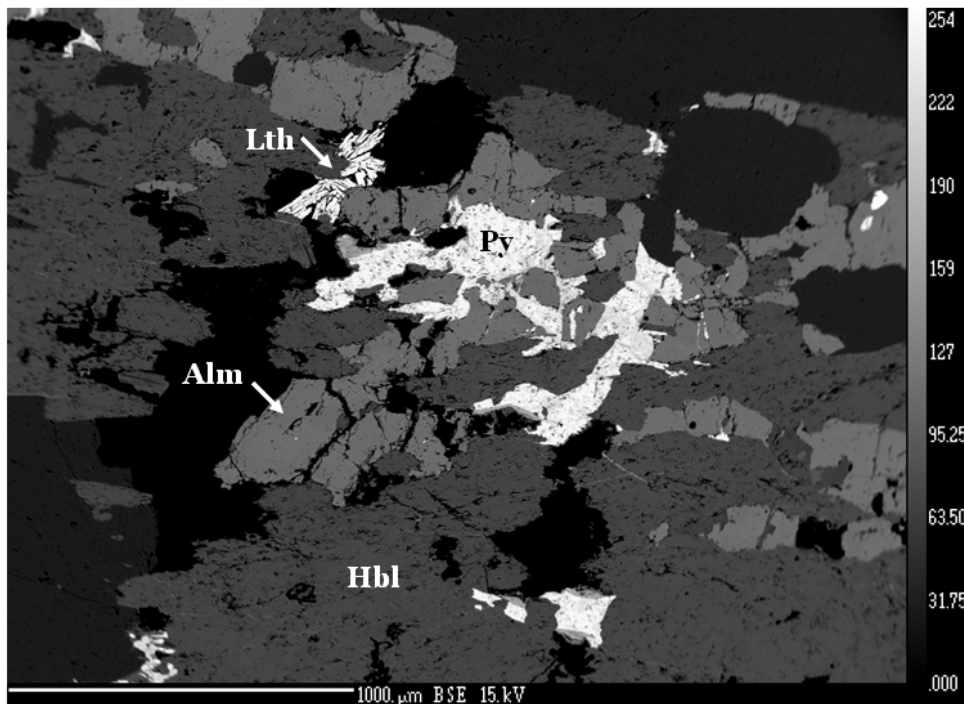


**Figure C.1.17** Amphibole with almandine, pyrite, and lanthanite-(Ce) in the quartz core at locality KIN-130.

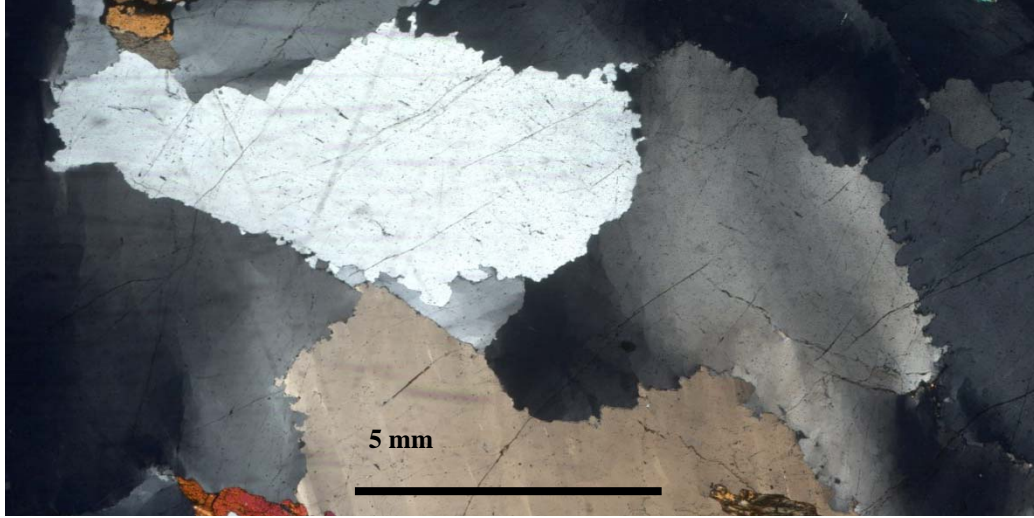


**Figure C.1.18** Undulose extinction and migratory boundaries visible in the quartz within the core at locality KIN-130.

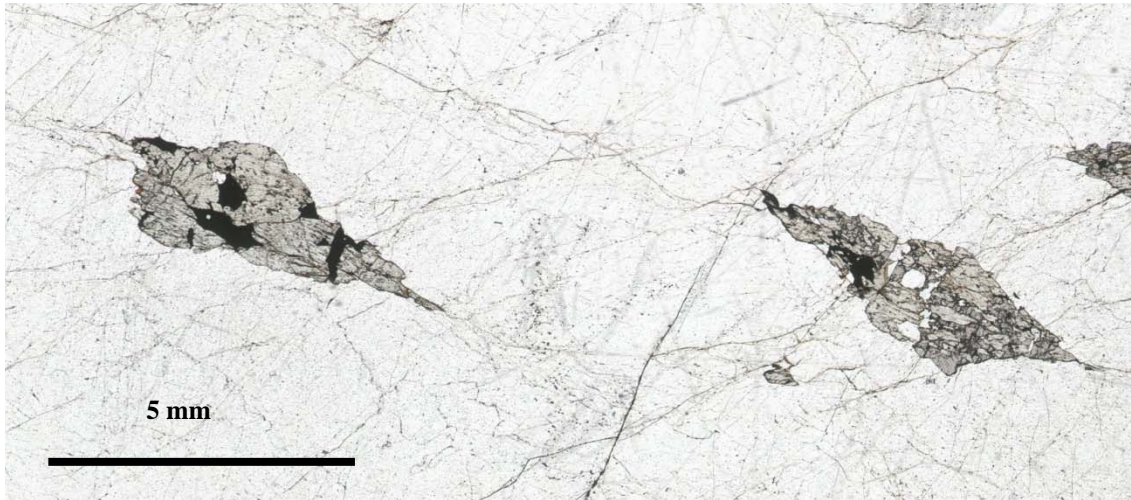


**Figure C.1.19** Primary amphibole grains demonstrating cleavage planes within quartz in the quartz core from locality KIN-130.



**Figure C.1.20** Quartz core with visible quartz and red garnet at locality KIN-134. The top of the photo shows the contact between the core and the intermediate zone .

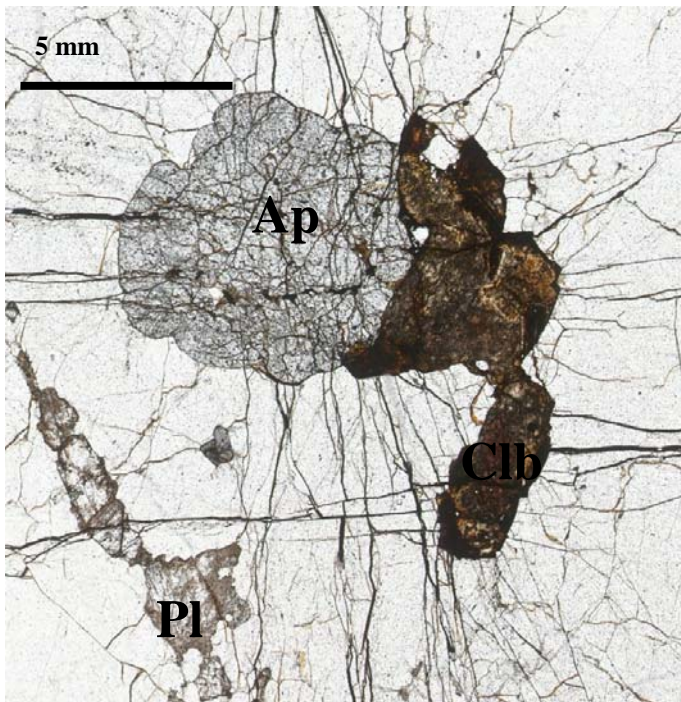


**Figure C.1.21** Allanite and apatite within quartz in sample Rad 2c.

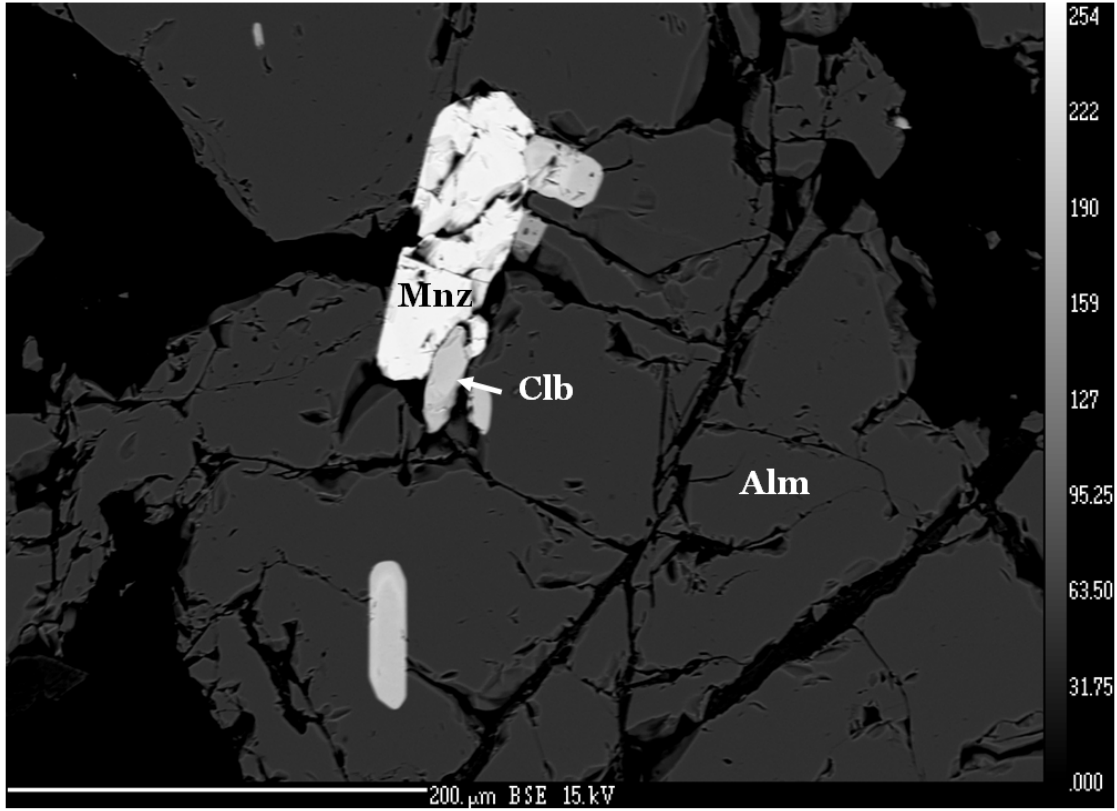


**Figure C.2.1** Ferrocolumbite and monazite-(Ce) within almandine in sample PGM1.

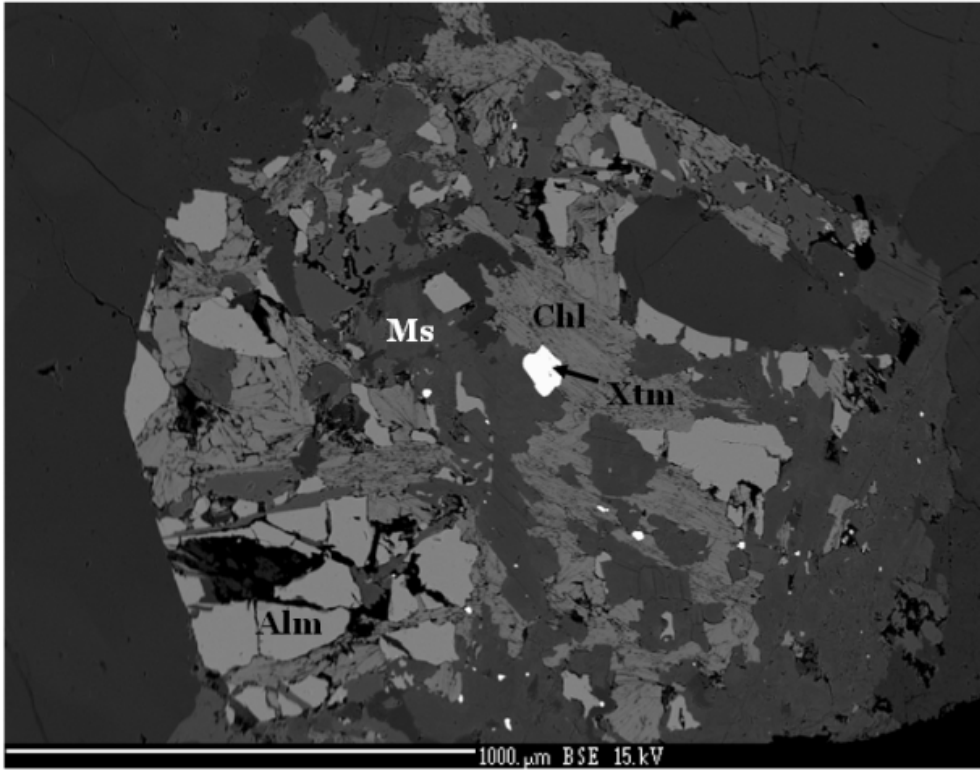


**Figure C.3.1** Primary garnet with secondary muscovite, chlorite, and xenotime in sample G17a.

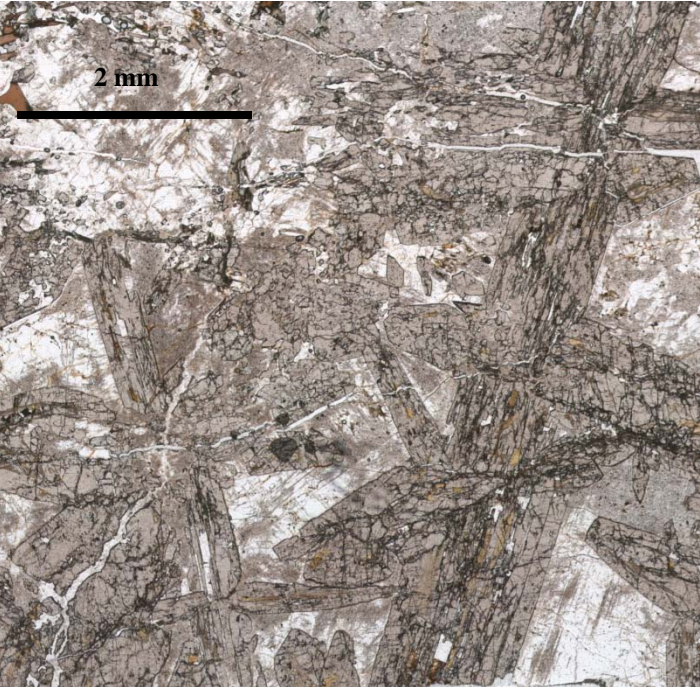


**Figure C.4.1** Secondary ferriallanite grains in syenite sample JBTDR018.

# U-Pb Geochronology of Zircons from Pegmatite by Laser Ablation ICP-MS Methods

J.K. Mortensen and D. Newton, Pacific Centre for Isotopic and Geochemical Research  
January 29, 2016

## Introduction

A sample of pegmatite (KIN-135), comprising several small hand specimens, was submitted to the Pacific Centre for Isotopic and Geochemical Research (PCIGR) for U-Pb zircon dating. Zircons were separated from the sample using conventional crushing, grinding, wet shaking table, heavy liquids and magnetic techniques.

## Analytical Methodology

Zircons from the sample were analyzed using laser ablation (LA-) ICP-MS methods, employing methods as described by Tafti et al. (2009). Instrumentation employed for LA-ICP-MS dating of zircons at the PCIGR comprises a New Wave UP-213 laser ablation system and a ThermoFinnigan Element2 single collector, double-focusing, magnetic sector ICP-MS. All zircons greater than about 50 microns in diameter were picked from the mineral separates and were mounted in an epoxy puck along with several grains of the  $337.13 \pm 0.13$  Ma Plešovice zircon standard (Sláma et al., 2007), together with a Temora 2 reference zircon, and brought to a very high polish. The surface of the mount was washed for 10 minutes with dilute nitric acid and rinsed in ultraclean water prior to analysis. The highest quality portions of each grain, free of alteration, inclusions, or possible inherited cores, were selected for analysis. Line scans rather than spot analyses were employed in order to minimize elemental fractionation during the analyses. A laser power level of 40% was used. A 25 micrometer spot size was used. Backgrounds were measured with the laser shutter closed for ten seconds, followed by data collection with the laser firing for approximately 35 seconds. The time-integrated signals were analysed using Iolite software (Patton et al., 2011), which automatically subtracts background measurements, propagates all analytical errors, and calculates isotopic ratios and ages. Corrections for mass and elemental fractionation were made by bracketing analyses of unknown grains with replicate analyses of the Plešovice zircon standard. A typical analytical session at the PCIGR consists of four analyses of the Plešovice standard zircon, followed by two analyses of the Temora2 zircon standard ( $416.78 \pm 0.33$  Ma), five analyses of unknown zircons, two standard analyses, five unknown analyses, etc., and finally two Temora2 zircon standards and four Plešovice standard analyses. The Temora2 zircon standard was analysed as an unknown in order to monitor the reproducibility of the age determinations on a run-to-run basis. Final interpretation and plotting of the analytical results employed the ISOPLOT software of Ludwig (2003). All sample preparation and data acquisition were done by J.K. Mortensen. CL imaging, data reduction and report preparation were by J.K. Mortensen and D. Newton.

## Analytical Results and Interpretation

The zircons that were recovered from the pegmatite sample showed euhedral to subhedral morphologies, and mainly consisted of equant to moderately elongate prismatic grains with large facets and simple terminations. No older inherited zircon cores in any of the

grains were visible from and initial examination under a binocular microscope, and it was expected that the zircons would display relatively simple isotopic systematics. The results of the 20 individual analyses are listed in Table 2, and are shown graphically in Figure 1. All of the analyses were concordant, and all but 2 analyses give overlapping error ellipses (at a  $2\sigma$  level; Fig. 1A). A weighted average of the  $^{206}\text{Pb}/^{238}\text{U}$  ages for these 18 analyses is  $79.5 \pm 0.9$  Ma, which is interpreted to give the crystallization age of the sample.

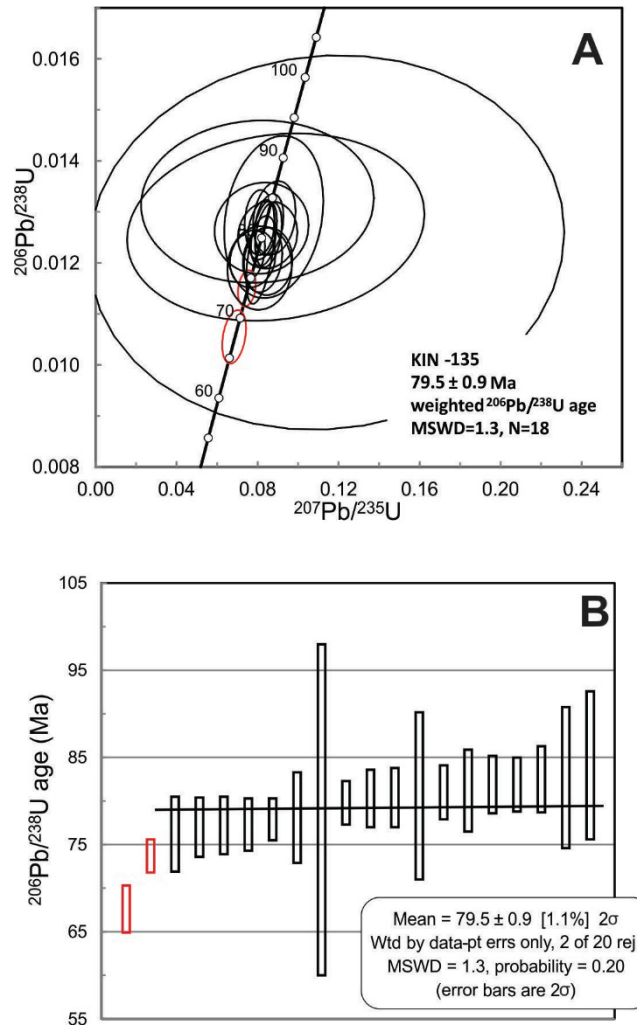


Figure 1. Conventional concordia plot of the analytical data for zircons from sample KIN-135. Error ellipses in Figure 1A and error boxes in Figure 1B are shown at the  $2\sigma$  level. Analyses shown in red were excluded from the calculated weighted average age.

The zircons were imaged with CL methods after the analyses were completed, and despite the apparently euhedral to subhedral external morphology exhibited by the grains, and the simple U-Pb systematics, the CL showed remarkable internal complexity. CL images for all of the grains are shown in Figure 2, and detailed images of three selected grains are shown in Figure 3, with the positions of the individual analysis tracks outlined. The CL images indicate that the bulk of each zircon grain consists of concentric

zoned zircon displaying concentric zoning that extends continuously out to individual external crystal facets. In all of the grains, however, this regular concentric zoning is overprinted by highly irregular, patchy zones with completely different CL characteristics that appears to completely destroy the original zoning. This patchiness is interpreted to reflect a younger alteration process that has affected the grains. All of the individual line scans that were analyzed during this study crossed both concentrically zoned zircon and at least some of the altered patches; however, the analytical data indicates that the age and composition of the altered zircon is indistinguishable from the original material. The alteration must therefore have occurred very soon after the initial crystallization of the zircon. In addition to the patchy alteration that affected the bulk of the grains, there is clear evidence from the CL images for some of the grains for resorption followed by overgrowth by probable metamorphic zircon. Figure 3B shows one grain that displays an irregular, scalloped resorption boundary (shown by the dotted red line) that has been overgrown by vaguely zoned metamorphic zircon.

All of the analyses, including the two that gave slightly younger  $^{206}\text{Pb}/^{238}\text{U}$  ages (analyses 11 and 19 in Fig. 3B and C, respectively), were from the concentrically zoned igneous zircon; hence, we interpret the younger ages for these two analyses to reflect minor post-crystallization Pb-loss rather than a younger zircon growth event. The age of the metamorphic zircon overgrowths is unknown at this point.

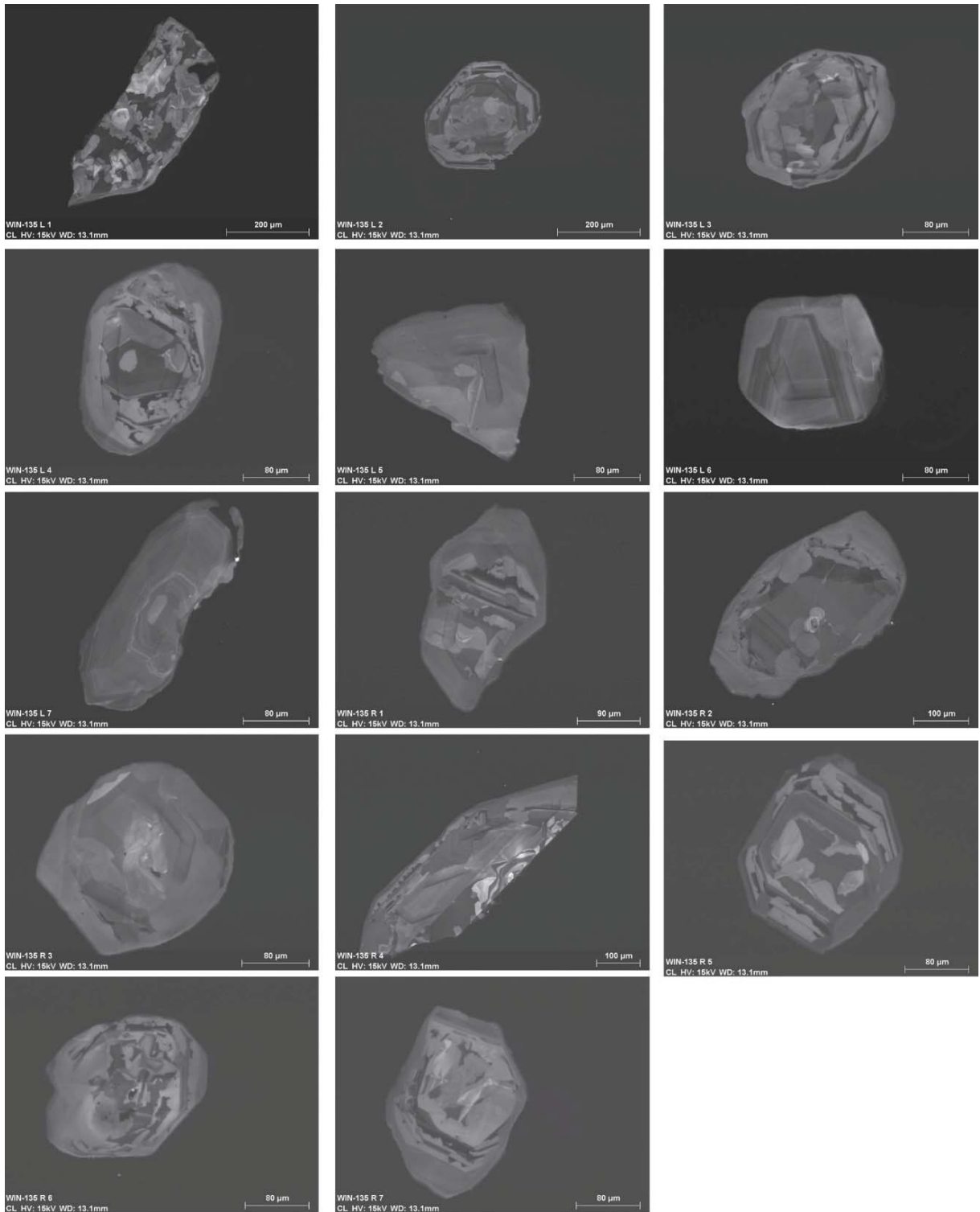


Figure 2. CL images of analyzed zircon grains from sample KIN-135.

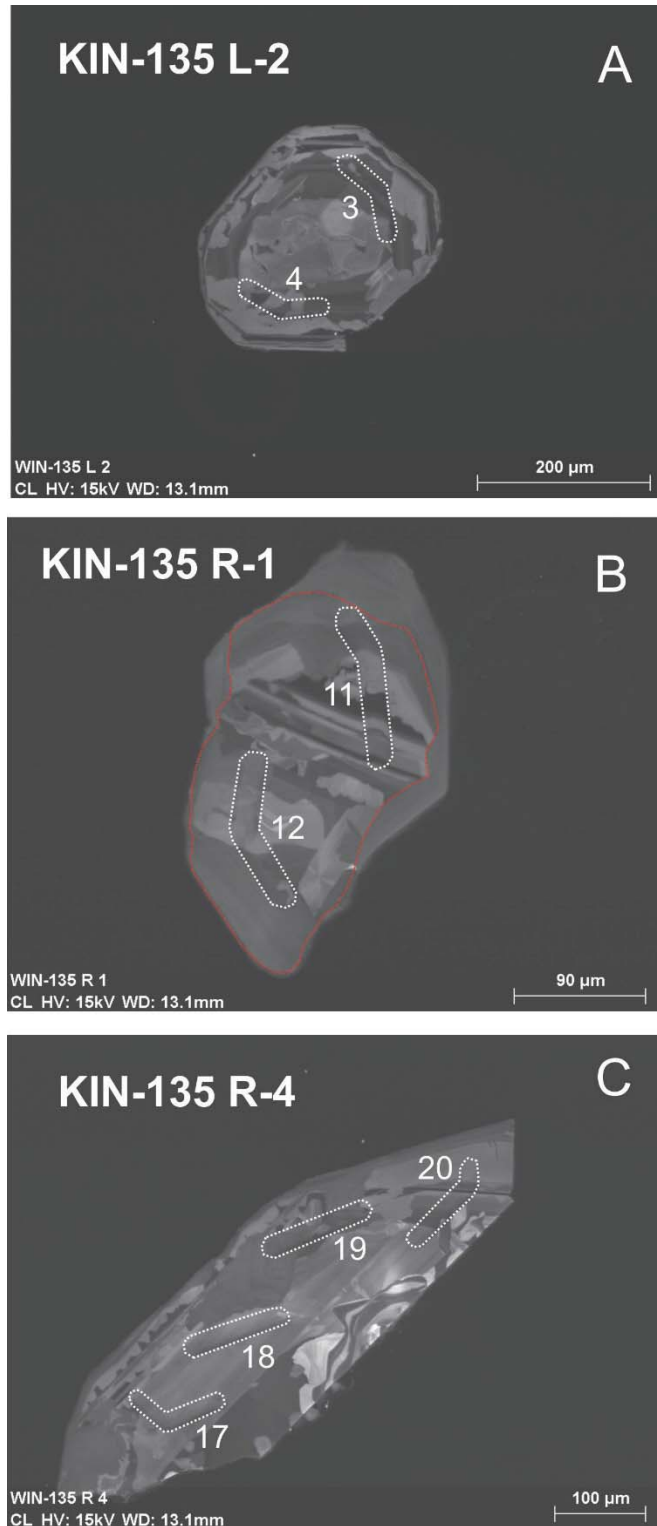


Figure 3. CL images of three of the zircon grains analyzed. Numbered dotted areas show the tracks of individual analyses (which correspond to analyses in Table 1). Red dotted line in B shows the interpreted metamorphic zircon rim that mantles the concentrically zoned igneous core.

Table 1. Zircon U-Pb laser ablation ICP-MS analytical data

Sample no.	Isotopic Ratios					Isotopic Ages					Background Corrected Mean Counts Per Second										
	<sup>207</sup> Pb/ <sup>235</sup> U	2σ (abs)	<sup>206</sup> Pb/ <sup>238</sup> U	2σ (abs)	ρ	<sup>207</sup> Pb/ <sup>206</sup> Pb	2σ (abs)	<sup>207</sup> Pb/ <sup>235</sup> U	2σ (Ma)	<sup>206</sup> Pb/ <sup>238</sup> U	2σ (Ma)	<sup>207</sup> Pb/ <sup>206</sup> Pb	2σ (Ma)	Hg202	Pb204	Pb206	Pb207	Pb208	Th232	U235	U238
<b>KIN-135</b>																					
KIN_135_1	0.088	0.020	0.0129	0.0013	0.20	0.052	0.013	84.0	19.0	82.7	8.1	170	430	-25	-11	1846	89	9019	528008	704	97356
KIN_135_2	0.081	0.013	0.0119	0.0007	0.04	0.051	0.009	77.0	12.0	76.2	4.3	160	270	11	-6	1499	76	993	63153	592	83517
KIN_135_3	0.089	0.060	0.0127	0.0015	0.14	0.210	0.120	53.0	62.0	80.6	9.6	-1900	1200	11	13	193	10	7101	429633	75	10558
KIN_135_4	0.088	0.009	0.0129	0.0006	0.18	0.050	0.005	85.0	8.0	82.5	3.8	180	180	-20	-4	4147	216	16272	986372	1580	224845
KIN_135_5	0.082	0.006	0.0122	0.0008	0.54	0.045	0.003	79.4	5.4	78.1	5.2	30	140	-46	-29	14994	702	10902	680117	6368	816494
KIN_135_6	0.080	0.047	0.0132	0.0013	0.04	0.027	0.060	66.0	48.0	84.1	8.5	-1750	960	-5	3	309	14	4392	278643	116	15343
KIN_135_7	0.081	0.006	0.0128	0.0005	0.06	0.049	0.005	79.8	5.6	81.9	3.3	110	150	-31	16	7595	352	17672	1033597	2980	421302
KIN_135_8	0.082	0.006	0.0127	0.0005	0.29	0.047	0.004	80.0	5.6	81.0	3.1	50	130	32	12	6838	322	9839	613360	2760	374178
KIN_135_9	0.085	0.010	0.0120	0.0005	0.04	0.051	0.006	81.2	9.4	77.0	3.4	140	200	-43	-7	1798	90	426	26165	732	103885
KIN_135_10	0.083	0.008	0.0121	0.0005	0.19	0.052	0.005	79.2	7.3	77.2	3.3	180	180	30	4	2401	122	671	43502	1003	140181
KIN_135_11	0.068	0.005	0.0106	0.0004	0.32	0.046	0.004	67.0	4.6	67.6	2.7	40	130	-57	-24	10036	478	513	30868	4936	659055
KIN_135_12	0.078	0.004	0.0122	0.0004	0.35	0.048	0.003	76.7	4.0	77.9	2.4	90	110	-37	-5	15232	731	6137	393445	6435	882496
KIN_135_13	0.083	0.005	0.0124	0.0004	0.26	0.050	0.003	80.6	4.7	79.8	2.5	150	130	-17	-8	5835	290	3311	208269	2469	335898
KIN_135_14	0.085	0.005	0.0126	0.0005	0.33	0.050	0.004	83.3	5.1	80.3	3.3	190	130	-10	8	15637	772	9260	613673	6574	907629
KIN_135_15	0.114	0.096	0.0124	0.0030	0.06	0.051	0.063	90.0	86.0	79.0	19.0	0	1400	85	79	404	24	1690	130897	154	21270
KIN_135_16	0.082	0.019	0.0127	0.0007	0.07	0.063	0.021	78.0	18.0	81.2	4.7	-200	340	57	-1	799	35	282	16748	319	45834
KIN_135_17	0.078	0.009	0.0121	0.0005	0.13	0.049	0.007	77.3	8.8	77.3	3.0	50	200	-2	2	1587	80	4876	320102	679	94521
KIN_135_18	0.085	0.012	0.0126	0.0005	0.08	0.061	0.010	82.0	12.0	80.4	3.4	60	230	-29	-11	1304	65	3772	251476	531	73760
KIN_135_19	0.075	0.004	0.0115	0.0003	0.23	0.048	0.003	73.1	3.4	73.7	1.9	90	110	-11	0	14333	686	1160	76049	6647	912716
KIN_135_20	0.086	0.006	0.0128	0.0005	0.27	0.049	0.004	82.8	5.5	81.9	3.1	160	130	5	-2	5733	281	4699	313342	2433	329833

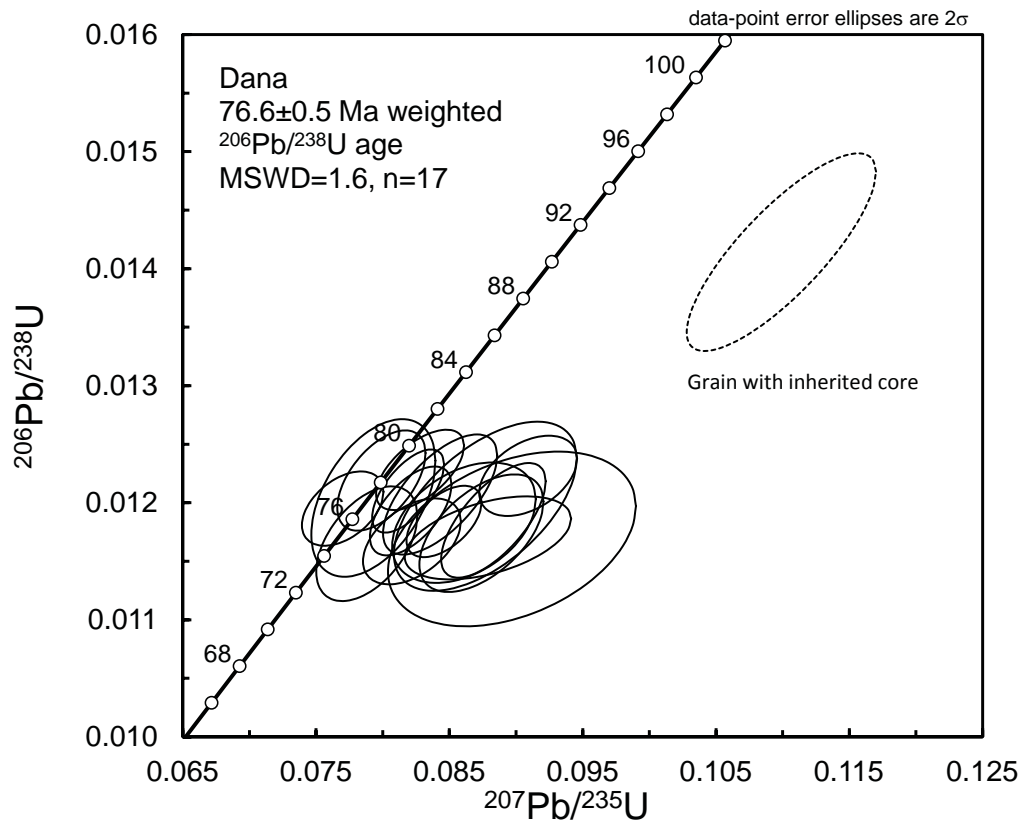
## References

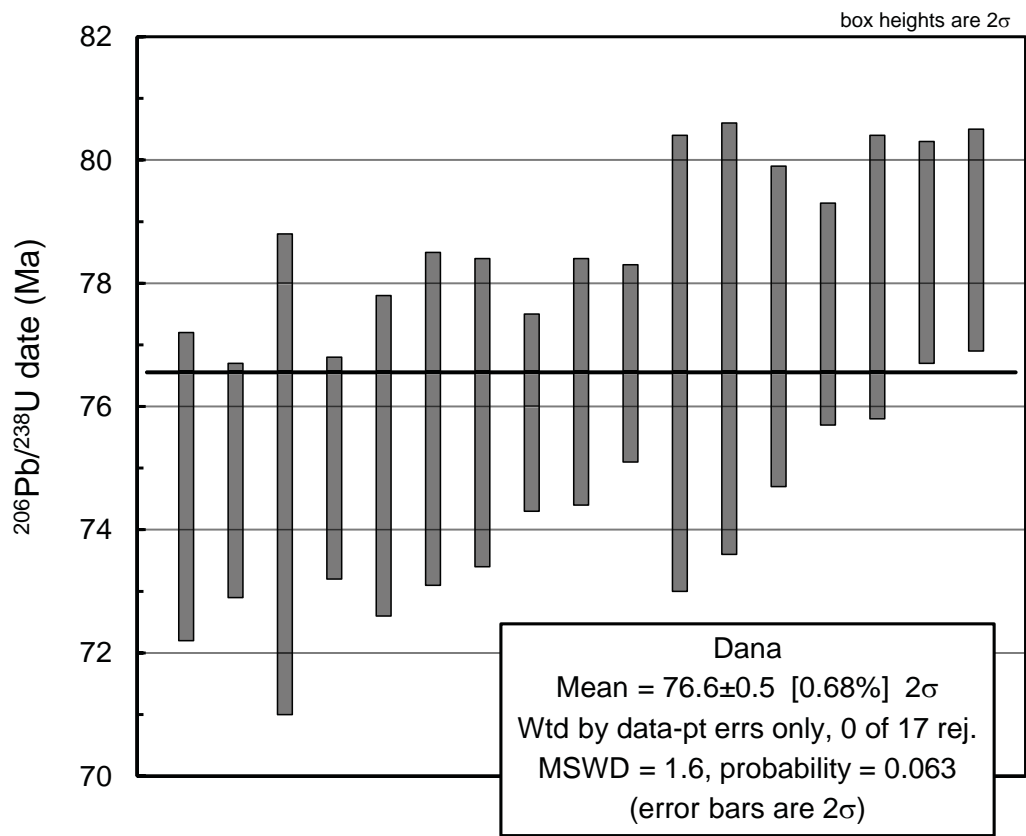
Ludwig, K., 2003, Isoplot/Ex, version 3: A geochronological toolkit for Microsoft Excel: Berkeley, California, Geochronology Center, Berkeley.

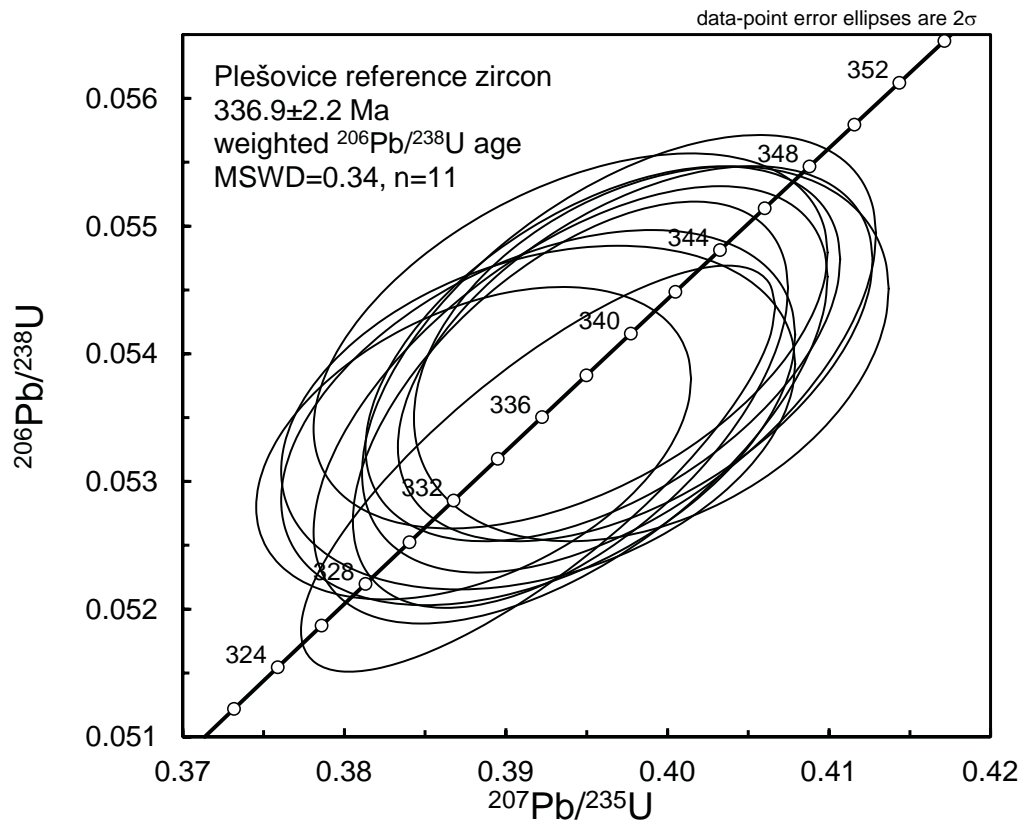
Patton, C., Hellstrom, J., Paul, B., Woodhead, J. Hergt, J., 2011. Iolite: freeware for the visualization and processing of mass spectrometry data; *Journal of Analytical Atomic Spectroscopy*, 26, pp. 2508-2518.

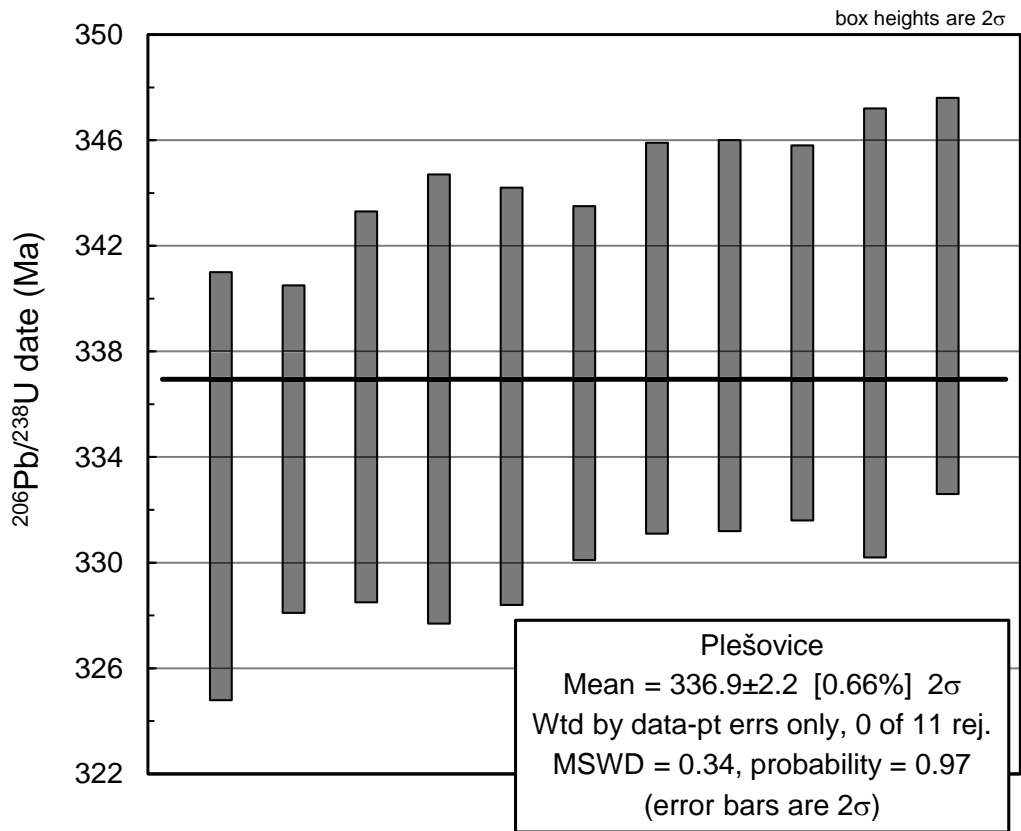
Sláma, J., Košler, J., Condon, D.J., Crowley, J.L., Gerdes, A., Hanchar, J.M., Horstwood, M.S.A., Morris, G.A., Nasdala, L., Norberg, N., Schaltegger, U., Xchoene, B., Tubrett, M.N. and Whitehouse, M.J., 2007, Plešovice zircon — A new natural reference material for U–Pb and Hf isotopic microanalysis; *Chemical Geology*, 249, 1-35.

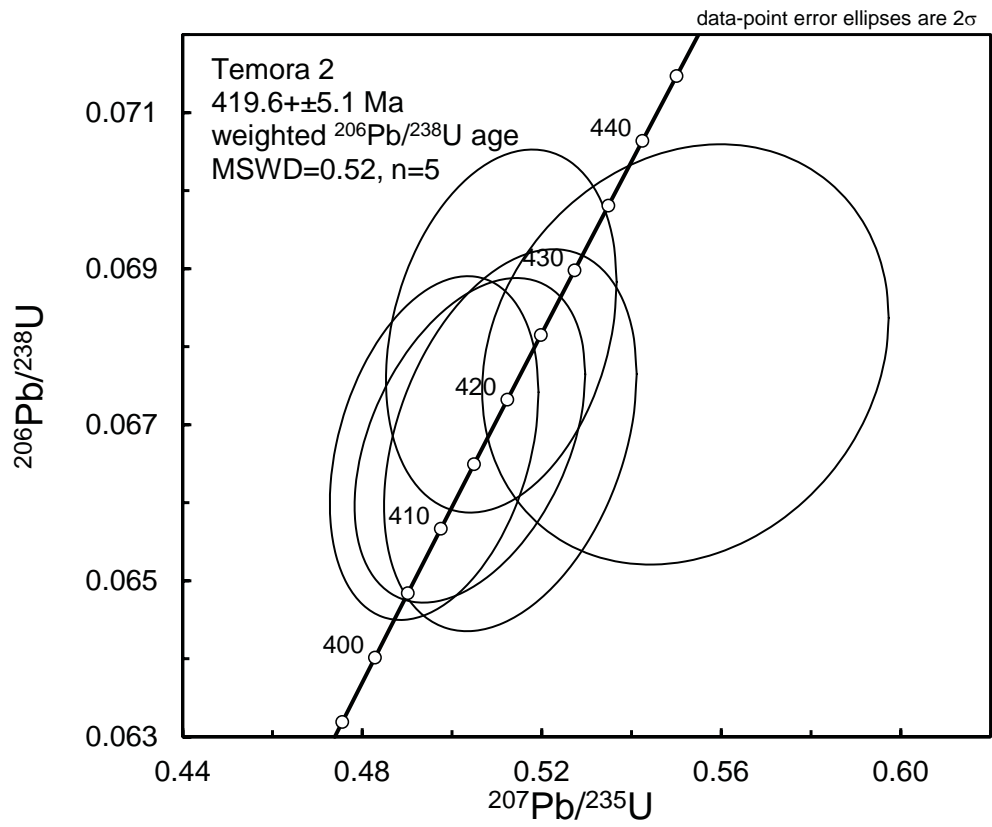
Tafti, R., Mortensen, J.K., Lang, J.R., Rebagliati, M. and Oliver, J.L., 2009, Jurassic U-Pb and Re-Os ages for newly discovered Xietongmen Cu-Au porphyry district, Tibet: Implications for metallogenic epochs in the southern Gangdese Belt; *Economic Geology*, v. 104, pp. 127–136

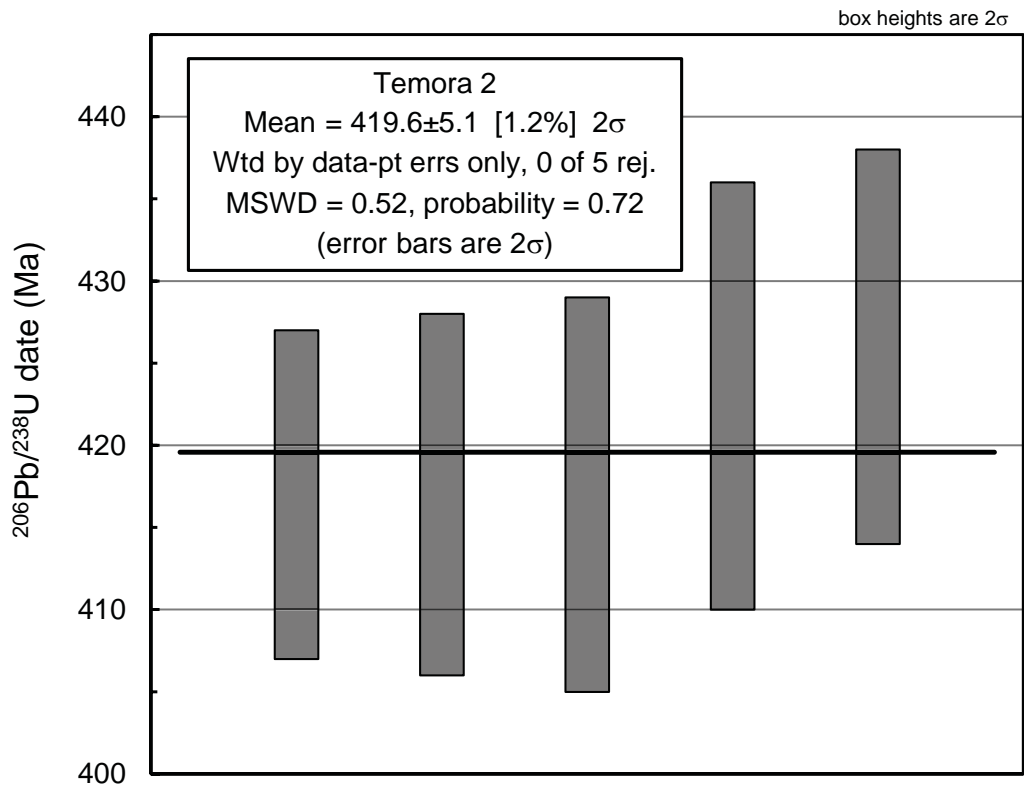












Laser ablation data table

analysis ID	Source file	207Pb/235U ± 2se (abs)	206Pb/238U ± 2se (abs)	Rho 68-75	207Pb/206Pb ± 2se (abs)	207Pb/235U (Ma) ± 2se (Ma)	206Pb/238U (Ma) ± 2se (abs)	207Pb/206Pb ± 2se (abs)	Hg202 (CPS)	Pb204 (CPS)	Pb206 (CPS)	Pb207 (CPS)	Pb208 (CPS)	Th232 (CPS)	U235 (CPS)	U238 (CPS)						
Dana sample																						
DANA_1	2.FIN2	0.0909	0.003	0.01223	0.00028	0.42464	0.0532	0.0023	88.2	2.8	78.5	1.8	313	89	40	21	27328	1438	355	5294	5718	677529
DANA_2	3.FIN2	0.0883	0.0032	0.01185	0.0004	0.67626	0.0526	0.0021	85.8	3	75.9	2.5	321	90	9	25	60944	3177	1025	17913	12502	1548073
DANA_3	4.FIN2	0.0879	0.0051	0.0117	0.00029	0.4605	0.055	0.0033	85	4.7	75	1.8	340	120	12	17	15963	871	246	1911	3562	411539
DANA_5	6.FIN2	0.0861	0.0044	0.01183	0.00042	0.38691	0.0532	0.0029	84.2	4	75.8	2.7	310	110	19	15	29179	1477	465	6650	6209	742443
DANA_6	7.FIN2	0.0843	0.0035	0.01207	0.00042	0.64727	0.0527	0.0023	82.2	3.2	77.3	2.6	300	95	48	18	49495	2578	635	15117	10570	1256377
DANA_7	8.FIN2	0.0788	0.0031	0.01165	0.0004	0.48806	0.0497	0.0023	77	2.9	74.7	2.5	183	95	3	23	36841	1749	265	6264	8022	966414
DANA_8	9.FIN2	0.0821	0.0025	0.01193	0.00031	0.58667	0.0513	0.002	80.2	2.4	76.4	2	244	82	23	41	58556	2885	559	11610	12818	1491013
DANA_9	10.FIN2	0.0874	0.0038	0.01174	0.00041	0.53425	0.0532	0.0026	85	3.5	75.2	2.6	330	100	50	14	39027	2028	549	9662	8423	1008501
DANA_10	11.FIN2	0.0822	0.003	0.01167	0.0003	0.46502	0.0521	0.0023	80	2.8	74.8	1.9	271	89	-3	16	17760	919	181	1662	3964	473504
DANA_11	12.FIN2	0.077	0.0025	0.01195	0.00026	0.44743	0.0472	0.0019	75.5	2.4	76.7	1.6	69	78	0	11	22345	1045	42	1662	4876	571783
DANA_12	13.FIN2	0.0897	0.0076	0.01169	0.00061	0.37352	0.0569	0.0055	87.1	7.1	74.9	3.9	440	210	-13	25	27251	1483	656	7538	5755	704232
DANA_13	14.FIN2	0.0799	0.0027	0.01219	0.00035	0.5427	0.0483	0.0021	78.2	2.5	78.1	2.3	117	86	-4	16	59306	2813	112	6345	12544	1477847
DANA_14	15.FIN2	0.0819	0.0022	0.0121	0.00029	0.63774	0.0489	0.0018	79.8	2	77.5	1.8	143	74	42	11	67310	3234	340	8284	13945	1667114
DANA_15	16.FIN2	0.1099	0.0058	0.01414	0.00069	0.81139	0.0583	0.0025	106.4	5.5	90.5	4.4	513	93	9	48	65933	3871	2042	27028	11752	1433938
DANA_16	17.FIN2	0.0793	0.0038	0.01204	0.00055	0.46515	0.0478	0.0025	77.4	3.5	77.1	3.5	130	110	5	12	27097	1303	73	4047	5797	684501
DANA_17	18.FIN2	0.0877	0.0056	0.01197	0.00059	0.56843	0.0538	0.0033	85.2	5.2	76.7	3.7	340	130	-1	13	37926	1941	462	8974	8497	950628
DANA_18	19.FIN2	0.0846	0.0023	0.01184	0.00025	0.53612	0.0521	0.0019	82.4	2.1	75.9	1.6	280	79	6	12	48545	2480	583	15102	10591	1257541
DANA_19	20.FIN2	0.0828	0.0027	0.01228	0.00028	0.60163	0.0484	0.0019	80.9	2.6	78.7	1.8	130	80	1	-11	46216	2182	175	6962	9932	1168094
Plešovice reference zircon																						
Z_Plešovice_1	PL1.FIN2	0.396	0.012	0.054	0.0012	0.50195	0.0535	0.0021	338.1	9	338.5	7.4	330	83	24	-8	18723	950	423	6266	877	104111
Z_Plešovice_2	PL2.FIN2	0.399	0.012	0.054	0.0012	0.34467	0.0535	0.0023	341.6	9	338.7	7.1	329	86	29	4	16382	842	415	6370	769	90826
Z_Plešovice_3	PL3.FIN2	0.394	0.013	0.0536	0.0014	0.5814	0.0538	0.0021	334.9	9.6	336.2	8.5	334	82	6	12	20413	1044	479	8276	961	113268
Z_Plešovice_4	PL4.FIN2	0.388	0.011	0.0533	0.001	0.40931	0.0517	0.002	332	8.2	334.3	6.2	267	80	19	4	24058	1212	615	9986	1118	134577
Z_Plešovice_5	PL5.FIN2	0.394	0.011	0.0536	0.0013	0.5711	0.0539	0.0021	336.2	8.2	336.3	7.9	348	78	22	3	27302	1414	725	11128	1280	154311
Z_Plešovice_6	PL6.FIN2	0.397	0.013	0.054	0.0014	0.54533	0.0539	0.0022	338.7	9.3	338.7	8.5	369	83	3	6	19158	1029	455	7802	883	109423
Z_Plešovice_7	PL7.FIN2	0.392	0.013	0.0535	0.0011	0.31048	0.053	0.0024	335.1	9.6	336.8	6.7	305	89	4	4	15229	797	358	6090	734	87824
Z_Plešovice_8	PL22.FIN2	0.392	0.013	0.0535	0.0012	0.4397	0.0529	0.0022	334.4	9.1	335.9	7.4	320	87	36	3	17547	925	440	7300	838	101691
Z_Plešovice_9	PL23.FIN2	0.398	0.012	0.054	0.0012	0.49715	0.0544	0.0023	339.9	8.8	338.6	7.4	335	78	8	7	19644	1023	459	7781	947	111440
Z_Plešovice_10	PL24.FIN2	0.394	0.013	0.0541	0.0012	0.46819	0.053	0.0021	337.2	9.1	340.1	7.5	311	82	0	-10	21061	1102	546	8382	992	121002
Z_Plešovice_11	PL25.FIN2	0.392	0.012	0.0531	0.0013	0.79722	0.0527	0.0021	334.7	8.6	332.9	8.1	307	82	6	-8	20857	1088	591	8628	1031	122567
Temora2 zircon (monitor)																						
Z_Temora2_1	TEM1.FIN2	0.511	0.021	0.0682	0.0019	0.26901	0.0541	0.0028	415	14	426	12	330	110	28	6	12245	643	1039	13706	488	54490
Z_Temora2_2	TEM2.FIN2	0.504	0.021	0.0668	0.0017	0.40484	0.0548	0.0026	411	14	417	10	369	97	1	8	10190	537	740	10051	364	45886
Z_Temora2_3	TEM3.FIN2	0.496	0.019	0.0667	0.0018	0.32264	0.054	0.0025	407	12	417	11	352	96	6	-12	11052	585	1017	13230	410	49842
Z_Temora2_4	TEM13.FIN2	0.552	0.037	0.0679	0.0022	0.17334	0.0579	0.0041	446	24	423	13	510	140	-3	-1	4393	261	563	6868	176	20104
Z_Temora2_5	TEM14.FIN2	0.513	0.023	0.0668	0.002	0.34408	0.0557	0.003	419	16	417	12	410	110	25	7	5806	318	808	10293	222	26424

## Analytical Methodology

Zircons were analyzed using laser ablation (LA) ICP-MS methods, employing methods as described by Tafti et al. (2009). Instrumentation employed for LA-ICP-MS dating of zircons at the PCIGR comprises a New Wave UP-213 laser ablation system and a ThermoFinnigan Element2 single collector, double-focusing, magnetic sector ICP-MS. All zircons greater than about 50 microns in diameter were picked from the mineral separates and were mounted in an epoxy puck along with several grains of the  $337.13 \pm 0.13$  Ma Plešovice zircon standard (Sláma et al., 2007), together with a Temora 2 reference zircon, and brought to a very high polish. The surface of the mount was washed for 10 minutes with dilute nitric acid and rinsed in ultraclean water prior to analysis. The highest quality portions of each grain, free of alteration, inclusions, or possible inherited cores, were selected for analysis. Line scans rather than spot analyses were employed in order to minimize elemental fractionation during the analyses. A laser power level of 40% was used. A 25 micrometer spot size was used. Backgrounds were measured with the laser shutter closed for ten seconds, followed by data collection with the laser firing for approximately 35 seconds. The time-integrated signals were analysed using Lolite software (Patton et al., 2011), which automatically subtracts background measurements, propagates all analytical errors, and calculates isotopic ratios and ages. Corrections for mass and elemental fractionation were made by bracketing analyses of unknown grains with replicate analyses of the Plešovice zircon standard. A typical analytical session at the PCIGR consists of four analyses of the Plešovice standard zircon, followed by two analyses of the Temora2 zircon standard ( $416.78 \pm 0.33$  Ma), five analyses of unknown zircons, two standard analyses, five unknown analyses, etc., and finally two Temora2 zircon standards and four Plešovice standard analyses. The Temora2 zircon standard was analysed as an unknown in order to monitor the reproducibility of the age determinations on a run-to-run basis. Final interpretation and plotting of the analytical results employed the ISOPLOT software of Ludwig (2003).

## References

- Ludwig, K., 2003, Isoplot/Ex, version 3: A geochronological toolkit for Microsoft Excel: Berkeley, California, Geochronology Center, Berkeley.
- Patton, C., Hellstrom, J., Paul, B., Woodhead, J., Hergt, J., 2011. Lolite: freeware for the visualization and processing of mass spectrometry data; *Journal of Analytical Atomic Spectroscopy*, 26, pp. 2508-2518.
- Sláma, J., Košler, J., Condon, D.J., Crowley, J.L., Gerdes, A., Hanchar, J.M., Horstwood, M.S.A., Morris, G.A., Nasdala, L., Norberg, N., Schaltegger, U., Xchoene, B., Tubrett, M.N. and Whitehouse, M.J., 2007, Plešovice zircon — A new natural reference material for U–Pb and Hf isotopic microanalysis; *Chemical Geology*, 249, 1-35.
- Tafti, R., Mortensen, J.K., Lang, J.R., Rebagliati, M. and Oliver, J.L., 2009, Jurassic U-Pb and Re-Os ages for newly discovered Xietongmen Cu-Au porphyry district, Tibet: Implications for metallogenic epochs in the southern Gangdese Belt; *Economic Geology*, v. 104, pp. 127–136